AFFDL–TR–75–152
ADA 025 746

# FRACTOGRAPHIC EVALUATION OF FRACTURE SPECIMENS

Grumman Aerospace Corporation
Bethpage, New York

MARCH 1976

TECHNICAL REPORT AFFDL–TR–75–152
FINAL REPORT FOR PERIOD MARCH 1975 – DECEMBER 1975



AIRFORCE FLIGHT DYNAMICS LABORATORY
AIR FORCE WRIGHT AERONAUTICAL LABORATORIES
AIR FORCE SYSTEMS COMMAND
WRIGHT-PATTERSON AIR FORCE BASE, OHIO 45433

NOTICE

When Government drawings, specifications, or other data are used for any purpose other than in connection with a definitely related Government procurement operation, the United States Government thereby incurs no responsibility nor any obligation whatsoever; and the fact that the Government may have formulated, furnished, or in any way supplied the said drawings, specifications, or other data, is not to be regarded by implication or otherwise as in any manner licensing the holder or any other person or corporation, or conveying any rights or permission to manufacture, use, or sell any patented invention that may in any way be related thereto.

This report has been reviewed by the Information Office (OI) and is releasable to the National Technical Information Service (NTIS). At NTIS, it will be available to the general public, including foreign nations.

This report has been reviewed and is approved for publication.

ROBERT M. ENGLE
Project Engineer

R. M. Bader

ROBERT M. BADER, Chief
Structural Integrity Branch
Structures Division

FOR THE COMMANDER

Gerald G. Leigh

GERALD G. LEIGH, Lt Col, USAF
Chief, Structures Division

Copies of this report should not be returned unless return is required by security considerations, contractual obligations, or notice on a specific document.

UNCLASSIFIED

SECURITY CLASSIFICATION OF THIS PAGE *(When Data Entered)*

| REPORT DOCUMENTATION PAGE | | READ INSTRUCTIONS BEFORE COMPLETING FORM |
|---|---|---|
| 1. REPORT NUMBER<br>AFFDL-TR-75-152 | 2. GOVT ACCESSION NO. | 3. RECIPIENT'S CATALOG NUMBER |
| 4. TITLE *(and Subtitle)*<br>FRACTOGRAPHIC EVALUATION OF FRACTURE SPECIMENS | | 5. TYPE OF REPORT & PERIOD COVERED<br>Final Technical Report<br>March 1975 – December 1975 |
| | | 6. PERFORMING ORG. REPORT NUMBER |
| 7. AUTHOR(s)<br>P.D. Bell, W.J. Feeney | | 8. CONTRACT OR GRANT NUMBER(s)<br>F33615-75-C-3042 |
| 9. PERFORMING ORGANIZATION NAME AND ADDRESS<br>Grumman Aerospace Corporation<br>Bethpage, New York 11714 | | 10. PROGRAM ELEMENT, PROJECT, TASK AREA & WORK UNIT NUMBERS<br>Project 486U<br>Task 486U0208 |
| 11. CONTROLLING OFFICE NAME AND ADDRESS<br>Air Force Flight Dynamics Laboratory<br>Wright-Patterson Air Force Base<br>Dayton, Ohio 45433 | | 12. REPORT DATE<br>MARCH 1976 |
| | | 13. NUMBER OF PAGES<br>187 |
| 14. MONITORING AGENCY NAME & ADDRESS *(if different from Controlling Office)* | | 15. SECURITY CLASS. *(of this report)*<br>UNCLASSIFIED |
| | | 15a. DECLASSIFICATION/DOWNGRADING SCHEDULE |

16. DISTRIBUTION STATEMENT *(of this Report)*

Approved for public release; distribution unlimited

17. DISTRIBUTION STATEMENT *(of the abstract entered in Block 20, if different from Report)*

18. SUPPLEMENTARY NOTES

19. KEY WORDS *(Continue on reverse side if necessary and identify by block number)*

| | | |
|---|---|---|
| Crack Closure | 2219-T851 Aluminum | Fractography |
| Crack Growth Interaction | Ti 6Al-4V Titanium | Electron Microscope |
| Mathematical Model | Retardation | |
| Overloads | Acceleration | |

20. ABSTRACT *(Continue on reverse side if necessary and identify by block number)*

This fractographic study of 2219-T851 aluminum and Ti 6Al-4V titanium was undertaken to investigate crack growth interaction effects in greater detail than was possible macroscopically. The specimens examined had been tested during the Crack Growth Analysis for Arbitrary Spectrum Loading Program, Air Force Contract No. F33615-72-C-1744. The transmission electron microscope was used for most measurements obtained.

DD FORM 1 JAN 73 1473 EDITION OF 1 NOV 65 IS OBSOLETE
S/N 0102-014-6601 |

UNCLASSIFIED

SECURITY CLASSIFICATION OF THIS PAGE *(When Data Entered)*

It was concluded that there is a one-for-one relationship between striations and loading cycles for the approximate striation size range from 1 to 50 micro inch. It was shown that striation spacing data, obtained along the centerline and edges of the fracture faces, correlated closely with macroscopic data obtained from the specimen surfaces. The plane strain plastic zone diameter described the overload affected crack length for specimens tested under plane strain conditions. The existence of delayed retardation was neither confirmed nor denied by this study, but a theory using plasticity and internal growth was proposed to explain delayed retardation as a surface phenomenon. The ratio of the closure level after one overload cycle to the stabilized closure level for the overload, decreased with increasing overload ratio. This ratio was larger for titanium than for aluminum at a given overload ratio. A local increase in striation spacing just prior to an overload was credited to stretching of the existing fracture surface by the overload. The stretch bands produced by the first few consecutive overload cycles were found to be much greater than could be calculated. The number of overload cycles required to achieve stabilized conditions of crack growth was found to be approximately 200 for both materials.

Discrete compression spikes or compression spikes applied prior to tensile overloads had negligible influence on subsequent crack growth, but compression spikes applied after tensile overloads tended to offset the retarding effect of the overload on subsequent crack growth in titanium. For constant amplitude loading, striation spacing was about 90% greater in 3/4-in. thick titanium than in 1/4-in. thick titanium, but the retardation parameters developed for the 1/4-in. thick material applied equally well to the 3/4-in. thick material.

## FOREWORD

This report describes a fractographic investigation of fatigue crack growth interaction effects in airframe structural materials, performed by Grumman Aerospace Corporation, Bethpage, New York, from March 15, 1975 through October 31, 1975 under Air Force Contract F33615-75-C-3042. Specimens tested under Air Force Contract F33615-72-C-1744, "Crack Growth Analysis for Arbitrary Spectrum Loading," were examined.

The work was sponsored under Project 486U, "The Advanced Metallic Structures - Advanced Development Program" (AMS-ADP), Task 486U02, "Applied Fracture Mechanics" Air Force Flight Dynamics Laboratory (AFFDL) with Mr. Robert M. Engle (AFFDL/FBE) as project engineer.

The program was conducted by personnel of the Structural Mechanics and Metallurgy Sections of the Grumman Aerospace Corporation under the supervision of F. Berger, Manager, Advanced Development, Systems Engineering. The project engineer and principal investigator was P. D. Bell and the chief electron microscopist was W. J. Feeney. Fractographic support was provided by R. Messler, J. Winn and P. Brofman. Mr. A. Wolfman provided the impetus for this program.

The report was submitted by the authors on October 31, 1975.

TABLE OF CONTENTS

TABLE OF CONTENTS (Cont)

LIST OF ILLUSTRATIONS

LIST OF ILLUSTRATIONS (Cont)

LIST OF ILLUSTRATIONS (Cont)

LIST OF ILLUSTRATIONS (Cont)

LIST OF ILLUSTRATIONS (Cont)

LIST OF ILLUSTRATIONS (Cont)

LIST OF TABLES

## LIST OF SYMBOLS

$a$ - Crack length or half-length, in.

$a_{min}$ - Crack length at minimum striation spacing, in.

$\Delta a$ - Crack growth increment since overload, in.

$\Delta a_{dr}$ - Crack length over which striation spacing decreased after an overload, in.

$B$ - Empirical exponent

$c$ - Surface crack half-length, in.

$C$ - Crack growth rate equation coefficient

$C_f$ - Crack closure factor, ratio of the stress (or load) at closure to the maximum applied stress (or load)

$C_{f_o}$ - Crack closure factor at R = zero

$d_s$ - Striation spacing or width, in.

$\frac{da}{dN}$ - Crack growth rate, in./ cycle

$\frac{\Delta a}{\Delta N}$ - Average crack growth rate, in./cycle

$f_n$ - Ratio of the measured striation spacing to the calculated constant amplitude crack growth rate for identical crack lengths and loads

$f(\frac{a}{t}, W)$ - Factor relating stress intensity to stress (or load)

$I_L$ - TEM objective lens current, ampere

$K$ - Maximum baseline stress intensity, ksi$\sqrt{in.}$

$K_{c_b}$ - Stress intensity at crack closure for baseline loading, ksi$\sqrt{in.}$

$K_{c_{OL}}$ - Stress intensity at crack closure for overload, ksi$\sqrt{in.}$

$K^1_{c_{OL}}$ - Stress intensity at crack closure after one overload cycle, ksi$\sqrt{in.}$

$K_{min}$ - Minimum baseline stress intensity, ksi$\sqrt{in.}$

$K_{OL}$ - Maximum overload stress intensity, ksi$\sqrt{in.}$

$K_{st}$ - Stress intensity at threshold of stable tear, ksi$\sqrt{in}$.

$\Delta K$ - Applied stress intensity range, ksi$\sqrt{in}$.

$\Delta K_{eff}$ - Effective stress intensity range, $K - K_{c_b}$ or $K_{OL} - K_{c_{OL}}$, ksi$\sqrt{in}$.

M - Magnification

n - Empirical crack growth rate equation exponent

N - Number of low load cycles

$N_L$ - Number of lines

$N_{OL}$ - Number of overload cycles

$N_s$ - Number of striations

$N_{sat}$ - Number of overload cycles to achieve stabilized closure and crack growth conditions

$\Delta N_s$ - Number of cycles since overload application or load change

O/L - Overload ratio, $S_{OL}/S$, $K_{OL}/K$ or $P_{OL}/P$

P - Maximum baseline load, lb

$P_{c_b}$ - Baseline load at crack closure, lb

$P_{c_{req}}$ - Closure load required to match crack growth rates and/or striation spacing, lb

$P_{min}$ - Minimum baseline load, lb

$P_{OL}$ - Maximum overload magnitude, lb

R - Stress ratio, $S_{min}/S$, $K_{min}/K$ or $P_{min}/P$

$R_c$ - Stress ratio for negative minimum stress or load

S - Maximum baseline stress, ksi

$S_{c_b}$ - Crack closure stress for baseline stress, ksi

$S_{c_{OL}}$ - Crack closure stress for overload stress, ksi

$S_{c_1}$ - Crack closure stress after one overload cycle, ksi

$S_{min}$ - Minimum baseline stress, ksi

$S_{OL}$ - Maximum overload stress, ksi

$t$ - Specimen thickness, in.

$W$ - Specimen width, in.

$\gamma_1$ - Ratio of closure stress (or load) after one overload cycle to the stabilized closure stress (or load) for the overload

$\delta$ - Plane strain plastic zone diameter, in.

$\rho$ - Plane stress plastic zone radius, in.

$\sigma_y$ - Tensile yield stress, ksi

$\mu$ - Micron ($10^{-6}$ meter) when used on photographs, otherwise micro ($10^{-6}$) when used with inches

## ABBREVIATIONS

CCA - Calculated constant amplitude

CCP - Center cracked panel

CTA - ASTM Compact Tension Specimen Geometry

CTB - Modified Compact Tension Specimen Geometry

C/T - Compression/tension

PD - Propagation direction

SEM - Scanning electron microscope

TEM - Transmission electron microscope

T/C - Tension/compression

## SUMMARY

This program is one in a series of research and development programs undertaken by the United States Air Force to develop methods and data needed to design against fracture in military aircraft. This fractographic program was directed to the investigation of fatigue crack growth interaction effects under spectrum loading conditions.

The program consisted of performing quantitative fractographic evaluations of fatigue crack growth specimens, fabricated from 2219-T851 aluminum and Ti 6Al-4V titanium, which were tested under Air Force Contract No. F33615-72-C-1744, "Crack Growth Analysis for Arbitrary Spectrum Loading" (Ref 1). Specimens which had been subjected to constant amplitude loading, single discrete and periodic overloads, low-to-high loading and compression spikes, applied singly or in combination with tensile overloads were examined.

The results of this program were used to verify and modify the Crack Closure Model developed during the Ref 1 program. In general, this program verified the Ref 1 program results, and in some cases, provided a more precise definition of crack growth interaction effects. It produced contradictory results regarding the retardation parameters for single overloads. It confirmed that the amount of crack growth which occurred during an overload exceeded the value calculated by using crack closure criteria.

## Section 1

## INTRODUCTION

The fractographic examination of failed components has often provided valuable clues to the mechanism and cause of failure. Examination of fractures which resulted from fatigue loading disclosed unique characteristics which are related to the loading sequences present in a fatigue environment. The nature of loading and unloading results in a discontinuous crack propagation process which is evident on the fracture surface. This characteristic discontinuity, referred to as a fatigue striation, is the topographical result of a single application and relaxation of load. A striation possesses a unique dimension of length which is, among other factors, a measure of the distance a fatigue crack would propagate during one load application. The microscopic measurement of such spacing yields information on the incremental crack growth rate. The examination and measurement of striation spacing, before, during, and after significant events in the flawed life of a component, can yield useful information on the interaction of various parameters such as the state of applied stress as well as the history of stress loading.

The objective of this program, initiated by the United States Air Force, was to perform a fractographic study of the test specimens from Air Force contract No. F33615-72-C-1744, "Crack Growth Analysis For Arbitrary Spectrum Loading" (Ref 1), to determine whether or not a refinement of the Crack Closure Model, developed during the Ref 1 program, was possible with the aid of fractography. The Crack Closure Model is a mathematical model which provides improved predictive capability for crack growth under variable amplitude loading. Because the model is empirical in nature, some assumptions were required during its development. The results of this effort were used to verify and, where applicable, modify those assumptions.

To date, the quantification of fatigue striation data has not been extensively employed on test specimens failed by complex alternating load interaction conditions. The limited prior striation measurement efforts of other investigators depended on the measurement of striation data from photographic

negatives or prints. This photographic approach is very time consuming because a great deal of striation data is required to overcome inherent striation measurement scatter. The technique employed in this contract utilized a more direct approach of striation measurement, designed to obtain a greater number of data points. The striations were measured directly on the transmission electron microscope magnification-calibrated, phosphorescent viewing screen. This technique enabled numerous traverses to be made through events which helped to overcome striation data scatter problems.

Fractographs which supplement results reported in the main text are presented in the Appendix.

## Section 2

## MATERIALS AND PROCEDURES

### 2.1 MATERIALS SELECTION

The materials selection and crack growth testing procedures are described in detail in Ref 1. The materials examined were 2219-T851 aluminum and Ti 6Al-4V titanium alloys. Most of the specimens examined were nominally 1/4-in. thick. A few measurements were obtained from a 3/4-in. thick titanium specimen to investigate the effect of thickness on striation spacing subsequent to a single overload cycle. The test specimens were either compact tension or center-cracked panel (CCP) specimens. The compact tension specimens were of either ASTM standard geometry (CTA) or a modified geometry (CTB) as described in Ref 1.

### 2.2 EXPERIMENTAL PROCEDURES

#### 2.2.1 Transmission Electron Microscope (TEM)

The measurements in this program were performed primarily on the JEOL JEM-6A electron transmission microscope which has a resolution of 25Å. In practice, striation spacings of approximately 2 μ-in. could be consistently measured. This particular microscope is ideally suited to this type of measurement because of the ease of viewing through three port windows and because the specimen stage drive is fitted with micrometer movements which enable accurate measurements of distance traversed along the replicas.

Replica preparation for the transmission electron microscope proceeded as follows:

- Cellulose acetate impressions were made of the clean fracture surfaces
- The plastic impressions were shadowed with chrome at a $45^{o}$ angle in a Denton Vacuum Evaporator D-502 and then coated with carbon as the plastic replica turned continuously

- The particular area of the fracture to be viewed was then cut from the coated plastic replica and placed on a transmission microscope specimen grid
- The grids were then placed inside a reflux condenser to dissolve away the plastic and leave only the chrome-shadowed carbon impression of the fracture surface. This thin chrome-shadowed carbon film is transparent to the electron beam of the microscope, whereas the original plastic impression was not.

Equipment Calibration - The TEM was calibrated by scribing a 1-in.-diameter circle on the projection screen. Then, a diffraction grating replica with 28800 lines per inch was placed in the TEM and the number of lines within the 1-in. circle were counted at a variety of lens current and magnification range settings. The magnification (M) was determined by

$$M = \frac{28800}{N_L} \tag{1}$$

where $N_L$ was the number of lines within the 1-in. circle. The magnification was then plotted against the current setting to provide a calibration curve which was accurate to within ± 8 percent due to intermediate lens hysteresis effects. In practice, the striation spacing, $d_s$, was determined by:

$$d_s = \frac{1}{N_s M} \tag{2}$$

where $N_s$ was the number of striae within the 1-in. circle and M was determined from the calibration curve using the lens current at which striation readings were taken. The calibration curves were monitored and revised at intervals as deemed necessary.

The specimen was held in a stage movement which was driven through two (a left and a right) micrometers. The micrometers (calibrated in 0.01 mm increments) were not direct reading because of the movement reduction obtained by the mechanical linkage between the exterior and interior of the TEM. The above-mentioned diffraction grating was used to calibrate the micrometer readings to the actual stage movement. This was accomplished by

traversing a course normal to the diffraction lines for 28.8 lines (.001 in. actual movement). It was determined that 5.6 mm change in the micrometer reading corresponded to an actual (stage) movement of 1 mm.

### 2.2.2 Supporting Equipment

Additional supportive work was performed on the AMR-1000 scanning electron microscope (SEM) (150 Å resolution). The lower magnification capability along with greater depth of field was helpful in locating particular events, such as high peak load slip lines and specimen edge effects. The fracture surfaces were prepared for scanning by coating the surface with pure gold in a vacuum evaporator. The addition of gold on both the aluminum and titanium fracture surfaces improved the fatigue striation contrast and resolution.

Low power stereo light microscopes were also used to locate events on specimens and on replicas and as an aid in mounting and preparing replicas.

## 2.3 ANALYTICAL PROCEDURES

The data reduction procedures were straightforward and basically the same for each of the types of measurements obtained. First, the location of the event of interest was determined by observing the specimens and/or the replicas as required using optical techniques. The replica was prepared as described above and placed in the TEM. The image was then scanned to locate the event. This may have been, in the case of a single overload, for example, an over-sized striation, a slip band, or a dimpled area. For the case of a single overload, the location of the leading edge of the event was recorded by obtaining coordinate readings along its length using the left and right micrometer drives. Then, one or more traverses were made both before and after the event. During these traverses, the number of striae within the 1-in. circle were counted at various points and recorded. The TEM intermediate lens current, $I_L$, and the coordinates of each point were also recorded. The average striation spacing was calculated from Eq 2 and a contour plot, typified by Fig. 1, was made. The perpendicular distance from the leading edge of the slip band to each striation measurement location was scaled to obtain a cross plot as shown in Fig. 2. These plots were obtained by assuming that the leading edge of the slip band coincided with the crack length, based on surface

measurements, at which the overload was applied. Because the slip band was not typically a straight, smooth or even continuous line (Fig. 1), it was necessary to work along each traverse using a nominal location for the slip band. This procedure undoubtedly added to the data scatter, especially right after load changes. Plots such as Fig. 2 formed the basis for all analytical evaluations of the measured data.

## 2.4 DISCUSSION OF ERRORS

There were several sources of error related to either the experimental or analytical procedures. As mentioned earlier, the TEM intermediate lens has an accuracy of ± 8% due to electro-magnetic hysteresis effects. A pin cushion distortion condition was observed during the early use of the TEM. As a result, the 1-in. diameter circle was calibrated as described in Subsection 2.2.1 of this report and, except for special cases, all subsequent striation spacing measurements were taken within that circle. Another source of error is related to the carbon replicating technique. The replicas are smoother than the fracture face resulting in greater angles between adjacent crystallographic planes (grains) on the replica than on the specimen with a resultant tendency to distort the striation spacing.

Brittle striations with associated secondary cracking were discounted because preliminary investigations indicated that the resultant striation spacing values were much greater than nearby ductile striation values for both materials examined.

A mixed mode topography, composed of fatigue striations and small amounts of cleavage, was observed in titanium under high stress intensity conditions. The striation spacing measurements obtained under these conditions may have introduced some error.

In many cases, striations were discontinuous. In others, the width of a striation or slip band varied from place to place along its length. These problems were overcome to a great extent by making multiple measurements.

Several possible error sources were related to electron microscope operator techniques. These included difficulties in identifying events, potential striation counting errors and the inclusion of partial striations in the count.

These error sources were negated by employing simultaneous operators. Multiple traverses through the events of interest were also made to reduce errors. Wherever possible, the TEM magnification was adjusted so that only whole striations were counted.

While the potential sources of error were numerous, the careful selection of measurement sites and the redundant measuring systems (multiple operators and/or multiple traverses) produced microscopic data which agreed very closely with macroscopically obtained data. The quality of the data obtained was considered to be very good and quantitative comparisons of microscopic and macroscopic data were possible throughout the investigation.

## Section 3

## RESULTS AND DISCUSSION

The objective of making microscopic measurements was to obtain quantitative values of striation spacing as a function of crack length, overload cycles or low load cycles for various loading perturbations. These results, in turn, were to be used to modify, if appropriate, the Crack Closure Model developed in Ref 1.

The measurement procedures were generally straightforward, as described in Section 2. Measurements obtained for aluminum were fairly easy to make, due to the large grain size, relative to the crack extensions involved. On the other hand, the small titanium grain size caused considerable difficulty quantifying the striae. In some cases for titanium, the striations were so discontinuous that consecutive striation spacing measurements could not be obtained. In these cases, the striation data were plotted as a function of crack length.

The majority of the data, to be reported below, was generally satisfactory but in some cases gave unexpected and contradictory results in relation to the Crack Growth Analysis program of Ref 1.

### 3.1 CORRELATION OF MICROSCOPIC AND MACROSCOPIC CRACK GROWTH

The objective of these measurements was to determine whether or not there is a one-for-one correlation between striations and loading cycles. Specimens subjected to constant amplitude loading were selected for this study. The criteria for selection were: a) the striation spacing should be at least five μ-in. in size, and b) the maximum stress intensity should be below the stable tear stress intensity threshold (30 ksi$\sqrt{\text{in.}}$ for aluminum and 72.5 ksi$\sqrt{\text{in.}}$ for titanium) as reported in Ref 1. Note that all of the aluminum data were obtained from the same specimen (AG-25-1P) which was selected as being representative of all aluminum specimens. The titanium specimens were similarly selected. The specimens examined, along with pertinent data are presented in Table 1.

They consisted of a 2219-T851 aluminum and two Ti 6Al-4V titanium specimens. Stress ratios, R, of 0.05 and 0.50 were examined for each material.

### 3.1.1 2219-T851 Aluminum

Figure 3 presents striation spacing data for a specimen subjected to constant amplitude loading with a stress ratio, R, of 0.05. Measured values of striation spacing, $d_s$, are plotted against crack length, a. These data were taken from a single replica over a length of about 0.055 in. The data were fit, using a least squares procedure, to a linear equation as a function of crack length, a, (assumed to be correct over this short length). A scatter band, fit to the most extreme data, indicates variations of as much as +23% and -45% from the best-fit line. Although this scatter appeared to be large, the least squares curve compared favorably with a similar line calculated from the crack growth Eq 1a of Ref 1 for 2219-T851 aluminum:

$$\frac{da}{dn} = 1.96 \times 10^{-9} \left[(1 + 0.6R)\Delta K\right]^{3.34} \qquad (3)$$

This equation is valid for $0 \leq R \leq 0.5$. The difference between the two lines ranges from 5% to 16%.

Figure 3b presents the same data plotted against $\Delta K$. When the data in Figure 3b were fit to the Paris equation: $da/dN = C\Delta K^n$, the exponent n was 5.68 which is measurably higher than the value (3.34) from Eq 3. In order to compare Eq 3 with the data, the exponent n was set to 3.34 (from Eq. 3) and a least squares analysis was performed to obtain C. (See Fig. 3b.) The rates (striation spacings) obtained are 13% less than those from Eq 3.

The conclusion drawn was that the data obtained over such a short crack extension, and therefore small increase in stress intensity, could not be analyzed to obtain the exponent n. As a result, eight additional replicas, spanning a total crack extension of 0.34 in., were fabricated. The data obtained are presented in Fig. 4. These data clearly show a trend of increasing $d_s$ with increasing crack length even though considerable scatter is still present. These data were converted to stress intensity and re-plotted in Fig. 5.

A least squares analysis produced:

$$d_s = 2.53 \times 10^{-9} \Delta K^{3.36} \qquad (4)$$

The exponents of Eq 3 and 4 compare favorably and Eq 4 yields values of $d_s$ which are only 15% greater than the rates from Eq 3. A further analysis of the crack growth rate data from the Crack Growth Analysis program (Ref 1), between $5 \times 10^{-6}$ and $5 \times 10^{-5}$-in./cycle with R = 0.50 was performed (Fig. 6). The least squares equation for these data is also presented in Fig. 5 and provides even closer agreement than Eq 3 with the striation data.

Figure 7 presents $d_s$ versus crack length for a specimen subjected to constant amplitude loading where R = 0.05. The striation spacing was again assumed to be a linear function of a, and a least squares analysis was performed. It can be seen that the least squares curve closely parallels the curve calculated from Eq 3.

These results demonstrate that quantitative striation values equivalent to crack growth rates, may be obtained from striation spacing measurements obtained from the 2219-T851 aluminum material under steady-state conditions. Although individual values of $d_s$ may possess considerable scatter, when a sufficient number of measurements are obtained, the resultant best-fit curves provide excellent correlation with macroscopically-obtained crack growth rates.

### 3.1.2 Ti 6A1-4V Titanium

Figure 8 presents striation spacing data for a titanium specimen subjected to constant amplitude loading with R = 0.05. The striation spacing was fit to the linear equation in Fig. 8a and compared to a curve calculated from Eq 1c of Ref 1:

$$\frac{da}{dN} = 5.9 \times 10^{-10} \left[(1 + .7R)\Delta K\right]^{3.08} \qquad (5)$$

This equation is valid for titanium for $0 \leq R \leq 0.7$. Although there is considerable scatter in individual data points, the best-fit curve is only from 47% to 21% lower than the curve generated using Eq 5.

Figure 8b shows that a Paris equation, fit to the data, would have a very high slope (exponent). Therefore, in order to compare Eq 5 with the data, the slope was set at 3.08 and a least squares analysis was performed to obtain C

so that: $d_s = 5.65 \times 10^{-10} \Delta K^{3.08}$. This equation yields values of $d_s$ which are 14% lower than the crack growth rates from Eq 5.

Ten replicas for the same specimen, spanning $1.05 \leq a \leq 1.41$, were prepared to determine whether or not a microscopically determined value of n (Paris equation exponent), which compared favorably with the macroscopically determined n, could be obtained. These data are presented in Fig. 9 and 10. Figure 10 shows that the least squares solution for both C and n in the Paris equation provides excellent agreement with crack growth rates obtained using Eq 5.

Figure 11 presents data for a specimen subjected to constant amplitude loading with a stress ratio of 0.50. It can be seen that the least squares fit agrees to within 15% with Eq 5.

These results demonstrate that, like the aluminum, individual titanium data points possess considerable scatter. However, they also show that when analyzed as described above, the microscopic data agree very closely with the macroscopically obtained data.

### 3.1.3 Summary

The data obtained for both materials at both stress ratios indicate that there is a one-for-one relationship between striations and cycles of applied load. The crack growth rate equations (3 and 5) taken from Ref 1 were obtained from the least squares fit to a variety of specimen configurations, loading conditions and stress ratios. The mean striation size and the crack growth rates calculated by using these equations, were found to differ by amounts which are well within typical values of scatter for macroscopic data. Although it appeared that individual striation values tended to possess more scatter (relative to the mean) than was obtained from macroscopic data, it will be shown in Subsection 3.2 of this report that, generally, the scatter in microscopic data was approximately the same as the scatter in macroscopic data.

There were two basic limitations associated with using striation data to obtain crack growth rates. The first occurred when the striation spacing was too small to be resolved (i.e., $< 10^{-6}$ in.). In this case, crack growth rates

could only be obtained macroscopically by averaging crack growth increments over large numbers of cycles. The second situation occurred when the stress conditions caused topography other than ductile striae. Dimple rupture, cleavage, brittle striae and extensive plasticity produced specimen topography which either defied quantification or, in the case of brittle striations, yielded misleading values of striation spacing. When the proper crack growth conditions did exist, crack growth rates could be determined from striation spacing data.

## 3.2 SURFACE AND FRACTURE FACE CORRELATION

These measurements were performed to determine whether or not there are any differences between microscopic striation spacing taken from the fracture face and from macroscopic crack growth data obtained during fatigue testing from the specimen surfaces. Fracture face measurements were generally obtained along the centerline of the specimens. In some cases, data were also taken from the fracture face along a line parallel to the centerline data, but at a distance approximately 0.05 in. from the edge of the specimen surface. Table 2 summarizes the specimens examined along with other pertinent data.

### 3.2.1 2219-T851 Aluminum

Figure 12 presents striation spacing, $d_s$, and average crack growth rate, $\Delta a/\Delta N$, plotted against crack length for a 2219-T851 aluminum center-cracked panel which was subjected to constant amplitude loading with a stress ratio of 0.05. The round solid symbols are striation spacing values while the solid square symbols are values of $\Delta a/\Delta N$ obtained optically on the specimen surface during the Ref 1 test program. The values of $\Delta a/\Delta N$ are plotted at the average crack length for the crack extension increment, $\Delta a$.

Scatter bands for each type of data are also presented. It can be seen that the scatter bands for both types of data agree closely. Further, the mean behavior of both data sets compare favorably. The conclusion drawn is that there is a direct correspondence between microscopic striation spacing and macroscopic crack growth rates.

Figures 13 through 15 present similar data for aluminum specimens subjected to single discrete overload cycles. Microscopic and macroscopic data

are plotted both before and after the overload application. There are very few macroscopic data points in these figures because of the limited crack extension (.05 to .07 in.) under consideration. In Fig. 13, the $\Delta a/\Delta N$ data average 10 micro-in. per cycle, while the striation spacing averages approximately 12 micro-in. This difference of 20% is well within typical values of scatter for crack growth rates.

It is interesting to note that the 1.25 overload ratio produced essentially no retardation (subsequent reduction in striation size). There is, however, a significant increase in striation spacing immediately before and after the overload. This phenomenon will be discussed further in Subsection 3.3.2 of this report.

Figure 14 shows that striation spacing data obtained both along the centerline of the fracture face (solid circles) and along the edge (open circles) agree both quantitatively and qualitatively (see also Appendix Fig. A-1). Both indicate that immediately after the overload cycle, $d_s$ decreases rapidly to a minimum value of around 6 micro-in. The macroscopic $\Delta a/\Delta N$ data agree qualitatively with the $d_s$ data, but the limited number of $\Delta a/\Delta N$ data points make a quantitative evaluation difficult. The single $\Delta a/\Delta N$ data point at a = 1.285 in. is of the same magnitude as the $d_s$ data and is located to provide a reasonable approximation to the $d_s$ behavior. The remaining $\Delta a/\Delta N$ points are too widely separated to provide more than a gross description of the crack growth behavior.

It can be seen in Fig. 15 that the centerline and edge $d_s$ data again agree closely. In this case, however, the differences between the macroscopic and microscopic data are more pronounced. For a crack length greater than 0.51 in. the $\Delta a/\Delta N$ data average 12 micro-in. per cycle while the $d_s$ average is between 8 and 9 micro-in. In the area immediately after the overload, both types of data are approximately equal in magnitude.

Considering all of the data of Fig. 12 through 15, it can be concluded that the macroscopic $\Delta a/\Delta N$ and microscopic $d_s$ data agree closely. In most cases, the quantitative values are well within reasonable scatter bounds.

### 3.2.2 Ti 6Al-4V Titanium

Striation spacing and $\Delta a/\Delta N$ data are plotted against crack length in Fig.

16 for a titanium specimen which was subjected to constant amplitude loading with a stress ratio of 0.05. It can be seen that, like the aluminum data of Fig. 12, these data compare favorably. The microscopic data possess a somewhat larger scatter band than the macroscopic data. In this case, the width of the microscopic scatter band on the right side of the figure is controlled by the two $d_s$ values at crack lengths of 1.320 and 1.420 in. If these two values were neglected, both scatter bands would be nearly the same. The $\Delta a/\Delta N$ data tend to be slightly lower than the $d_s$ data.

Figures 17 through 19 present similar data for titanium specimens which were subjected to single discrete overloads. In Fig. 17, where the overload ratio was 1.25, the macroscopic data are more scattered than the microscopic data. The microscopic data indicate that the overload cycle had little effect on subsequent striation spacing. Reference 1 concluded that overloads, where O/L = 1.25, had negligible effect on subsequent crack growth. Again, the data taken along the edge of the fracture face (open circles) agree closely with those gathered along the centerline (solid circles).

It can be seen that the edge and centerline data also agree closely in Fig. 18. There the overload ratio was 1.5 and the overload caused a significant reduction in the striation size immediately after the overload application. Again, the macroscopic data possess considerably more scatter than the microscopic data.

Figure 19 shows the data resulting from two overload applications. The overloads (O/L = 1.8) were separated by 0.053 in. Centerline and edge data agree closely through the first overload. (Edge data were not gathered through the second overload.) Although the macroscopic data exhibit considerable scatter, they do yield a qualitative description of the crack growth behavior.

Figures 16 through 19 show that the microscopic and macroscopic data agree fairly well. The $\Delta a/\Delta N$ data tend to possess more scatter than the $d_s$ data except for the constant amplitude loading case (Fig. 16). The correlation between $d_s$ data taken along the centerline and edges of the fracture faces agree very closely. The microscopic data provide a much finer description of the crack growth behavior subsequent to an overload than do the macroscopic data.

### 3.2.3 Summary

Microscopic striation spacing data, gathered both along the centerline and edges of the fracture faces, compare favorably with macroscopic data taken from the specimen surfaces for both materials. The macroscopic data for single overload events tend to possess more scatter than the striation data. This is a result of the inability to accurately measure crack growth on the specimen surfaces to a sufficiently small scale. Another reason may have been related to the differences in the internal and external crack growth behavior during, and immediately after the overload application. Figures 63 through 66 provide a visual illustration of this effect which will be discussed in Subsection 3.3.2 of this report.

## 3.3 SINGLE OVERLOADS

It was found during the Ref 1 program that crack growth retardation due to overloads was the single most important phenomenon associated with spectrum loading. This section deals with the overload affected crack length, delayed retardation, and crack front curvature and plasticity effects caused by the application of single, discrete overload cycles.

### 3.3.1 Affected Crack Length

An item of significant interest in modeling crack growth interaction effects is the crack length or distance in front of the crack tip which is effected by an overload application. This distance, generally referred to as the plastic zone size, defines a crack growth increment over which the crack growth rate is retarded (the observed crack growth rate is lower than the rate which would have existed if the overload had not been applied). Mathematical crack growth prediction models which are currently available specify the plastic zone radius as the affected length. The crack closure model (Ref 1) uses the plane stress plastic zone radius, while the Willenborg, et. al. (Ref 2) and Wheeler (Ref 3) models use either the plane stress or plane strain plastic zone radii as appropriate to the actual stress conditions.

The objective of the measurements discussed below was to determine, as accurately as possible, the crack length which is affected by the application of a single overload cycle. The technique employed was to measure striation spac-

ing before and after an overload application. These data were plotted against crack length. The calculated constant amplitude crack growth (CCA) rate, obtained from either Eq 3 or from Eq 5, were also plotted on the same figure. The crack length at which the striation spacing returned to steady-state conditions, using the CCA curve as a reference, was then determined. The affected crack length was taken as the difference between the crack length at the return to steady-state crack growth conditions and the crack length at which the overload was applied. No allowance was made for growth during the overload, except that the maximum stress intensity of the overload was limited to 90% of the stable tear threshold, $K_{st}$. It was determined in Ref 1 that $K_{st}$ was 30 ksi $\sqrt{in.}$ for aluminum and 72.5 ksi $\sqrt{in.}$ for titanium (Table 3). Table 4 summarizes the specimens examined, along with other pertinent data.

3.3.1.1 2219-T851 Aluminum - The experimental results for the aluminum data are presented in Fig. 20 through 25. Figure 20 presents the results taken along the centerline of a specimen subjected to an overload with O/L = 1.25. It can be seen that the overload cycle caused very little effect on the striation spacing except that the scatter near the overload increased. This figure shows the CCA curve and a least squares fit to all of the data. The least squares analysis assumed that the slopes of the CCA and least squares curves were equal. Technically, the CCA curve is not a straight line but was assumed to be so over this short amount of crack extension. The least squares analysis showed that the mean striation spacing was about 30% greater than the calculated crack growth rates. This value is well within typical crack growth scatter limits.

Figures 21 and 22 (also see Fig. A-1) for centerline and edge locations respectively, show similar data for a specimen subjected to a single overload cycle with O/L = 1.5. In addition to the striation spacing, $d_s$, the CCA curve, the plane stress plastic zone radius, $\rho$, and the plane strain plastic zone diameter, $\delta$, are shown. The two parameters $\rho$ and $\delta$ are defined by

$$\rho = \frac{1}{2\pi}\left(\frac{K_{OL}}{\sigma_y}\right)^2 \qquad (6)$$

$$\delta = \frac{1}{2\sqrt{2}\pi}\left(\frac{K_{OL}}{\sigma_y}\right)^2 \qquad (7)$$

where $K_{OL}$ is the maximum stress intensity caused by the overload and $\sigma_y$ is the material tensile yield stress. Reference 1 reported $\sigma_y$ as 54.7 ksi for aluminum and 130 ksi for titanium. The crack closure model (Ref 1) uses Eq 6 while the other models (Ref 2 and 3) would use $\delta/2$ for the two materials examined, as plane strain conditions prevailed. Both figures show that $\rho$ is larger than the affected length. Values of $\delta/2$ and $\delta$ provide a good fit to the data in Fig. 21 and 22 respectively. The CCA curve agrees closely with the data for $a < a_{OL}$ and $a > a_{OL} + \delta$.

Figure 23 (also see Fig. A-2)shows the data and other parameters for a specimen subjected to O/L = 1.8. The data are contrary to all others taken, in that a 1.8 overload ratio always produced a significant reduction in $d_s$ subsequent to the overload. In the figure the overload has negligible effect on striation spacing and the affected crack length cannot be determined.

Figure 24 (also see Fig. A-2) presents data for the same specimen but at a larger crack length. In this case, the overload did produce a significant reduction in striation spacing. Based on the trend of the data subsequent to $a_{OL}$, $\delta$ accurately describes the affected crack length for this event.

In Figure 25 (also see Fig. A-3), where O/L = 1.8, the affected crack length appears to be greater than $\delta$ and perhaps even greater than $\rho$.

Of the six data sets presented, two suggest that $\delta$ is the appropriate value and one each indicate that something less than or greater than $\delta$ yield a good definition of the affected crack length. There is only one case (Fig. 21) which indicates that the plane stress plastic zone radius best describes the affected length. The remaining two data sets do not provide an indication of the affected crack length.

3.3.1.2 Ti 6Al-4V Titanium - The titanium affected crack length results are presented in Fig. 26 through 32 in the same form as the aluminum results.

Figures 26 and 27 present the results where the overload ratio was 1.25. Like the aluminum, this value of O/L (1.25) had negligible effect on the striation spacing. Therefore, no conclusion on affected length could be reached.

Figures 28 and 29 (also see Fig. A-4 and A-5) present the centerline and edge results for a case where O/L = 1.5. In both cases, the plane strain plastic zone diameter best describes the affected crack length. The CCA curve yields a reasonable fit to the $d_s$ data before the overload and again at $a > a_{OL} + \delta$. Interestingly, the centerline data show immediate retardation (the minimum $d_s$ occurred immediately after the overload) while the edge data reflect delayed retardation (the minimum striation spacing occurred some distances after the overload). This phenomenon will be discussed in Subsection 3.3.3.

Figures 30 through 32 (also see Fig. A-6) show similar data where the overload ratio was 1.8. In Fig. 30 and 31 the data were obtained along the centerline of the specimen and in Fig. 31 the results from two overloads separated by 0.053 in. are shown. Figure 32 shows edge data. In all four of these cases, the plane strain plastic zone diameter provides the best description of the affected crack length.

For the eight events presented here, six indicate that $\delta$ gives the best definition of the affected length. The two remaining cases were for O/L = 1.25 and did not reveal any pertinent information.

3.3.1.3 Summary - It was concluded that the plane strain plastic zone diameter best describes the affected crack length for the specimens investigated. A total combination of fourteen specimens, locations or events were observed. Of these, eight indicated a definite tendency to correlate with $\delta$. One suggests a value $< \delta$ and another $> \delta$. The remaining four yielded no information. Therefore, eight of the ten useful cases indicate that $\delta$ is the appropriate parameter to define the affected crack length.

This conclusion is substantiated by the fact that in all cases plane strain crack growth conditions existed as evidenced by an almost total lack of shear lips on the fracture faces. In addition, it seems appropriate that the affected crack length should extend to the edge of the elastic-plastic interface. While a variety of models have been suggested to describe the shape of

the plastic zone for different materials, it is generally accepted that the Irwin plastic zone radius expression (Ref 4) describes the half length of the plastic area for small scale yielding in most materials. The total extent of plasticity would therefore be the plastic zone diameter.

It should also be pointed out that $\delta$ is about 71% of $\rho$. In cases of single, discrete overload applications, this difference may be significant. However, during typical aircraft spectrum crack growth, it is questionable as to whether the overall crack growth life is very sensitive to the affected length expression. This is due to the frequency of occurrence of load changes and the quasi-constant process of updating the location of the elastic-plastic interface.

### 3.3.2 Delayed Retardation

Delayed retardation occurs when the minimum crack growth rate (or striation spacing) subsequent to an overload application does not occur immediately after the overload. Several investigators (Ref 5 through 8) have reported this phenomenon. Many others (i.e., Ref 1) have not.

The objective of the measurements reported below was to determine whether or not delayed retardation existed for the materials investigated. The specimens examined (Table 5) were selected randomly from those available, except that the striation spacing and stable tear constraints described in Subsection 3.1 were observed. A qualitative evaluation of the data revealed that delayed retardation did not occur for most of the specimens examined. A subsequent, quantitative analysis of the data, assuming that delayed retardation did not occur, was performed. The results of this analysis were found to agree conceptually with the results of Ref 1.

3.3.2.1 Qualitative Analysis - The striation spacing was normalized by dividing it by the calculated CCA growth rate. This normalization procedure was employed as the events investigated were comprised of a variety of crack lengths, baseline and overloads and overload ratios. By normalizing the results, the data analysis was reduced to a consistent and manageable task. The CCA values neglected the overloads. The resultant values of this ratio (de-

fined as $f_n$) were plotted against crack length along with the extent of the plane strain plastic zone diameter, $\delta$, and plane stress plastic zone radius, $\rho$. A typical plot is shown in Fig. 33 (also see Fig. A-1). This plot is representative of most of the data gathered. There was a fair amount of scatter prior to the overload, but subsequent to the overload, the scatter was measurably reduced. The data tend to group around a value of $f_n = 1$ both before and well after the overload. The data are also typical in that it is difficult to determine whether or not delayed retardation occurred. Immediately after the overload, values of $f_n$ range from 0.43 to 0.88. It is generally accepted that when delayed retardation occurs, the minimum crack growth rate (striation spacing) occurs when the crack propagates 1/8 to 1/4 of the way through the affected length. If the first five data points immediately after the overload are temporarily discarded, the remaining data extend forward from 1.2845 in. The gap between the overload crack length (1.282 in.) and the remaining data is 0.0025 in., or about 15% of $\delta$ and 10% of $\rho$. It is possible to have missed or to have been unable to resolve the decay in $f_n$ over the first 10% to 15% of the affected length. If $f_n$ had decayed from around unity to a value of approximately 0.5, then it could be concluded that delayed retardation occurred. Based on the data of Fig. 33, it would be very difficult to reach such a conclusion.

The first phase of the analysis consisted of examining the data as described above. All of the normalized data are presented in Fig. 34 through 55. Twenty-two events on ten different specimens were examined, the results of which are presented in Table 6.

Seven events did not show any significant transient behavior subsequent to the overload application (notes 1 and 2 in Table 6). All four of the O/L = 1.25 cases in addition to one O/L = 1.8 case were in this category. Based on the results obtained in Ref 1, for cases where the overload ratio was 1.25, it was not expected that a single overload cycle would have a significant impact on subsequent crack growth behavior. This is confirmed by the microscopic data. For the case where the overload ratio was 1.8 (Fig. 41), the striation spacing prior to the overload was 5 $\mu$-in. (Fig. 23). It is probable that the striation spacing subsequent to the overload was on the order of 1 $\mu$-in., a value too small to be resolved with the techniques used in this program. In each of these five cases, there was no systematic reduction of $f_n$ within any

of the crack growth increments which might define the affected crack length (i.e., $\delta$ or $\rho$). The remaining two data sets (Fig. 45 and 46) (also see Fig. A-2 and A-3) were gathered subsequent to overloads where large scale yielding had occurred. Further, in these figures, the overloads had been applied so close together that the affected crack length (based on plane stress conditions) from a previous overload apparently overlapped the overload crack length of interest. As a result, the values of $f_n$ are nominally constant at a value of approximately 0.2. These last results are consistent with all of the previously mentioned crack growth retardation models. Those models predict that in situations where overloads are applied before a crack can grow out of the affected length caused by a previously applied overload, the crack growth rates are constantly depressed below their unretarded values.

The data from six events were classified as showing no delayed retardation. This result is based on the fact that the striation spacing increased from some minimum value immediately after the overload, in a more-or-less orderly manner, until $f_n$ approached unity.

Four events indicated that delayed retardation occurred. In these cases (Fig. 38, 39, 43 and 50 (also see Fig. A-3 through A-5)), there appears to be a definite tendency for the striation spacing after the overload to decrease from a value of $f_n$ which was nominally the same as the values of $f_n$ prior to the overload, to a measurably lower value as the crack length increased. In addition to these four events, five other events are listed in Table 6 as possibly portraying delayed retardation. The crack lengths at which the minimum spacings were estimated to have occurred, $a_{min}$, are tabulated in Table 7 for all nine events where delayed retardation may have occurred. Other pertinent data are also included.

It can be seen from Table 7 that the minimum value of $f_n$ ranges from 0.3 to 0.7 and that the ratio of $\Delta a_{dr}$ to $\delta$ ranges from 0.092 to 0.455. (The parameter $\Delta a_{dr}$ defines the crack length increment over which the striation spacing decreased with increasing carck length.) There is no systematic variation of either the minimum $f_n$ or $\Delta a_{dr}/\delta$ with material, overload ratio, or overload stress intensity. This conclusion is verified in Fig. 56. Although it appears in Fig. 56d that there is a systematic variation of minimum $f_n$ with overload stress intensity, Fig. 56b indicates that the minimum $f_n$ is independent of

overload ratio. These two figures conflict and the data in Fig. 56d is considered to be coincidental and is explained as follows. Consider a series of single overload tests where the overload stress intensity is held constant and the baseline stress (stress intensity) is varied. The overload ratio becomes a function of the baseline stress. Intuitively, the minimum value of $f_n$ would be expected to decrease with decreasing baseline stress. The crack growth rate equations of Ref 1 which are based on crack closure concepts provide a verification:

$$\left(\frac{da}{dN}\right)_{ret} = C\left[\frac{K-K^1_{c_{OL}}}{1-C_f}\right]^n \tag{8}$$

$$\left(\frac{da}{dN}\right)_{C.A.} = C\left[\frac{K-K_c}{1-C_f}\right]^n \tag{9}$$

Equations 8 and 9 define the retarded and constant amplitude crack growth rates respectively, where

$K$ = maximum baseline stress intensity

$K_c$ = baseline stress intensity at crack closure

$K^1_{c_{OL}}$ = stress intensity at crack closure caused by the single overload cycle

$C_f$ = closure factor (ratio of closure stress to maximum applied stress)

The ratio of Eq 8 and 9 is the parameter $f_n$. For convenience, the minimum stress intensity is taken as zero so that:

$$f_n = \left[\frac{K-K^1_{c_{OL}}}{K-K_c}\right]^n \tag{10}$$

For one overload cycle, $K^1_{c_{OL}}$ was given in Ref 1 as $\gamma_1 K_{c_{OL}}$, or, for R = 0, $K^1_{c_{OL}} = \gamma_1 \cdot C_{f_o} \cdot O/L \cdot K$ where $O/L = K_{OL}/K$ and $C_{f_o}$ is the closure factor at R = 0. Similarly, $K_c = K\, C_{f_o}$ so that Eq 10 can be rewritten as:

$$f_n = \left[\frac{1 - \gamma_1\, O/L\, C_{f_o}}{1 - C_{f_o}}\right]^n \tag{10a}$$

It was shown in Ref 1 that $\gamma_1$ and $C_{f_o}$ are material constants so that f is some function of the overload ratio only and is independent of the baseline or overload stress intensity.

It was concluded that, qualitatively, the data do not reveal whether or not delayed retardation is a real phenomenon. As a result, a quantitative analysis was performed.

3.3.2.2 Quantitative Analysis - The first qualitative approach did not reveal whether or not delayed retardation occurred as the evidence was inconclusive. The second approach consisted of assuming that delayed retardation did not exist. The fifteen cases (Table 6) which provided sufficient data were analyzed.

The general crack closure equation of Ref (1)

$$S_c = S_{c_1} - (S_{c_1} - S_{c_b}) \left(\frac{\Delta a}{\delta}\right)^B \tag{11}$$

was assumed to apply, where

$S_c$ = general closure stress (or load)

$S_{c_1}$ = closure stress (or load) after one overload

$S_c$ = closure stress (or load) for baseline stress

$\Delta a$ = crack growth increment since the overload

$\delta$ = plane strain plastic zone diameter (used in place of the plane stress plastic zone radius, $\rho$)

B = empirical exponent.

The crack growth rate based on an effective stress range for $0 < \Delta a < \delta$ is given by

$$\frac{da}{dN} = C \left[ \frac{S - S_c}{1 - C_{f_o}} f(a) \right]^n \tag{12}$$

where S is the baseline maximum stress, $S_c$ is given by Eq 11 and f(a), which is a function of specimen geometry, relates stress to stress intensity. If it is assumed that $S_{c_1}$ is some constant, $\gamma_1$, times the stabilized closure level for the overload, $S_{c_{OL}}$, Eq 12 becomes

$$\frac{da}{dN} = C\left\{\frac{S - \left[\gamma_1 S_{c_{OL}} - \left(\gamma_1 S_{c_{OL}} - S_{c_b}\right)\left(\frac{\Delta a}{\delta}\right)^B\right]}{1 - C_{f_o}} f(a)\right\}^n \tag{12a}$$

The constant amplitude crack growth rate for the baseline load is given by

$$\left(\frac{da}{dN}\right)_{CA} = C\left[\frac{S - S_{c_b}}{1 - C_{f_o}} f(a)\right]^n \tag{13}$$

The ratio of Eq 12a to Eq 13 is $f_n$ so that

$$f_n = \left\{\frac{S - \left[\gamma_1 S_{c_{OL}} - \left(\gamma_1 S_{c_{OL}} - S_{c_b}\right)\left(\frac{\Delta a}{\delta}\right)^B\right]}{S_b - S_{c_b}}\right\}^n \tag{14}$$

The unknowns were assumed to be $\gamma_1$ and B while the exponent n was 3.34 and 3.08 for aluminum and titanium respectively (from Eq 3 and 5).

A least squares procedure was used to determine the best fit values of $\gamma_1$ and B for each of the data sets in the previously described figures. The results of this analysis are shown in Table 8. These results are based on all of the striation data points between $a_{OL}$ and $a_{OL} + \delta$ except as noted in Table 8. In three cases (notes 1 through 3 of Table 8), some of the data immediately after the overload were excluded because the least squares search routine could not find a satisfactory solution. It should be noted that the crack growth increments over which the data were excluded comprised less than about 10% of the plane strain plastic zone diameter in all three cases.

The values of $\gamma_1$ are plotted against overload ratio in Fig. 57. The data indicate that the effectiveness of a single overload cycle is a function of both material and overload ratio. The values obtained here for $\gamma_1$ averaged 0.83 and 0.75 for O/L = 1.5 and 1.8 for aluminum, and 0.93 and 0.81 for O/L = 1.5 and 1.8 for titanium.

It can be seen from Eq 14 that for $\Delta a$ equal to zero, the value selected for $\gamma_1$ has a significant influence on initial crack growth rate (or $f_n$) immediately after the overload. For example, if the overload ratio for an aluminum specimen were 1.5 and $\gamma_1$ were 0.667 (Ref 1) the value of $f_n$ at $\Delta a = 0$ is unity and the overload would have no effect on subsequent growth. However, if $\gamma_1$ were taken as 0.83 (for O/L = 1.5) then $f_n$ would be 0.52. The initial crack growth rate for the second case would be about half of that for the first case. A large variation in the initial value of $f_n$ also affects the number of cycles required to propagate the crack through the overload affected crack length. Therefore, an increase in $\gamma_1$ causes an increase in that number of cycles. Because the crack closure model predictions of Ref 1 were generally good, the new values of $\gamma_1$ would tend to degrade those predictions unless some compensating factors are also introduced.

One modification, already proposed, was to use the overload plane strain plastic zone diameter, rather than the plane stress radius, to define the overload affected crack length. This effect is shown schematically in Fig. 58. If the areas between each of the two curves and $f_n$ = unity are equal, the number of cycles required to transverse the affected length will be equal. The results obtained thus far are, therefore, consistent: a reduced affected length combined with increased values of $\gamma_1$.

An examination of Eq 14 shows that for $\gamma_1$ equal to unity and $\Delta a$ equal to zero, $f_n$ would also be unity when $S_{cOL}$ is equal to $S_{cb}$. This case represents constant amplitude loading (i.e. O/L = 1.0). By definition, then, any expression defining $f_n$ as a function of O/L must pass through the point O/L = 1, $f_n$ = 1 on Fig. 57. It can be seen that the straight lines (shown dashed in Fig. 57):

$$\gamma_1 = 1.312 - 0.312\ (O/L) \text{ for aluminum} \qquad (15a)$$

$$\gamma_1 = 1.213 - 0.213\ (O/L) \text{ for titanium} \qquad (15b)$$

provide good fits to the data over the range of interest. Although there are some indications to the contrary (i.e. Ref 16), it is reasonable to assume that the effective closure level does not decrease from the existing value as a result of an overload. If it did, an overload would cause acceleration rather than retardation. Based on this assumption, there is a lower bound to the values of $\gamma_1$ as a function of overload. For the case where R = 0, the stabilized closure load for the overload is simply O/L · $P_{cb}$, where $P_{cb}$ is the stabilized closure load for the baseline loading. The closure load after one cycle must be greater than, or equal to, the existing closure load so that:

$$\gamma_1 \cdot O/L \cdot P_{c_b} \geq P_{c_b} \tag{16}$$

and

$$\gamma_1 \geq \frac{1}{O/L} \tag{17}$$

Equation 17 is plotted as the solid line in Fig. 57. Equations 15a and 17 are equal for O/L = 3.21. This implies that for aluminum with O/L values greater than or equal to 3.21, a single overload cycle would have no effect on subsequent crack growth. A similar result was obtained for titanium where O/L = 4.70. Experience indicates that this is probably not the case, so it must be concluded that although Eq 15a, b provide good fits to the available data, they must be in error for larger overload ratio values.

Another parameter which affects the total number of cycles is the exponent B in Eq 14. Figure 59 shows how the area under the curves depends on B. The number of cycles required to propagate the crack through the affected length increases as the value of B increases. The values of B obtained from the least squares procedure (Table 8) possess considerable scatter and have a very large range (i.e., 0.26 to 20.7). Further, Fig. 60 shows that there is no consistent behavior of B with respect to either overload ratio or material.

Large values of B yield an $f_n$ curve which is almost flat through the affected length, a behavior which would provide a good fit to the data of, for instance, Fig. 43. The bulk of the data do not behave in the same manner as those of Fig. 43 so that both the data and the value B of 20.7 are atypical. The other large value of B was obtained for the data of Fig. 39. Referring to

that figure, it can be seen that the data do not return to a value of $f_n$ = unity after the overload. These data are also not typical of the bulk of the data. If the values of B associated with Fig. 39 and 43 are discarded, the remaining values average 0.97 which compares favorably with the value of 1.0 developed in Ref 1.

Equation 14 is plotted along with the usable data in Fig. 61. The exponent B was taken as unity while Eq 15a, b were used to define $\gamma_1$. It can be seen that in most cases, Eq 14 yields a reasonable fit to the data. It can be concluded that these parameters should be incorporated in the crack closure model of Ref 1. However, such an action is considered premature without an extensive re-analysis of the data of Ref 1 wherein the model predictions are compared with the data.

3.3.2.3 Summary - The data obtained from 22 specimens and/or events along both the centerline and edges of specimen fracture faces neither confirmed nor denied the existence of delayed retardation. A quantitative analysis of the usable data, regardless of delayed retardation indications, was performed assuming that delayed retardation did not occur. This analysis revealed that the ability of a single overload cycle to increase the crack closure level decreased with increasing overload ratio for both of the materials examined. These results agree with the results obtained in Ref 1. The crack closure exponent, B, was found to be nearly unity as reported in Ref 1.

### 3.3.3 Crack Front Curvature and Plasticity Effects

Delayed retardation has been observed by some investigators (Ref 5 and 7) on the surface of a specimen. Other investigators (Ref 6 and 8) have observed this behavior fractographically. The initial objective of these measurements was to develop a theory based on changes in crack front curvature to explain the delayed retardation phenomenon. However, attempts to measure crack front curvature before and after an overload for cases of small scale yielding were unsuccessful for the following reasons. At low power, the gross curvature at an overload could be measured, but the width of the overload crack front could not. At high magnifications the opposite was true; width could be measured, but the overall curvature could not be observed because of the

limited field of view. Further, the widths and the crack fronts were discontinuous and quite irregular at high power. Near the specimen edges (an area of importance) the event was almost always obliterated by rubbing of the fracture surfaces (fretting) caused by subsequent fatigue loading.

A review of the data presented in previous sections of this report revealed that the striation spacing immediately before an overload application increased significantly. Figure 20 clearly shows this increase and it can be observed to a lesser degree in Fig. 21-23, 25, 30-32. This phenomenon may be explained as follows: An overload causes additional plasticity near the crack tip. This plasticity tends to stretch existing striations near the tip resulting in exaggerated spacing. Based on these observations, another overload event, where it was known that extensive plasticity occurred, was examined. These results are presented in Fig. 62. There it can be seen that at about 0.005 in. before the overload the striation spacing began to increase. The area immediately before the overload (approximately 0.002 in.) had undergone such extensive plasticity that quantitative values for the striation spacing could not be obtained.

It was concluded that if the additional plasticity near the crack tip affected the apparent striation spacing prior to the overload, then it was more likely that this effect would exist in the highly plastic area subsequent to the overload. Therefore, several events where O/L = 1.8 and where significant plasticity occurred were examined. Figures 63a and 63b show overall views of several such events. Figure 63a shows that as a result of an overload application, there is a shear type of failure near the specimen surface. Figure 63b shows that considerable internal growth occurred during each overload. It also shows that the growth during the overload is much less on, or near, the surface, than the internal growth. It is also obvious in Fig. 63a that several changes in the contour of the fracture face occurred subsequent to, and not during, the overload application. Figure 63c shows the contours schematically.

The line ABC in Fig. 63c represents the crack front prior to the overload and is typical of all specimens or events examined regardless of material. One overload cycle caused a new crack front AB'C defining the internal growth.

The area ABCB'A consisted of dimples indicating that the material ruptured until the crack front arrived at the new stable configuration. Significantly, no appreciable growth occurred on the surface although the surface material was plastically deformed. As the specimen was subsequently cycled at the lower load the crack re-initiated on the surface (points A and C). Once the crack began to propagate again, it did so at a high rate and it also grew along a new plane (ADB' or CD'B') following the general direction of the surface deformations which were oriented at about $45^{o}$ to the gross crack growth plane. This area appeared to consist of a slip type of crack extension. The crack propagation through this region was very rapid and occurred in comparatively few cycles.

Finally, the crack, having reached points D and D' continued to propagate until the crack front returned to the overall plane of the fracture face (A' B" C'). The area (DB'B"A') consisted of a fretted fatigue topography indicating that crack extension occurred as a result of fatigue cycling. During the period of measureable growth on the surface (ADA'), the movement of the crack front from B' to B'' was much less than on the surface. Once the crack front reached A'B"C' it began to propagate in a uniform manner, except that the rate of propagation was low. Interestingly, the geometry of the new front, A'B"C', was quite similar to the original front, ABC, just prior to the overload.

Figure 64 shows an extreme case of plasticity and internal growth, where both the mascroscopic crack length versus cycles curve and a perspective view of the fracture face are compared. It can be seen that optical measurements of crack extension were obtained while the crack front was in what may be called a transient condition. It is also apparent that, starting with the 4th and 5th data points, the crack growth rate was extremely high as reflected by the slope of the crack length versus cycles curve. At about 942,000 cycles, the slope of the a versus N curve decreased and was nominally constant for about 1000 cycles. It then began to increase monotonically with increasing cycles and crack length. There are two significant aspects of these results: a) crack propagation was apparently arrested on the surface for at least 300 cycles and b) several macroscopic crack extension measurements were obtained

when the crack front was in the shear and fretted fatigue areas.

Figure 65 presents similar results for a shorter overload crack length. The photograph shows the specimen edge profile. There was an arrest of at least 100 cycles on the specimen surface. Immediately afterward, the crack length increased rapidly to a value of approximately 1.46 in. reflecting a very high crack propagation rate.

The striation spacing data of Fig. 62 were used to compare microscopic and macroscopic data directly. Each striation spacing value subsequent to the overload dimpled area was assumed to represent the average crack growth rate over a small crack growth increment. The increment was taken as half the distance between the data point before and the data point after the point of interest. This crack growth increment was divided by the striation spacing value to obtain the incremental number of loading cycles required to transverse the crack growth increment. Then, the crack growth and cyclic increments were numerically integrated to obtain crack length versus cycles. These results are shown in Fig. 66 as "x" symbols. The data are displaced a distance of 0.0098 in. from the crack length where the overload was applied to account for the internal growth caused by the overload. The macroscopic surface measurements are shown by the dots. It can be seen that after about 800 cycles, both types of data agree closely. For the first 800 cycles, the data behave very differently. The microscopic data increase in a monotonic manner immediately after the overload. The macroscopic data behave in a very erratic manner, exhibiting, first crack arrest and then very high growth rates before quasi-stable growth conditions were established. The $\Delta a/\Delta N$ values were calculated for the macroscopic data of Fig. 66 and are compared in Fig. 67 with the microscopic data of Fig. 62. Although there is considerable scatter, the macroscopic data immediately after the overload are significantly higher than the striation spacing data. However, after the crack tip had advanced approximately 0.02 in., the two types of data tend to agree closely. The overload stress intensity for this event was 35.8 Ksi $\sqrt{\text{in.}}$ which produced a plane stress plastic zone radius of 0.068 in. The minimum macroscopic crack growth rate appears to have occurred after the crack propagated about 30% of the way through the plastic zone. This result is consistent with other investigators

(i.e., Ref 5, 6 and 8), who reported values ranging from 10 to 25 percent.

It can be concluded for cases involving large amounts of plasticity and measurable internal crack growth that the macroscopically observed data exhibit, first crack arrest, and then comparatively large crack growth rates immediately after an overload. These rates, combined with subsequent crack growth behavior might erroneously be interpreted as delayed retardation. It was shown that while it appeared that delayed retardation occurred on the surface, no such phenomenon was observed microscopically along the centerline of the specimen fracture face. The discussion comparing surface behavior with the behavior along the fracture face centerline can also be applied to measurements taken from the fracture face at some point between the centerline and the edge of the specimen. This would explain why delayed retardation has been observed on a microscopic level (i.e., Ref 6 and 8). As stated previously, if the plasticity caused by an overload can distort striations developed prior to the overload, it must have a significant effect on subsequent striation spacing.

The authors propose that the phenomena discussed above also apply for cases of small scale yielding and where small amounts of internal stable tear are caused by overloads. Some plasticity occurs during every overload application (and even during every cycle of the base load). Therefore, the degree of plasticity caused by an overload must control the duration of the arrest period and the amount of shear deformation on the specimen surfaces. This must also be true, to a lesser extent, in the interior of the specimen. Unless the amount of plasticity is sufficiently large, crack arrest may not occur so that initial high crack growth rates are observed. These high rates decay to a minimum value as the crack propagates and then increase until constant amplitude crack growth rates are resumed. This sequence produces what appears to be delayed retardation, but which is, in fact, a false effect caused by plasticity.

### 3.4 CRACK GROWTH ACCELERATION

A typical example of crack growth acceleration occurs when a cracked element or specimen is subjected to a low-high loading sequence. Immediately after the load change, the crack growth rate increases to a value which is

higher than the stabilized value which would have existed if the high load had not been preceded by the low load. This higher than normal crack growth rate is referred to as acceleration. Striation spacing measurements were obtained during this program from specimens which had been subjected to low-high loading sequences. The objective of these measurements was to convert the striation spacing values during the overloads to comparable crack closure levels. These results would then be used to obtain closure behavior as a function of the number of overload cycles. Four specimens were examined as outlined in Table 9. Some results were consistent in that the first cycle of the overload produced a stretch zone which was several times larger than the expected constant amplitude striation spacing for the overload. The striation spacing during the overload then rapidly decayed, in about five cycles, to a striation spacing which was approximately double the expected constant amplitude spacing. This spacing continued for approximately 50 cycles and then subsequently decayed to the expected striation spacing for the overloads. The expected striation spacing was the calculated constant amplitude crack growth rate for the overloads, neglecting the previous low loading.

### 3.4.1 2219-T851 Aluminum

Figure 68 (also see Fig. A-8) shows the striation spacing plotted against the number of overload cycles for an aluminum specimen subjected to successive multiple overloads which were 50% greater than the previous loads. The figure shows that the striation width caused by the first high load cycle is from five to nine times the expected constant amplitude crack growth rate. It was shown by von Euw, et. al., in Ref 8 that a similar result was obtained for 2024-T3 aluminum. There, the authors used crack closure arguments to provide better correlation of the calculated first overload striation width and the measured stretch zone widths. Although the closure concept did improve their correlation, an examination of their data at low values of $\Delta K_{eff}$ showed that the stretch zones were still approximately three times the calculated values.

The crack closure model of Ref 1 predicts a first overload cycle striation width of 21 μ-in. in Fig. 68. This value is twice the constant amplitude

value, but is still only 20% to 40% of the measured striation values. It was stated in Ref 8 that the striation widths decreased gradually over hundreds of cycles for 2024-T3 aluminum. It can be seen in Fig. 68 that for 2219-T851 aluminum, the decay is actually a two-stage process where the striation spacing decreased, in 3 to 5 cycles, to a value of approximately 20 μ-in., which was, in turn, almost double the constant amplitude rate. Subsequently, at about 50 cycles, the decay resumed and agreement with the constant amplitude curve occurred at around 200 cycles.

Figure 69 presents similar results where the overload ratio was 1.25 (also see Fig. A-9). The first overload cycle striation width averaged 50 μ-in. The crack closure model predicted a value of 23 μ-in. which was 46% of the measured values. The striation spacing again decayed in approximately five cycles to a first stage mean value of 26 μ-in., which was, in turn, 73% higher than the expected constant amplitude value of 15 μ-in.

It can be concluded, based on this limited data, that the stretch zone caused by the first overload cycle is several times larger than either the expected constant amplitude crack growth rate or the expected value based on crack closure considerations. These results are consistent with those of both Ref 8 and 9. In the latter reference, the authors observed similar behavior for aluminum, steel and titanium specimens subjected to single overload cycles. Further, the decay of the striation spacing to the stabilized or non-interacted value is apparently a two-stage process in which the striation spacing decays to about double the CCA rate after five cycles and then requires about 200 cycles to arrive at the final stabilized value.

### 3.4.2 Ti 6Al-4V Titanium

The data obtained from the two titanium specimens are presented in Fig. 70 and 71 (also see Fig. A-10 and A-11). Because of the greater difficulty in making measurements on the titanium, the data are not as complete as the aluminum data were. This is due principally to the smaller titanium grain size. In the aluminum, it was possible to locate long grains which included the overload event and many subsequent striations. The small grains in titanium, coupled with its basic heterogeneous texture made this impossible. In Fig.

70, where the overload ratio was 1.25, 26 successive striations were quantified. The width of the first striation is given as 32 μ-in., but based on the data trend, is probably greater than 40 μ-in. The CCA rate is 11 μ-in. and the Ref 1 crack closure model predicted a value of 17 μ-in., so that the measured value (40 μ-in.) was 3.6 and 2.4 times those respective expected values.

Like the aluminum results, the striation spacing quickly decayed, in approximately five cycles, to a value of about 19 μ-in., which is 73% greater than the CCA value. The replica used to obtain these data deteriorated significantly during examination. As a result, it was not possible to gather sufficient data to observe the subsequent decay to the CCA value.

The data of Fig. 71 were obtained from a specimen subjected to an overload ratio of 1.8. Due to extensive local plasticity, only the first five striations could be quantified. One additional striation, estimated to be for the 15th overload cycle was also observed. These data are far too sparse to arrive at any firm conclusions. The first cycle striation width is eight times the CCA rate. The crack closure model predicted a value of 27 μ-in., which is only 27% of the measured value. The data seem to indicate a first stage striation spacing of about 22 μ-in., a value which is again twice the CCA rate.

Although it was not possible to count striae continuously, it was possible to cross-plot striation spacing versus crack extension after the overloads began. These results are presented in Fig. 72 (also see Fig. A-11). It can be seen that the striation spacing decayed to the expected CCA value within the 500 overload cycles. The figure also shows that subsequent to the overloads (Point B) the low load striation and CCA values agree, except that immediately after point B, the spacing was less than 1 μ-in. and could not be resolved with the replicating technique employed.

It can be concluded that the titanium data behaved in much the same manner as the aluminum data. The first overload cycle striation width was much greater than expected. There also appeared to be a two-stage behavior which describes the subsequent striation spacing decay to the stabilized or expected values.

### 3.4.3 Summary

The objective of these measurements was to define crack closure behavior

as a function of number of overload cycles. Table 10 summarizes the results obtained. It can be seen in column 5 that the final (stage 2) striation spacings are substantially the same as the CCA values. Further, columns 2, 4 and 7 show that the spacings predicted by the crack closure model agree closely with the stage 1 striation spacings. It is also clear from column 6 that the measured first cycle spacings are always at least twice the predicted values.

The closure level prior to the overloads, which would be required to provide a crack growth rate equal to the observed striation width during the first overload, was determined from the crack growth equation of Ref 1.

$$d_s = \frac{da}{dN} = C\left[\frac{P_{OL} - P_{c_{req}}}{1 - C_{f_o}} f(\tfrac{a}{W}, t)\right]^n \qquad (18)$$

The constants C and n are the same as in Eq 3 and 5. The value of $C_{f_o}$ was determined (Ref 1) to be 0.4 for both materials while f(a/w, t) relates stress intensity to the specimen geometry. The parameter $P_{c_{req}}$ is the closure load required to fit the data and is shown schematically in Fig. 73. The values of $P_{c_{req}}$ were calculated and normalized by dividing them by the maximum baseline loading. These values are plotted in Fig. 74 against the overload ratio. The value of 0.41 at O/L = 1.0 is given by definition for a constant amplitude loading case with R = 0.05. It can be seen that the data lie very close to a straight line which passes through zero at O/L = 1.43. (Similar results, showing a reduction in closure level, were presented in Ref 10 through 12.) For overload ratios greater than 1.43, the required closure factor is negative (Fig. 74), implying a negative (compression) crack opening load. Although this phenomenon is physically possible, it does not logically fit the conditions. Because the applied minimum load always exceeded zero, the effective load range was merely taken as the difference between the maximum and minimum applied loads. Clearly, there are phenomena other than crack closure which contribute to the first cycle growth. These phenomena appear to influence not only the first cycle, but also the next few overload cycles. This conclusion is based on the fact that crack closure considerations yield striation spac-

ings which closely match the stage 1 measured values (Table 10, column 7).

Until additional work can be done in this area, a temporary improvement to the crack closure model of Ref 1 can be obtained by making $N_{sat}$, the number of cycles to saturation (stabilized overload growth) equal to approximately 200 for both materials. This modification does not properly predict the growth during the first few cycles, but should improve the subsequent predictions as shown in Fig. 75 and 76 (also see Fig. A-11). The first few cycles contribute comparatively small amounts of crack extension, so that the net error is small. It can be seen in Fig. 75 that by increasing the value of $N_{sat}$ from 13 (Ref 1) to 200 for aluminum, the predicted curve fits the data closely. In Fig. 76 although there is considerable scatter, the fit for titanium is improved by increasing $N_{sat}$ from 100 (Ref 1) to 200 cycles.

## 3.5 COMPRESSION EFFECTS

It was found during the Ref 1 program that compression spike loads, applied alone, or subsequent to a tensile overload spike produced very little effect on subsequent crack growth. Generally, only a compression/tension loading sequence produced subsequent retarded crack growth. The measurements described below were performed to determine in greater detail how the crack growth behavior was affected by these types of loading.

### 3.5.1 Compression Spikes

One compression spike event was investigated for each material. Figure 77 (also see Fig. A-12) shows the results for the aluminum specimen which was subjected to a 12-ksi compression spike superimposed on a constant amplitude loading of 6 ksi with R = 0.05. The figure shows the striation size plotted against crack length before and after the spike. The striation data are generally greater than the CCA rate curve. These data differ from the macroscopic $\Delta a/\Delta N$ data which are also plotted. The macroscopic data indicate that there was an abrupt decrease in the crack growth rate (retardation) after the compression spike. The microscopic data do not show such a trend. Further, the striation data do not exhibit the previously discussed striation spacing increase in the vicinity of the spike.

Similar data are presented in Fig. 78 for the titanium specimen. The striation data before and well after the compression spike are also higher than the CCA rate curve. In this case, the compression spike reduced the striation spacing immediately after the overload. Although there are only three data points, the macroscopic data tend to verify this result. The interesting aspect of these data is that the striation spacing was reduced by the application of a compression load. Intuitively, the opposite effect would be expected. Because tensile overloads tend to reduce subsequent striation spacing (and crack growth rates) compression loads would be expected to increase the spacing. Crack closure considerations indicate that compression loads tend to reduce the closure level, resulting in higher subsequent crack growth rates. The two sets of macroscopic data and one set of microscopic data are in direct contradiction to both intuitive and crack closure reasoning. The gross compression stresses were quite small compared to the yield stresses of both materials and, as a result, plasticity effects near the crack tip must be discounted as a factor. No explanation for the decreased striation spacing and macroscopic crack growth rates can be found.

Two figures from Ref 1, reproduced here as Fig. 79 and 80, show that the long range effects of the compression spikes are negligible for both materials because the macroscopically measured crack length versus cycles data agreed closely with calculated constant amplitude crack growth predictions which neglected the compression spikes. It must be concluded that although discrete compression spikes do affect subsequent crack growth rates to some degree, the fact that they have negligible long term effects on crack growth indicates that they may be discounted in crack growth calculations. However, this does not imply that their effects on crack growth during spectrum loading are negligible.

### 3.5.2 Tension/Compression and Compression/Tension Sequences

Figure 81 (also see Fig. A-13) presents striation spacing data for an aluminum specimen subjected to a tension/compression (T/C) sequence where O/L = 1.5 and $R_c$ = -3. The data exhibit a lot of scatter immediately after the T/C sequence but, based on the reduction of striation spacing they indicate that retardation

occurred. The CCA rate curve is shown to provide a good fit to the data well after the T/C sequence. A retarded crack growth rate (dash-dot) curve, calculated from Eq 12a and 15 and neglecting the compression spike is also shown. This retarded curve fits the data quite well in terms of both the minimum striation spacing and the distance required for the striation data to return to the CCA curve. The affected crack length was taken as the plane strain plastic zone diameter, $\delta$, caused by the tensile overload. These data indicate that the compression spike did not alter the influence of the tensile overload on subsequent crack growth.

The data of Fig. 82 are much less conclusive. For this case O/L = 1.5 and $R_c$ = -2. It can be seen that the striation spacing data subsequent to the T/C sequence possess considerable scatter. Unlike the data of Fig. 81, these data do not lie along the retarded crack growth curve. In fact, the data do not exhibit any particular, well behaved, trend at all. It might be concluded that the compression spike negated any tendency of the tensile overload to cause subsequent retarded growth rates (reduced striation spacing).

The data of the two figures (81 and 82) yield contradictory results which are further confused by the fact that the event which showed retardation (Fig. 81) was subjected to a more severe compression spike (-18 ksi) than the other event where the compression spike was -12 ksi where no retardation occurred. The data presented here do not provide sufficient evidence to conclude whether or not compression spikes applied subsequent to tensile overloads had an effect for 2219-T851 aluminum.

Figure 83 presents striation spacing data for a titanium specimen which was subjected to a tension compression sequence where O/L = 1.5 and $R_c$ = -1.5. The striation spacing data prior to and well after the T/C loads lie about 25% above the CCA rate curve. A least squares analysis was performed on all of the data except for the points within the plane strain plastic zone diameter, $\delta$. The slope of the least squares curve was set equal to that of the CCA curve and provides a good description of those data points. Using the least squares curve as a reference, the data indicate that the T/C sequence sharply reduced the subsequent striation spacing. After the crack propagated

a distance roughly equal to $\delta$ the data again agreed with the least squares curve. The figure also shows a retarded crack growth rate (dash-dot) curve which was calculated using Eq 12a and 15 for a single overload and which neglected the compression spike. The crack growth rate values obtained were multiplied by 1.25 to account for the difference between the least squares and CCA curves. It can be seen that the retarded curve qualitatively defines the data trend but that it predicts values which are less than the data. This probably reflects the effect of the compression spike, a conclusion which is indirectly supported by Fig. 84.

Figure 84 shows data for an event where the loads were reversed and the specimen was subjected to a compression/tension (C/T) sequence. A least squares procedure was used to provide a better fit to the data before and well after the C/T sequence. In this case, the least squares curve was 76% greater than the CCA curve. It can be seen that, neglecting the compression spike, the retarded crack growth rates obtained from Eq 12a and 15 (multipled by 1.76 in this case) correlate closely with the data within the plastic zone diameter, $\delta$. In this case, the compression spike applied prior to the tensile overload did not modify the effect of the overload on subsequent crack growth behavior. Compression/tension sequence can therefore be treated as single overload spikes and the compression spike can be neglected. However, the data of Fig. 83 indicate that the compression portion of tension/compression sequences must be accounted for. The limited data obtained here are insufficient to define how the compression spike must be accounted for in titanium.

### 3.5.3 Summary

Fractographic examinations of specimens subjected to compression spikes and tension/compression and compression/tension sequences tend to support the conclusions of Ref 1. Compression spikes have negligible effect on subsequent crack growth for both materials. It could not be concluded whether or not compression spikes negate the retarding effects of preceding tensile overloads in 2219-T851 aluminum. The striation spacing data indicated that compression/tension sequences in titanium could be treated as tension spikes only. For titanium, a compression spike tends to offset the retarding effect on subsequent crack growth of a preceding tensile overload.

## 3.6 SINGLE PERIODIC OVERLOADS

It was shown in Ref 1 that the single periodic overload cases included the poorest predictions of the Crack Closure Model. Specifically, for the aluminum specimens with O/L = 1.8 and where the number of cycles between overloads was 500 and 1000 cycles, or with O/L = 1.25 and with 50 cycles between overloads, the model overpredicted the specimen lives by considerable amounts. For titanium, the predictions were generally good except where the overload ratio was 1.8 with frequencies of occurrence of the overloads of 500 and 1000 cycles. In these cases, the model underpredicted the specimen lives by significant amounts.

The objective of these measurements was to determine, if possible, how the striation spacing varied within the block of low loads. This task can not be performed macroscopically because of the extremely small crack extensions involved.

Four specimens were examined. The pertinent data are recorded in Table 11.

### 3.6.1 2219-T851 Aluminum

Figure 85 (also see Fig. A-14) presents striation spacing plotted against the number of low load cycles after the overload for an aluminum specimen with O/L = 1.25. In this case there were 50 low load cycles between overloads. The striation (stretch band) width for five different overload applications is shown to vary from 24.8 to 85.5 μ-in, averaging 41.3 μ-in. An interesting feature of these data is that the striation spacings for the first several cycles immediately after the overload are larger than the subsequent spacings for all three sequences examined. These results are contradictory because overloads generally reduce the subsequent striation spacing. At first, the increased magnitude of the first few cycles was attributed to delayed retardation. However, this phenomenon must be discounted as being part of a delayed retardation sequence as the total crack extension in each block of 50 low load cycles was nominally 0.0005 in., while the plane strain plastic diameter, $\delta$, caused by the overload was 0.0146 in. The crack propagated only 3% of the way through $\delta$. In situations where delayed retardation has been observed, the

crack growth rate decayed to a minimum value after the crack tip had propagated 1/8 to 1/4 of the way through the affected crack length. The value of 3% obtained here is far too small. The increased striation spacing of the first few cycles was finally attributed to plasticity effects, which was discussed in Subsection 3.3.3 of this report.

If the striation spacing of the first six or seven cycles is discounted, the average $d_s$ for the remaining cycles is 10.9 μ-in. compared to a calculated constant amplitude crack growth rate for the low loads (neglecting the overloads) of 18.3 μ-in. per cycle. If it is assumed that the crack closure load is nominally constant through each block, then the closure level can be calculated as outlined below:

$$\frac{(d_s)_{AVG}}{\left(\frac{da}{dN}\right)_{CA}} = \left[\frac{P_b - \bar{P}_c}{P_b - P_{b_c}}\right]^n \qquad (19)$$

where $(d_s)_{AVG}$ = Average Striation Spacing = 10.9 μ-in.

$\left(\frac{da}{dN}\right)_{CA}$ = CCA crack growth rate = 18.3 μ-in./cycle

$P_b$ = Low level maximum load = 500 lb

$P_{b_c}$ = Closure load for low level = 206 lb*

$P_c$ = Average closure load (lb)

$n$ = Crack growth exponent from Eq 3 = 3.34

*Obtained from Eq 16 and 21 from Ref 1.

The average closure value, $\bar{P}_c$, was found to be 248 lb. The steady-state closure value for the overload (625 lb, $R_{eff}$ = 0.04) was found to be 256 lb from Eq 16 and 21 of Ref 1. These two values (the average closure level and the steady-state overload closure level) indicate that when the overloads are applied frequently, the average closure level which exists is nominally the closure level associated with the overloads. Reference 1 showed how the aver-

age closure level could be calculated using this type of loading sequence, a technique which is verified by these results.

A review of the closure model revealed that the model calculates and maintains a closure load of 255 lb after the first few blocks of loads. These results are consistent, but do not explain why the model overpredicted the life of this specimen as shown in Fig. 86a. As a result of this discrepancy, the macroscopic data for this specimen were examined and are presented in Fig. 87 (also see Fig. A-14) where the striation spacing and average macroscopic crack growth rates are plotted against the crack length. It can be seen that at the crack length which was examined (a = 1.44 in.) the macroscopic rate, calculated constant closure rate and striation spacing all agree closely. In general, the macroscopic rates are 25% to 35% greater than the rates calculated using a constant closure load of 255 lb (for the overload). It can be seen that for crack lengths less than about 1 in., the macroscopic rates are as much as three times the calculated values. The poor prediction (from the crack closure model, Fig. 86) can therefore be attributed to the vast differences in measured and calculated crack growth rates at small crack lengths. A second prediction was made using the Ref 1 model with an initial crack length of 1 in. It can be seen in Fig. 86b that the correlation is significantly better. Starting at a crack length of 1 in. the predicted life is 33% greater than the experimental life. This value is consistent with the difference between calculated and average crack growth rates.

Figure 87 also shows that at short crack lengths, the average macroscopic crack growth rates are even higher than those calculated using a constant closure load of 206 lb, the value for the low load. This difference in observed and calculated rates can only be explained by the growth during the overload. For example, at the crack length of 1.44 in, the average striation spacing for the last 43 low load cycles was previously stated as being 10.9 μ-in. The spacing for the first seven cycles averages 14 μ-in. and the growth during the overload averages 41.3 μ-in. The overall average striation spacing for 51 cycles (including the overload) is 11.9 μ-in. which is almost identical to the average macroscopic growth rate (12 μ-in. at a = 1.44 in.). The significant aspect of these results is that presently conceived crack closure con-

cepts can not properly predict the growth during the overload (Subsection 3.4 of this report) or, apparently, the growth during the first few low load cycles. At short crack lengths, where the average growth during the low load is only 1 or 2 μ-in., the growth during the overloads is probably proportionately much greater. This would explain why the actual crack growth rates are so much higher (a factor of 3) than the calculated rates.

Figure 88 (also see Fig. A-15) presents $d_s$ versus cycles data for an aluminum specimen subjected to overloads with O/L = 1.8 and $N_{OL}/N$ = 1/500. The striation spacing behavior is similar to the preceding case. The overload striation width is 31.5 μ-in. and the first two striae after the overload average 21 μ-in. The spacing decayed rapidly to an average value of 2.9 μ-in. This value compares to a CCA rate of 12.6 μ-in. for the low loads (neglecting the overloads). The average closure load for $d_s$ = 2.9 μ-in. was calculated using the constant closure technique (Eq 19) as 316 lb. This lies between the values of 206 lb and 365 lb for the low loads and overload respectively. When the overload closure level (365 lb) was used, the rate was calculated to be 0.9 μ-in./cycle. It is obvious from the data that the average closure load, if that is the appropriate parameter to be used, increases as a function of the number of cycles after the overload. In fact, the closure load necessary to predict the spacing of 21 μ-in. for the first two cycles is 157 lb, a value which is less than the low load closure level.

Reference 12 showed that the crack opening load (here, interpreted as the closure load) was depressed as a result of applying several overload cycles. The crack closure model (Ref 1) does not predict this type of behavior and the data obtained during the fractographic program are far too sparse to be used to modify that model. As in the previously discussed case, the closure model calculates and maintains a closure level which is nominally the same as the overload closure level. A technique suitable for modifying the closure model has not been developed. Such a modification will require a further, more complete, fractographic program to examine single periodic overload specimens or an analytical program employing elastic-plastic finite element models.

### 3.6.2 Ti 6A1-4V Titanium

Two titanium specimens, the first with O/L = 1.25 and $N_{OL}/N$ = 1/50 and the second with O/L = 1.8 and $N_{OL}/N$ = 1/500, were examined.

Figure 89 presents striation spacing versus cycles after the overload for O/L = 1.25 and $N_{OL}/N$ = 1/50. In this case, the model over-predicted the test life by 30%. It can be seen in the figure that, unlike the aluminum data, the striation spacing is not large (relative to the bulk of the data) immediately after the overload. The average spacing for all of the low loads is 7.3 μ-in. This value compares closely with an average macroscopic $\Delta a/\Delta N$ value of 7.7 μ-in. per cycle, which includes the growth during the overload. The average overload striation width is 29.6 μ-in. Subtracting this value from the macroscopic $\Delta a/\Delta N$ gives an average $\Delta a/\Delta N$ for the low loads only, of 7.3 μ-in., yielding exact agreement between average microscopically and macroscopically measured values.

At the crack length of 1.4 in., the crack closure model yields an average crack growth rate of 9.0 μ-in./cycle including growth during the overload. This rate is based on an average closure level of 340 lb, and compares with closure levels of 330 lb and 410 lb for the low loads and overload respectively. The model predicts a closure level which is quite close to the closure level for the low loads. The average macroscopic $\Delta a/\Delta N$ value of 7.7 μ-in./cycle reflects an average closure load of 363 lb, which is only 7% higher than that calculated by the model. In this case, then, the closure model predicts values which compare favorably with measured values in all respects. The model even predicts an overload striation width of 27.4 μ-in. which is almost identical to the average value of 29.6 μ-in.

Figure 90 presents striation spacing versus crack extension after the overload for a case where O/L = 1.8 and $N_{OL}/N$ = 1/500. As previously discussed, the titanium under some conditions did not yield clear microscopic data and, in this case, it was not possible to obtain continuous striation spacing measurements. As a result, the data were plotted against crack extension rather than cycles after the overload. The figure shows considerable scatter, typical of some of the titanium measurements.

The growth during the overload cycle averaged 108μ-in. for five measurements, while the constant amplitude crack growth rate for the overload at this crack length is 214 μ-in./cycle. In this case only, the measured striation width was less than the CCA rate for the overload.

The crack extension between overloads (including the overload growth) was calculated to be 0.0024 in. based on the average macroscopic $\Delta a/\Delta N$ of 4.8 μ-in./cycle. Therefore the crack grew about 85% of the way through the plane strain plastic zone diameter caused by the overload. On this basis, it would be expected that the striation spacing would be close to the constant amplitude crack growth rate just before the second overload was applied. It can be seen that this is not the case as the largest value of $d_s$ observed was about 19 μ-in. (excluding the overloads) which is approximately one half of the CCA rate. The figure also shows a general tendency for the striation spacing to decrease subsequent to the overload to an average value of about 4 μ-in. This implies that the closure load increased subsequent to the overload. The average spacing of 4-μ in. reflects an average closure load of 735 lb which compares with values of 429 lb and 760 lb for the low loads and overload respectively. The average closure load is, therefore, 96% of the overload closure level. The closure model predicts a rate of 13.5 μ-in./cycle (including the overload) at a = 1.5 in., which reflects an average closure level load of 588 lb. Although the closure model predicted an overall life which was 69% of the test life (Fig. 91), the predicted average crack growth rate is 2.8 times the measured rates at this crack length. Therefore, the model tends to predict lives which are about one third the test lives when a = 1.5 in. The differences in predicted and observed lives are not this great because the model predicted the crack growth behavior reasonably well up to a crack length of about 1.1 in. (Fig. 91). These results are directly opposite of those of Fig. 86 where the short crack prediction was poor while the long crack prediction was good. Generally, the model predicts average crack growth rates which increase with increasing crack length for both materials. Consider that the overload plastic zone size increases in approximately direct proportion to the crack length while the crack growth per block increases at some higher power of crack length. It can be concluded that the relationship be-

tween crack extension and plastic zone size is not properly handled by the model. The limited data obtained during this program are insufficient to discern the proper relationships and thereby modify the model. Further, the striation spacing behavior is inconsistent with the currently accepted concepts of crack closure behavior, in that the closure level apparently increased during the block of low load cycles when it was expected to decrease.

### 3.6.3 Summary

The fractographic examination of the four specimens revealed that the average crack growth rate during each block of loads is always less than the calculated crack growth rate for low loads. Growth during the overloads in aluminum specimens is measurably greater than can be calculated using crack closure concepts. The titanium overload $d_s$ value was close to the calculated value where O/L = 1.25, but was less than the CCA value where O/L = 1.8. In three of the four cases examined, the striation spacing immediately after the overloads was greater than the average spacing for the block of low loads and decayed fairly quickly to a stabilized value. These results directly contradict currently accepted closure concepts although they do support some analytical finite element results (Ref 12). Where overloads were applied every 50 low load cycles, the average closure level based on macroscopic $\Delta a/\Delta N$ data was close to the overload closure level. The crack closure model of Ref 1 tends to predict average crack growth rates which are initially much lower than the calculated values for long cracks, indicating a poor correlation between crack growth during the low loads and plastic zone size. The model does not properly predict the growth during the overloads for aluminum (Subsection 3.4) which accounts for the lower than actual overall growth rates obtained by the model. Insufficient data were collected to obtain more than a qualitative understanding of the mechanism of single periodic overload crack growth behavior.

## 3.7 THICKNESS EFFECTS IN TI 6Al-4V TITANIUM

A few 3/4-in. thick titanium specimens were tested during the Ref 1 program. Most specimens were 1/4-in. thick. Two 3/4-in. thick, single overload events were microscopically examined during this program to determine whether the material thickness had any effect on striation spacing (and crack growth rates) before and after an overload cycle.

The striation spacing data obtained from the centerline of the fracture face during this investigation are plotted against crack length in Fig. 92 and 93. Both figures show that the striation spacing data before and well after the overload are measureably larger than the CCA rate curves calculated from the 1/4-in. thick material parameters. Reference 1 showed that a limited amount of data, gathered under constant amplitude loading conditions with R = 0.05, tended to lie near the upper edge of the 1/4-in. thick data scatter band on a plot of crack growth rate versus stress intensity range. Those data are consistent with the striation spacing data obtained during this program. A least squares analysis was performed for the striation data of each figure. Those data which fell within the plastic zone diameter, $\delta$, were excluded and the slope of the least squares line was set equal to the CCA line. The least squares lines were 1.72 and 2.10 times the CCA lines in Fig. 92 and 93, respectively. It can be seen that the macroscopic $\Delta a/\Delta N$ data (boxes) obtained on the specimen surfaces agree closely with the least squares lines for crack lengths outside the affected crack length increment. It can be concluded that the macroscopic surface and microscopic centerline data agree closely and that the average uninteracted striation spacing (crack growth rates) for the 3/4-in. material are about 90% greater than those for the 1/4-in. thick material.

It was assumed when the least squares analyses were performed, that the plane strain diameter, $\delta$, defined the affected crack length. The data of both figures indicate that this was a valid assumption because, after the overload, they tend to return to agreement with the least squares curve at about the distance, $\delta$, measured from the overload crack length.

Retarded crack growth rates were calculated using Eq 12a and 15 except that Eq 12a was modified to account for the difference in crack growth rates between the 3/4-in. and 1/4-in. thicknesses. The crack growth coefficient, C, ($5.9 \times 10^{-10}$ for 1/4-in. thick titanium) was multiplied by 1.72 and 2.1 for the data of Fig. 92 and 93, respectively. The effectiveness of an overload, where O/L = 1.8, was assumed to be the same as for the 1/4-in. materials and Eq 15 was used without modification. It can be seen that the retarded growth rate curves (dash-dot) yield crack growths which are very similar to

the data. Therefore, the techniques developed to predict retarded crack growth for the 1/4-in. data can also be applied to the 3/4-in. thick material.

It should be noted that when the least squares analyses were performed, no allowance was made for the previously described buildup of striation spacing just prior to the overload. The data of both figures exhibit this tendency to a certain extent. If this phenomenon had been somehow accounted for, the least squares curves would have been slightly lower, and the calculated affected crack lengths and retarded growth rate curves would have been in better agreement with the data.

It can be concluded that the only apparent difference between the 3/4-in. and 1/4-in. material are the basic crack growth rates. Other parameters related to overload affected crack length and retarded crack growth behavior apply equally well to both material thicknesses.

## 3.8 PART THROUGH AND TRANSITION CRACKS

These investigations were initially intended to be directed to surface cracks subjected to high-low loading sequences. In addition to defining the aspect ratios of surface cracks, striation spacing data before and after a high-low load change were to be obtained. It was not possible to perform the latter task for two principal reasons. First, the number of test specimens where the high-low load change had been applied to surface cracks was quite limited. Second, in almost all cases, the striation spacing was extremely small because of the very small cracks, a problem further complicated by the retarding effect of the high loads on subsequent low load crack growth rates. The resulting striation widths were below the resolution limits of the replication process employed in this program. As a result, transition cracks, where the front surface lengths were measureably different from the back surface lengths, were used for most measurements.

### 3.8.1 2219-T851 Aluminum

The aluminum striation spacing results are presented in Fig. 94 and 95. Striation spacing measurements were made along the centerline of the specimens in a direction normal to the local crack front. It was assumed that where

stabilized or constant amplitude crack growth conditions existed, the CCA rates, calculated using the front and back surface half-crack lengths, should be respectively larger than and smaller than the striation data. Figure 94, which shows striation spacing plotted against the local crack extension after the load change, indicates that this assumption is nominally correct. The data prior to the load change lie near the CCA (min) curve which was calculated using the back surface (short) crack length. The CCA (max) curve was calculated using the front surface (long) crack length. The low load data gathered well after the load change lie near the CCA (max) curve. Because the total crack extension was only 0.04 in., the stress intensity did not vary significantly. The differences in crack growth behavior must therefore be attributed to scatter.

The data tend to indicate that the crack length affected by the high load cycles can be defined by the plane strain plastic zone diameter, $\delta$, caused by the last high load cycle. The two values shown for $\delta$ are based on the long and short cracks lengths. This conclusion is substantiated by the data of Fig. 95. Those data clearly show that $\delta$ can be used to calculate the affected crack length for multiple overloads as well as for single overload cycles.

The data of Fig. 95 also verify that the stress intensity can be based on some crack length between the front and back surface half-length. The data obtained well after the load change lie close to the CCA (min) curve, a result which conflicts with similar data in Fig. 94.

The data immediately after the load change in Fig. 95 imply that delayed retardation occurred. The striation spacing decreases with increasing crack length for about 0.004 in. Although delayed retardation subsequent to multiple overloads has been reported by a few authors (Ref 5), it is generally accepted that for multiple overloads, retardation should be immediate. This apparent delayed retardation can be explained by the same reasoning as given in Subsection 3.3.3 of this report.

### 3.8.2 Ti 6Al-4V Titanium

Figure 96 presents striation spacing plotted against crack extension after the change from a high load to a low load. In this case, the replica was made at the root of a part-through crack which was 84% of the way through the thickness. The figure also shows CCA curves calculated using a surface crack stress intensity solution and a through crack stress intensity solution where the crack length was taken as half the front surface crack length. It can be seen that the data prior to the load change lie close to the through crack CCA curve. This is probably because the surface crack stress intensity solution is too low at the crack depth-to-thickness ratio, a/t, of 0.84. The solution, taken from Ref 13 was developed so that at a/t = 1, the surface crack stress intensity solution, is equal to the through crack stress intensity solution based on the half-surface length of the surface crack. The surface crack stress intensity solution may actually be almost equal to the through crack solution for values of a/t close to unity.

No retardation was observed subsequent to the load change. This may be because the striation spacing was too small to be resolved. It can be seen that the plane strain plastic zone diameter caused by the high load is only about 0.003 in. If any retardation did occur, it may have been obscured by the data scatter. The data well after the load change lie between the surface and through crack CCA curves.

Figure 97 presents data for a titanium specimen with a transition crack which was subjected to a high-low loading sequence. In this case, the high load had a stress ratio, R, of 0.7 and the low load had a stress ratio of 0.5. The data were obtained near the centerline of the specimen fracture surface. The CCA (max) and CCA (min) curves were calculated using the front and back surface half lengths respectively. It can be seen that the striation spacing data prior to the load change lie between the CCA (max) and CCA (min) curves, a result consistent with the aluminum data of Subsection 3.8.1. Subsequent to the load change, the striation spacing averaged about 4 μ-in. The average predicted crack growth rate is between 8 and 22 μ-in., indicating that substantial retardation was caused by the high loads. Immediate retardation is also evident.

The maximum overload stress intensity was between 54 and 73 ksi$\sqrt{in.}$, values calculated using the back and front surface crack lengths respectively. These values are sufficiently high so that mixed mode, rather than plane strain crack growth conditions may have existed. As a result, the corresponding plane strain plastic zone diameters shown in the figure may be too small. Although the fracture surface did not reveal significant amounts of plasticity (i.e., dimples) plane stress plastic zone diameters may be more appropriate. This theory is supported by the fact that the striation spacing does not tend to increase after the load change over the crack extension investigated. The data indicate that the affected crack length may be significantly larger than the values calculated for plane strain conditions. If plane stress conditions were assumed, the calculated affected crack lengths would be 2.8 times those shown and the data of Fig. 97 would extend about 25% of the way through those dimensions, in which case, a measureable increase in striation spacing would not necessarily be expected.

### 3.8.3 Summary

Striation spacing data for aluminum and titanium specimens indicate that the stress intensity solution for transition cracks lies between the through crack stress intensities calculated from the front and back surface half crack lengths. The affected crack length for aluminum specimens subjected to a high-low loading sequence under plane strain conditions is the plane strain plastic zone diameter produced by the last high load cycle. Surface crack data obtained from a titanium specimen at a/t greater than 0.8 correlated more closely with crack growth rates calculated using a through crack stress intensity solution than with a surface crack stress intensity solution. The crack growth rates subsequent to the load change were not always retarded. This result was inconclusive as the minimum striation spacing may have been too small to resolve in some cases.

## Section 4

## SUGGESTIONS FOR FUTURE EFFORTS

This effort was intended to be, principally, a verification program. As such, it was useful in determining the overload affected crack length and the effectiveness of single overloads with values of O/L up to 1.8. Originally, it was thought that by examining a specimen subjected to a low-to-high loading sequence, crack closure behavior as a function of the number of overloads could be determined indirectly from the striation spacing for the first few overload cycles. As evidenced by the data presented in Subsection 3.4 of this report, the first few overload cycles do not conform to currently accepted closure concepts.

The crack extension which occurred during the first few overload cycles was found to be much greater than could be explained by current prediction methods during this program and by other investigators (Ref 8 and 9) as well. It was shown in Subsection 3.6 of this report that under certain conditions, this growth can be a large percentage of the total growth for a block of loads. The quantification of overload stretch zones was outside the scope of this program. It is therefore suggested that a systematic study of the characteristics of overload stretch zones be conducted using fractographic techniques. This study would attempt to relate overload stretch band widths and topography to material fracture toughness, overload stress intensity, overload ratio and other pertinent parameters. The angle of the slip band, relative to the gross fracture plane, or to the angle of low level fatigue striations may also be of interest. A product of this effort might also be to define the retardation parameters for several consecutive overloads, as opposed to one or many overloads.

The local increase in striation spacing before an overload occurred in many of the cases investigated. Elastic-plastic finite element analyses may provide further insight into the material stress state near the crack tip. Although a considerable number of such analyses have been performed for a

variety of problems, detailed information regarding element sizes before and after an overload and subsequent to cracking are not generally available in the literature. While some of the data currently available may be of use, it is suggested that elastic-plastic finite element analyses, specifically formulated to reveal information regarding element sizes and the stress-strain states near the crack tip, before, during and after an overload, could provide considerable insight into the real or apparent mechanisms of crack propagation. Such a program may also provide additional evidence to support our explanation for delayed retardation by revealing how much different the final, stress-free condition of material along the crack faces is from the condition when the crack was originally formed.

It is suggested that any future Air Force sponsored fractographic programs aimed at quantifying crack growth behavior be carefully planned. For example, the crack growth tests should be designed for fractographic or microscopic measurements, rather than for macroscopic measurements. This is because the measurement of striation unit size change along a crack length depends on the continuity of the bulk structure. This continuity is lost at grain boundaries and second phase particles in the common engineering alloys. The crystallographic orientation of the grain is also important in determining whether or not striations will be visible. From a purely fractographic point of view, in order to quantify striations easily, a large, elongaged-grain alloy with few second-phase particles would be preferable. A non-heat-treatable wrought aluminum that has been recrystallized is suggested. The fatigue crack path through one large grain would yield an extended clear record of striation spacing changes caused by load interactions. This idealized case, even though it would not be representative of an aircraft structural material, would be convenient in understanding basic changes in fatigue crack growth rates due to load interactions.

It is also suggested that for specialized fatigue crack growth tests, the macroscopic crack growth observations obtained while the specimen is in the fatigue test machine could be improved by viewing the specimen surface or a replica of the specimen surface using a high power bench microscope. It

may be very difficult to view the specimen directly due to vibrations and high frequency oscillations of the test machine, thereby necessitating replication procedures. For example, when it is desired to define the growth during, or immediately after, one or more overloads, crack extensions could be measured very accurately using such techniques.

## Section 5

## OBSERVATIONS AND CONCLUSIONS

This program has verified, through the use of fractography, some of the results obtained in the Ref 1 Crack Growth Analysis program. In some cases, it has provided additional detailed information and more refined results than were revealed during that program. In other cases, it has raised additional questions regarding the mechanisms of fatigue crack propagation.

The following conclusions and observations have been reached as a direct result of investigations performed during this program.

(1) There is a one-for-one relationship between striations and applied loading cycles. However, topography composed of dimple rupture, cleavage, brittle striations or plasticity can yield striation spacing values which do not agree with crack growth rate data.

(2) If striation data are obtained over a sufficient amount of crack extension, the data can be used to obtain crack growth rate versus stress intensity relationships.

(3) The threshold of striation resolution for the carbon replicating techniques as employed in this program is approximately $1 \times 10^{-6}$ in.

(4) Striation spacing data, obtained along the centerline and edges of the fracture faces, correlate closely. These data also agree very closely with macroscopic crack growth rate data obtained from the specimen surfaces.

(5) Overall, microscopic data possessed less scatter than the equivalent macroscopic data.

(6) The plane strain plastic zone diameter best described the overload affected crack length for specimens fabricated from both materials and tested under plane strain conditions.

(7) The data obtained during this program neither confirmed nor denied the existence of delayed retardation.

(8) The ratio of the closure level after one overload cycle to the stabilized closure level for the overload (the effectiveness of an overload) decreased with increasing overload ratio.

(9) The effectiveness of an overload was found to be greater for titanium than for aluminum at a given overload ratio.

(10) The crack closure exponent, B, was found to be close to unity as reported in Ref 1.

(11) A local increase in the striation width just prior to an overload was observed. This is believed to result from stretching of the existing free fracture surface.

(12) Plasticity effects and internal growth caused by an overload can explain delayed retardation as a surface phenomenon.

(13) The crack growth (striation width) caused by the first few consecutive overload cycles in a low-high loading sequence was from two to eight times the value predicted by currently accepted crack closure concepts.

(14) The number of overload cycles required to achieve stabilized crack growth conditions was found to be approximately 200 for both materials.

(15) Discrete compression spikes have a negligible effect on subsequent crack growth behavior.

(16) Compression spikes tend to offset the retarding effects of preceding tensile overloads in titanium, but a similar conclusion could not be reached for aluminum.

(17) Compression spikes applied prior to tensile overloads have a negligible effect on the retardation-producing characteristics of the overloads.

(18) In three of four single periodic overload cases examined, the striation spacing of the first few low level cycles after the overload was greater than the average spacing of the remaining cycles, a

result contrary to that expected. This is also believed to have resulted from stretching of the free fracture surface.

(19) The unexplained large growth caused by single overloads, applied periodically, can constitute a large percentage of the total growth in a single periodic overload sequence, resulting in much greater overall growth than expected.

(20) Constant amplitude crack growth rates (striation spacing) in 3/4-in. thick specimens was about 90% higher than equivalent 1/4-in. thick specimens.

(21) Retardation parameters (i.e., affected crack length and overload effectiveness) developed for 1/4-in. thick specimens were applicable to the 3/4-in. thick specimens when the differences in basic crack growth characteristics were accounted for.

(22) The transmission microscope techniques developed during this program were found to be very efficient in generating striation spacing data.

## REFERENCES


1. Bell, P.D. and Creager, M., "Crack Growth Analysis For Arbitrary Spectrum Loading," AFFDL-TR-74-129, Volume I, October 1974.

2. Willenborg, J., Engle, R. and Wood, H.A., "A Crack Growth Retardation Model Using an Effective Stress Concept," Technical Memorandum 71-1FBR, Air Force Flight Dynamics Laboratory, WPAFB, January 1971.

3. Wheeler, O.E., "Crack Growth Under Spectrum Loading," Report No. FZM-5602, General Dynamics Corporation, Forth Worth Division, June 1970.

4. McClintock, F.A. and Irwin, G.R., "Plasticity Aspects of Fracture Mechanics," ASTM STP 381, 1964.

5. Trebules, V.W., Roberts Jr., R., and Hertzberg, R.W., "Effect of Multiple Overloads in Fatigue Crack Propagation in 2024-T3 Aluminum Alloy," ASTM STP 536, July 1973.

6. Corbly, D.M. and Packman, P.F., "On the Influence of Single and Multiple Peak Overloads on Fatigue Crack Propagation In 7075-T6511 Aluminum," Journal of Engineering Fracture Mechanics, Vol. 5, 1973.

7. Gallagher, J.P. and Hughes, T.F., "Influence of Yield Strength On Overload Affected Fatigue Crack Growth Behavior in 4340 Steel, AFFDL-TR-74-27, June 1974.

8. vonEuw, E.F.J., Hertzberg, R.W. and Roberts, Richard, "Delay Effects in Fatigue Crack Propagation," ASTM STP 513, September 1972.

9. Hall, L.R., Shah, R.C. and Engstrom, W.L., "Fracture and Fatigue Crack Growth Behavior of Surface Flaws and Flaws Originating at Fastener Holes," AFFDL-TR-74-47.

10. Newman Jr., J. C. and Armen, Harry, Jr.: "Elastic-Plastic Analysis of a Propagating Crack Under Cyclic Loading," AIAA Paper No. 74-366, Pre-

sented at the AIAA/ASME/SAE 15th Structures, Structural Dynamics, and Materials Conference, Las Vegas, Nevada, April 17-19, 1974.

11. Newman Jr., J. C., "Finite-Element Analysis of Fatigue Crack Propagation - Including the Effects of Crack Closure," Ph. D. Thesis, Virginia Polytechnic Institute and State University, May 1974.

12. Newman Jr., J. C., "A Finite-Element Analysis of Fatigue Crack Closure," Presented at the ASTM Eighth National Symposium on Fracture Mechanics, Providence, R.I., August 1974.

13. Newman Jr., J. C., "Fracture Analysis of Surface- and Through-Cracked Sheets and Plates", Engineering Fracture Mechanics, 1973, Vol. 5, pp 667-689.

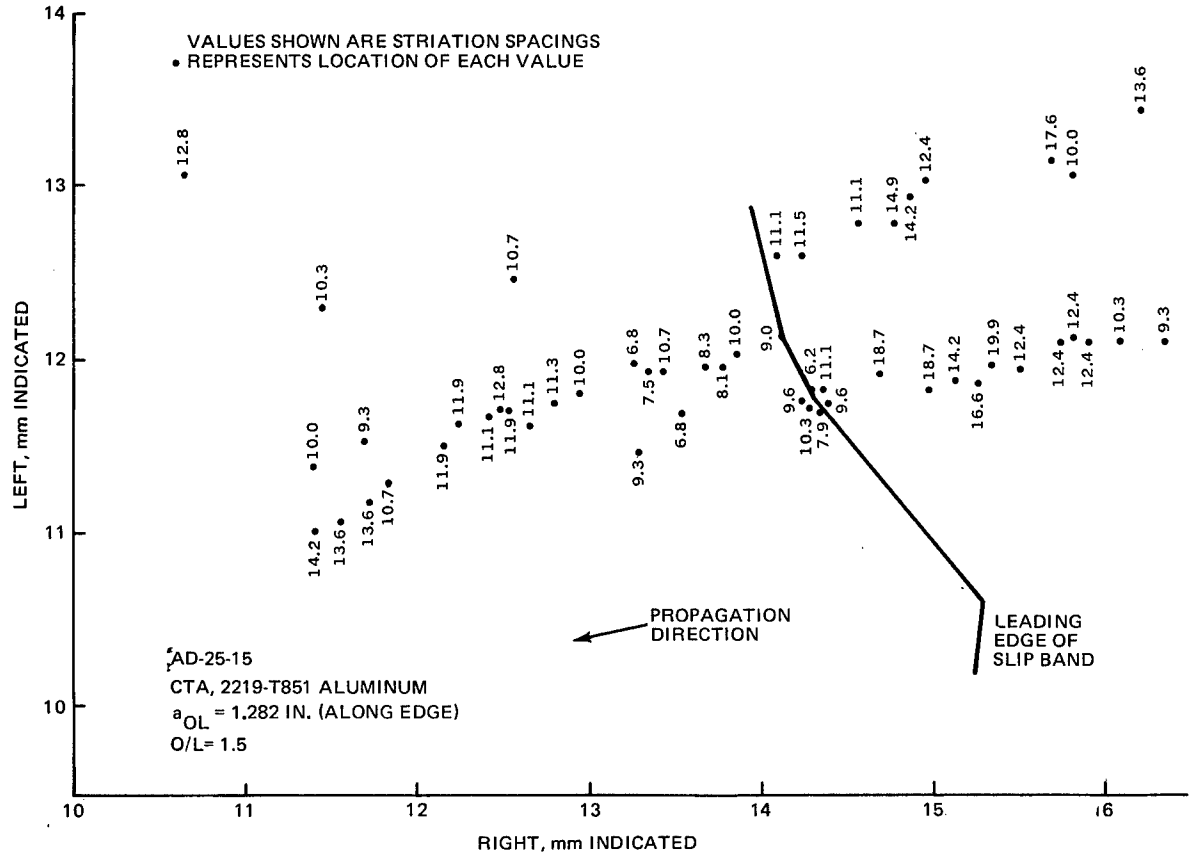


**Figure 1 Typical Contour Plot for a Single Overload Specimen**

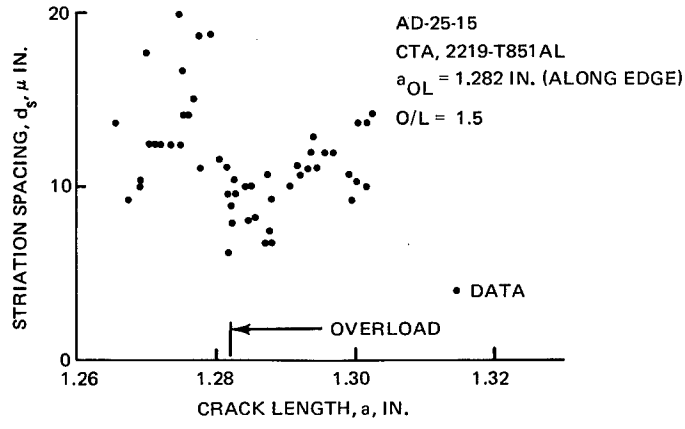


**Figure 2 Typical Striation Spacing vs Crack Length Plot**

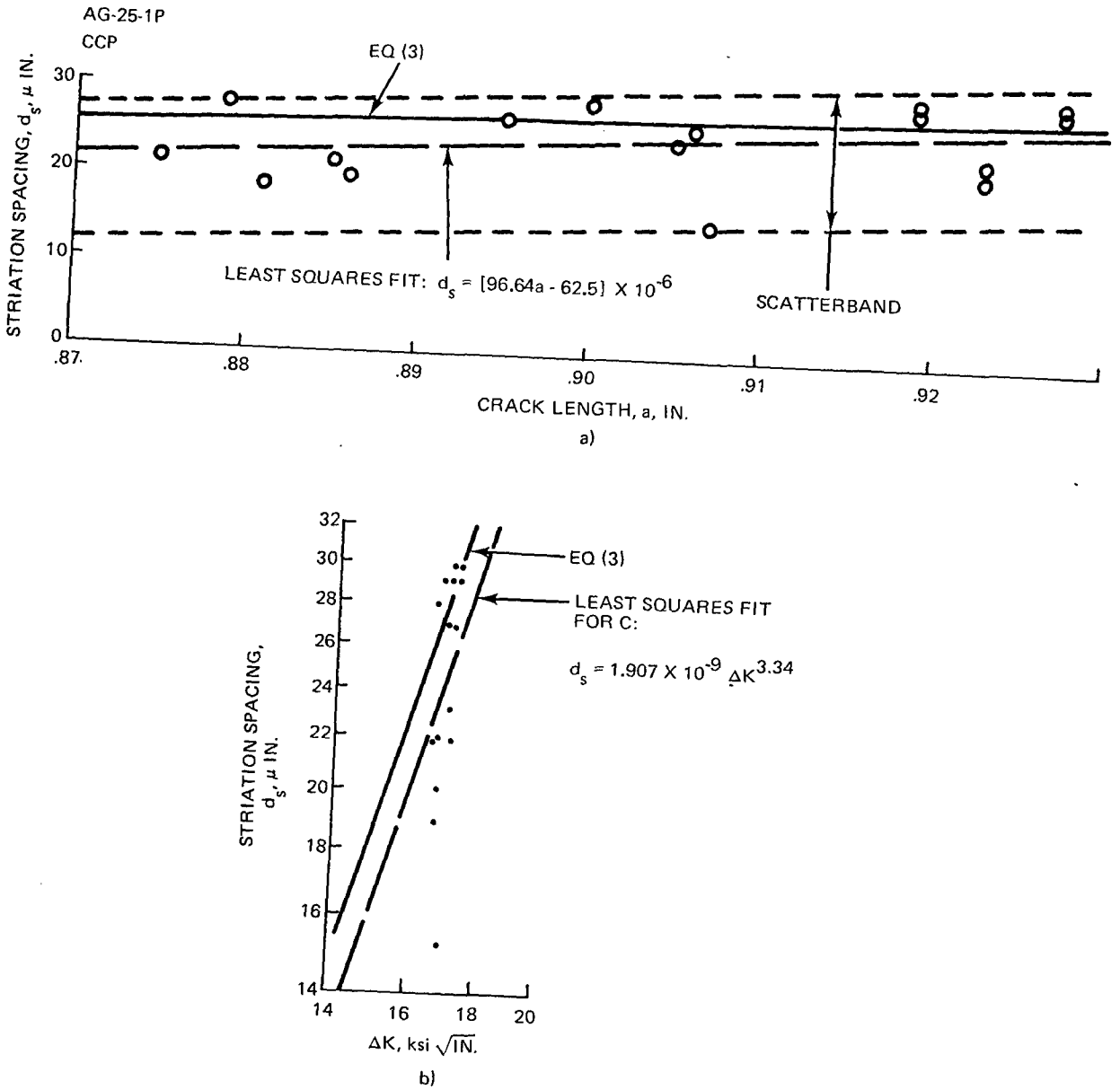


**Figure 3** Striation Spacing vs Crack Length, and Stress Intensity Range, 2219-T851 Aluminum, Constant Amplitude, R = 0.05

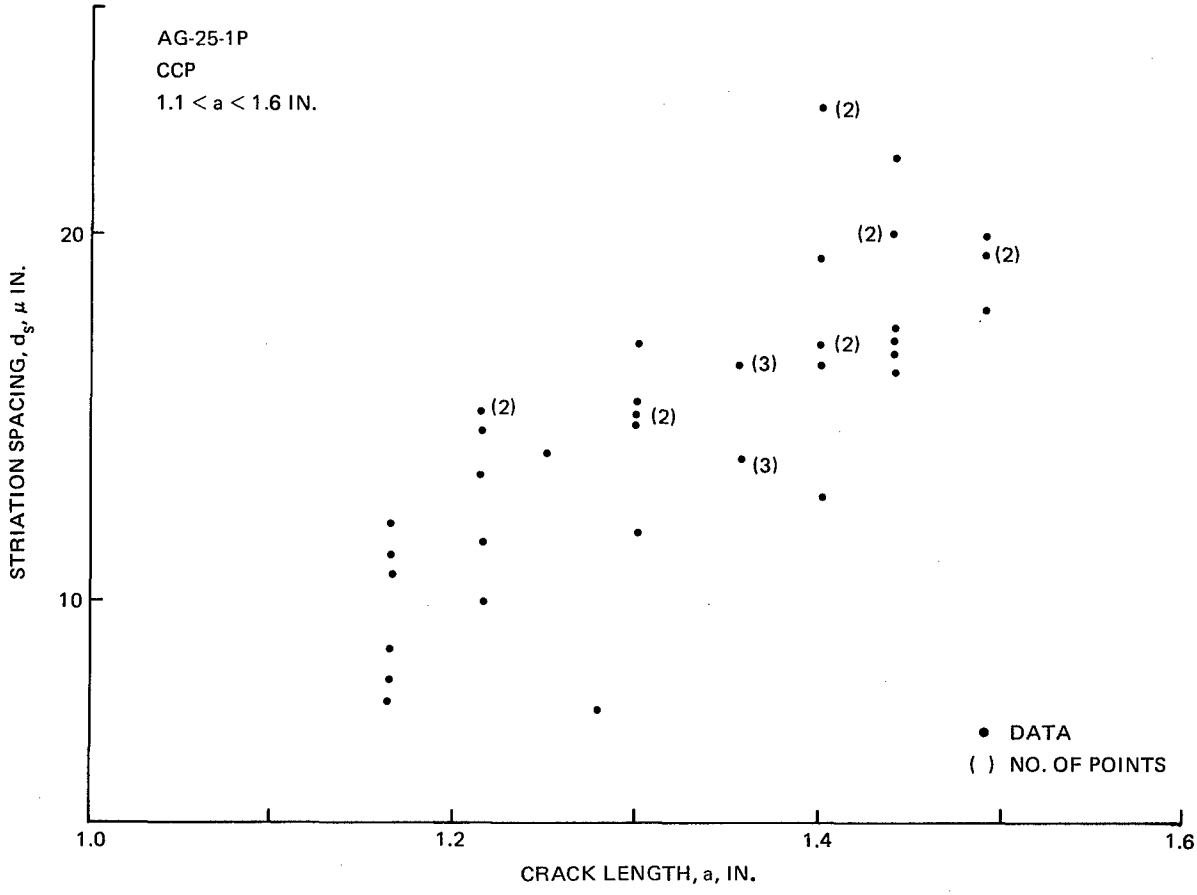


**Figure 4 Striation Spacing vs Crack Length, 2219-T851 Aluminum, Constant Amplitude R = 0.05**

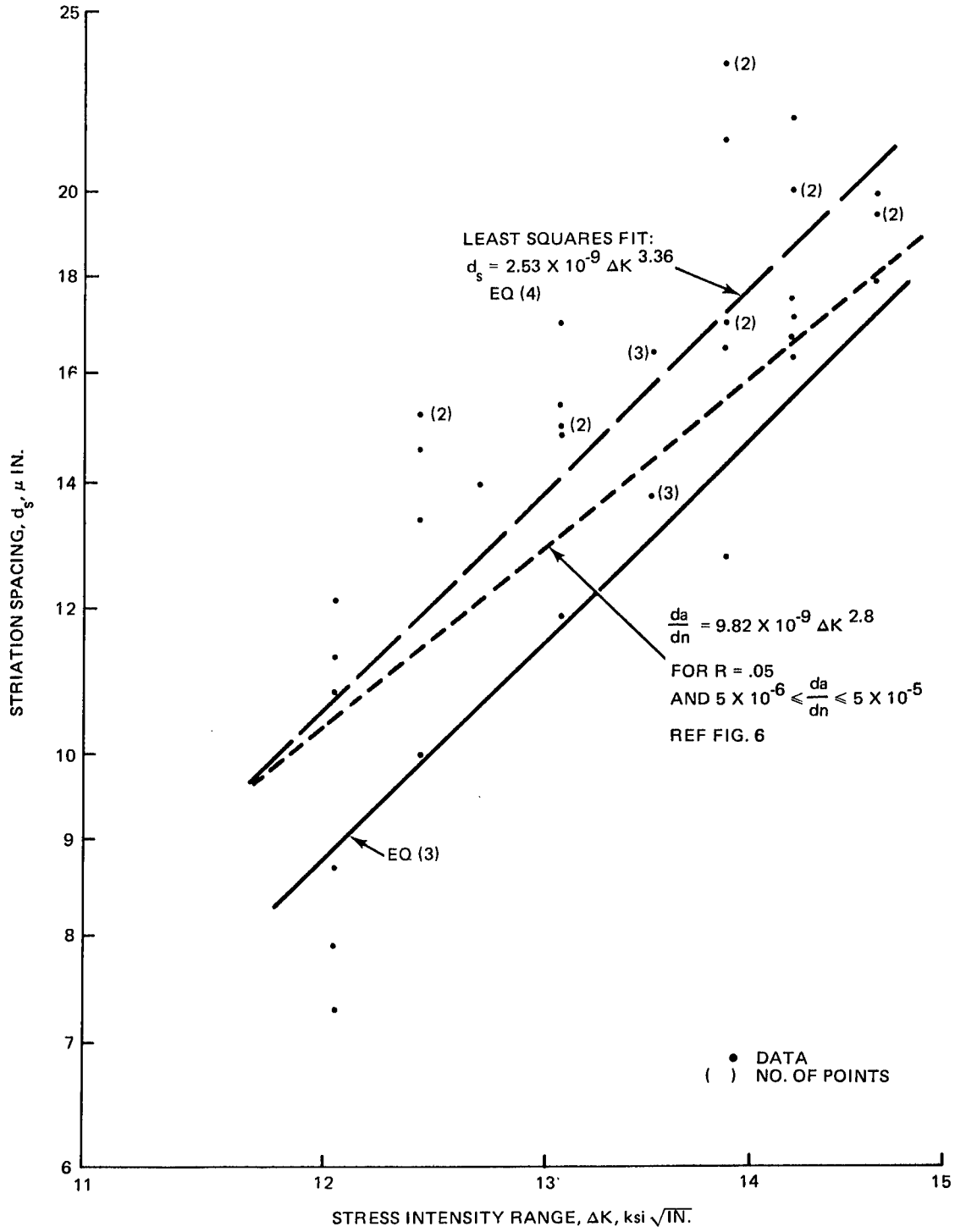


**Figure 5 Striation Spacing vs Stress Intensity Range, 2219-T851 Aluminum, Constant Amplitude, R = 0.05**

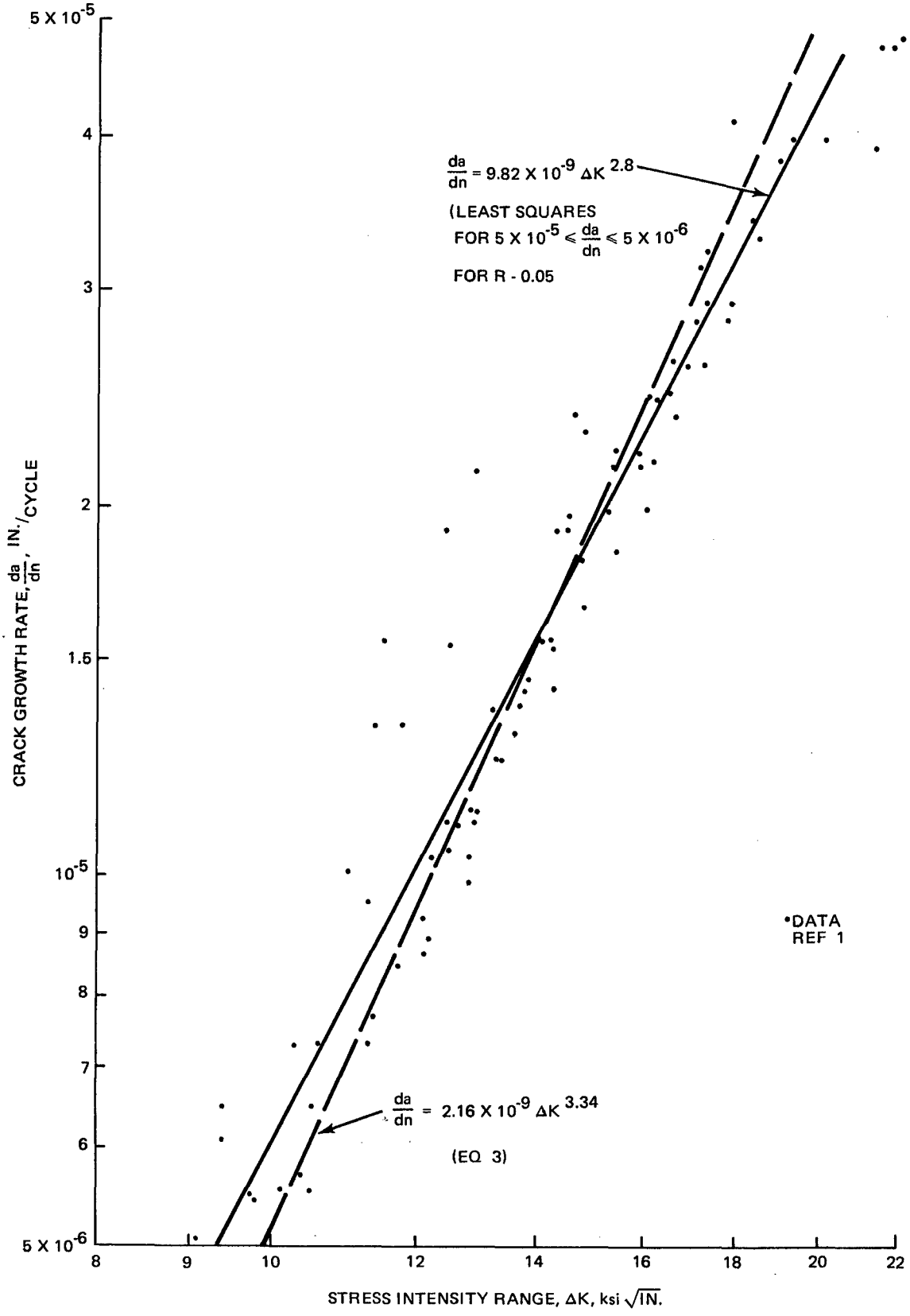


**Figure 6 Crack Growth Rate vs Stress Intensity Range, 2219-T851 Aluminum, Constant Amplitude, R = 0.05**

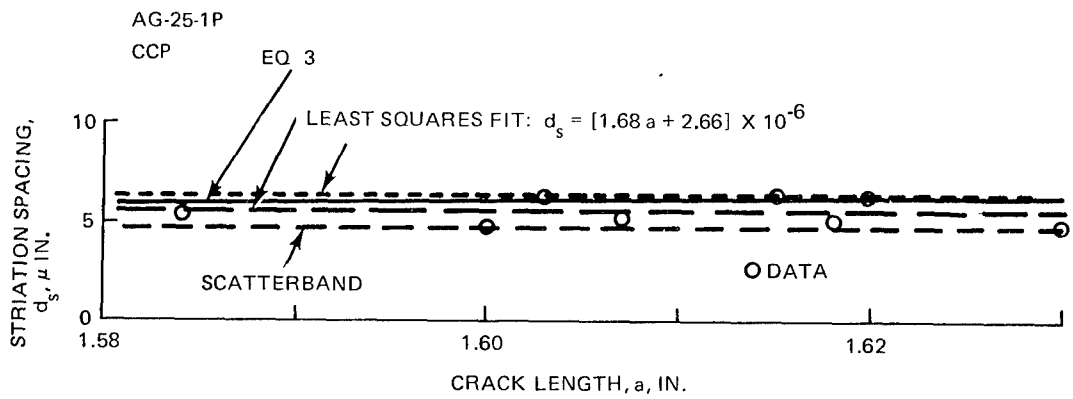


Figure 7 Striation Spacing vs Crack Length, 2219-T851 Aluminum, Constant Amplitude, R = 0.50

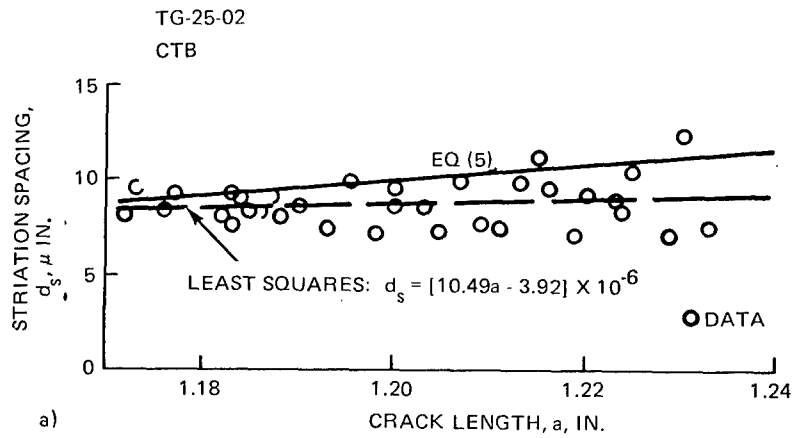


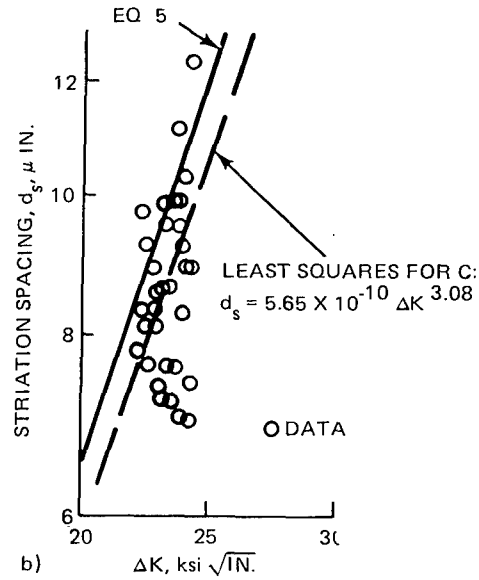


Figure 8 Striation Spacing vs Crack Length and Stress Intensity Range, Ti 6Al-4V Titanium, Constant Amplitude, R = 0.05

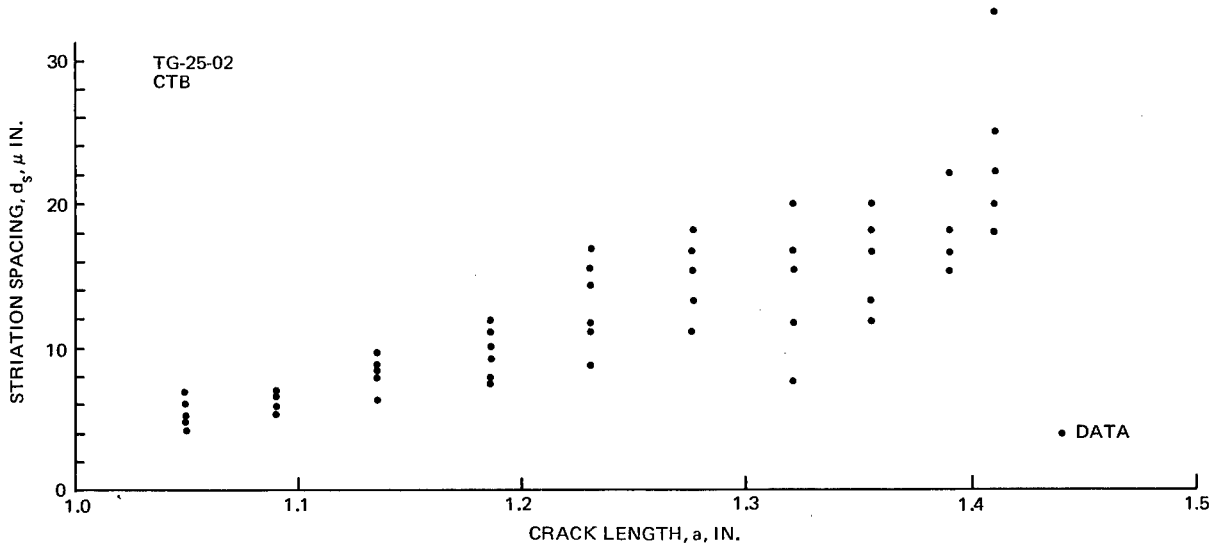


**Figure 9 Striation Spacing vs Crack Length, Ti 6Al-4V Titanium, Constant Amplitude, R = 0.05**

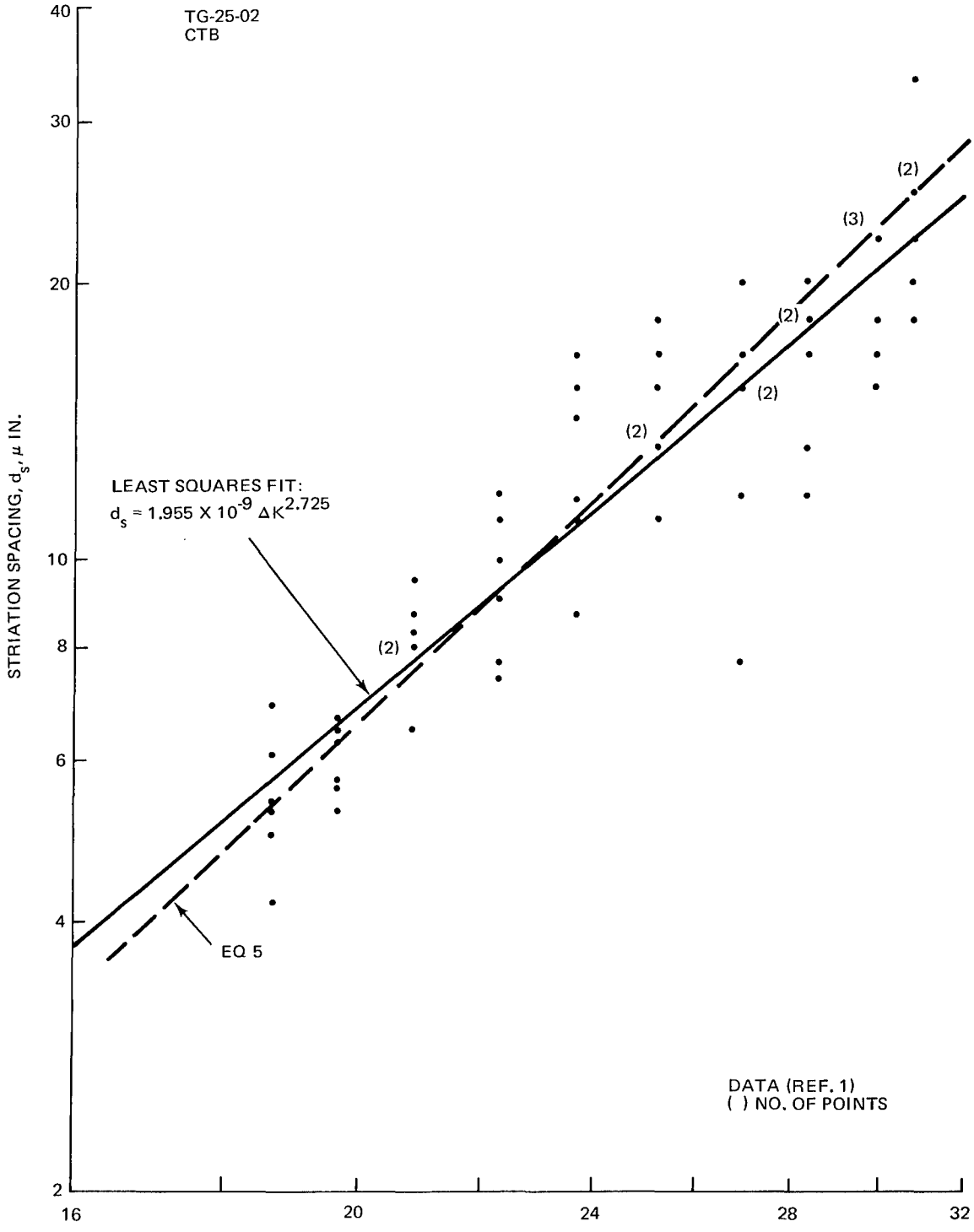


Figure 10 Striation Spacing vs Stress Intensity Range, Ti 6Al-4V Titanium Constant Amplitude, R = 0.05

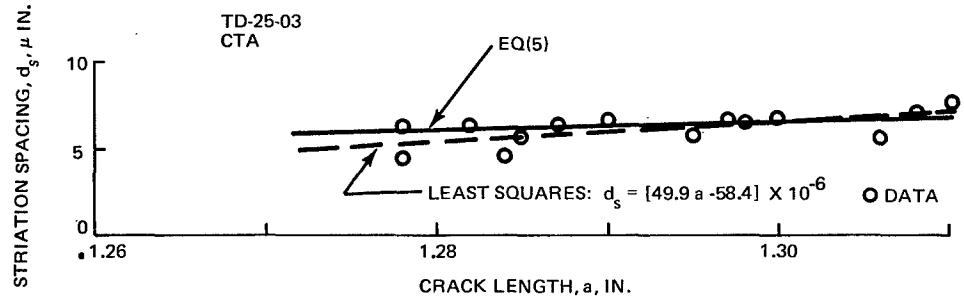


**Figure 11 Striation Spacing vs Crack Length, Ti 6Al-4V Titanium, Constant Amplitude, R = 0.50.**

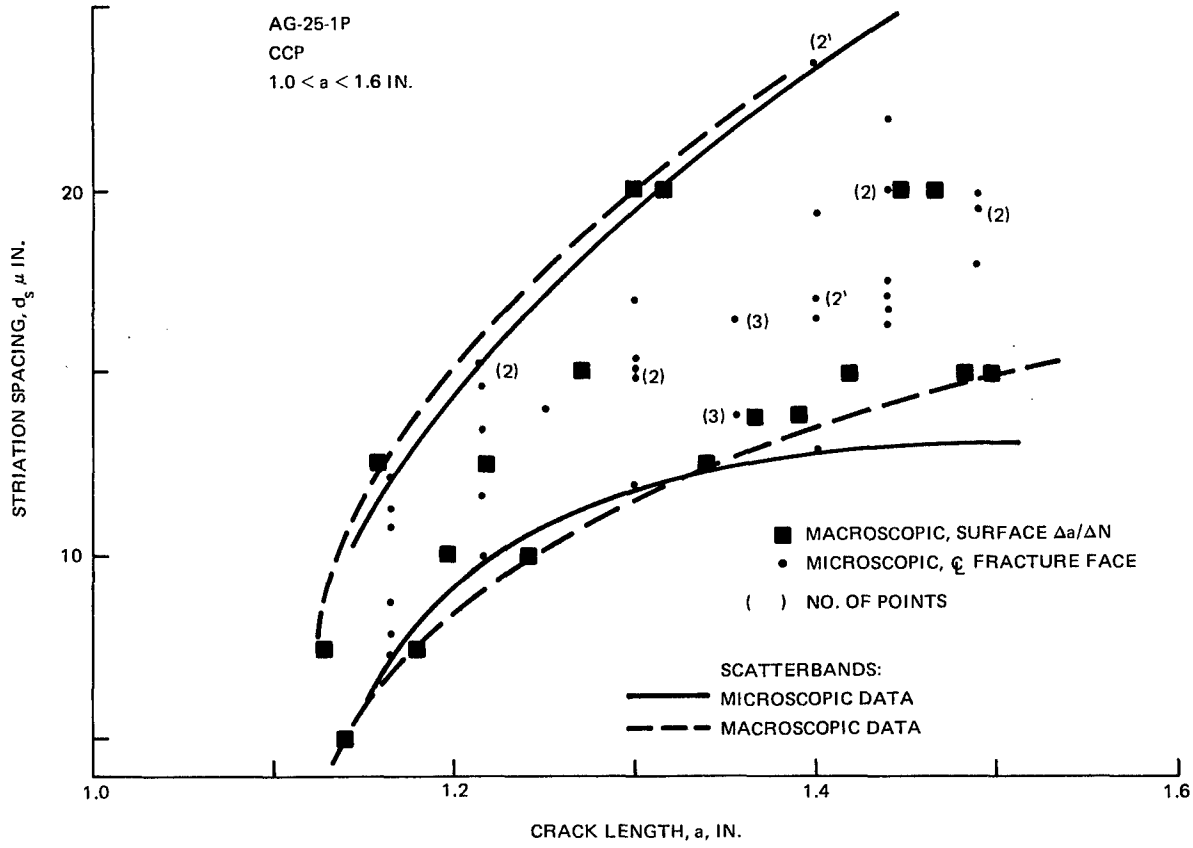


**Figure 12 Striation Spacing and Δa/Δn vs Crack Length, 2219-T851 Aluminum, Constant Amplitude, R = 0.05**

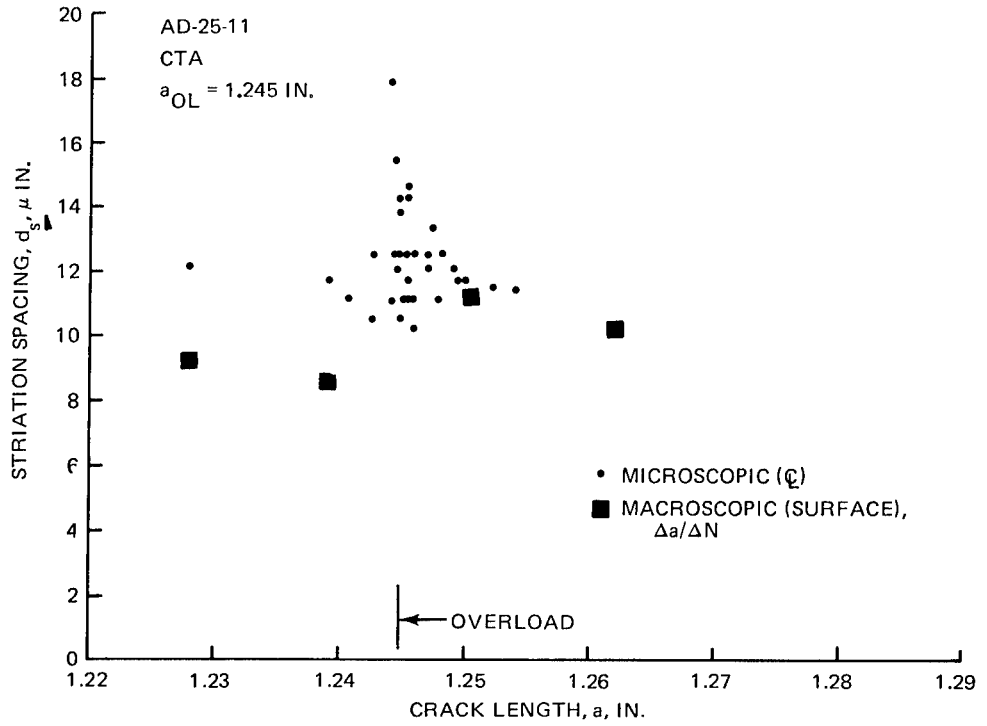


**Figure 13 Striation Spacing and Δa/ΔN vs Crack Length, 2219-T851 Aluminum, O/L = 1.25**

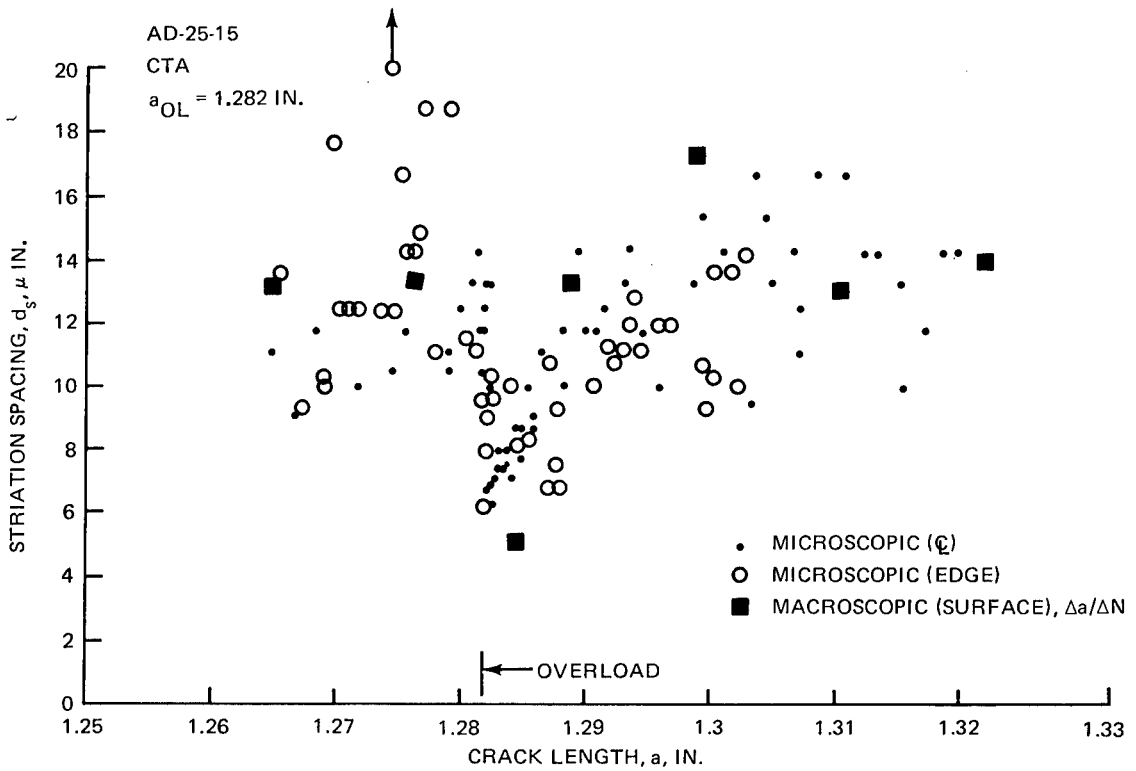


**Figure 14 Striation Spacing and Δa/ΔN vs Crack Length, 2219-T851 Aluminum, O/L = 1.5**

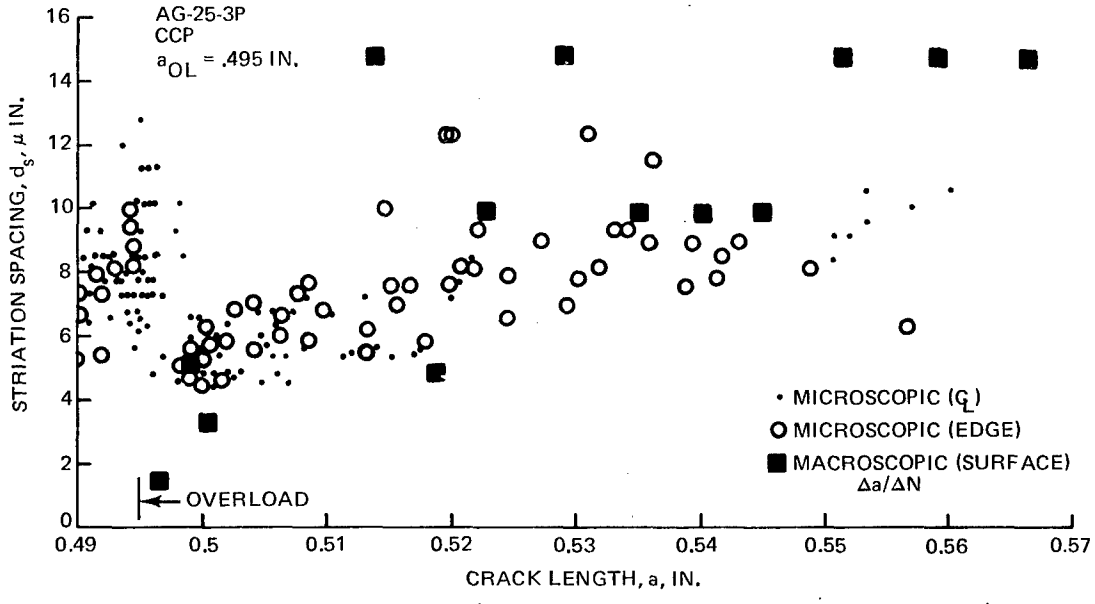


**Figure 15 Striation Spacing and Δa/ΔN vs Crack Length, 2219-T851 Aluminum O/L = 1.8**

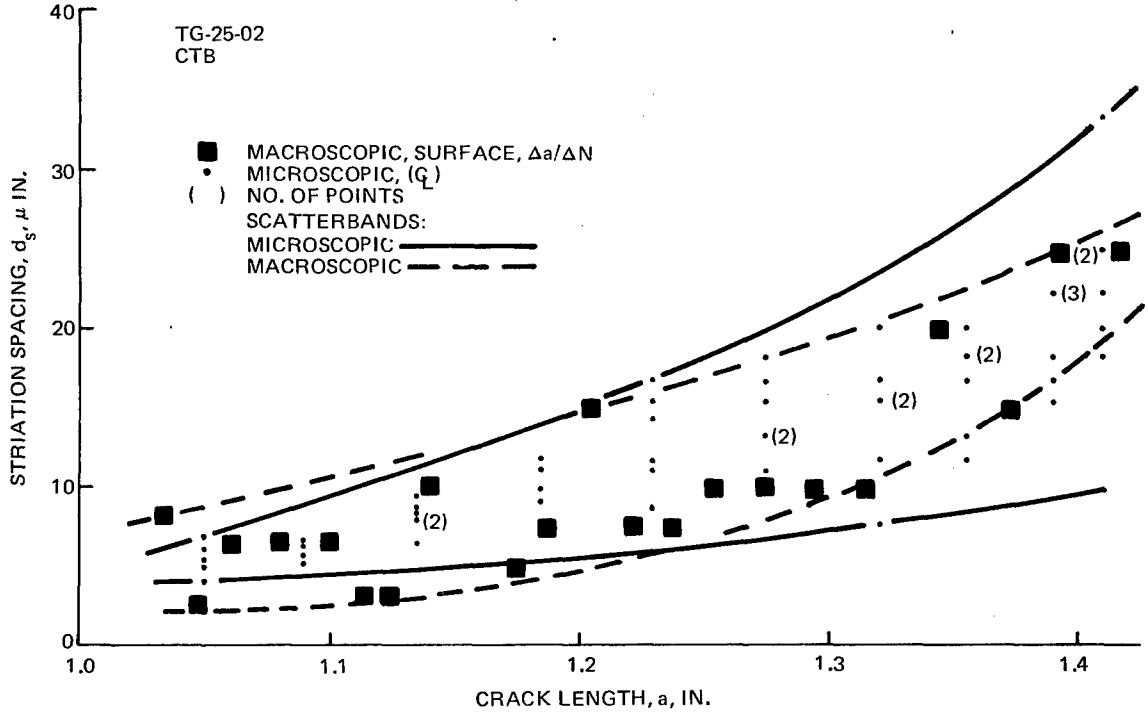


**Figure 16 Striation Spacing and Δa/ΔN vs Crack Length, Ti 6Al-4V Titanium, Constant Amplitude, R = 0.05**

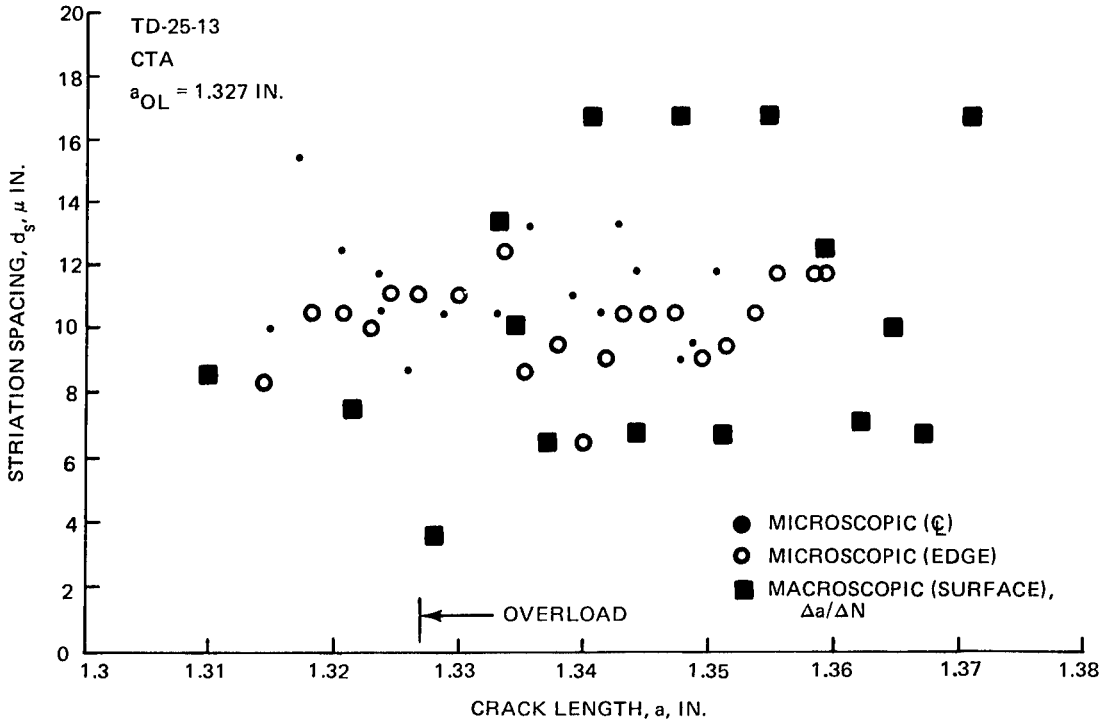


**Figure 17 Striation Spacing and Δa/ΔN vs Crack Length, Ti 6Al-4V Titanium, O/L = 1.25**

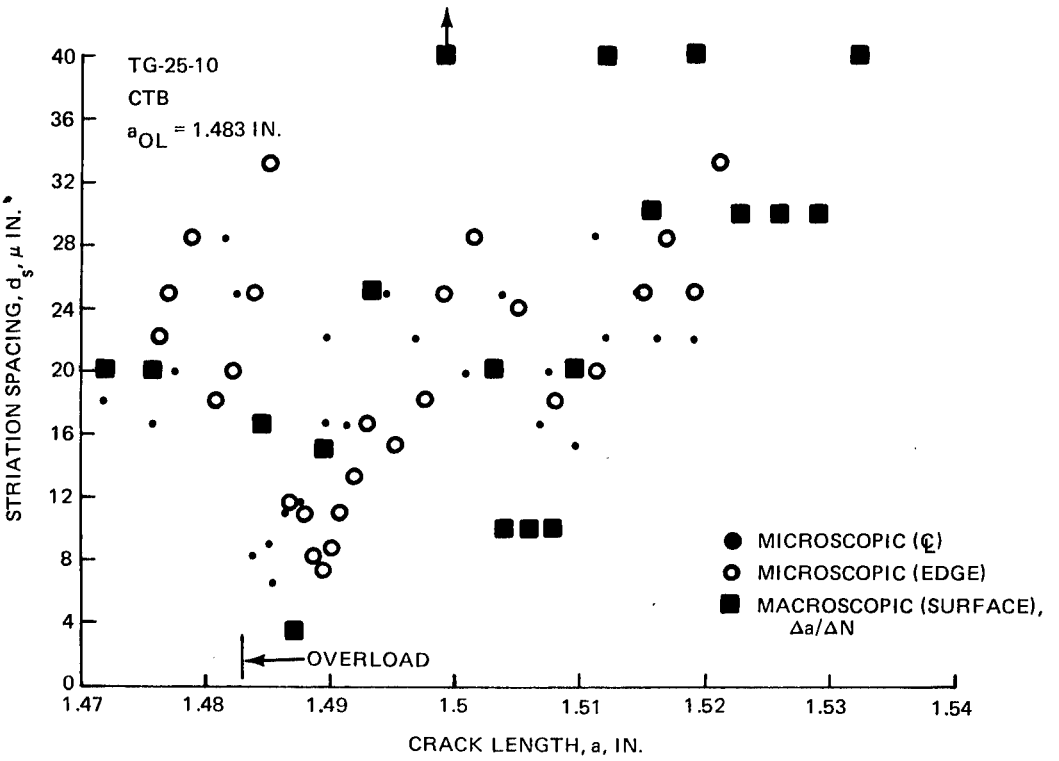


**Figure 18 Striation Spacing and Δa/ΔN vs Crack Length, Ti 6Al-4V Titanium, O/L = 1.5**

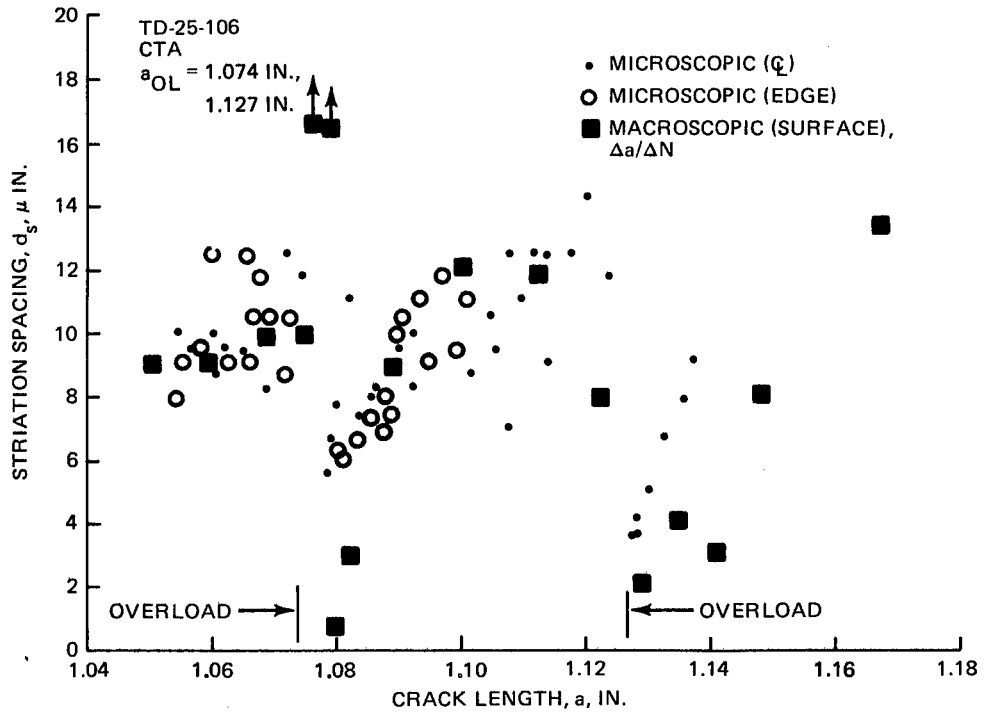


**Figure 19 Striation Spacing and Δa/ΔN vs Crack Length, O/L = 1.8, Ti 6AI-4V Titanium**

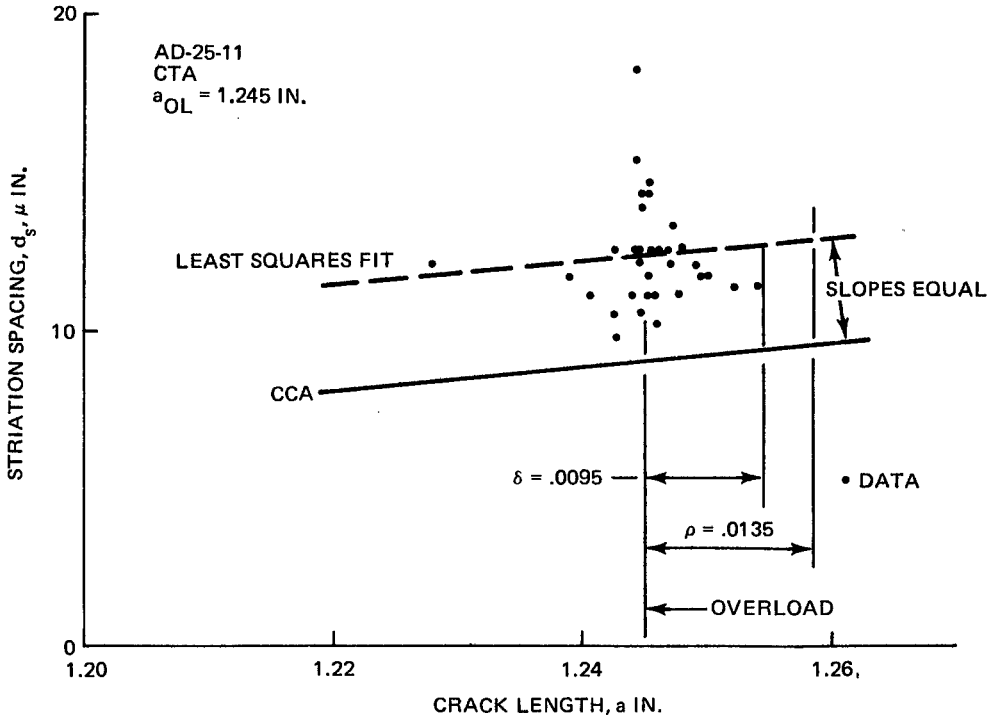


**Figure 20 Affected Crack Length, Centerline, O/L = 1.25, 2219-T851 Aluminum**

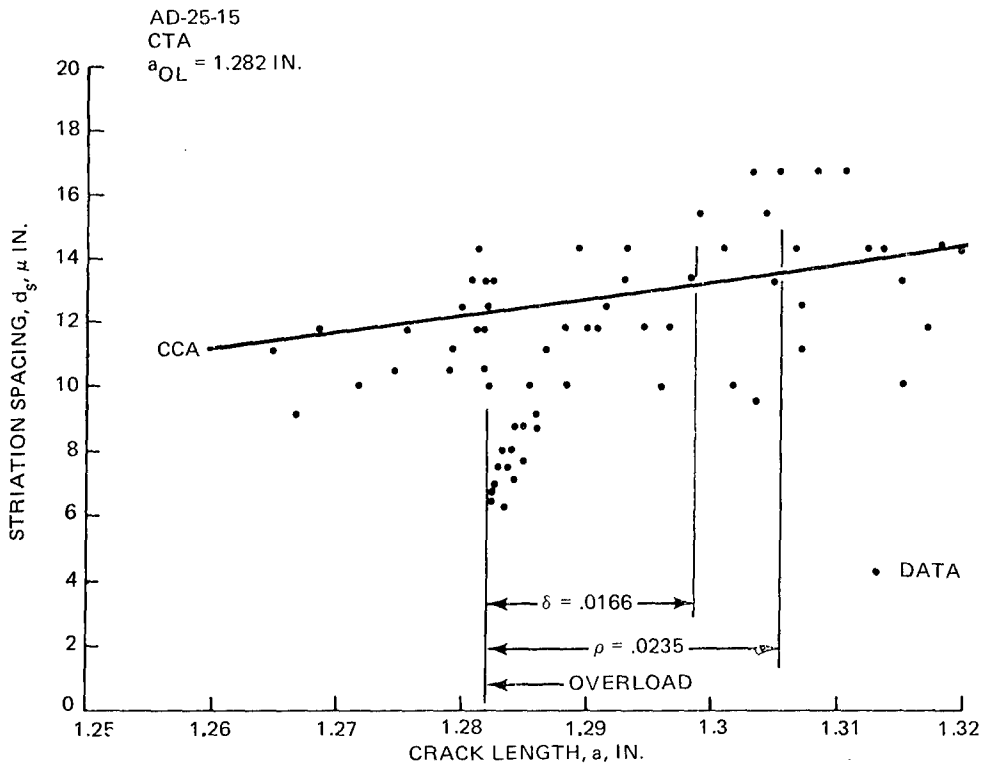


**Figure 21 Affected Crack Length, Centerline, O/L = 1.5, 2219-T851 Aluminum**

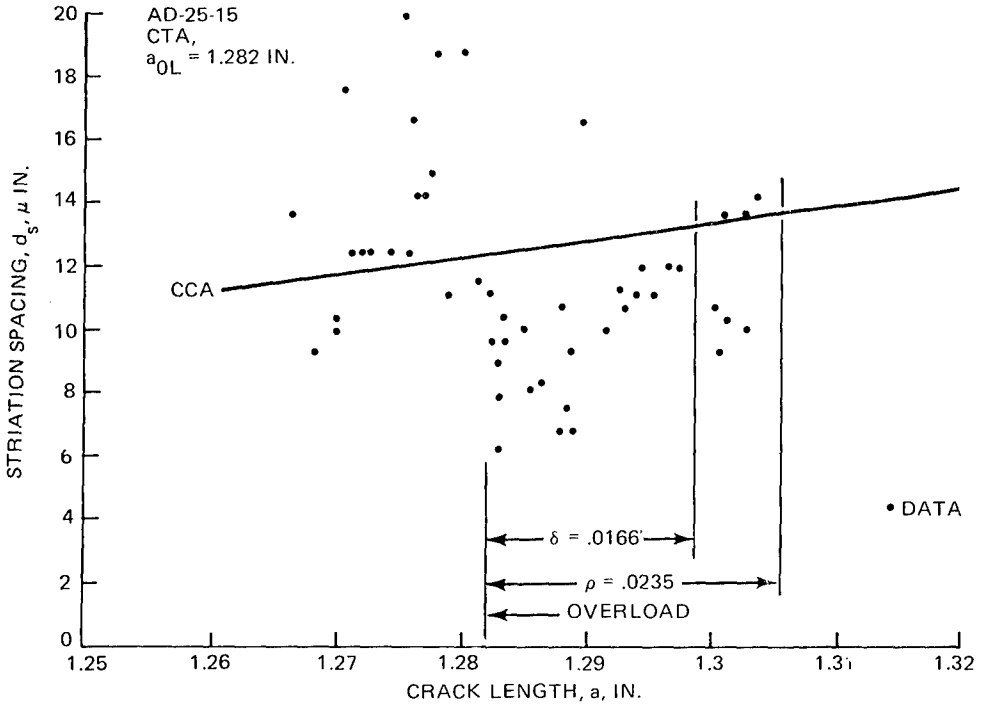


**Figure 22 Affected Crack Length, Edge, O/L = 1.5, 2219-T851 Aluminum**

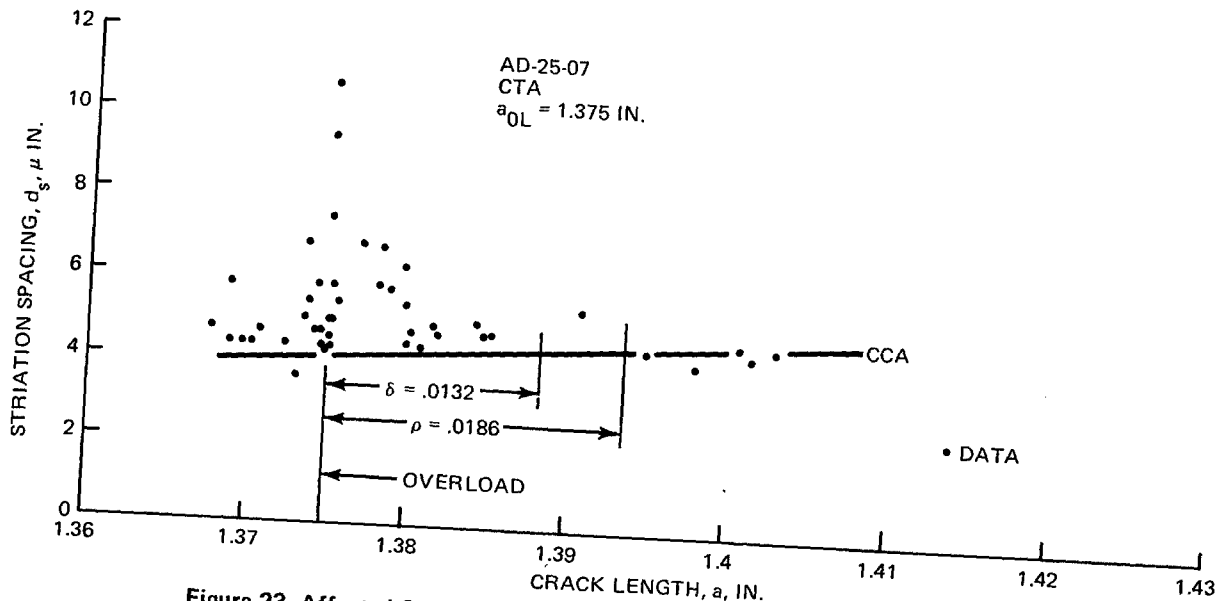


**Figure 23 Affected Crack Length, Centerline, O/L = 1.8, 2219-T851 Aluminum**

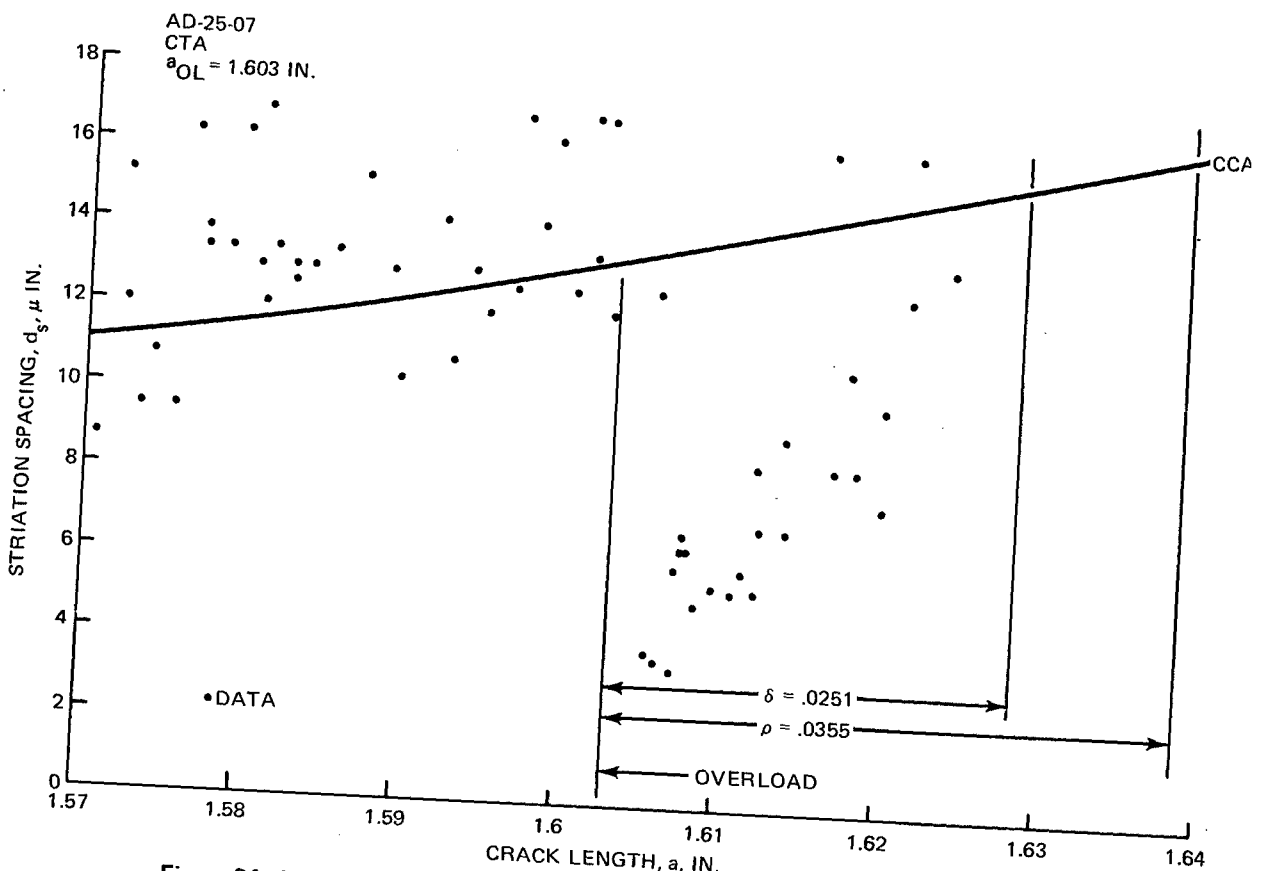


**Figure 24 Affected Crack Length, Centerline, O/L = 1.8, 2219-T851 Aluminum**

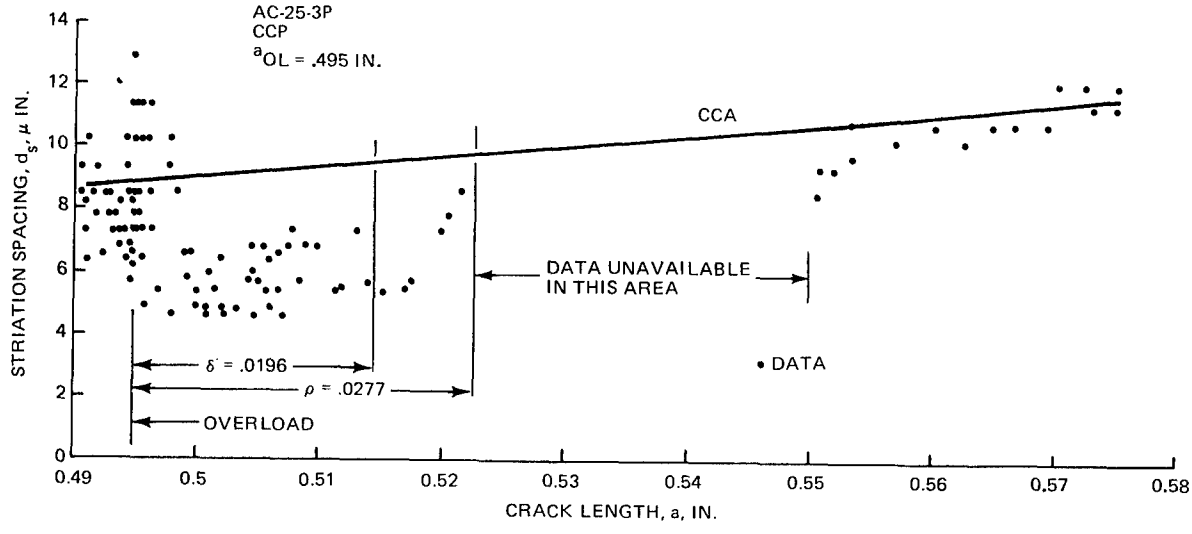


**Figure 25 Affected Crack Length, Centerline, O/L = 1.8, 2219-T851 Aluminum**

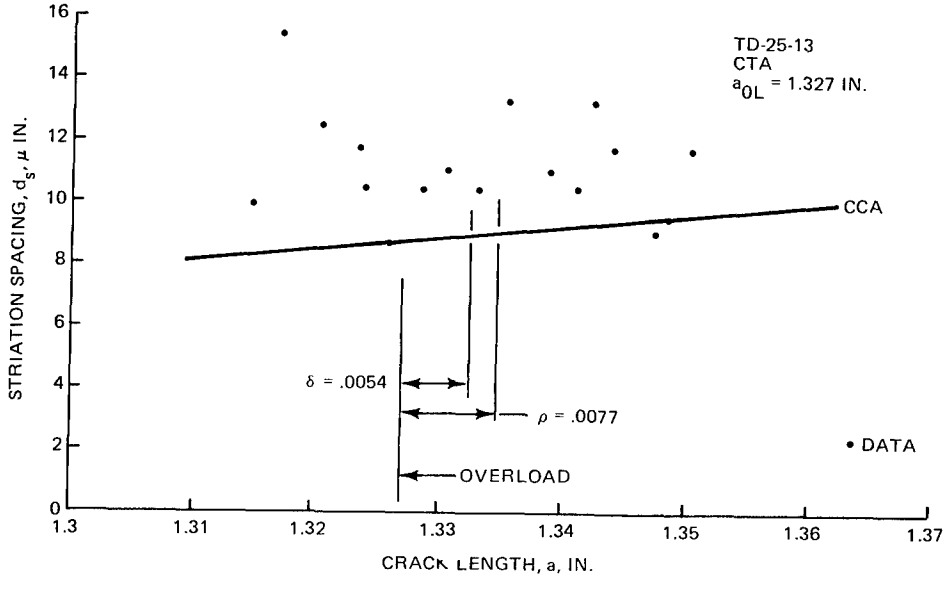


**Figure 26 Affected Crack Length, Centerline, O/L = 1.25, Ti 6Al-4V Titanium**

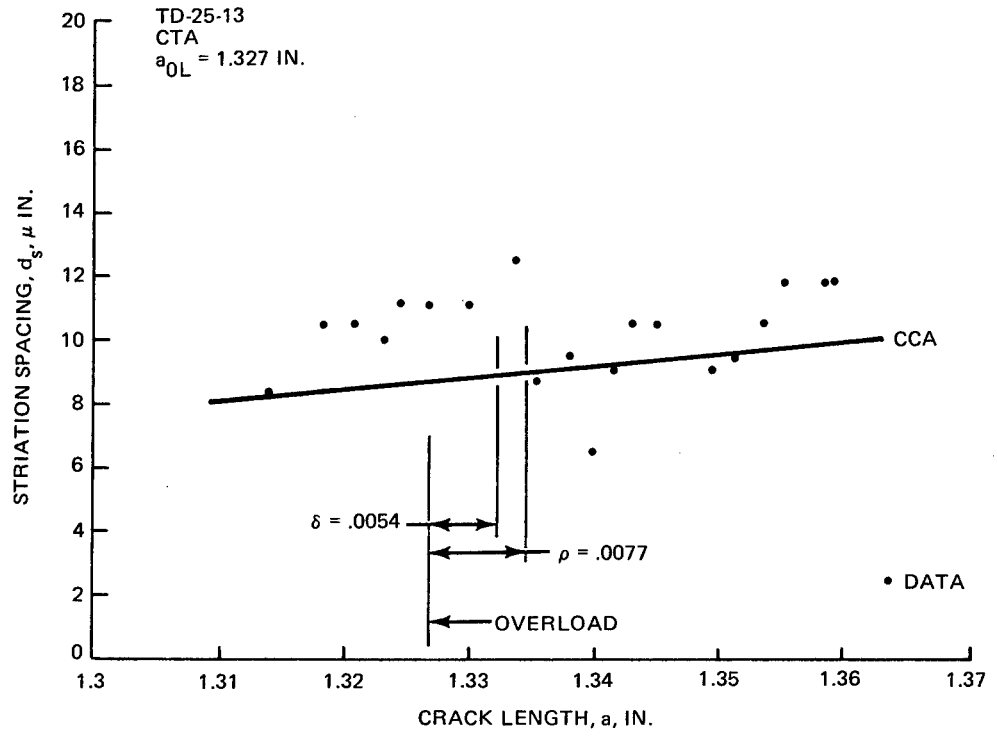


**Figure 27 Affected Crack Length, Edge, O/L = 1.25, Ti 6Al-4V Titanium**

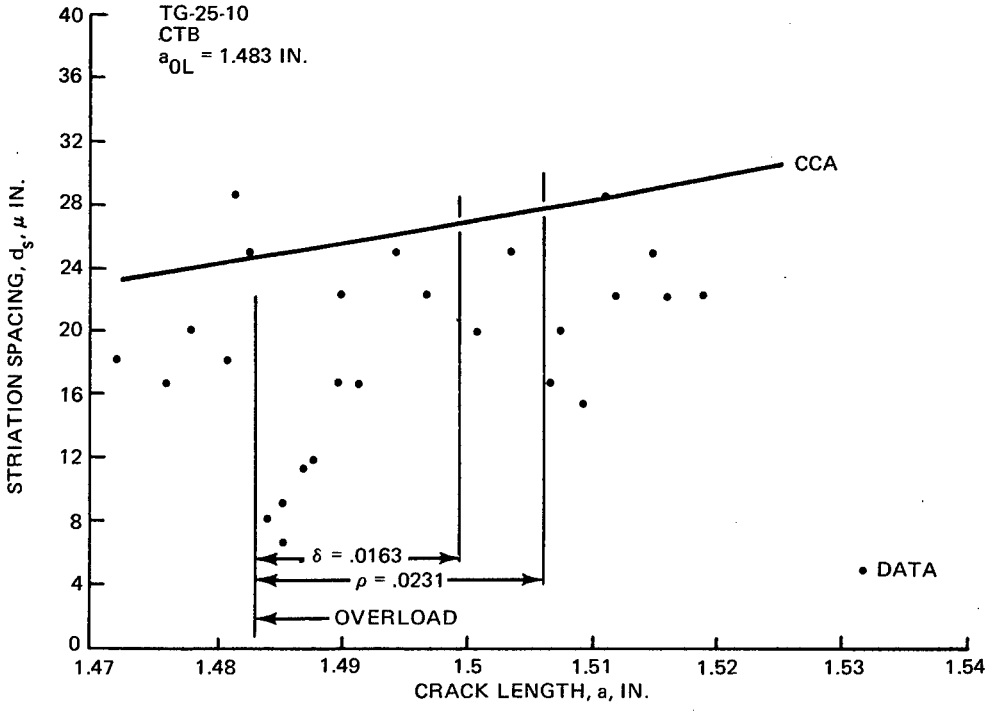


**Figure 28 Affected Crack Length, Centerline, O/L = 1.5, Ti 6Al-4V Titanium**

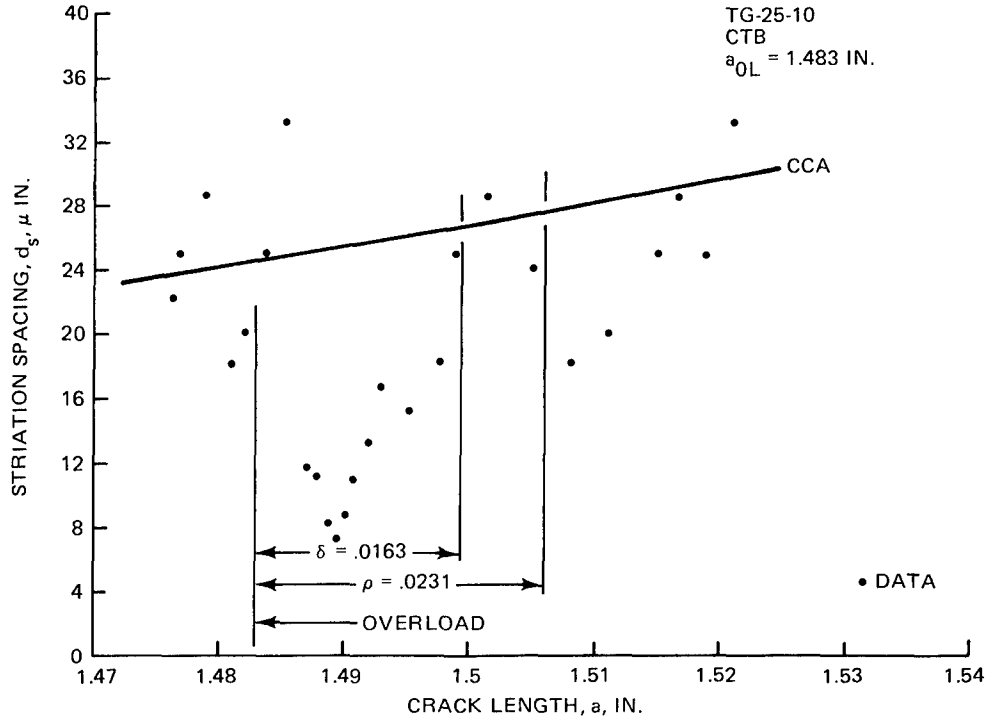


**Figure 29 Affected Crack Length, Edge, O/L = 1.5, Ti 6Al-4V Titanium**

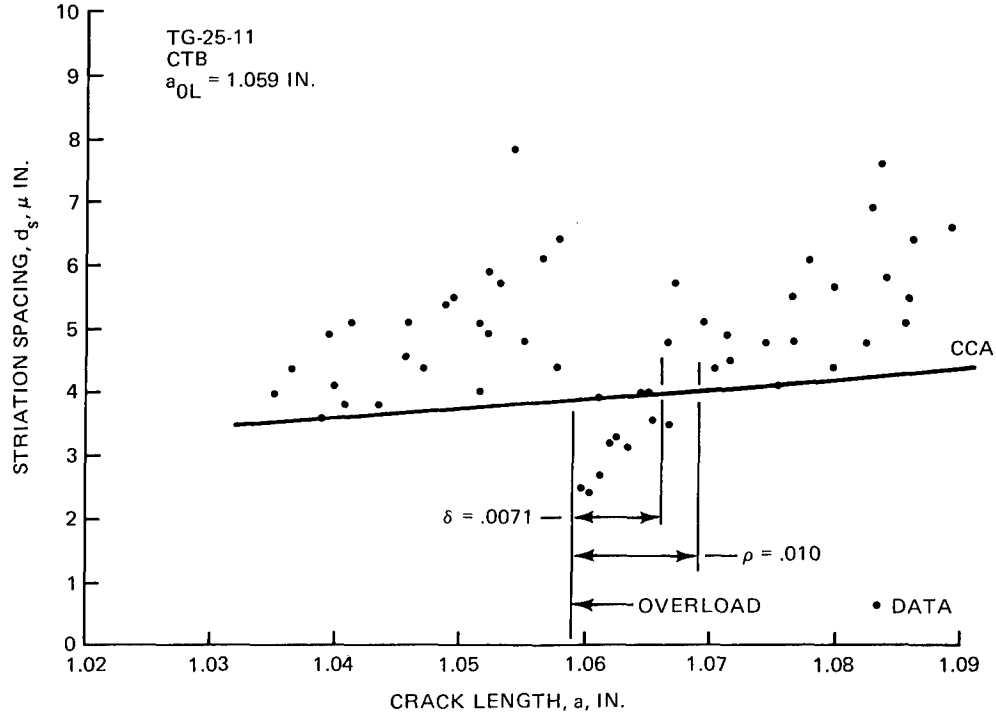


**Figure 30 Affected Crack Length, Centerline, O/L = 1.8, Ti 6Al-4V Titanium**

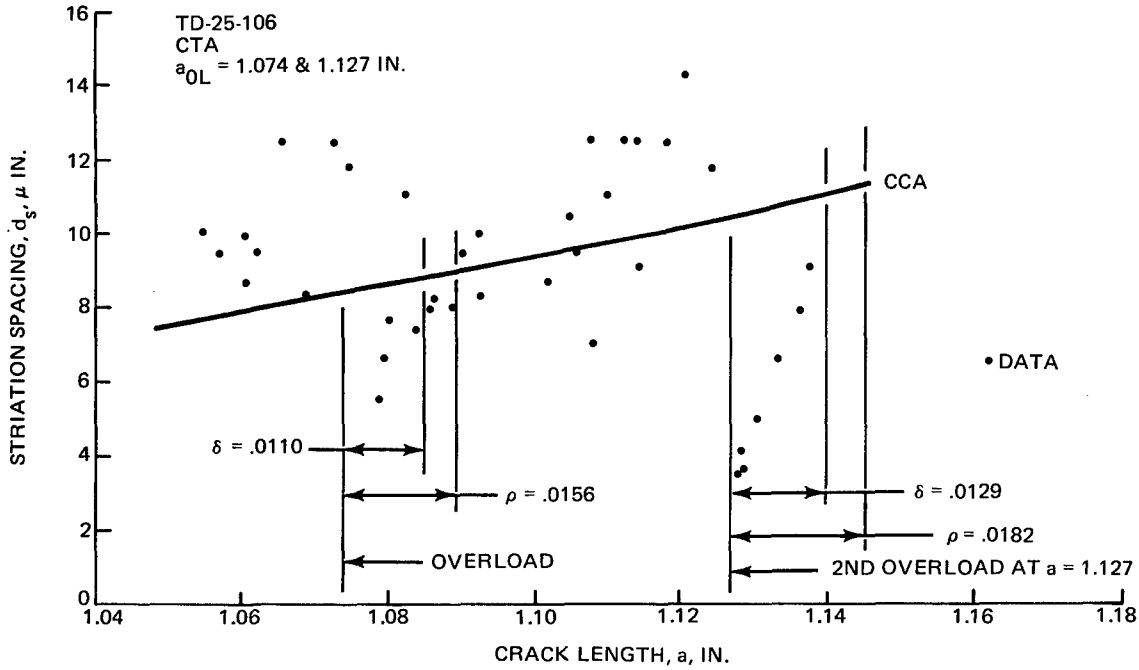


**Figure 31 Affected Crack Length, Centerline, O/L = 1.8, Ti 6Al-4V Titanium**

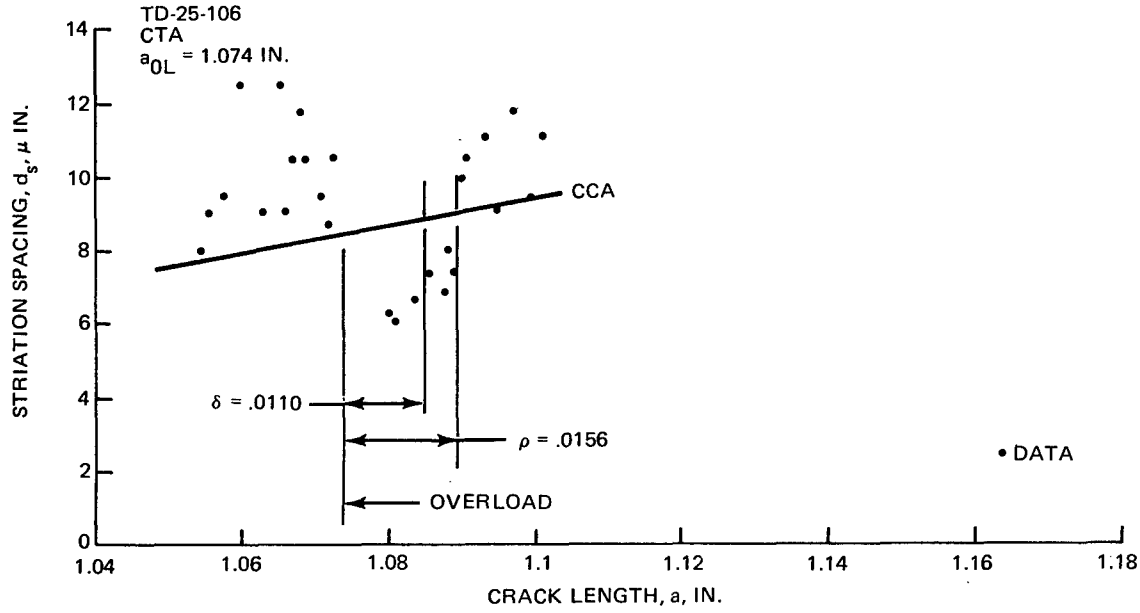


**Figure 32 Affected Crack Length, Edge, O/L = 1.8, Ti 6Al-4V Titanium**

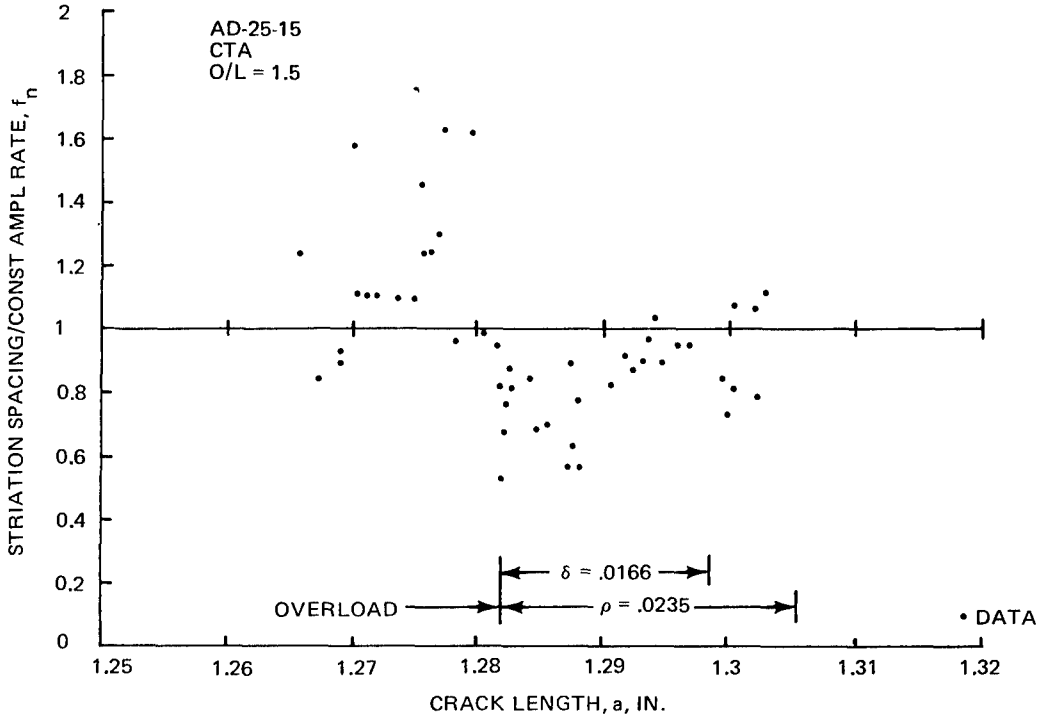


**Figure 33 Typical Plot of $f_n$ vs Crack Length**

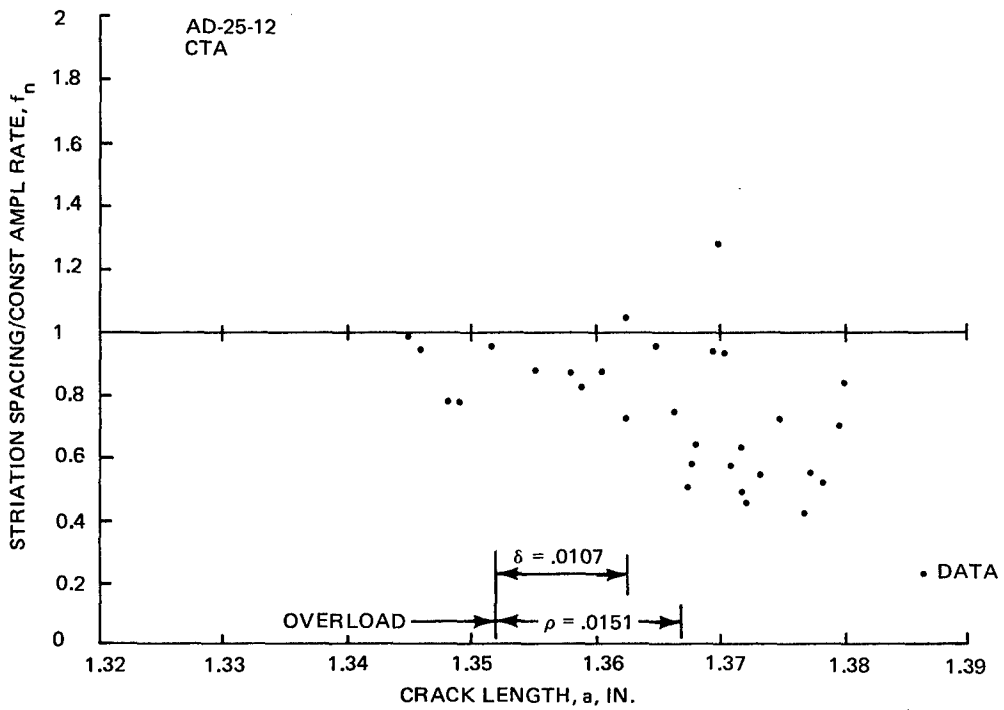


**Figure 34 Delayed Retardation, $a_{OL}$ = 1.352 In., Centerline, O/L = 1.25, 2219-T851 Aluminum**

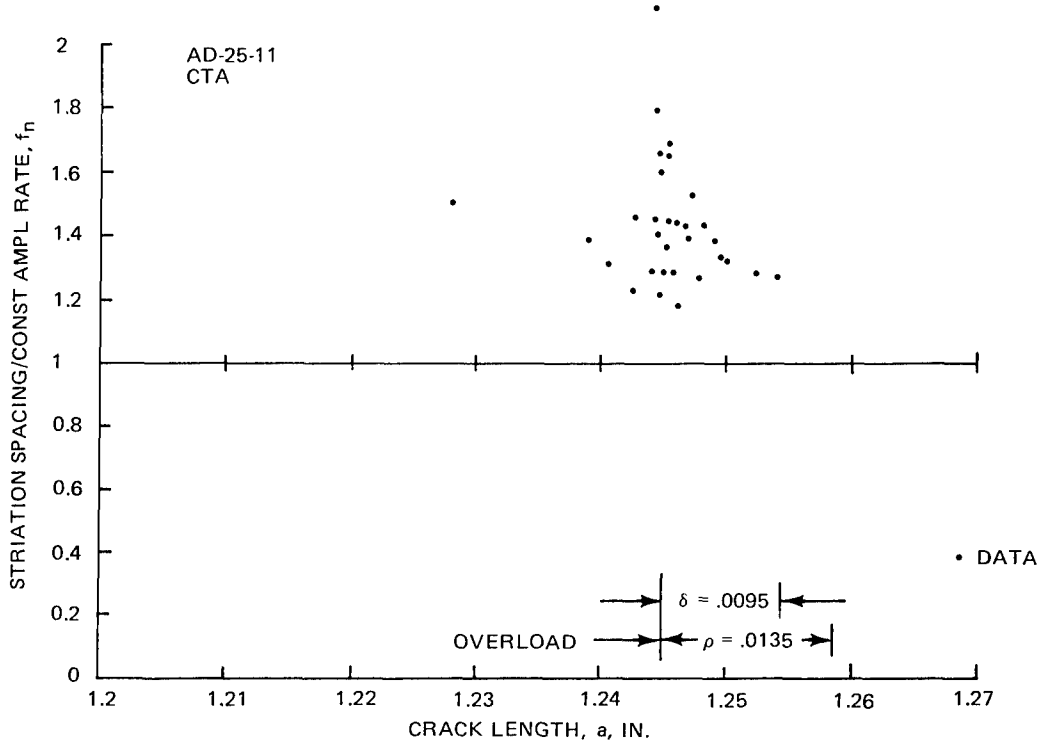


**Figure 35 Delayed Retardation, $a_{OL}$ = 1.245 In., Centerline, O/L = 1.25, 2219-T851 Aluminum**

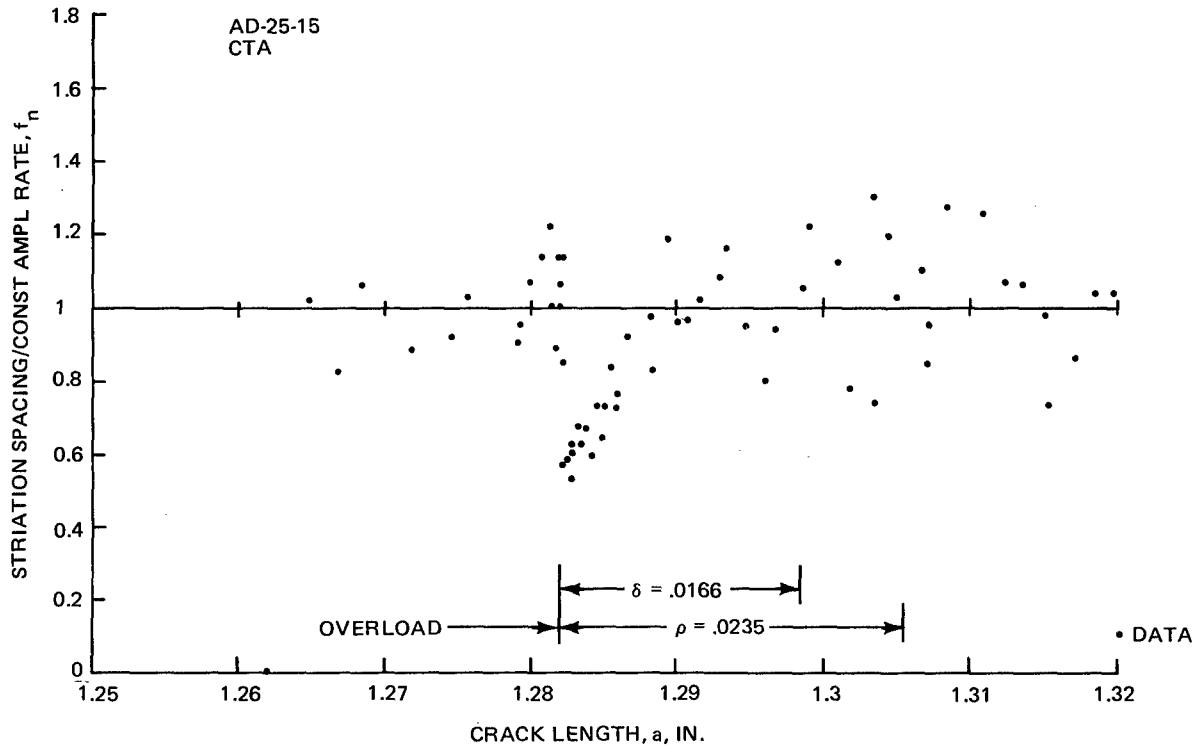


**Figure 36 Delayed Retardation, $a_{OL}$ = 1.282 In., Centerline, O/L = 1.5, 2219-T851 Aluminum**

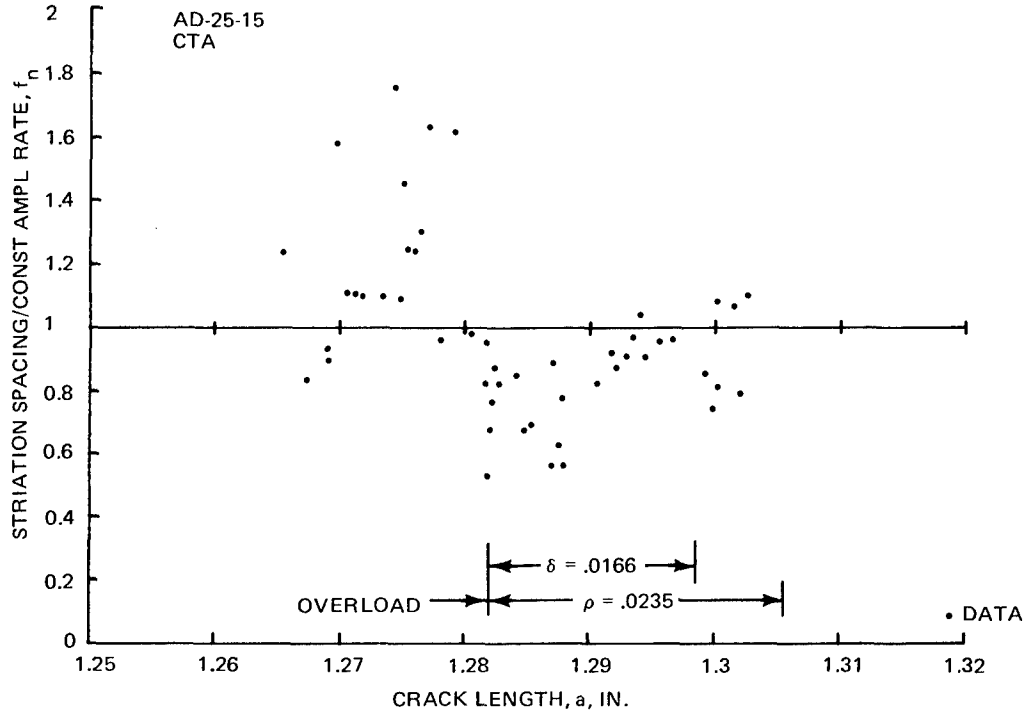


**Figure 37 Delayed Retardation, $a_{OL}$ = 1.282 In., Edge, O/L = 1.5, 2219-T851 Aluminum**

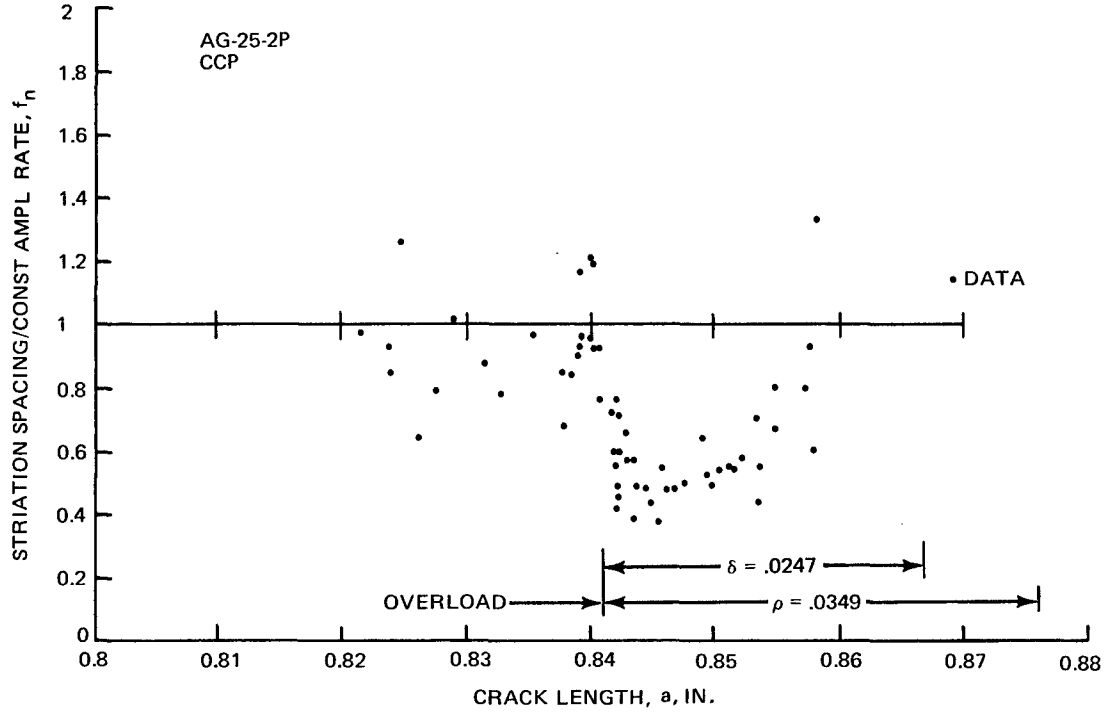


**Figure 38 Delayed Retardation, $a_{OL}$ = 0.841 In., Centerline, O/L = 1.5, 2219-T851 Aluminum**

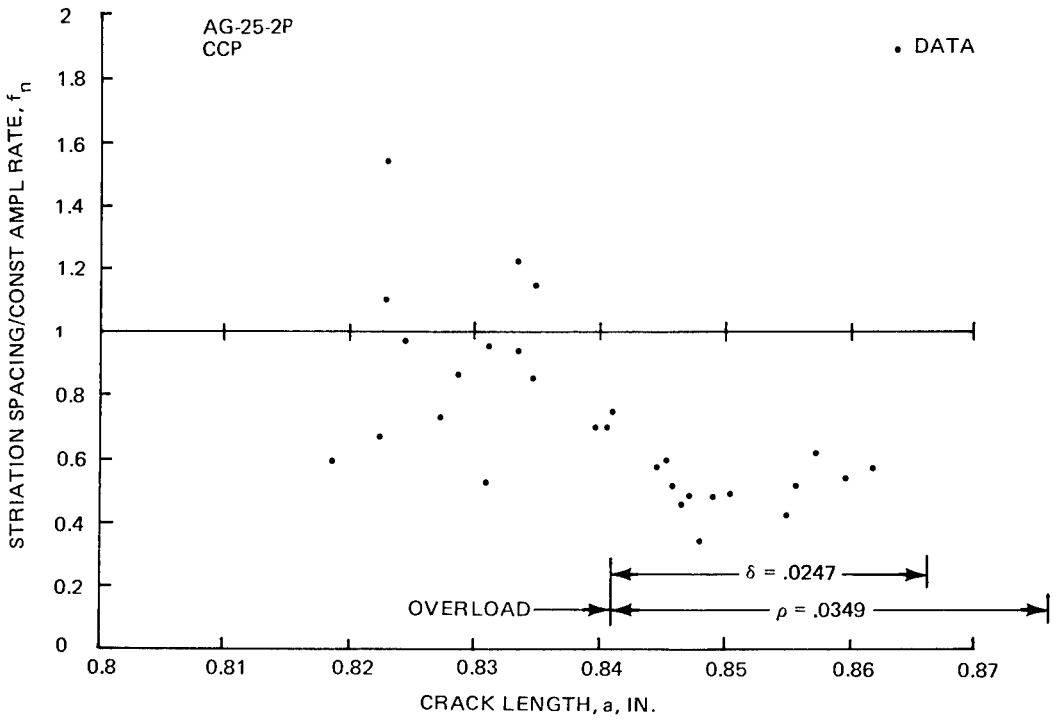


**Figure 39 Delayed Retardation, $a_{OL}$ = 0.841 In., Edge, O/L = 1.5, 2219-T851 Aluminum**

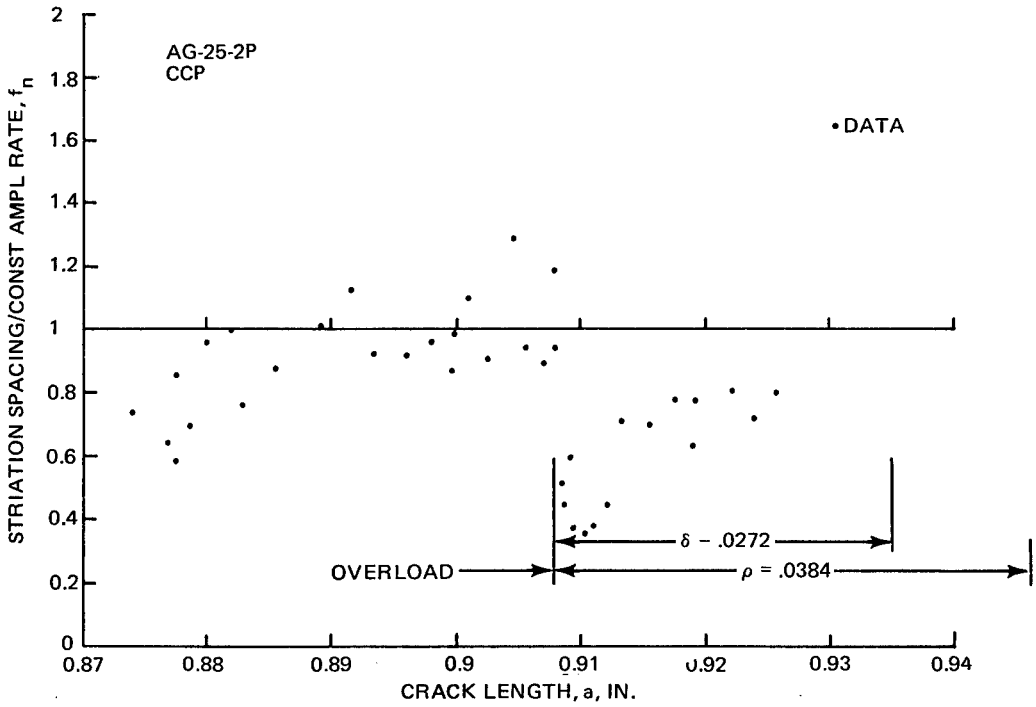


**Figure 40 Delayed Retardation, $a_{OL}$ = 0.908 In., Centerline, O/L = 1.5, 2219-T851 Aluminum**

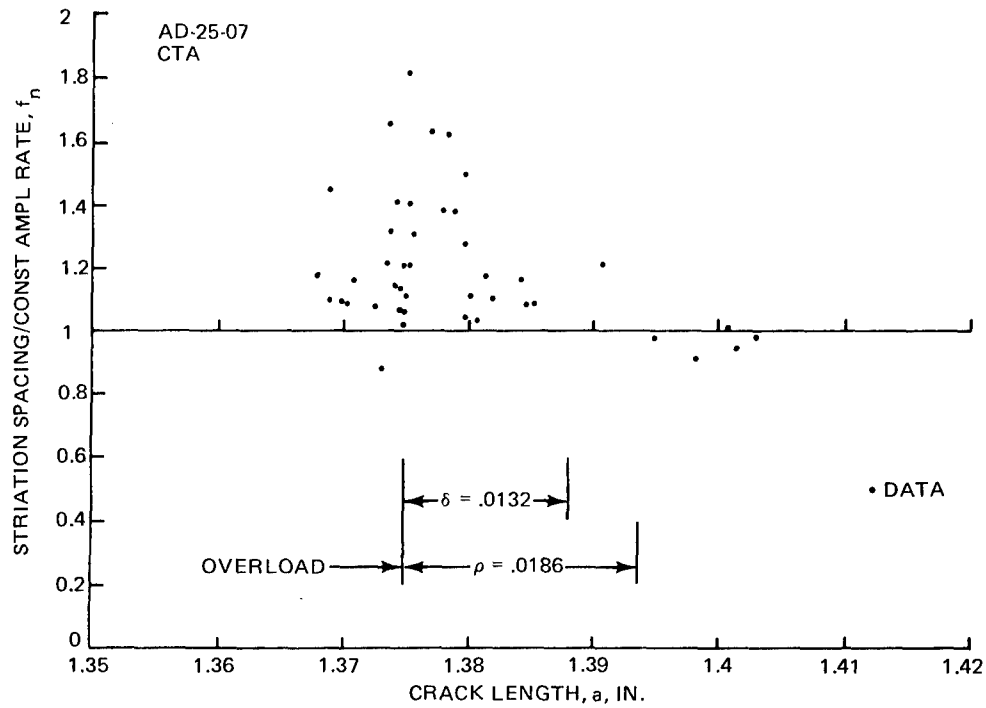


**Figure 41 Delayed Retardation, $a_{OL}$ = 1.375 In., Centerline, O/L = 1.8, 2219-T851 Aluminum**

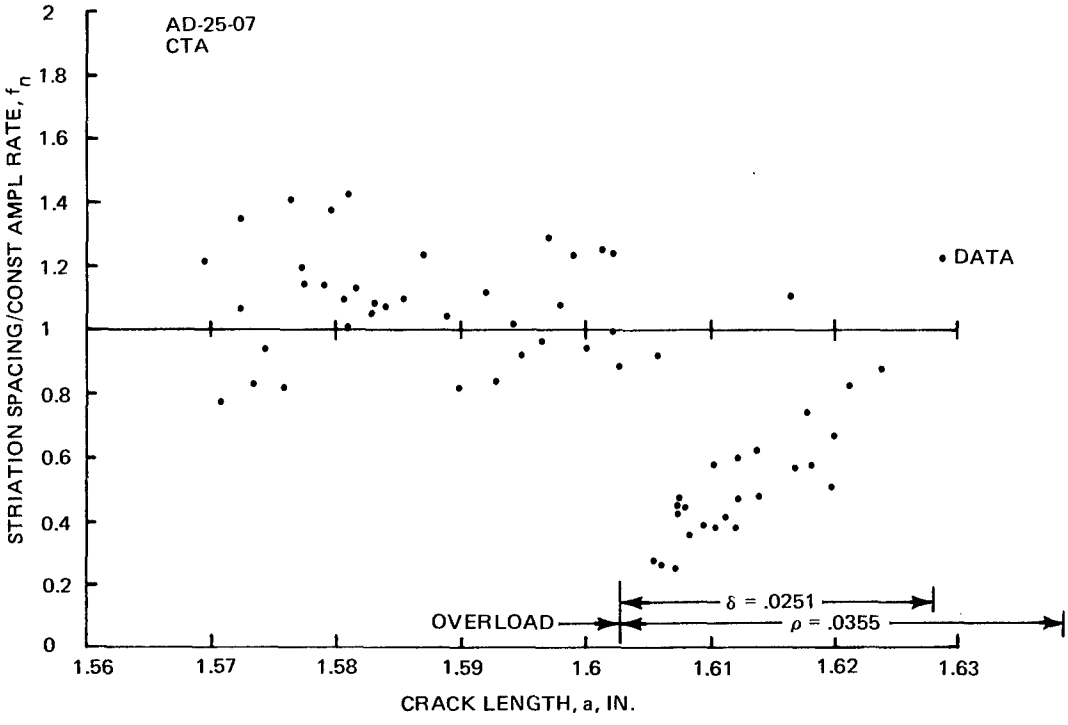


**Figure 42 Delayed Retardation, $a_{OL}$ = 1.603 In., Centerline, O/L = 1.8, 2219-T851 Aluminum**

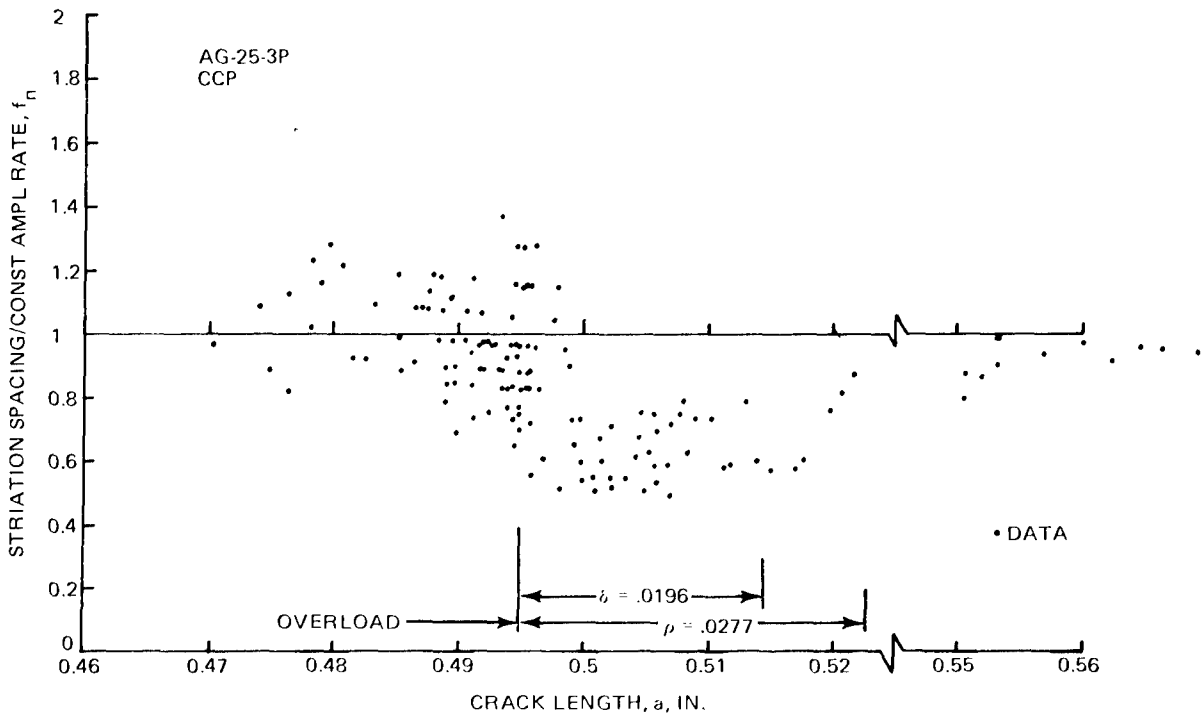


**Figure 43** Delayed Retardation, $a_{OL}$ = 0.495 In., Centerline, O/L = 1.8, 2219-T851 Aluminum

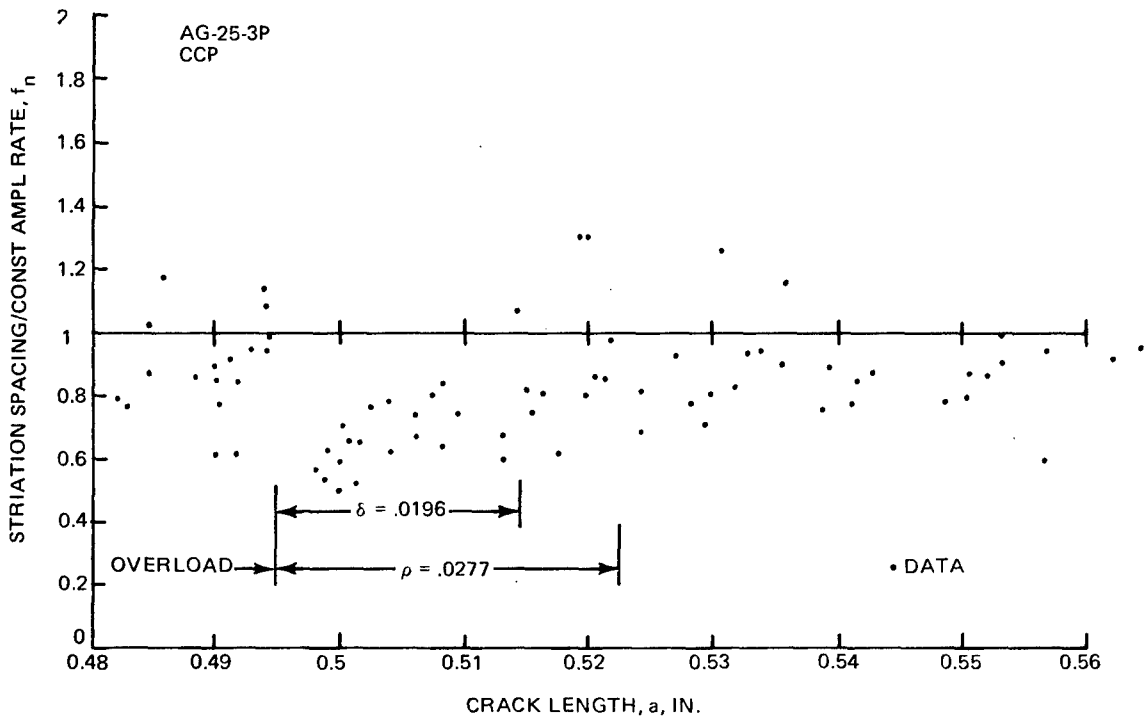


**Figure 44 Delayed Retardation, $a_{OL}$ = 0.495 In., Edge, O/L = 1.8, 2219-T851 Aluminum**

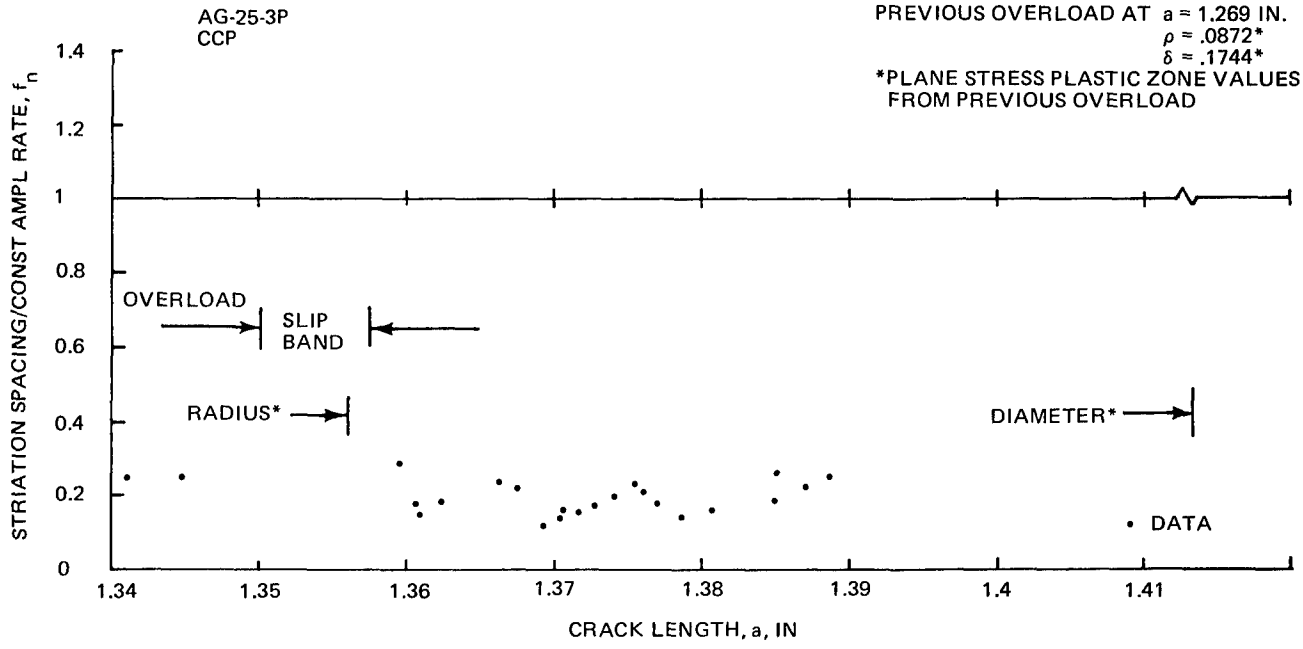


**Figure 45 Delayed Retardation, $a_{OL}$ = 1.35 In., Centerline, O/L = 1.8, 2219-T851 Aluminum**

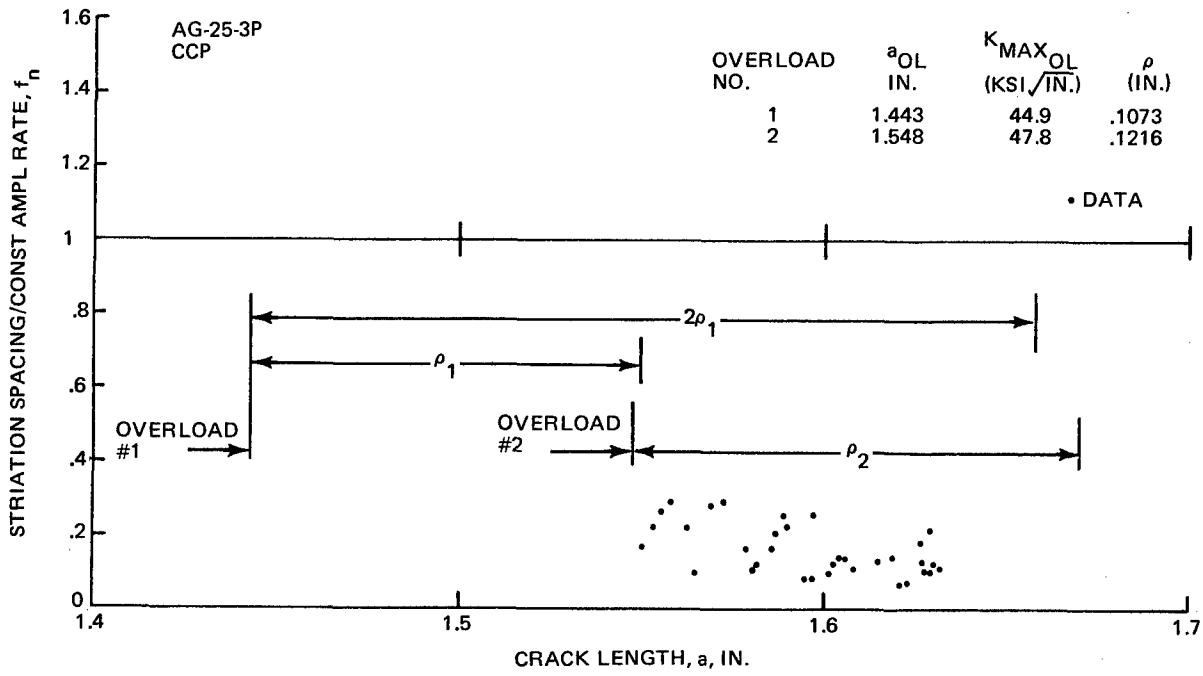


**Figure 46 Delayed Retardation, $a_{OL}$ = 1.548 In., Centerline, O/L = 1.8, 2219-T851 Aluminum**

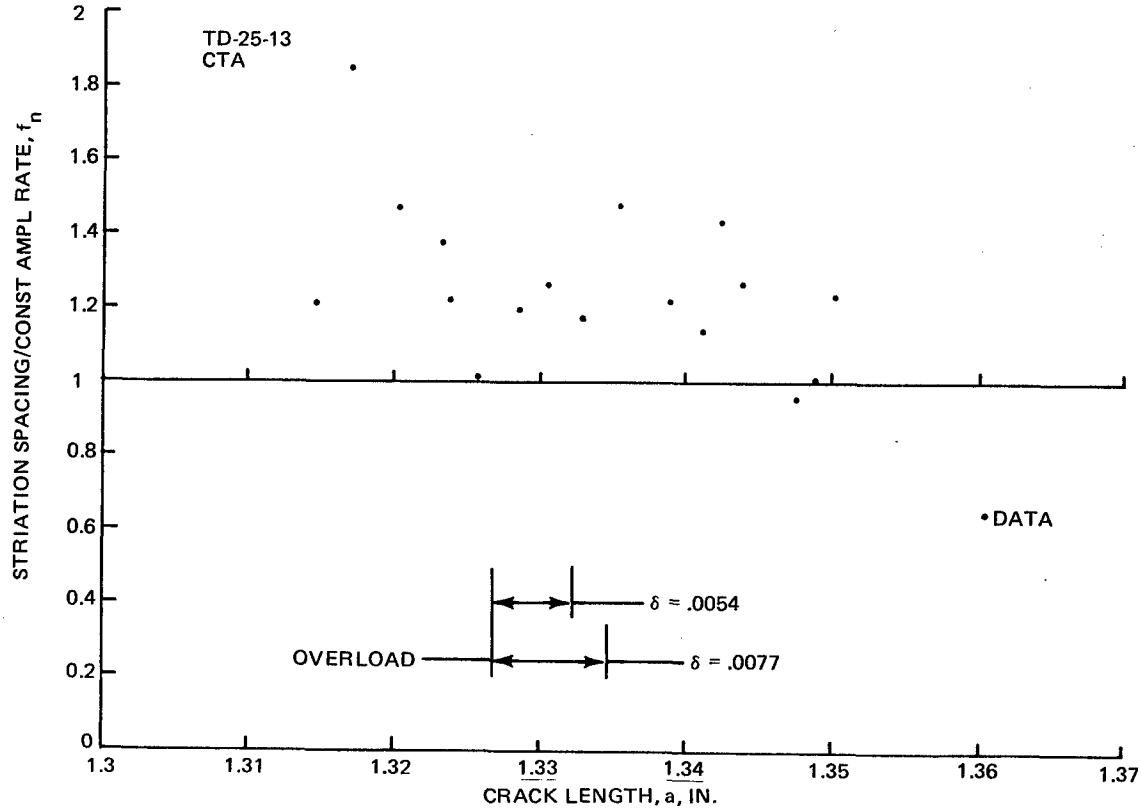


**Figure 47 Delayed Retardation, $a_{OL}$ = 1.327 In., Centerline, O/L = 1.25, Ti 6Al-4V Titanium**

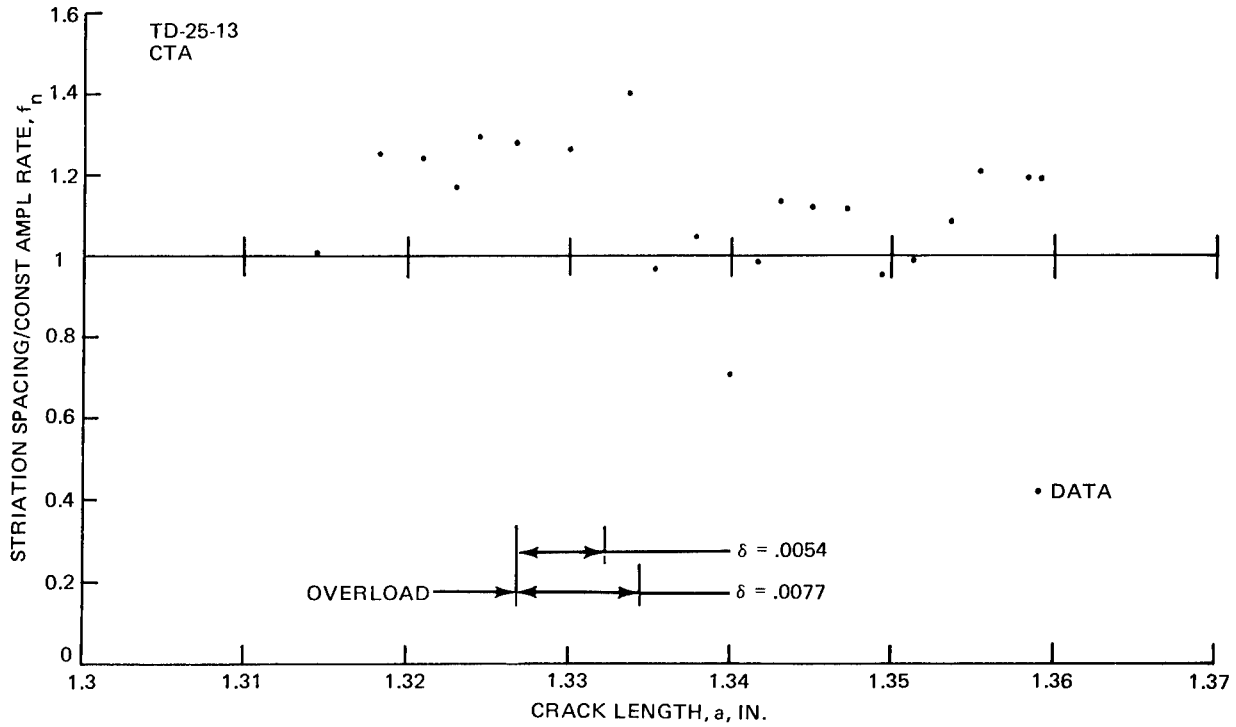


**Figure 48 Delayed Retardation, $a_{OL}$ = 1.327 In., Edge, O/L = 1.25, Ti 6Al-4V Titanium**

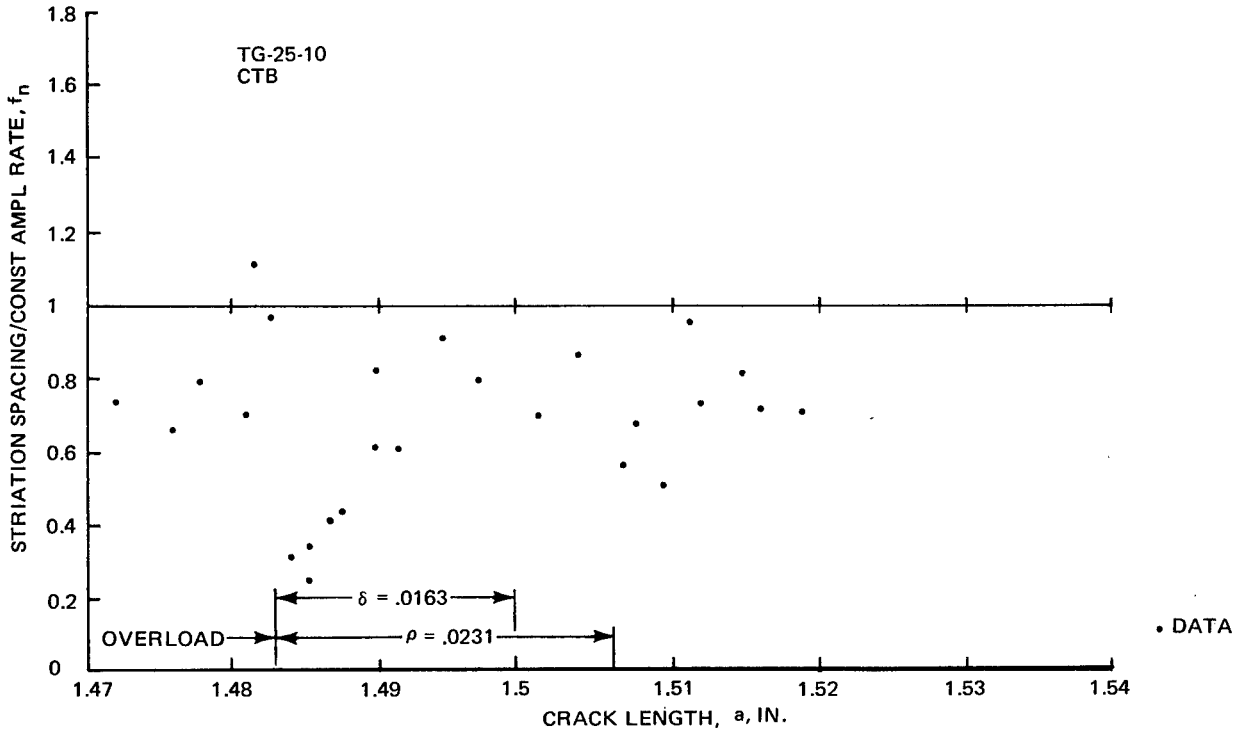


**Figure 49 Delayed Retardation, $a_{OL}$ = 1.483 In., Centerline, O/L = 1.5, Ti 6Al-4V Titanium**

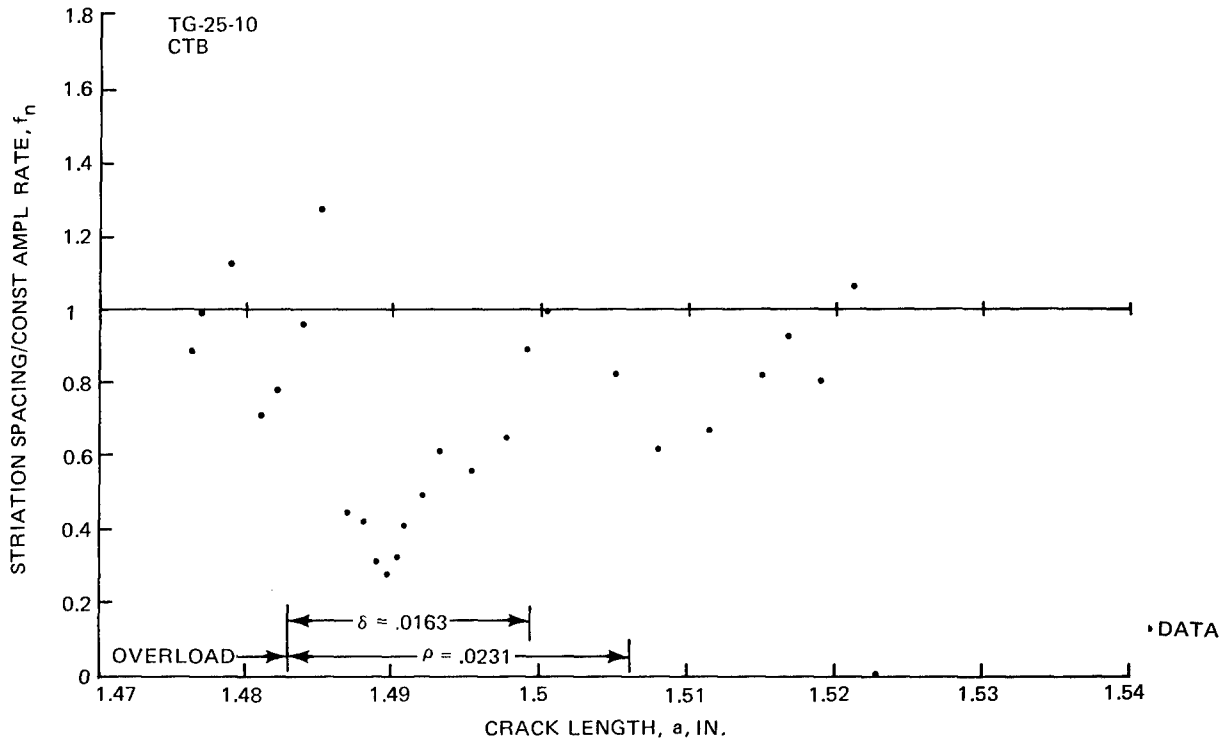


**Figure 50 Delayed Retardation, $a_{OL}$ = 1.483 In., Edge, O/L = 1.5, Ti 6Al-4V Titanium**

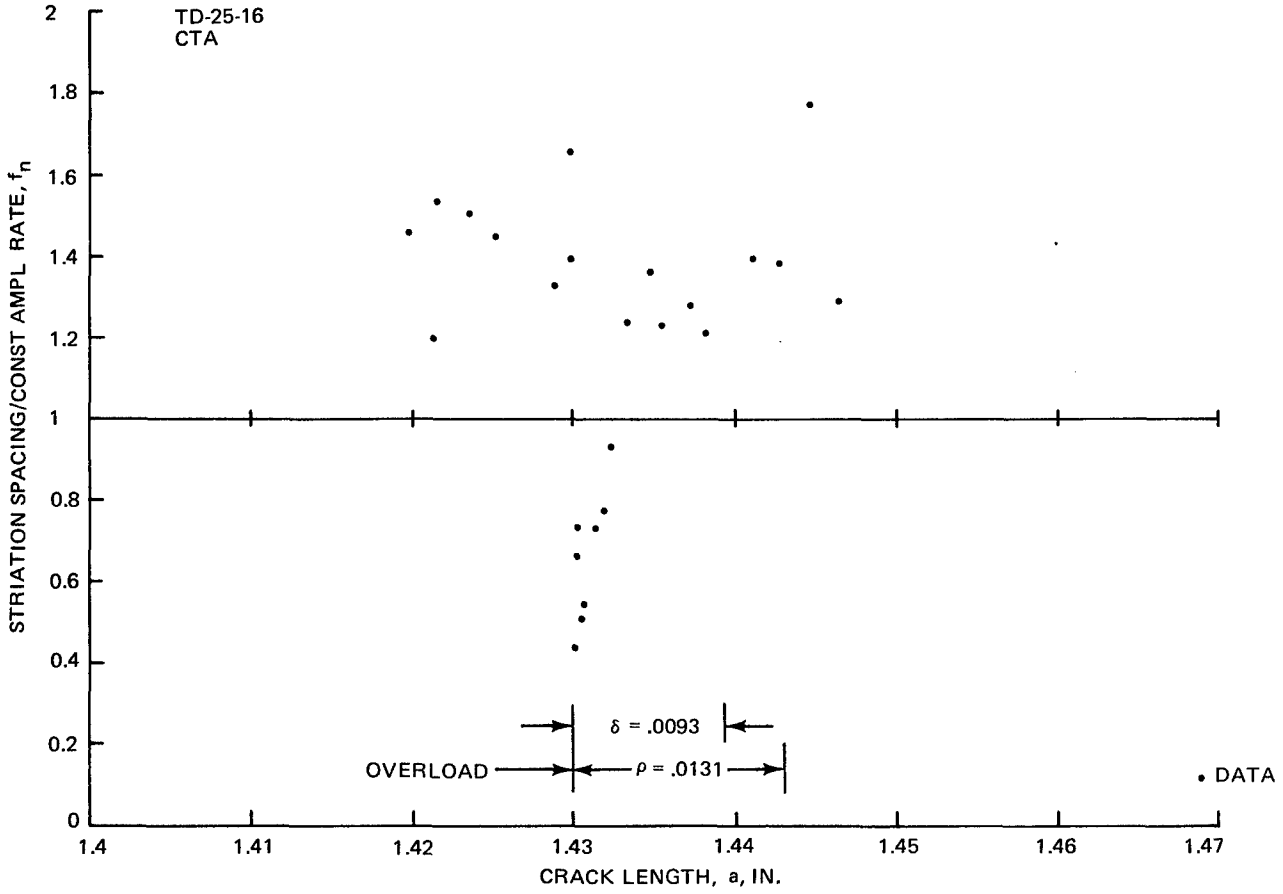


**Figure 51 Delayed Retardation, $a_{OL}$ = 1.43 In., Centerline, O/L = 1.5, Ti 6Al-4V Titanium**

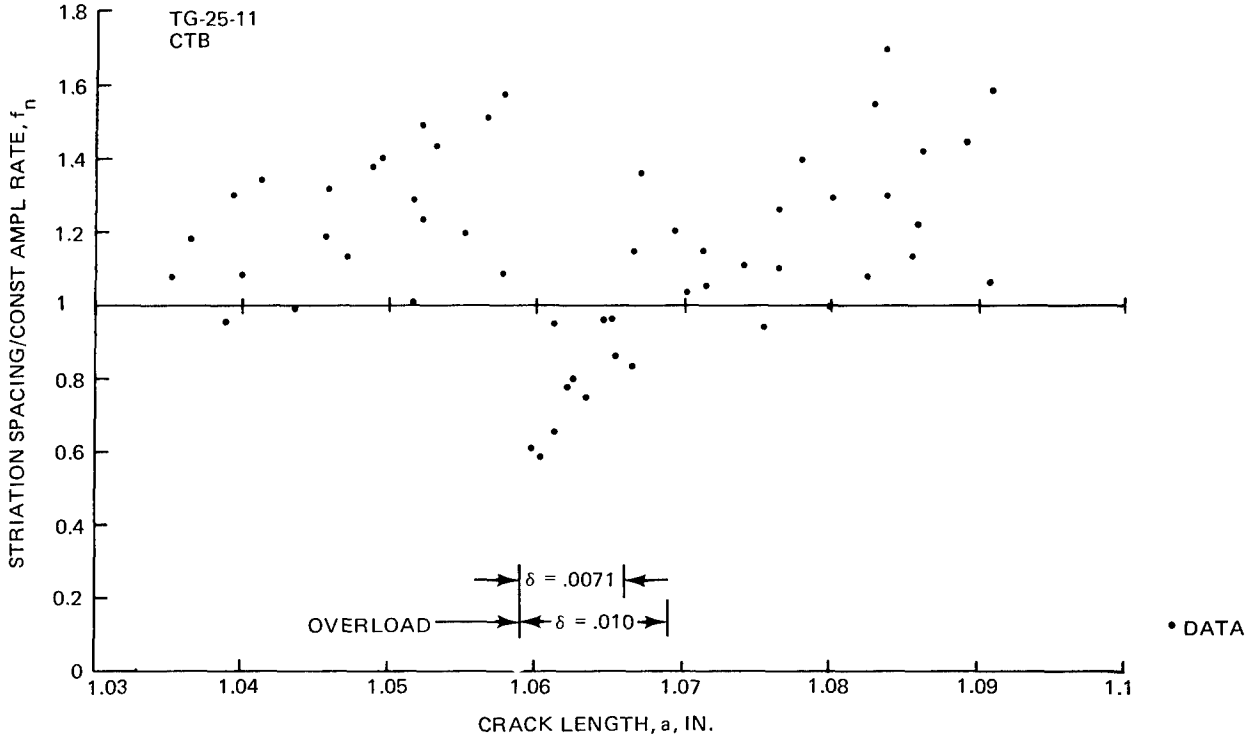


**Figure 52 Delayed Retardation, $a_{OL}$ = 1.059 In., Centerline, O/L = 1.8, Ti 6Al-4V Titanium**

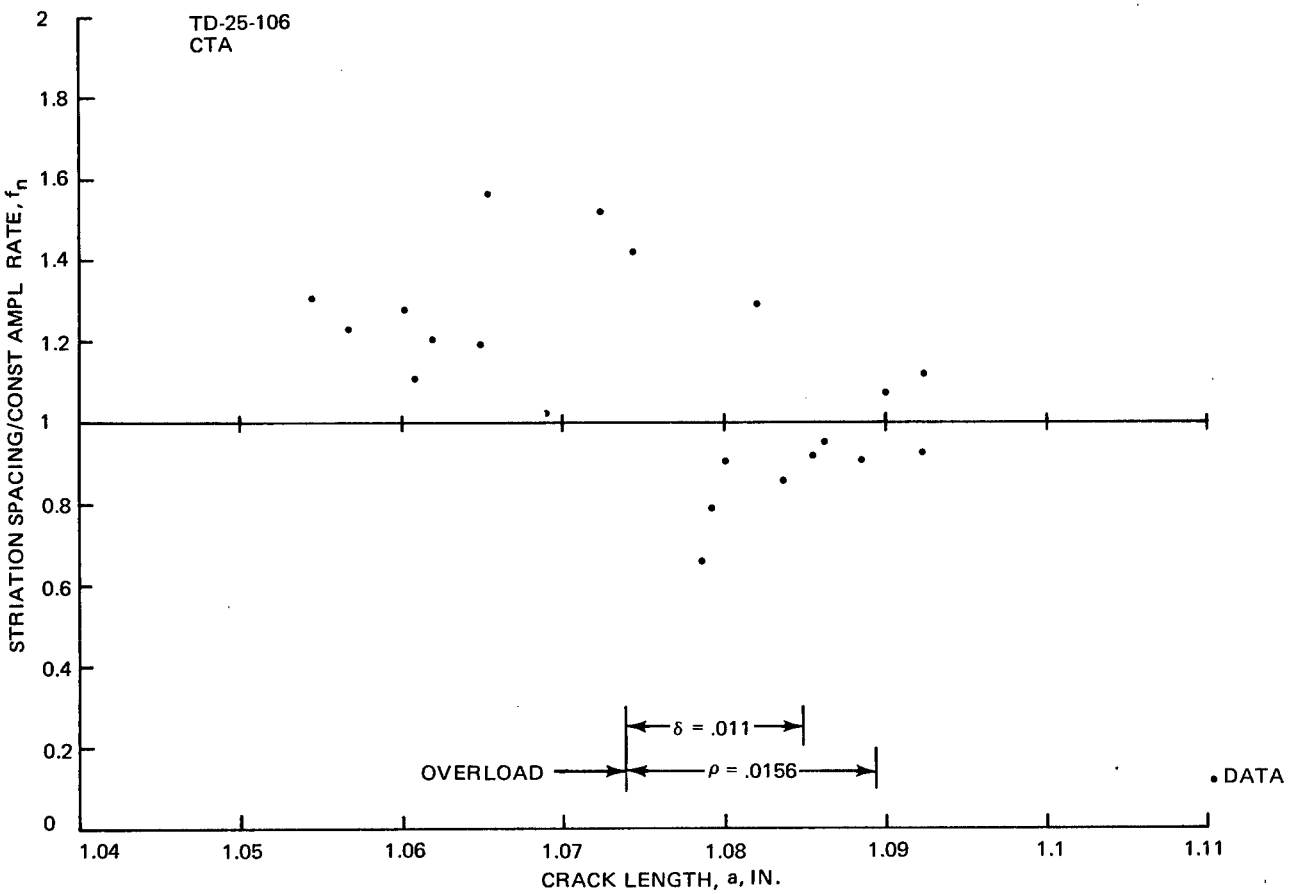


**Figure 53 Delayed Retardation, $a_{OL}$ = 1.074 In., Centerline, O/L = 1.8, Ti 6Al-4V Titanium**

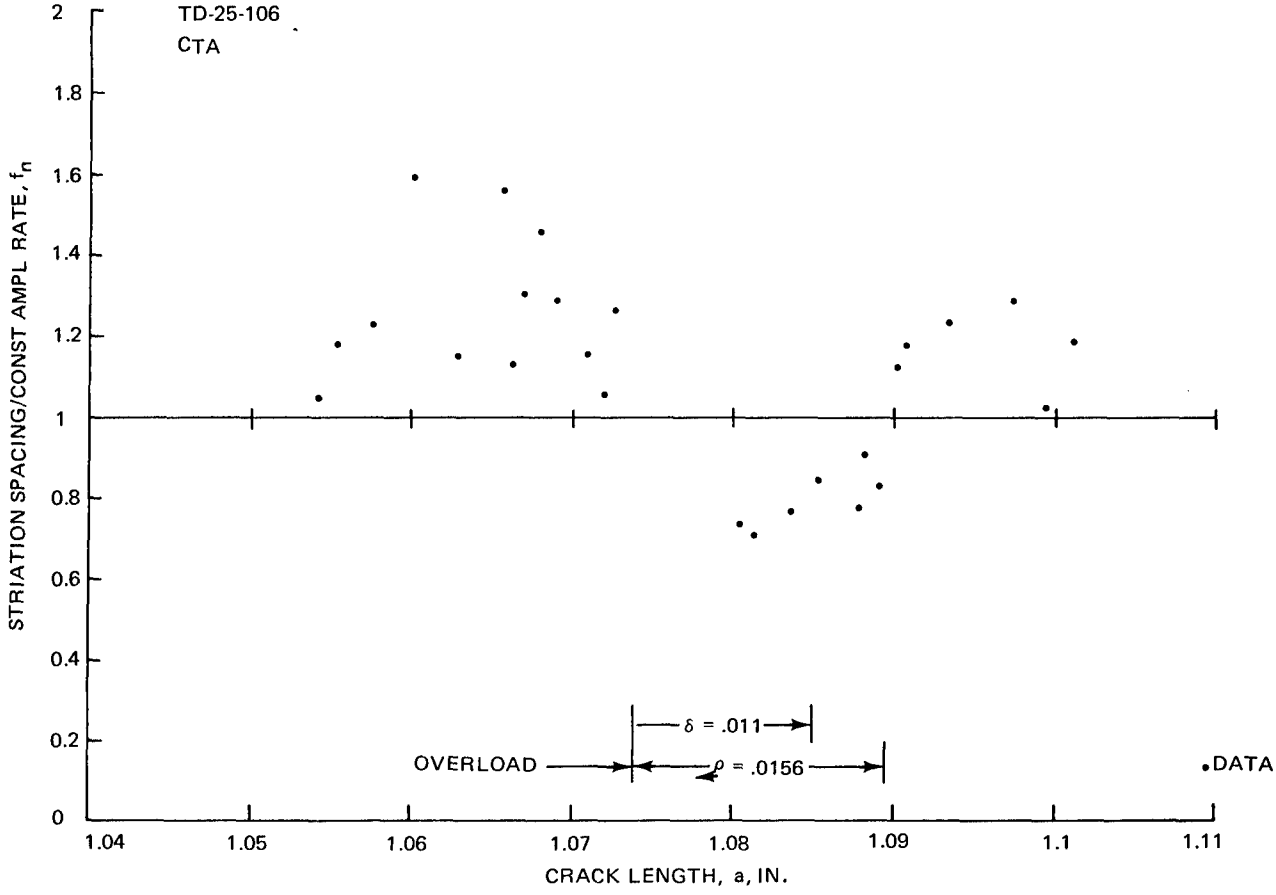


**Figure 54 Delayed Retardation, $a_{OL}$ = 1.074 In., Edge, O/L = 1.8, Ti 6Al-4V Titanium**

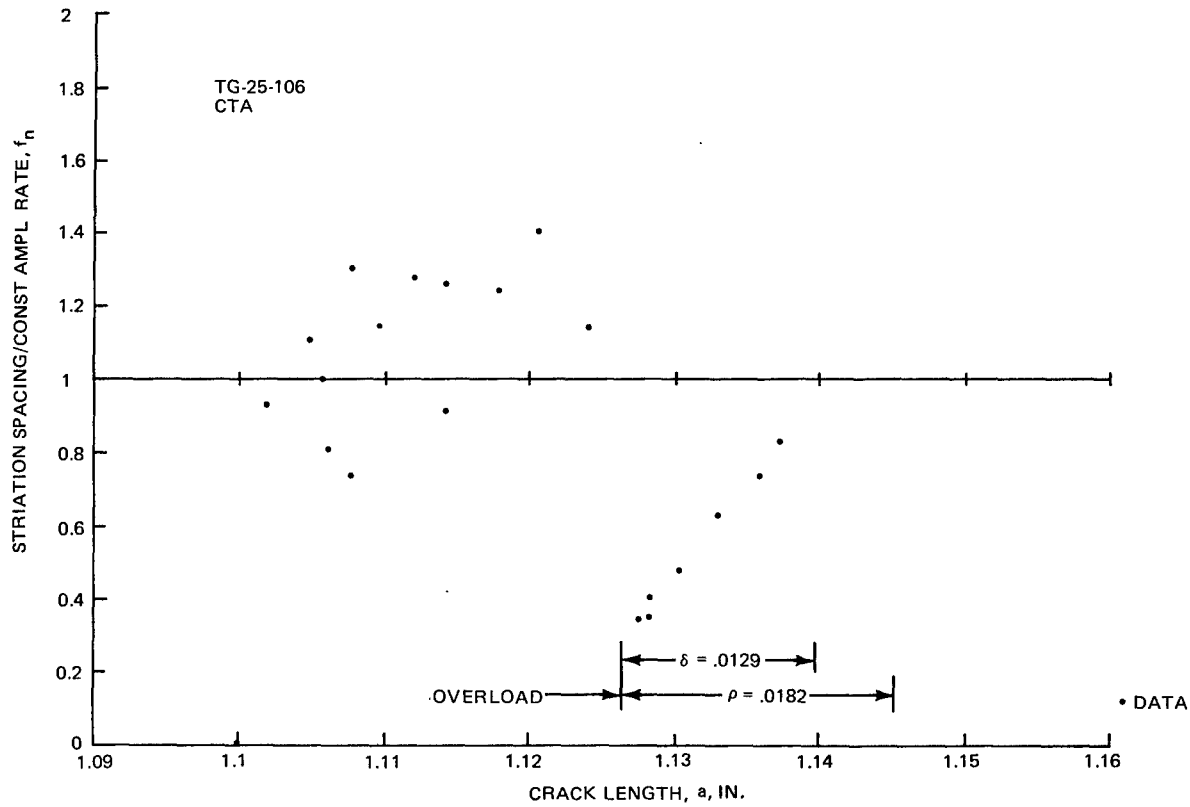


**Figure 55 Delayed Retardation, $a_{OL}$ = 1.127 In., Centerline, O/L = 1.8, Ti 6Al-4V Titanium**

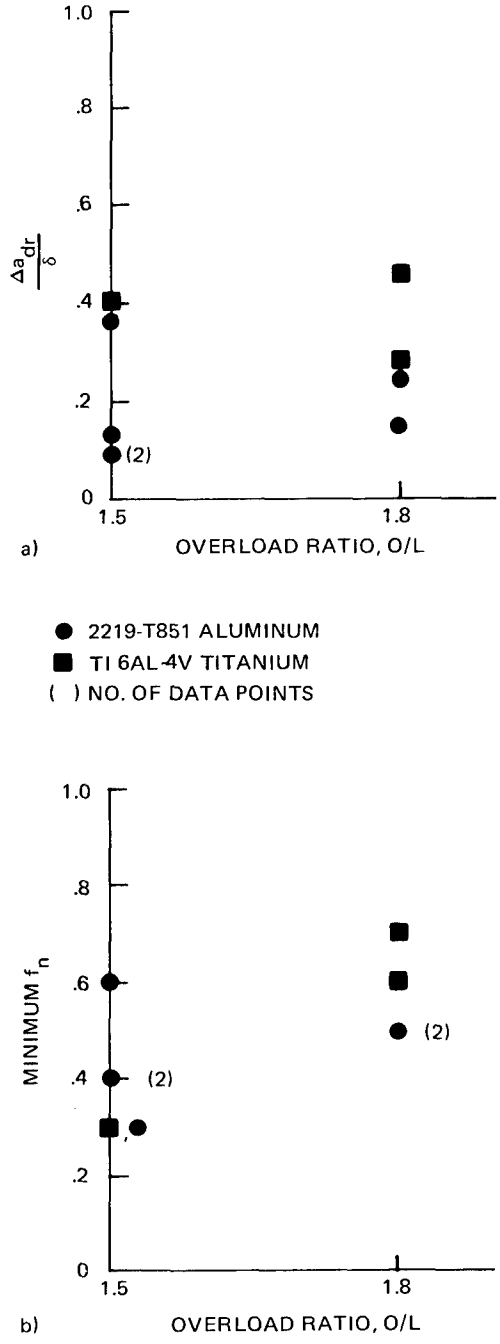


**Figure 56 Delayed Retardation Parameters (Sheet 1 of 2)**

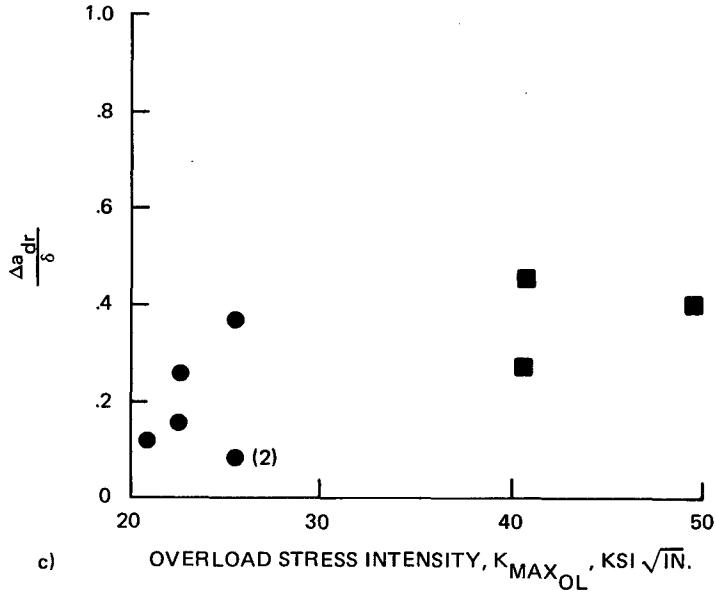


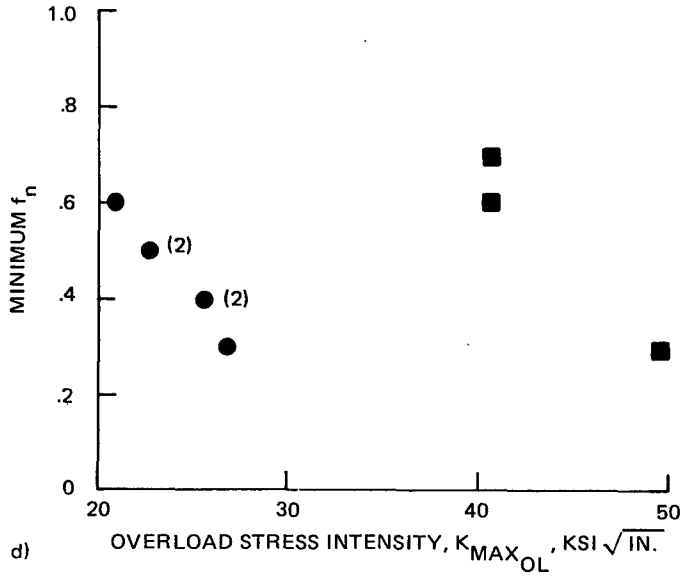


**Figure 56 Delayed Retardation Parameters (Sheet 2 of 2)**

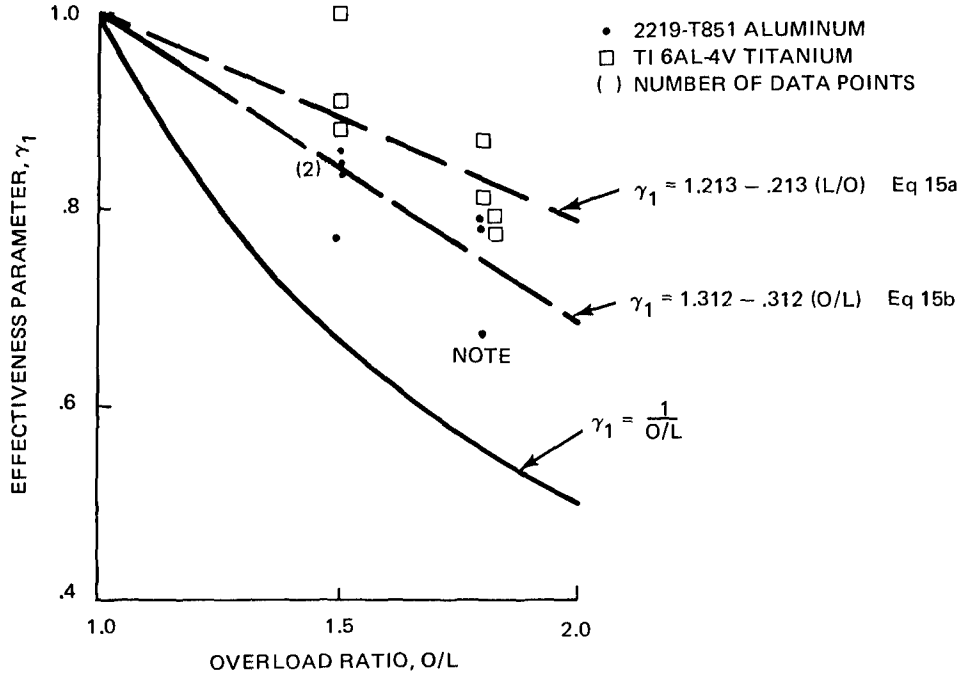


**Figure 57 Overload Effectiveness vs Overload Ratio**

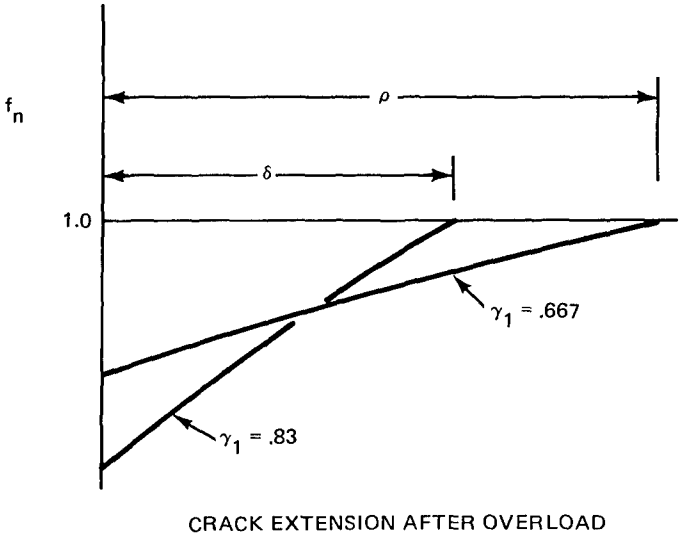


**Figure 58 Schematic of $f_n$ vs Crack Extension**

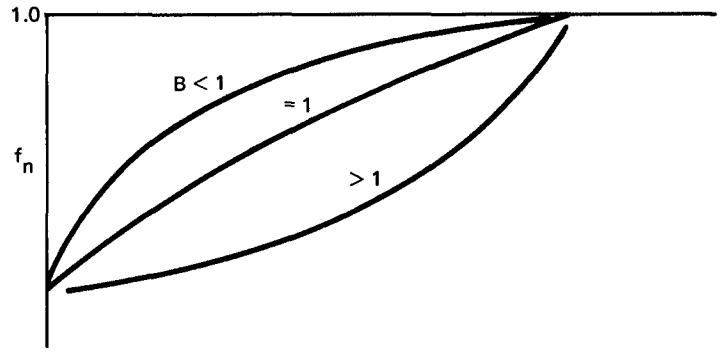


**Figure 59 Schematic of $f_n$ As a Function of B**

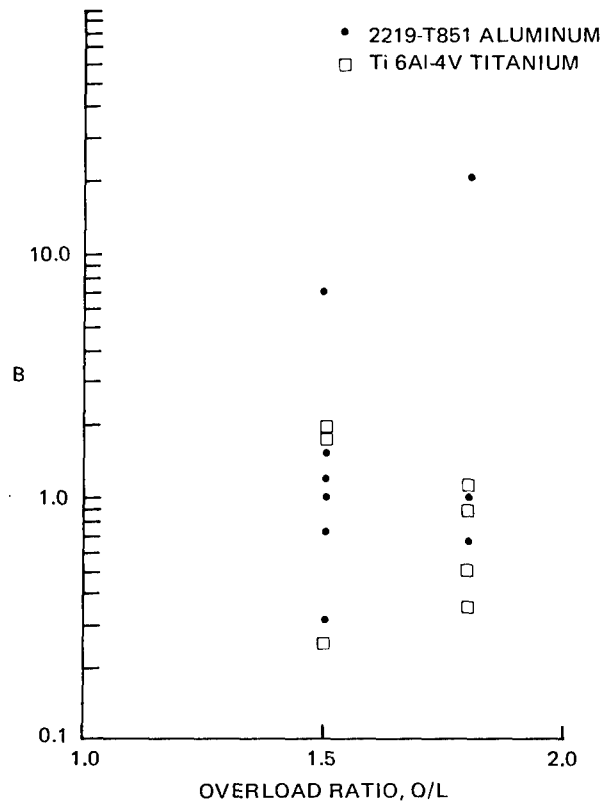


**Figure 60 Exponent B vs Overload Ratio**

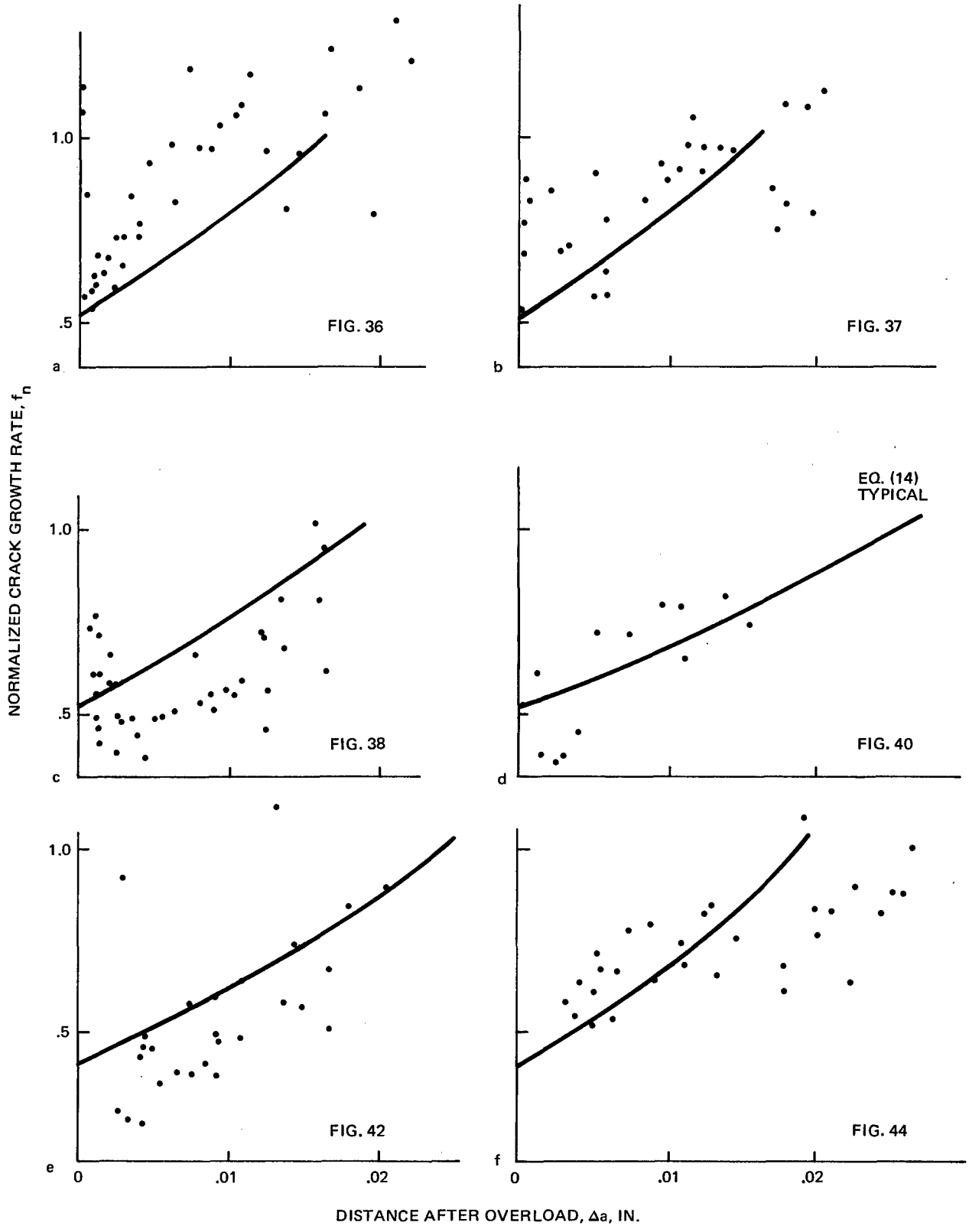


**Figure 61 Comparison of Equation 14 with Data (Sheet 1 of 3)**

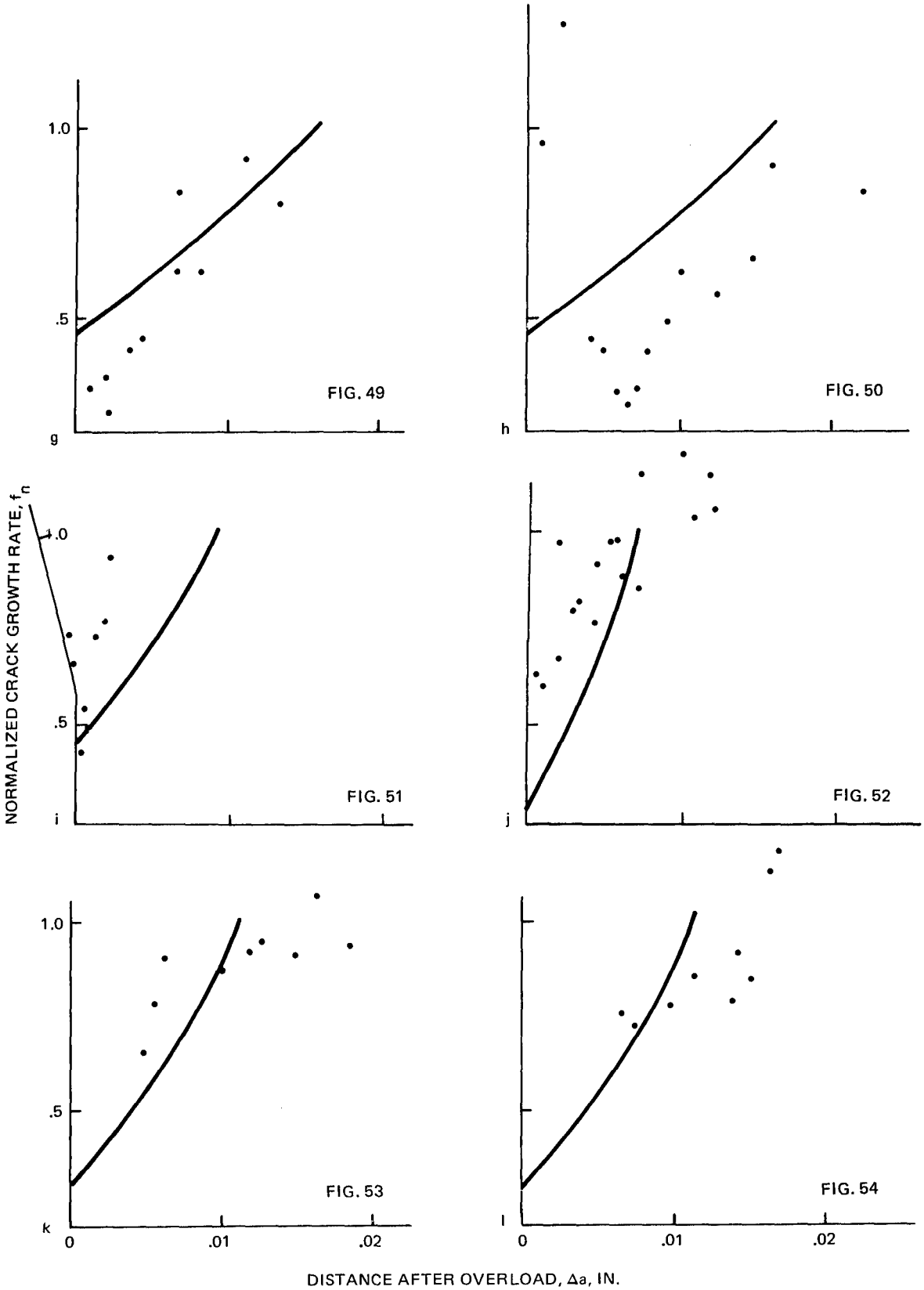


**Figure 61 Comparison of Equation 14 with Data (Sheet 2 of 3)**

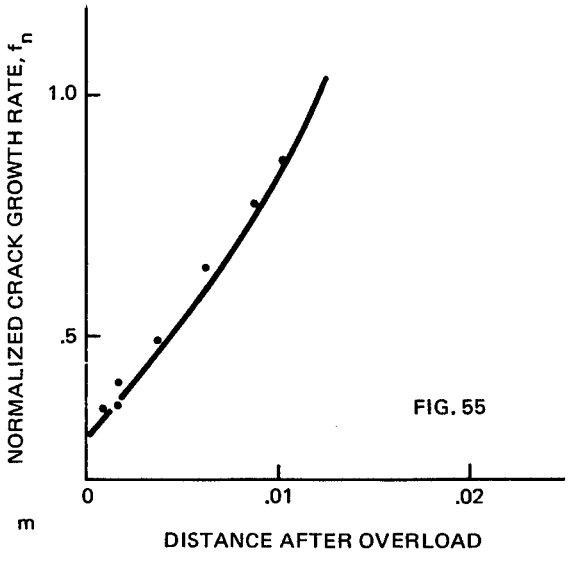


**Figure 61 Comparison of Equation 14 with Data (Sheet 3 of 3)**

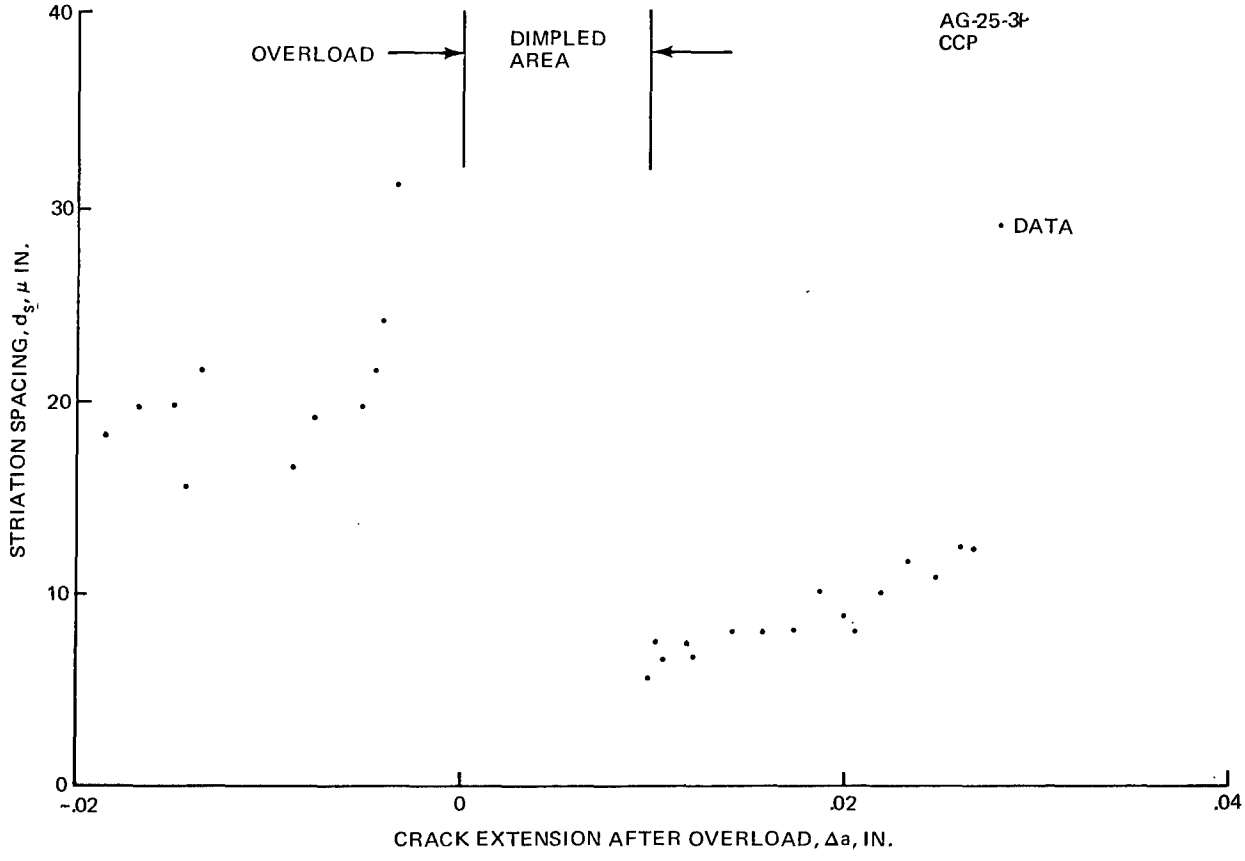


**Figure 62 Striation Spacing vs Distance After Overload, $a_{OL}$ = 1.263 In., Centerline, O/L = 1.8, 2219-T851 Aluminum**

Shear lips

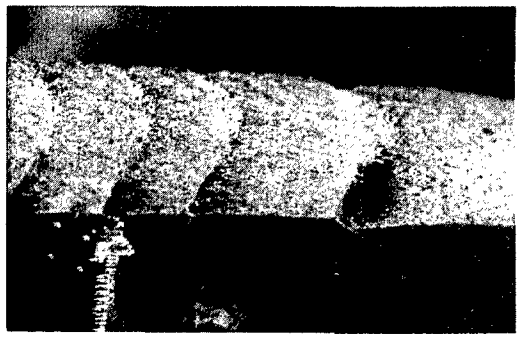

a. Contrast photographic lighting

Overload dimple topography

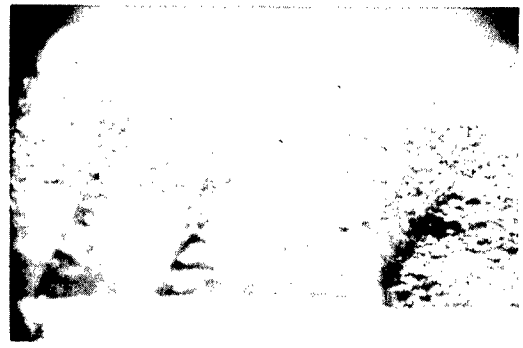

MAG: 10X

b. Diffuse Photographic lighting

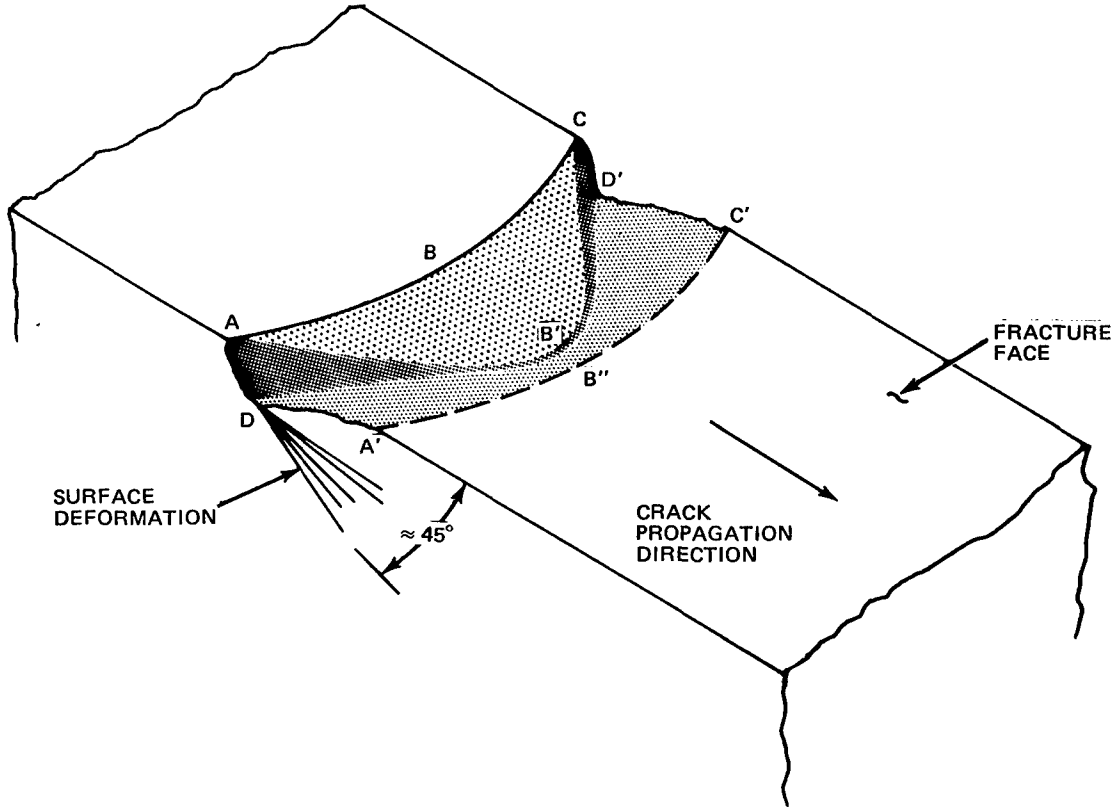


c. Schematic of Fracture Face in Vicinity of Overload Application

**Figure 63 Crack Curvature, $a_{OL}$ = 1.26 to 1.71 In., O/L = 1.8, 2219-T851 Aluminum**

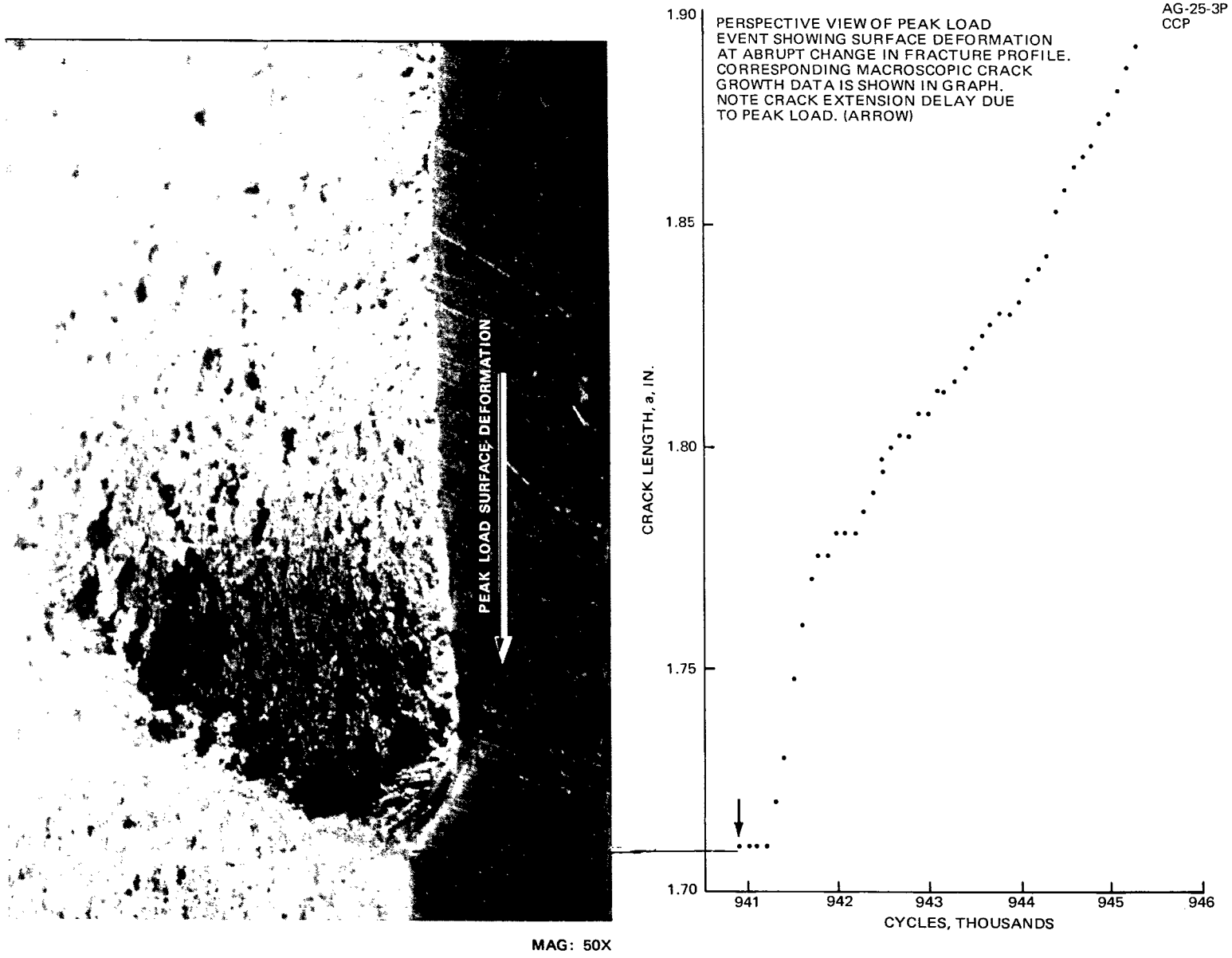


**Figure 64 Crack Curvature, $a_{OL}$ = 1.71 In., Edge, O/L = 1.8, 2219-T851 Aluminum**

FRACTURE SURFACE PROFILE AND CORRESPONDING MACROSCOPICALLY OBSERVED GROWTH DATA. NOTE CORRELATION BETWEEN PEAK LOAD EVENT ($a_{OL}$ = 1.45 IN.) AND DELAY IN CRACK GROWTH. (ARROW)

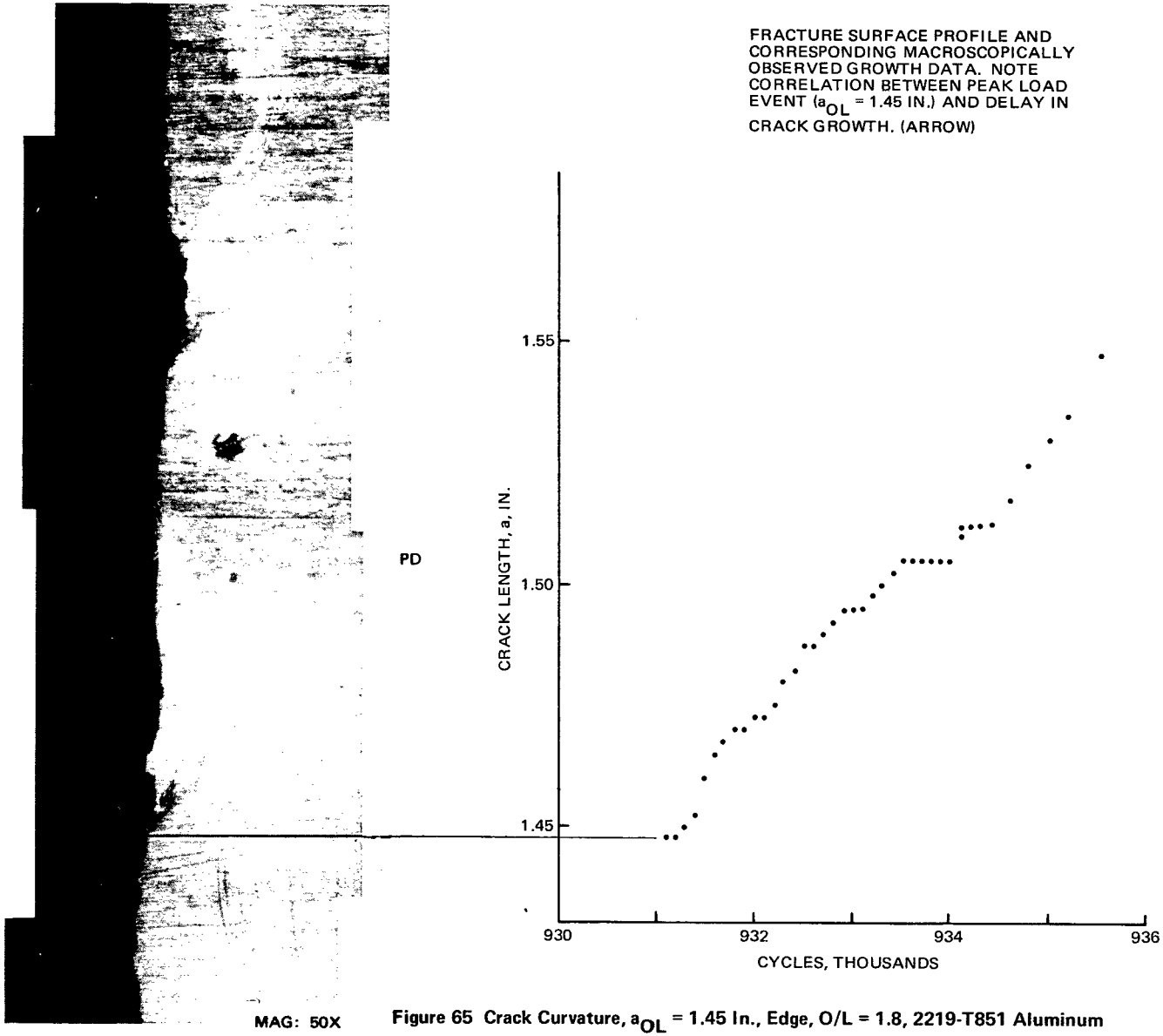


**Figure 65 Crack Curvature, $a_{OL}$ = 1.45 In., Edge, O/L = 1.8, 2219-T851 Aluminum**

AG-25-3P
CCP

FRACTURE SURFACE PROFILE AND CORRESPONDING MICROSCOPICALLY AND MACROSCOPICALLY OBSERVED GROWTH DATA. NOTE CORRELATION BETWEEN PEAK LOAD EVENT ($a_{OL}$ = 1.263 IN.) AND DELAY IN CRACK GROWTH. (ARROW)

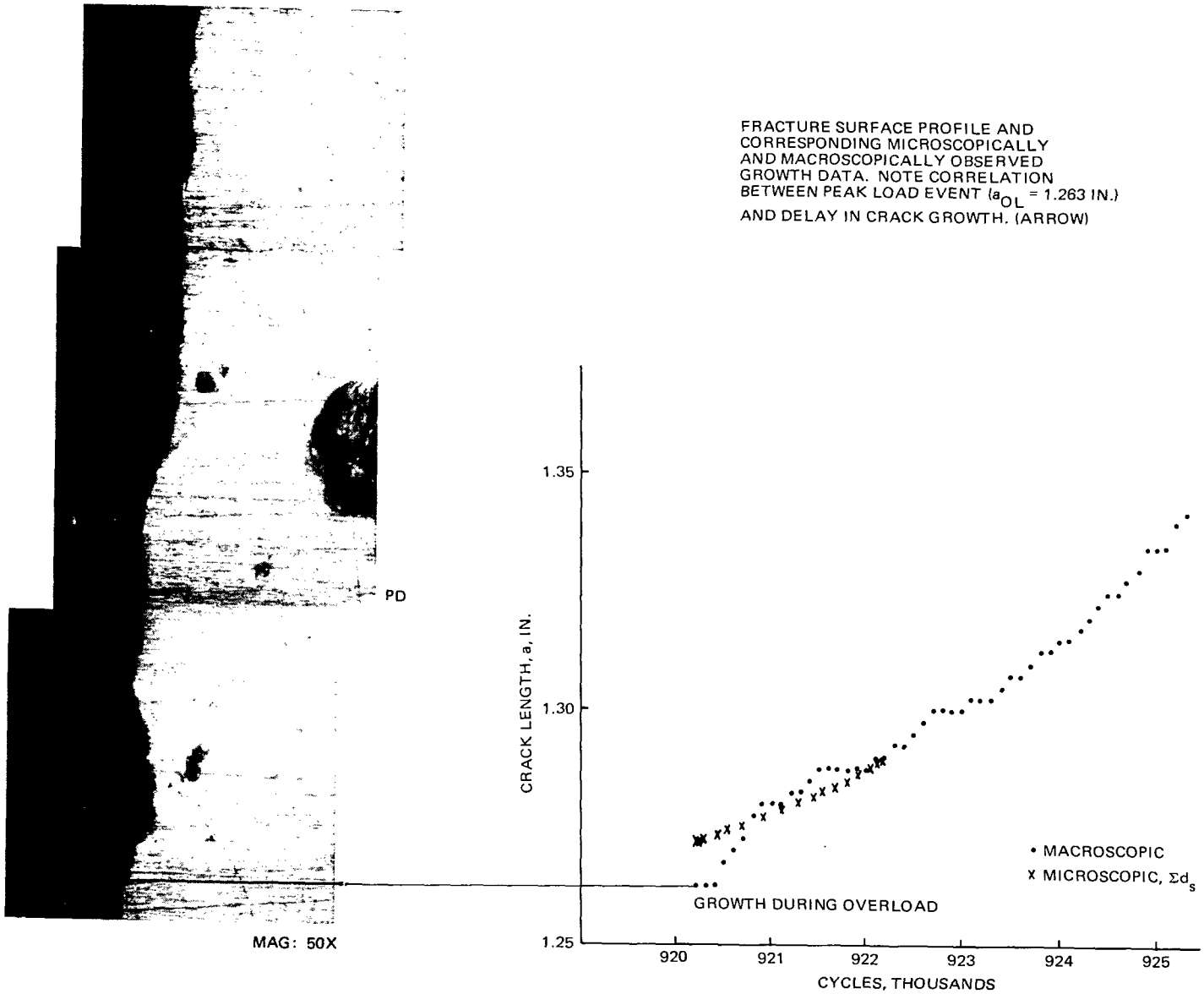


**Figure 66 Crack Curvature $a_{OL}$ = 1.263 In., O/L = 1.8, 2219-T851 Aluminum**

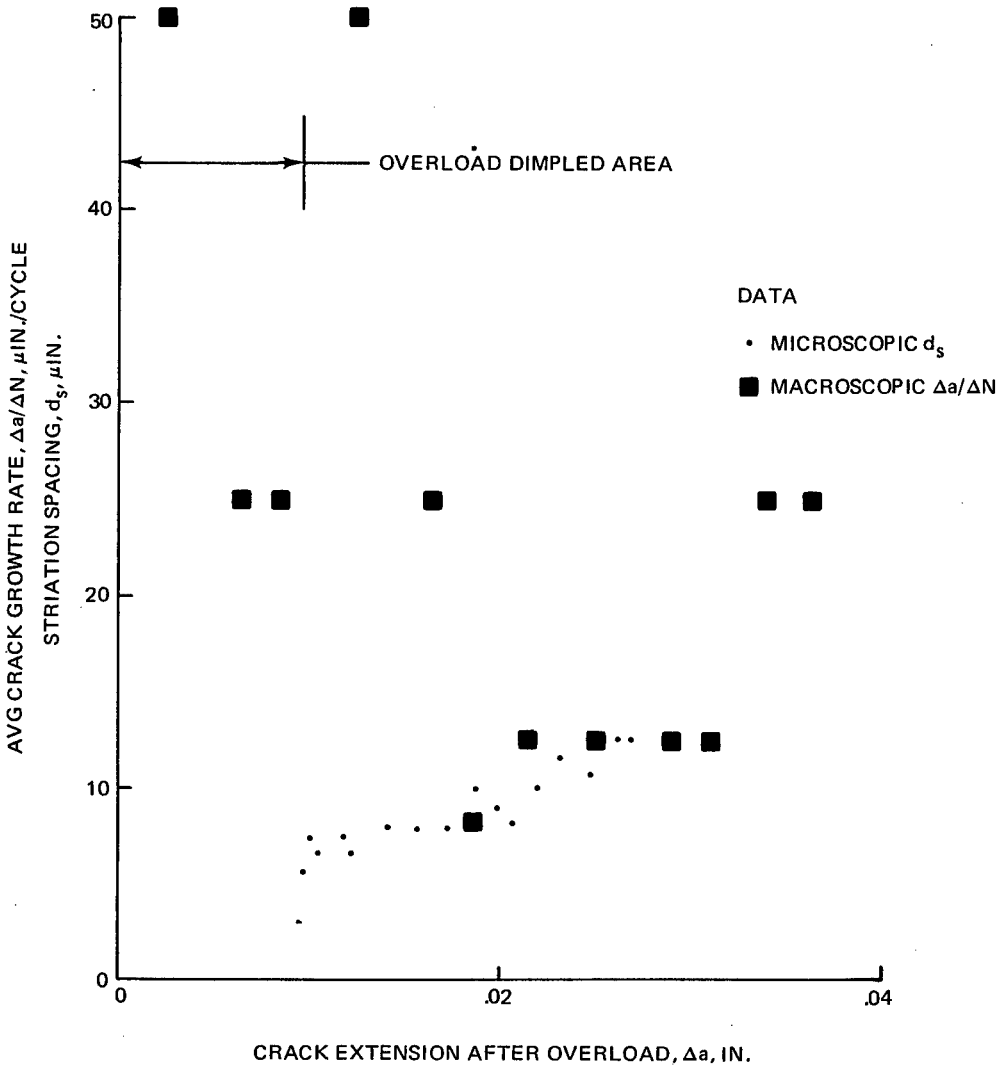


**Figure 67 Comparison of Micro- and Macroscopic Data After an Overload**

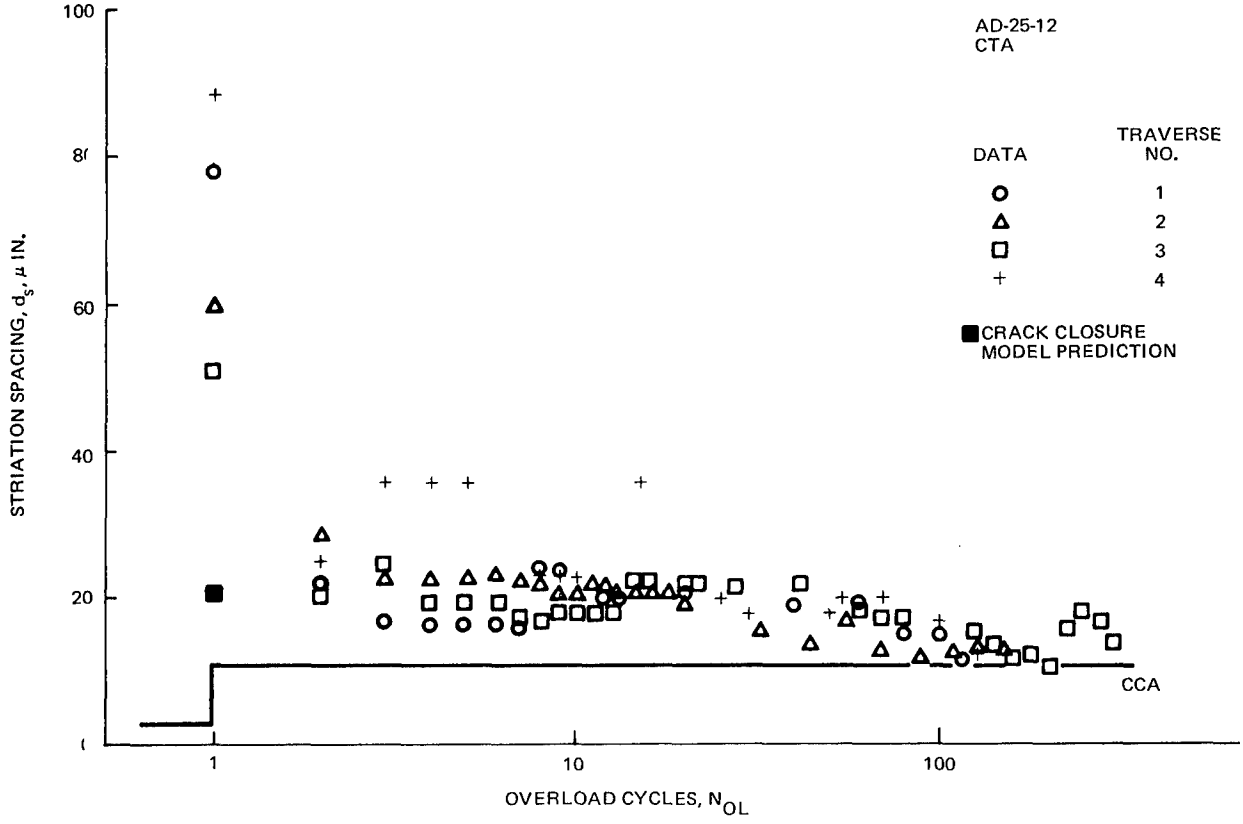


Figure 68 Acceleration, $a_{OL}$ = 1.069 In., O/L = 1.5, 2219-T851 Aluminum

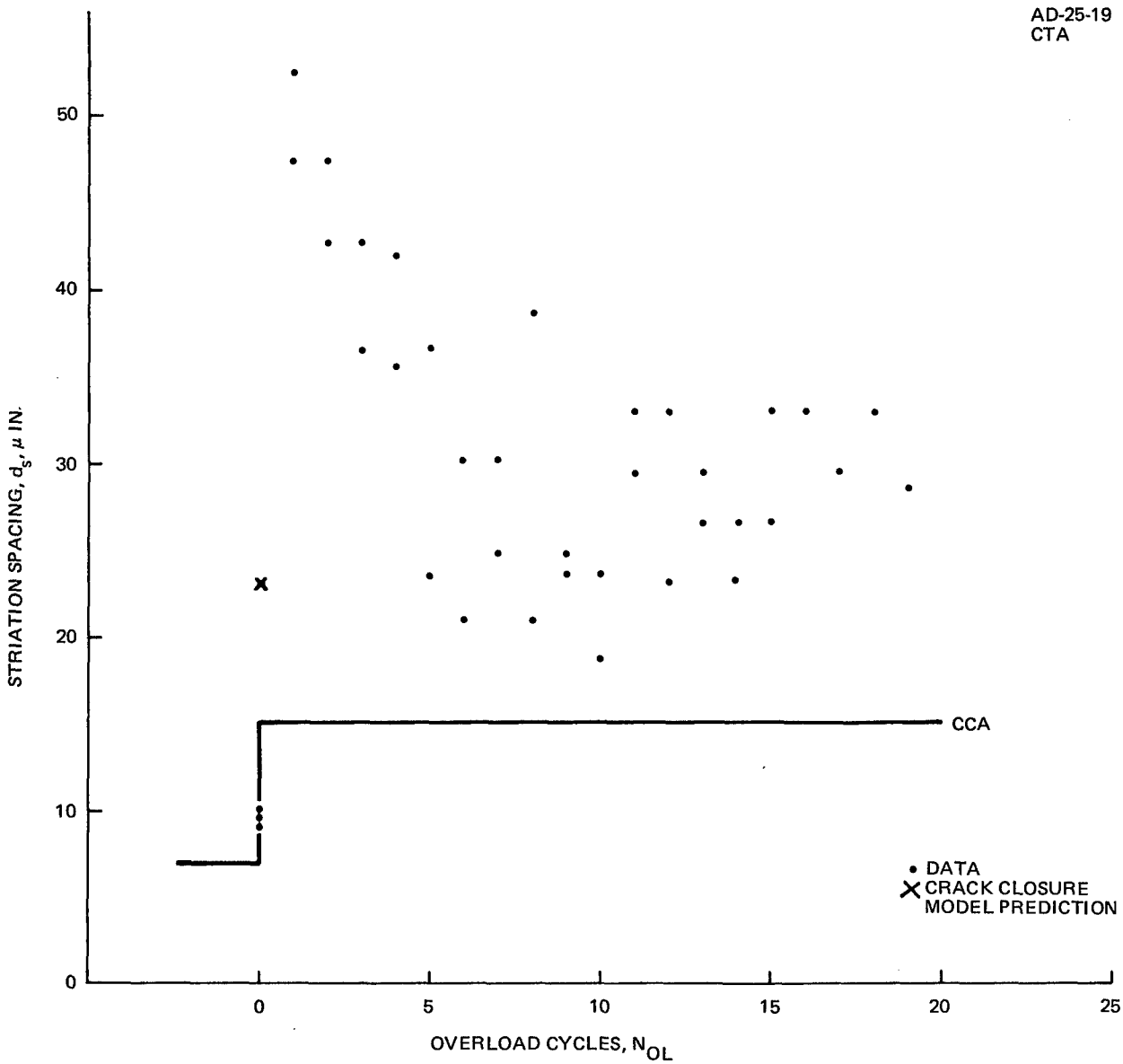


**Figure 69 Acceleration, $a_{OL}$ = 1.396 In., O/L = 1.25, 2219-T851 Aluminum**

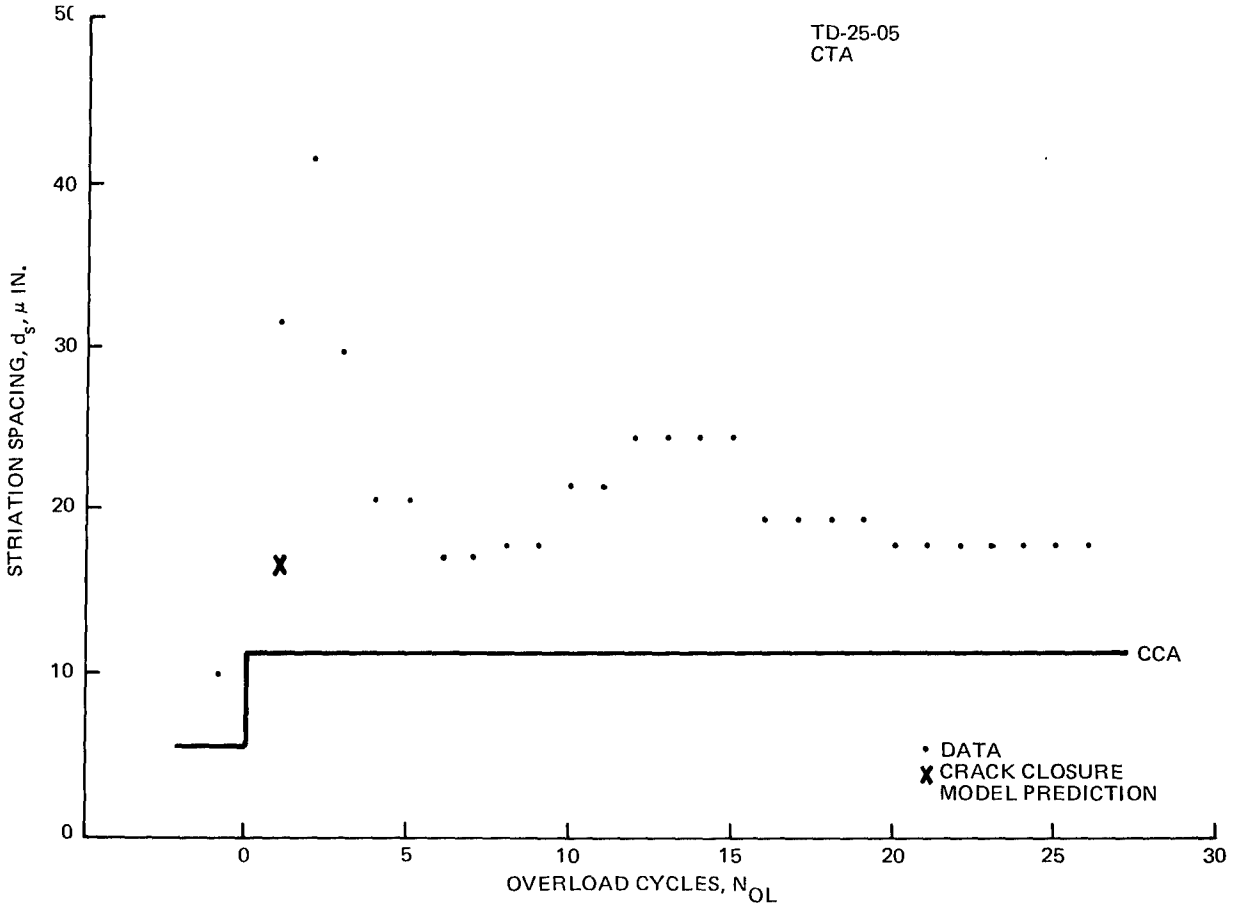


**Figure 70** Acceleration, $a_{OL}$ = 1.418 In., O/L = 1.25, Ti 6Al-4V Titanium

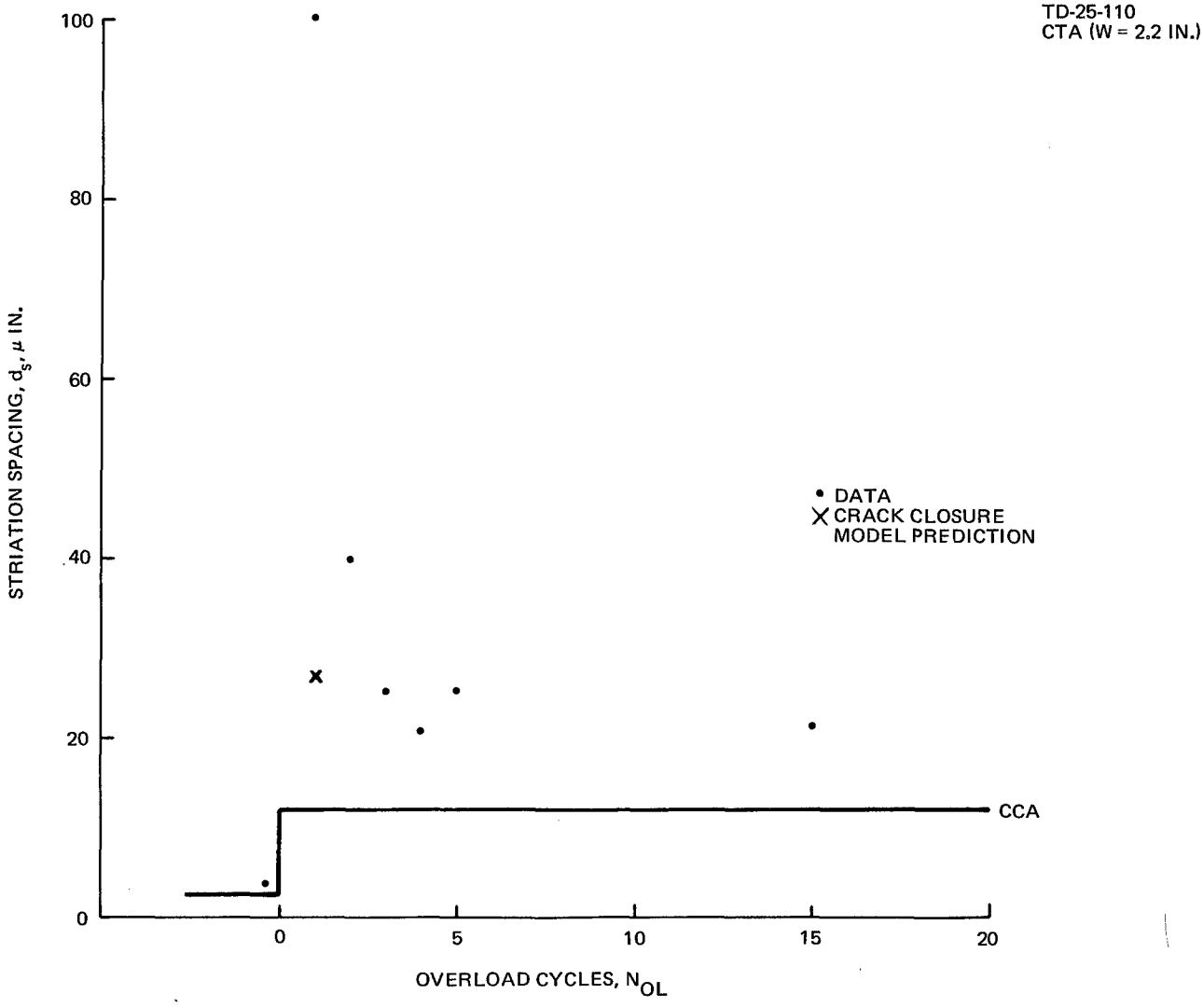


**Figure 71** Acceleration, $a_{OL}$ = 0.692 In., O/L = 1.8, Ti 6Al-4V Titanium

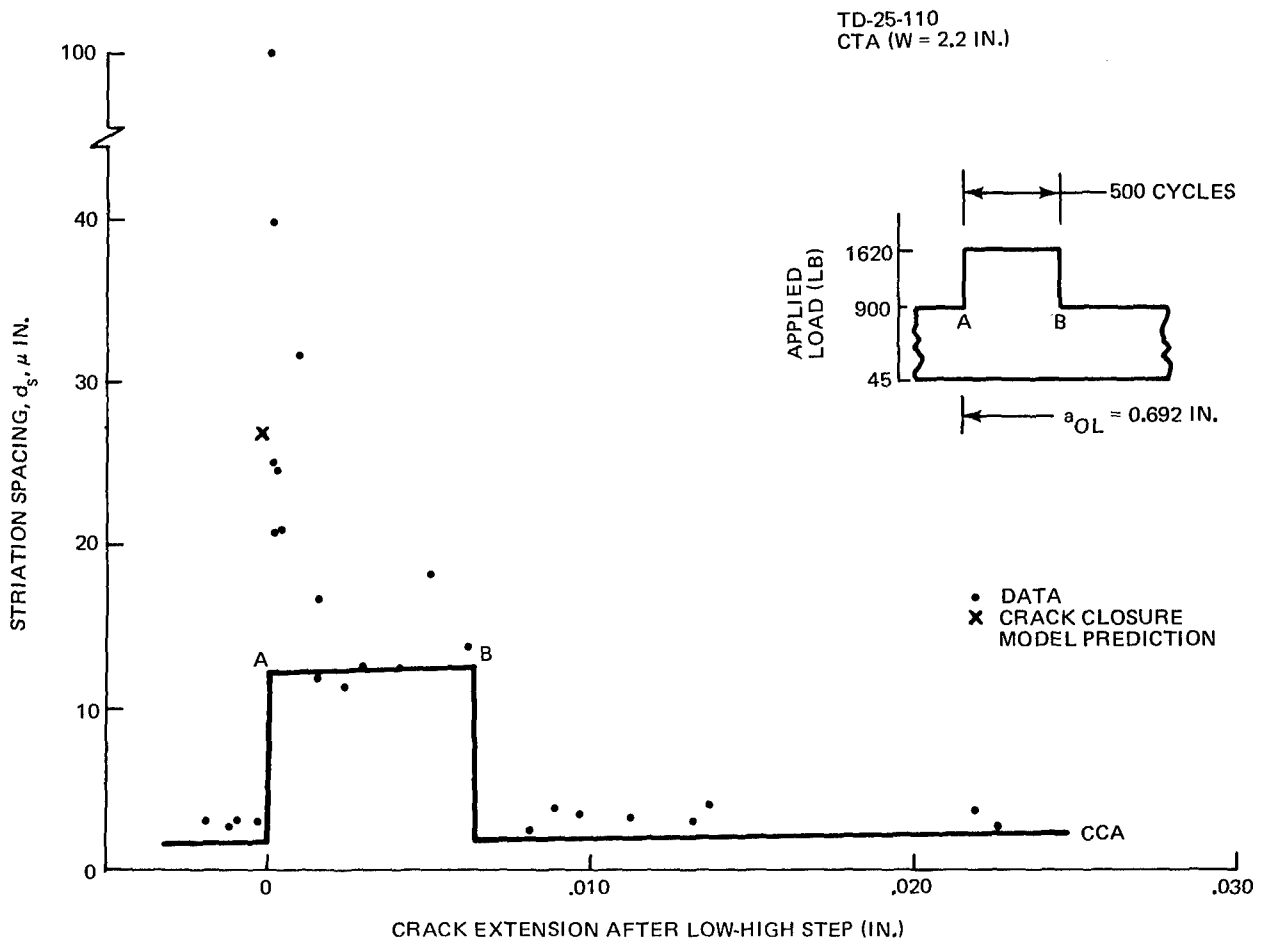


**Figure 72 Acceleration, Striation Spacing During Overloads**

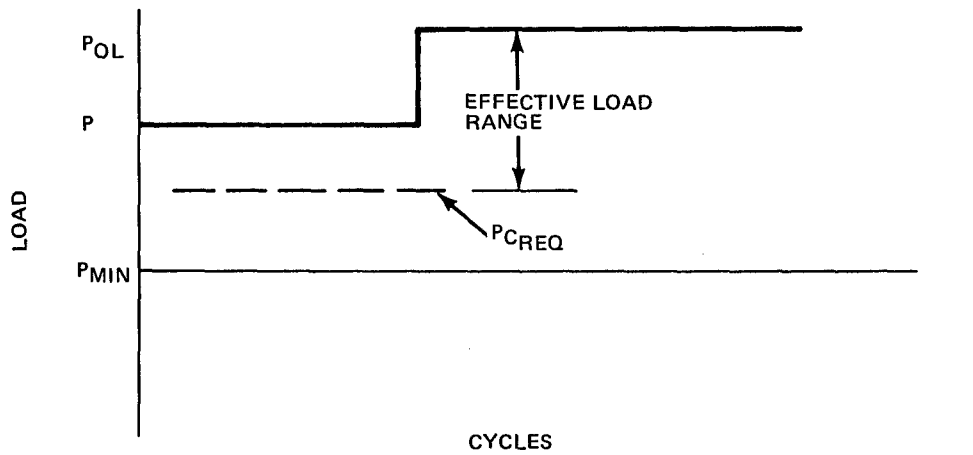


**Figure 73 Schematic of Required Effective Load Range For Low-High Loading Sequence**

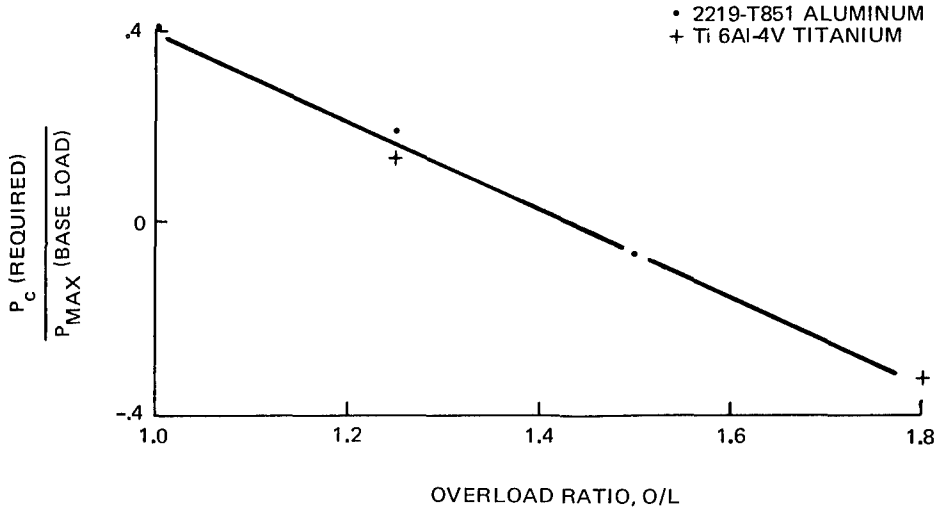


**Figure 74 Closure Level Required to Match Stretch Zone Measurements**

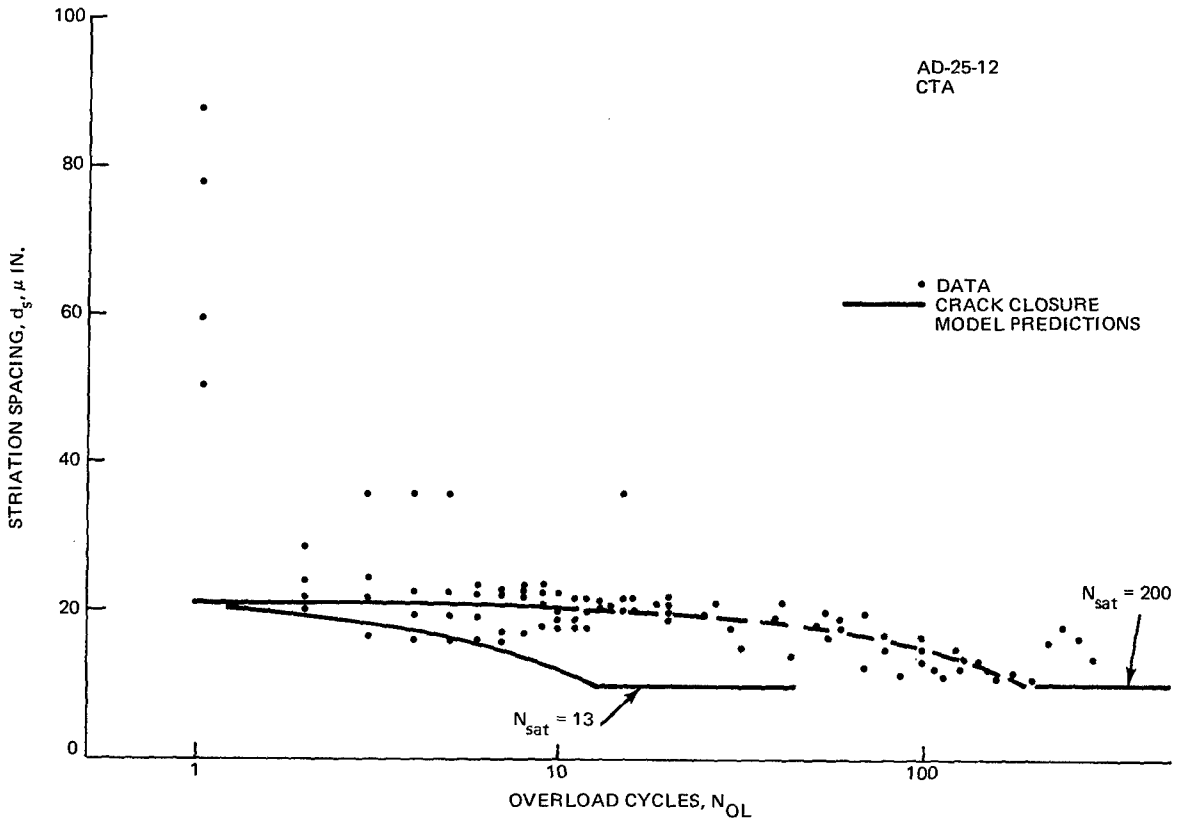


**Figure 75 Crack Closure Model Predictions for 2219-T851 Aluminum**

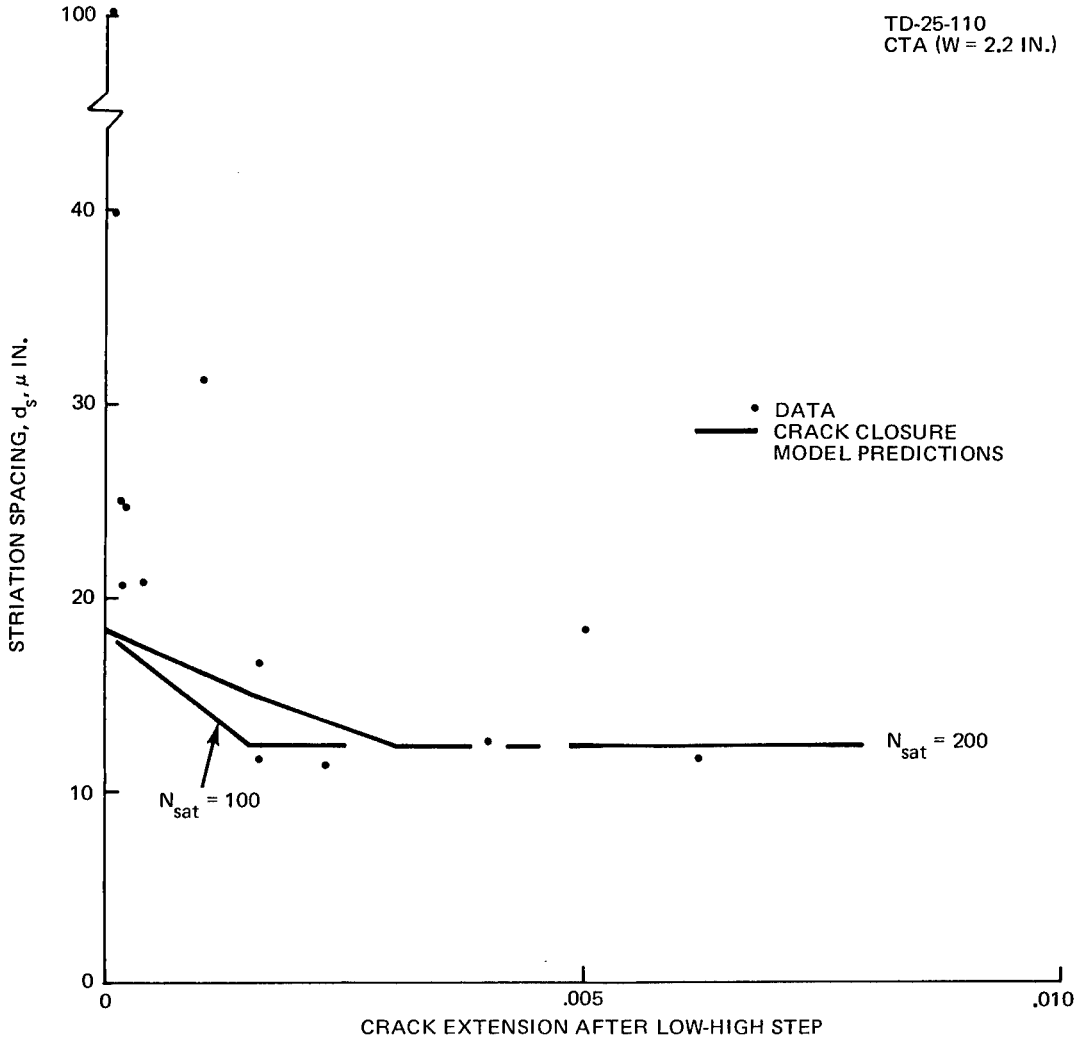


**Figure 76** Crack Closure Model Predictions for Ti 6Al-4V Titanium

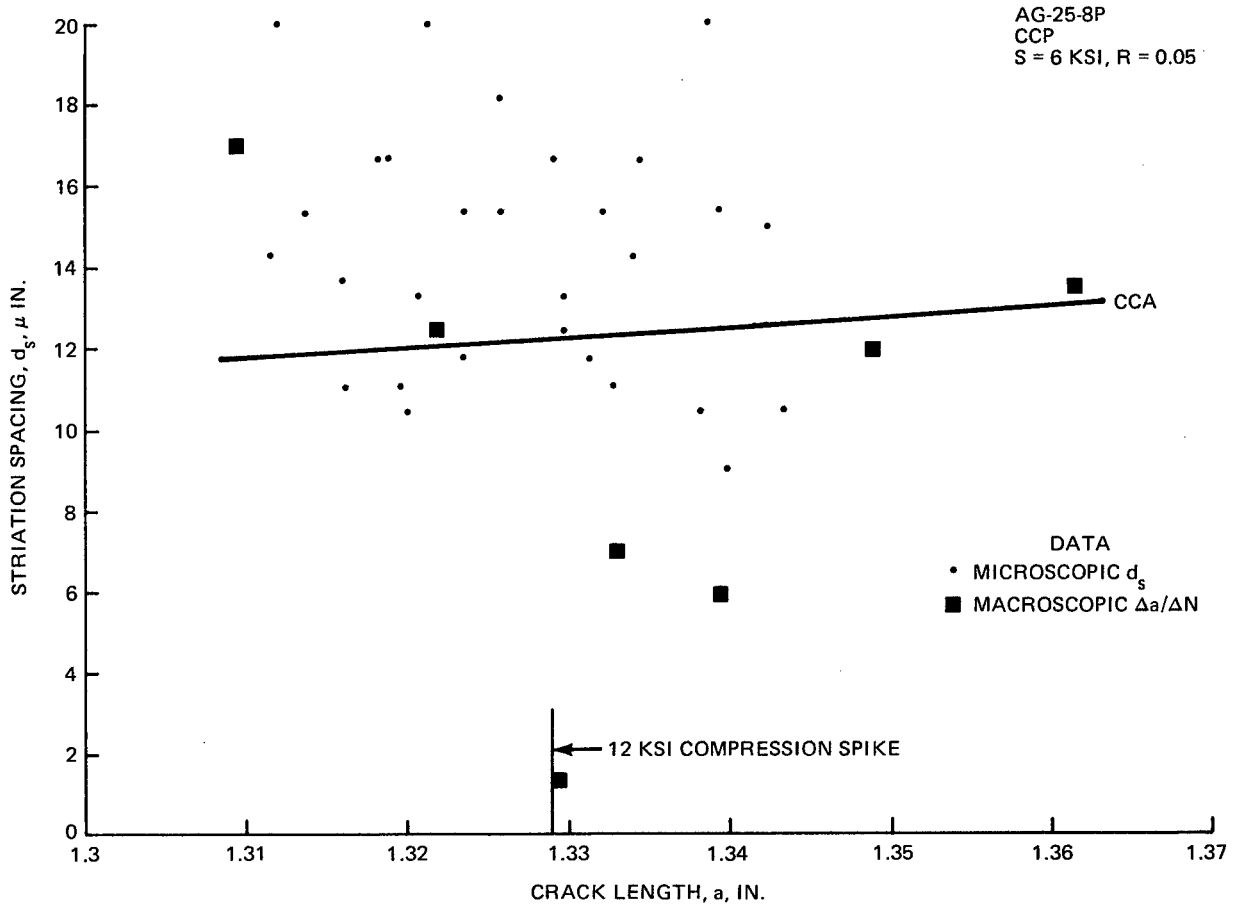


**Figure 77 Compression Spike, $R_C = -2$, $a_{ref} = 1.329$ In., 2219-T851 Aluminum**

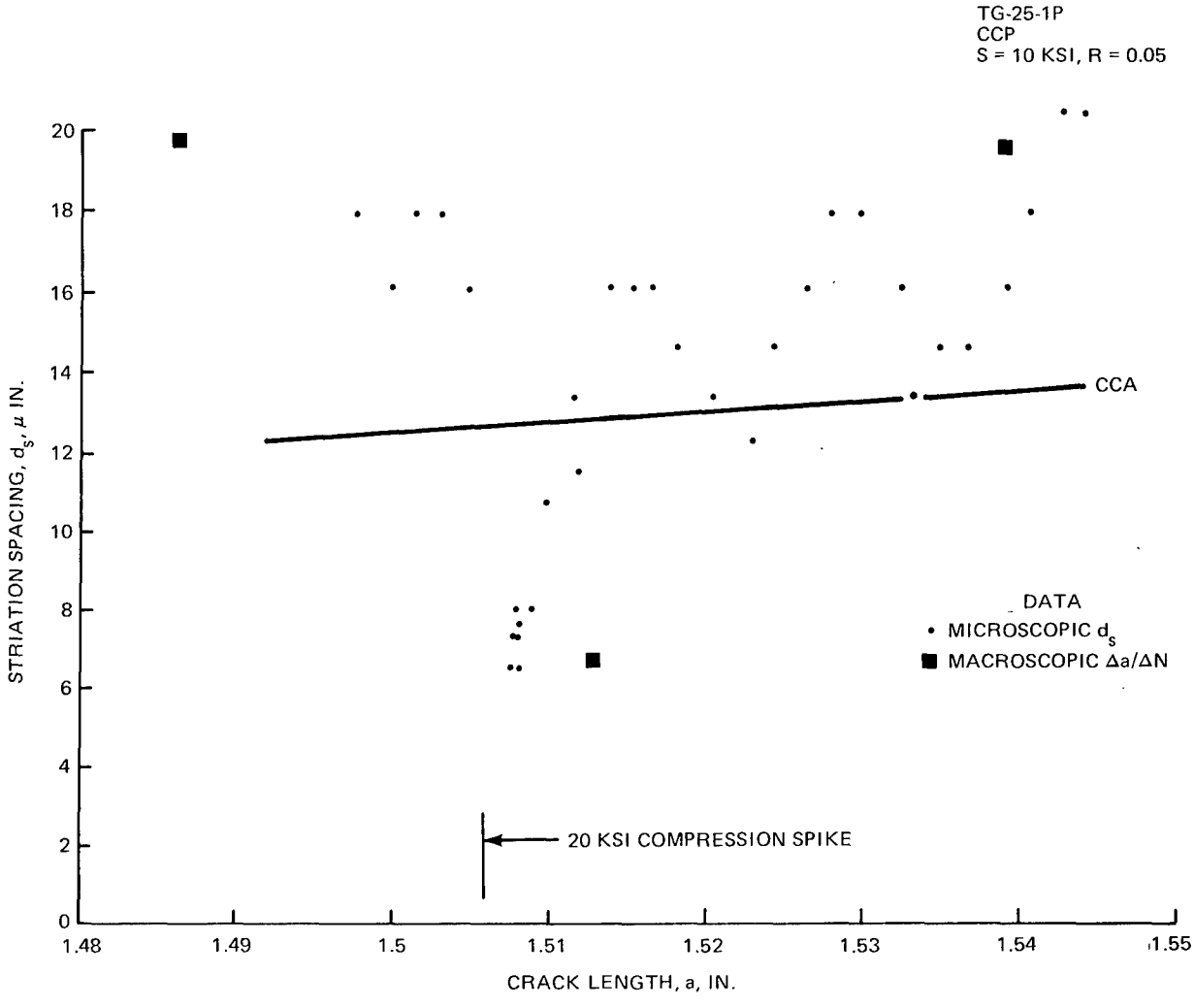


**Figure 78 Compression Spike, $R_C = -2$, $a_{ref} = 1.506$ In., Ti 6Al-4V Titanium**

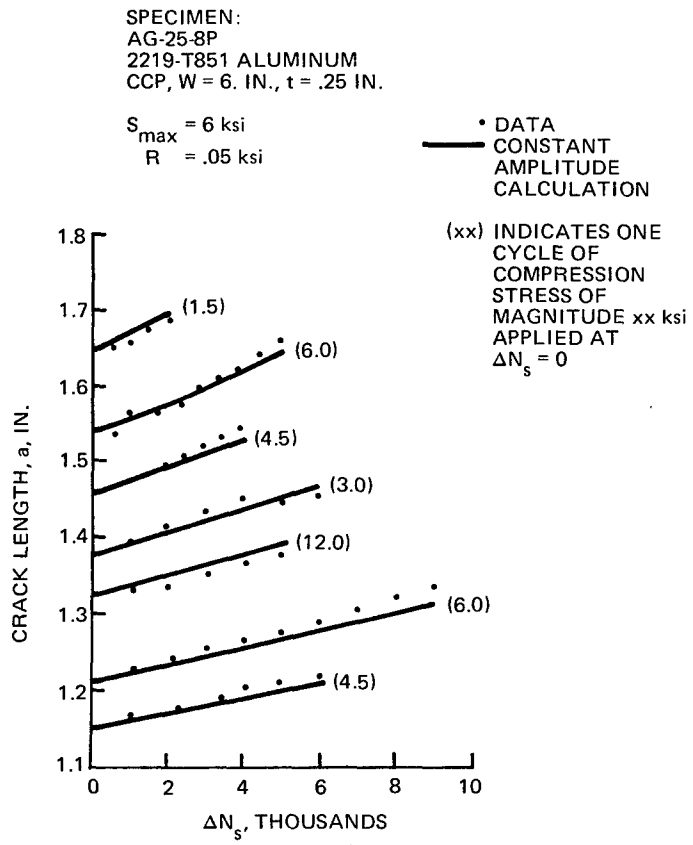


**Figure 79 Crack Length vs $\Delta N_s$ for Compression Spikes, Aluminum**

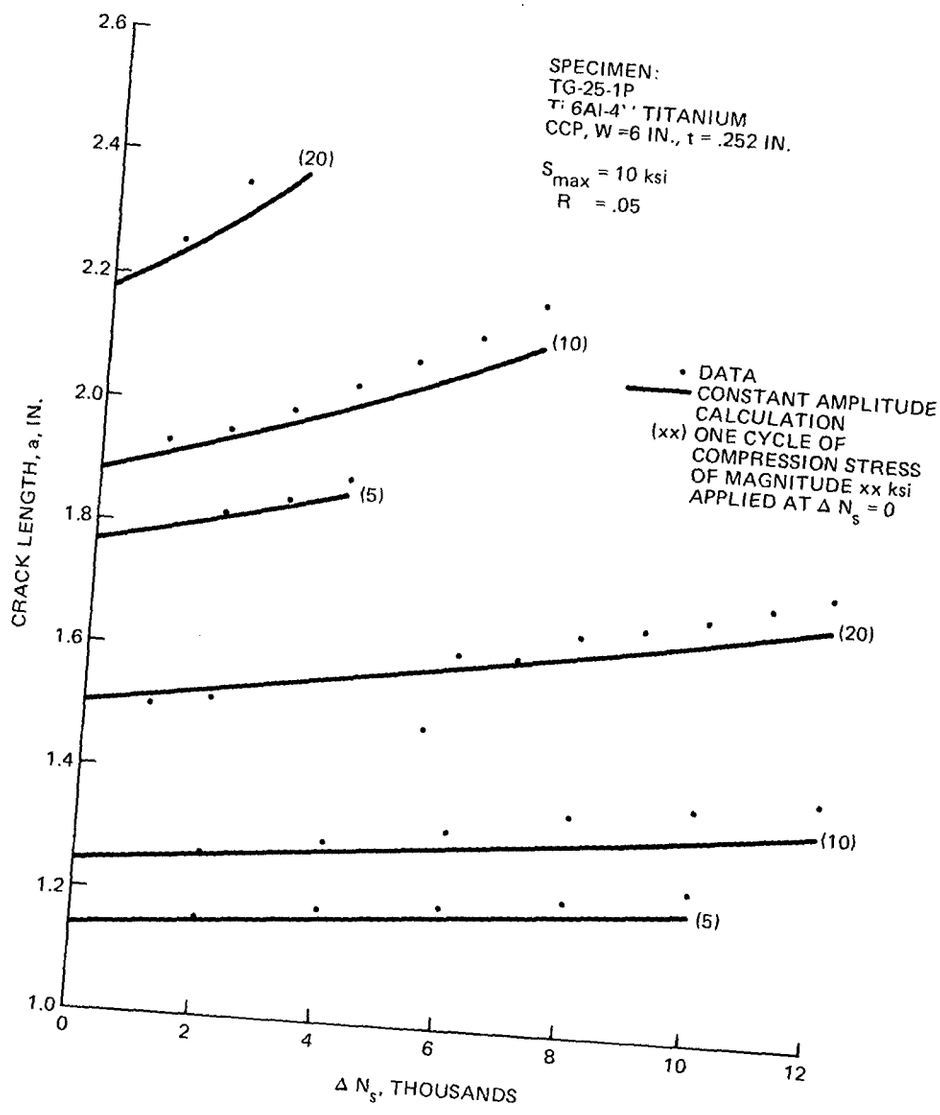


**Figure 80 Crack Length vs Δ $N_s$ for Compression Spikes, Titanium**

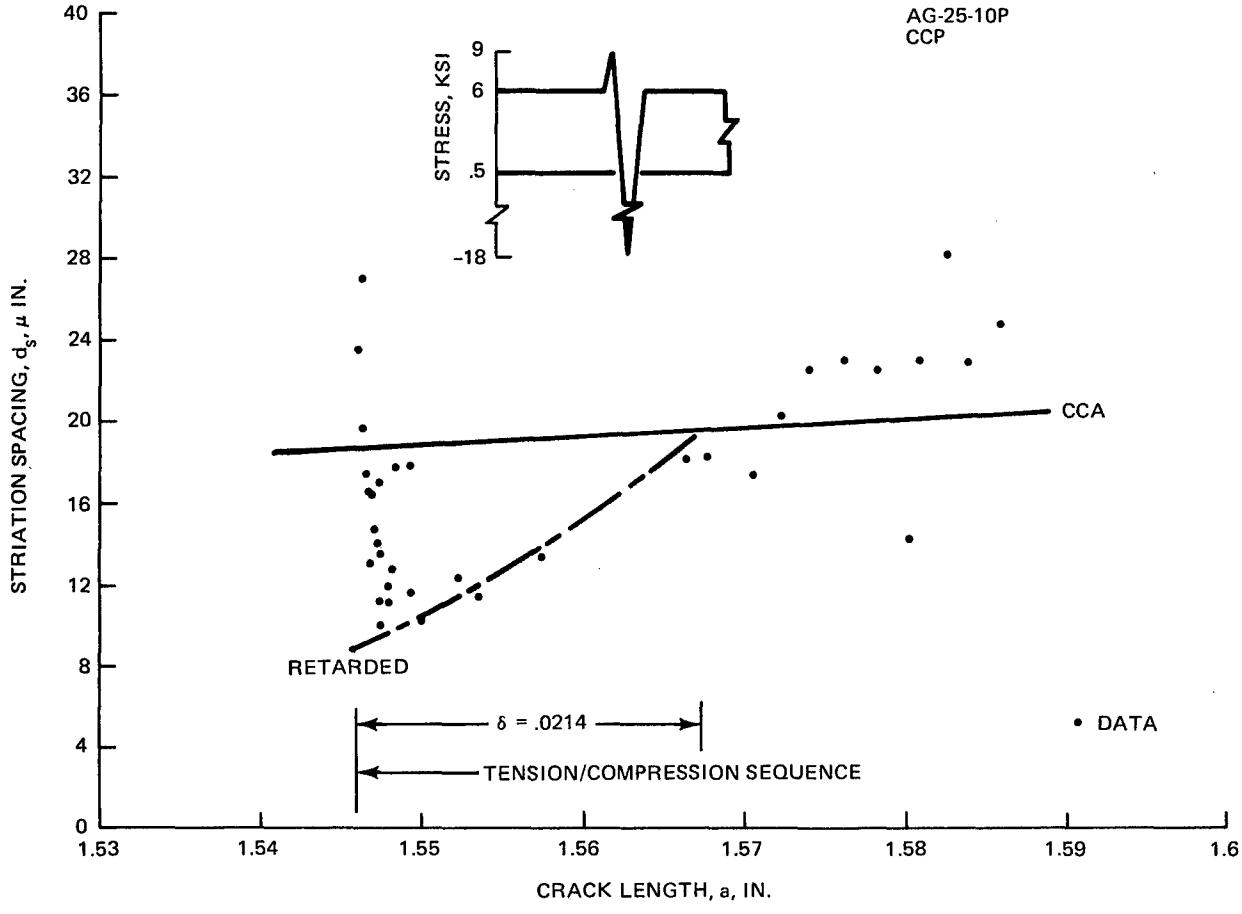


**Figure 81 Tension/Compression, O/L = 1.5, $R_C$ = -3, $a_{ref}$ = 1.546 In., 2219-T851 Aluminum**

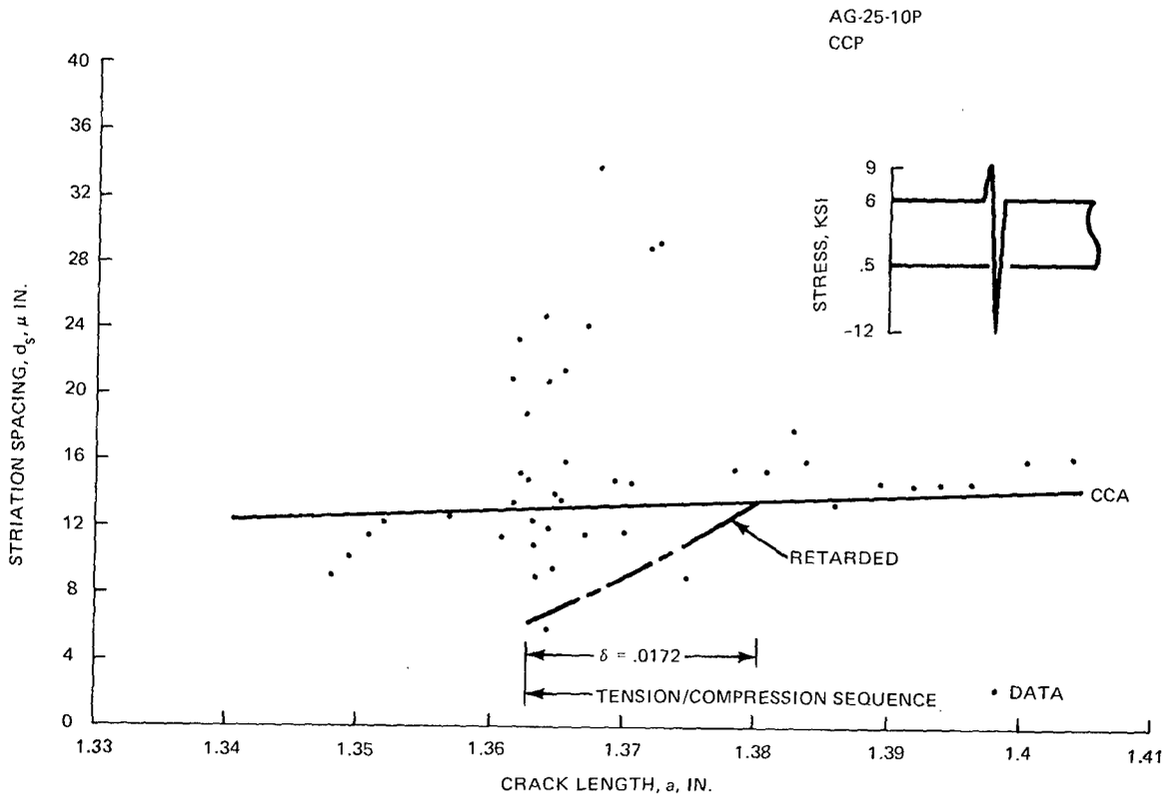


**Figure 82** Tension/Compression, O/L = 1.5, $R_C$ = -2, $a_{ref}$ = 1.363 In., 2219-T851 Aluminum

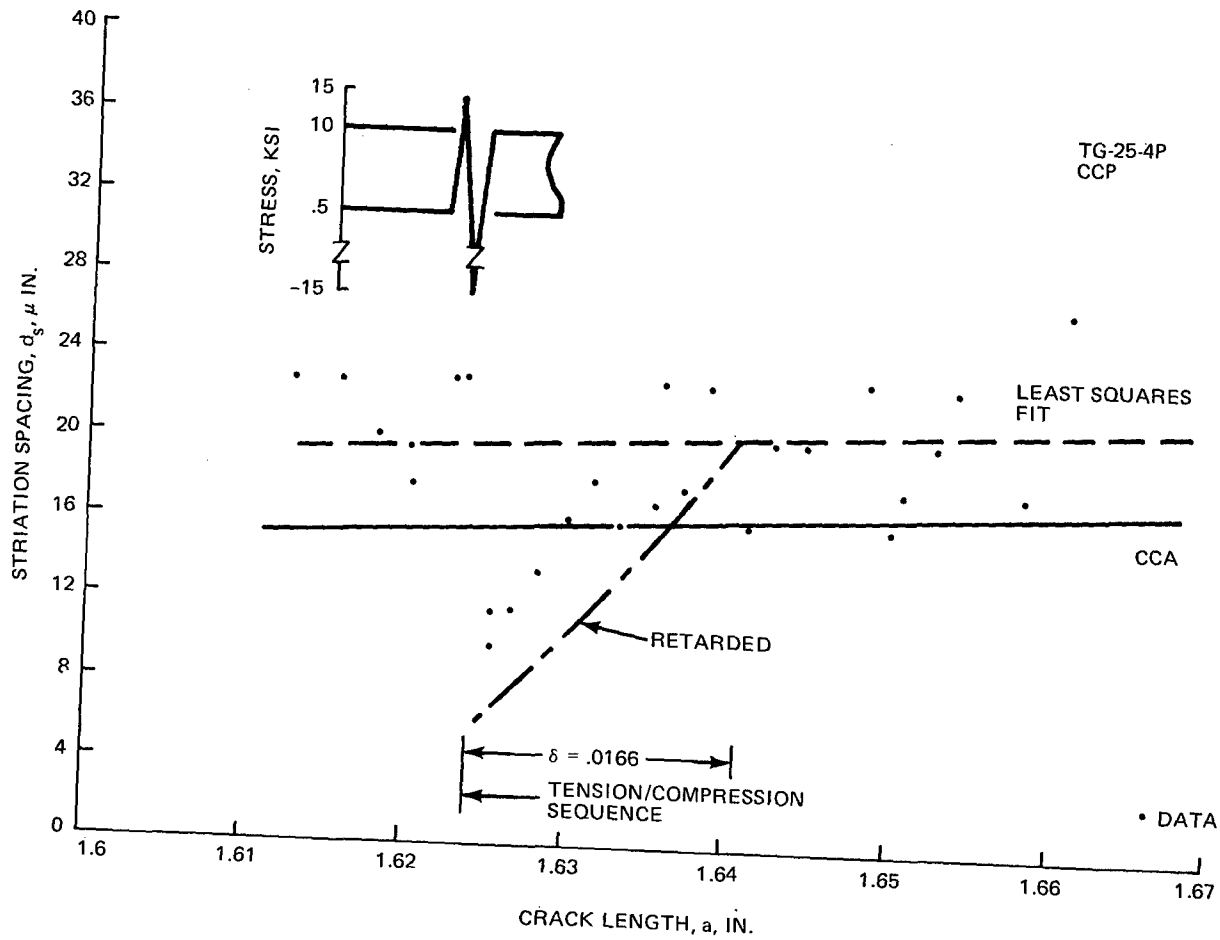


**Figure 83 Tension/Compression, O/L = 1.5, $R_C$ = -1.5, $a_{ref}$ = 1.624 In., Ti 6Al-4V Titanium**

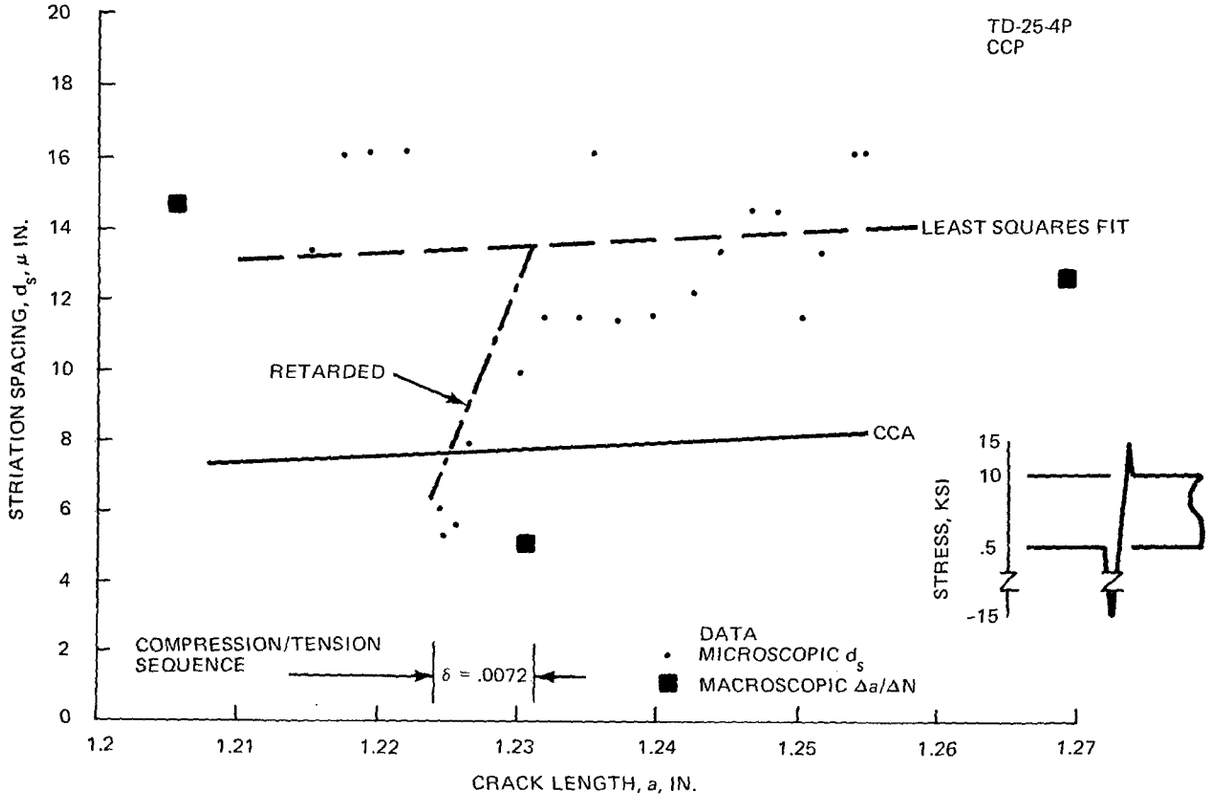


**Figure 84 Compression/Tension, O/L = 1.5, $R_C$ = -1.5, $a_{ref}$ = 1.224 In., Ti 6Al-4V Titanium**

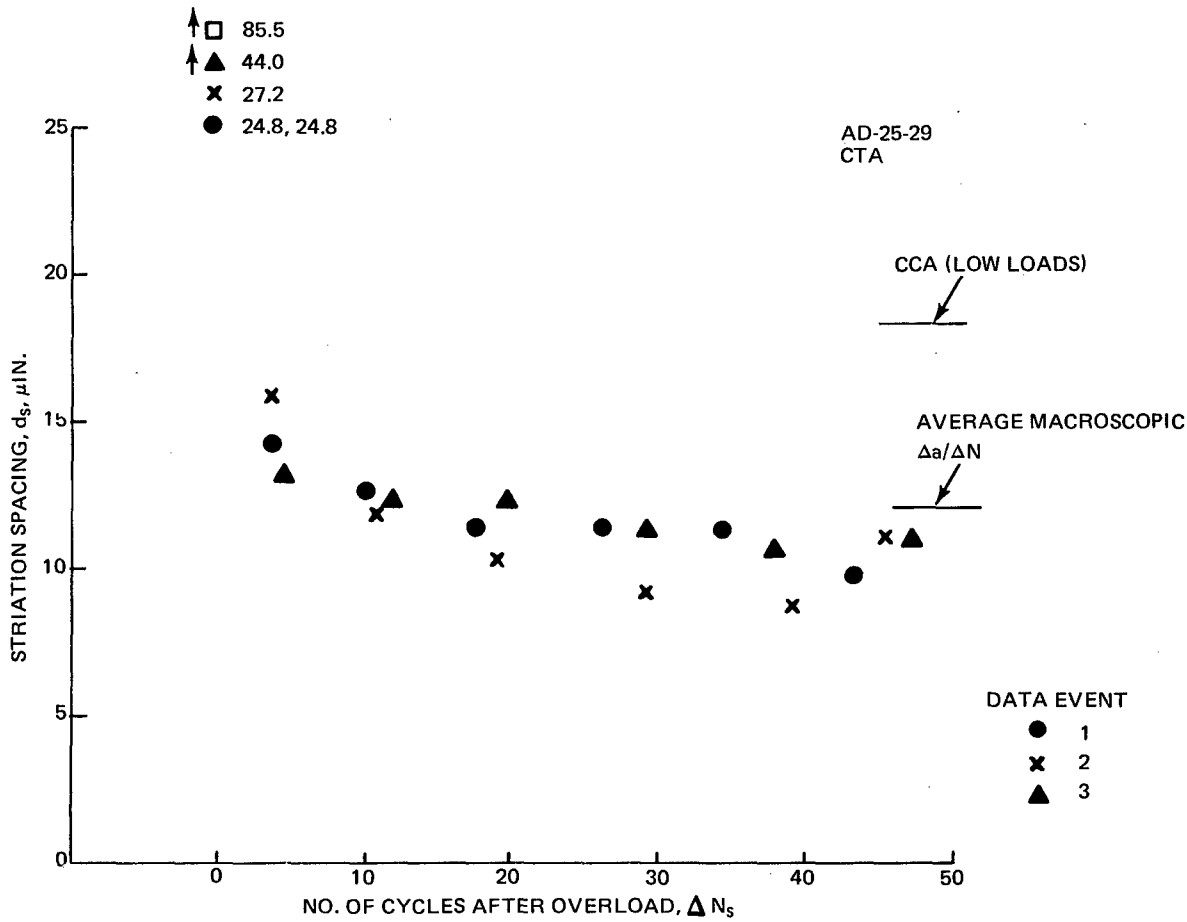


**Figure 85** Single Periodic Overloads, $a_{ref}$ = 1.44 In., O/L = 1.25, $N_{OL}/N$ = 1/50, 2219-T851 Aluminum

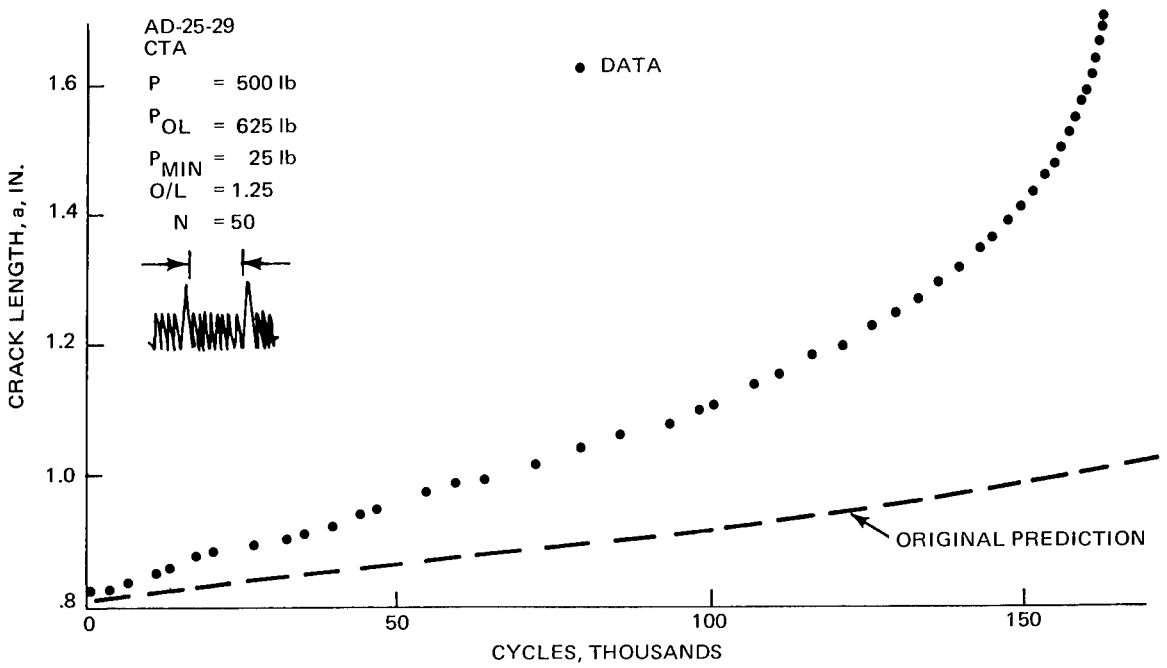


a. Original Prediction

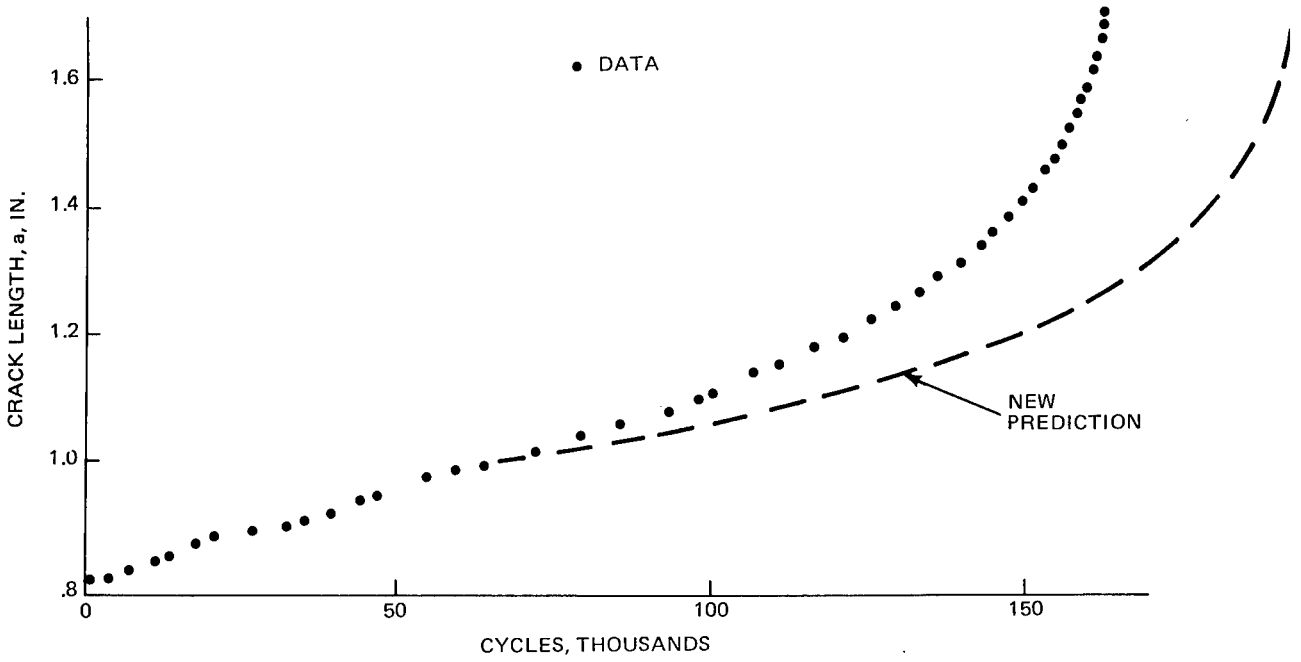


b. New Prediction

**Figure 86 Predicted a vs N for O/L = 1.25, N = 50, Single Periodic Overloads, 2219-T851 Aluminum**

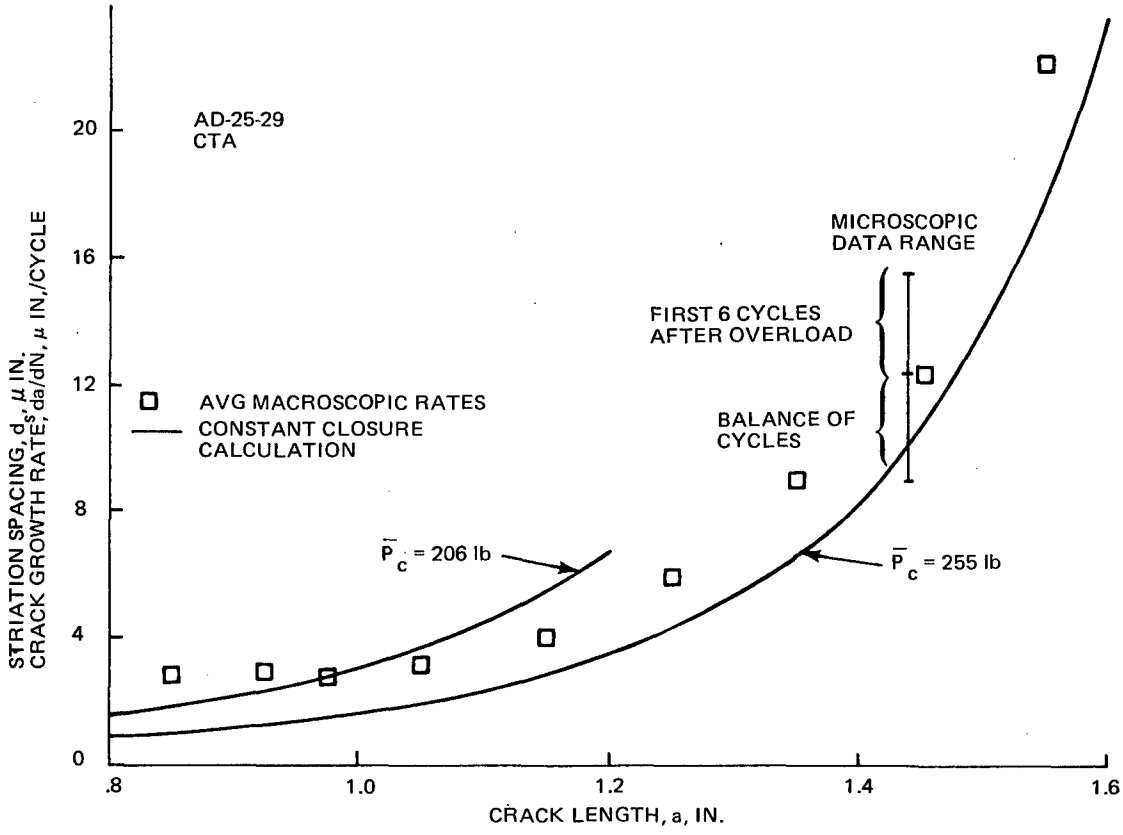


**Figure 87 Average Crack Growth Rates vs Crack Length, Single Periodic Overloads, 2219-T851 Aluminum**

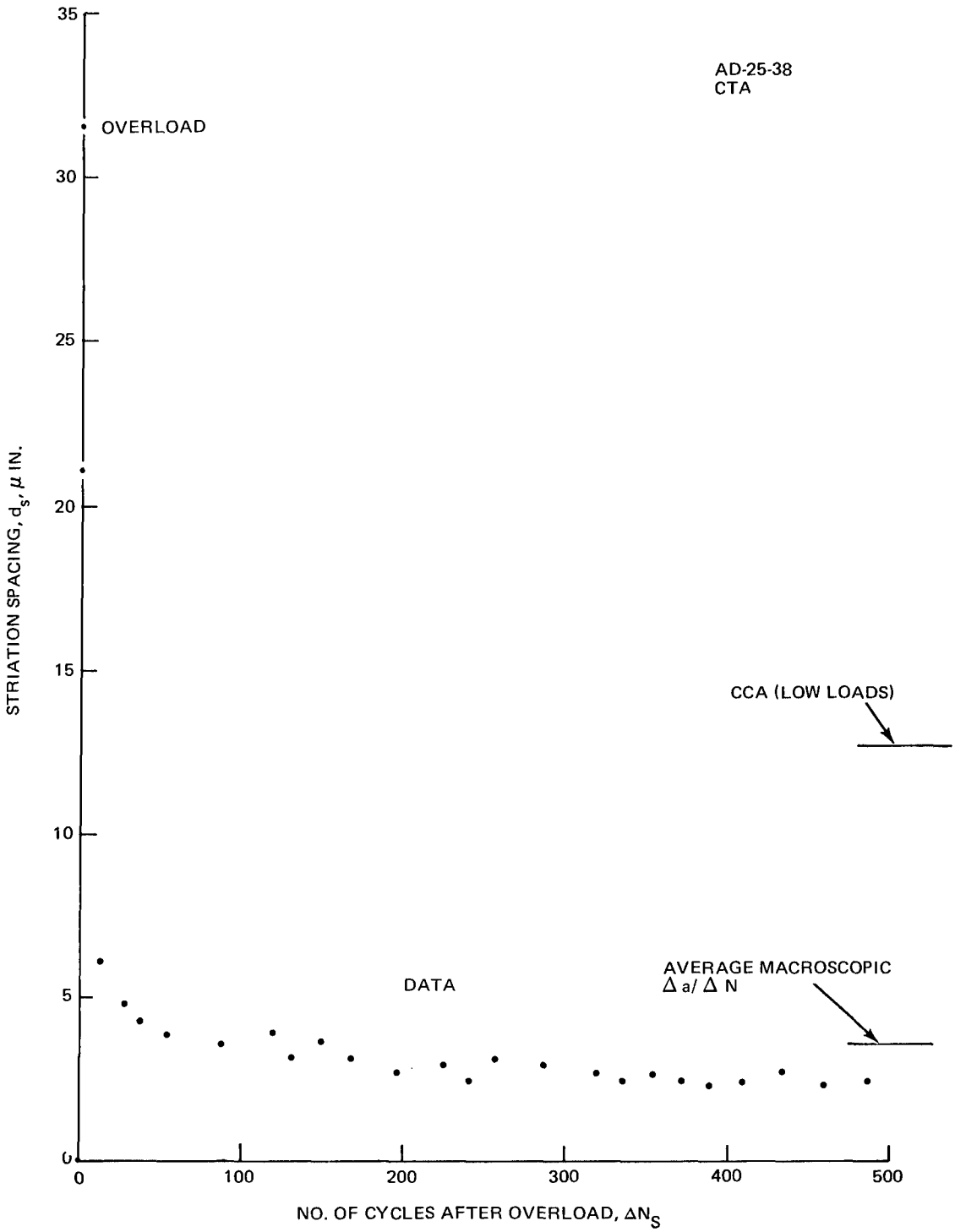


**Figure 88** Single Periodic Overloads, $a_{ref}$ = 1.36 In., O/L = 1.8, $N_{OL}/N$ = 1/500, 2219-T851 Aluminum

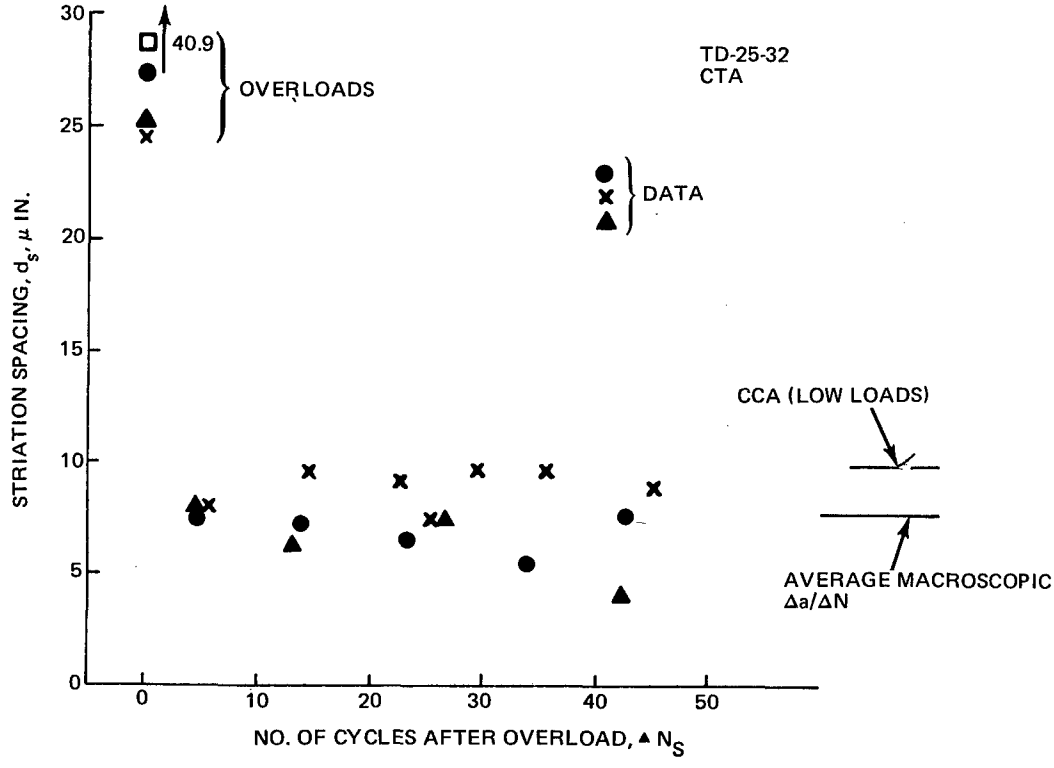


**Figure 89 Single Periodic Overloads, $a_{ref}$ = 1.4 In., O/L = 1.25, $N_{OL}$/N = 1/50, Ti 6Al-4V Titanium**

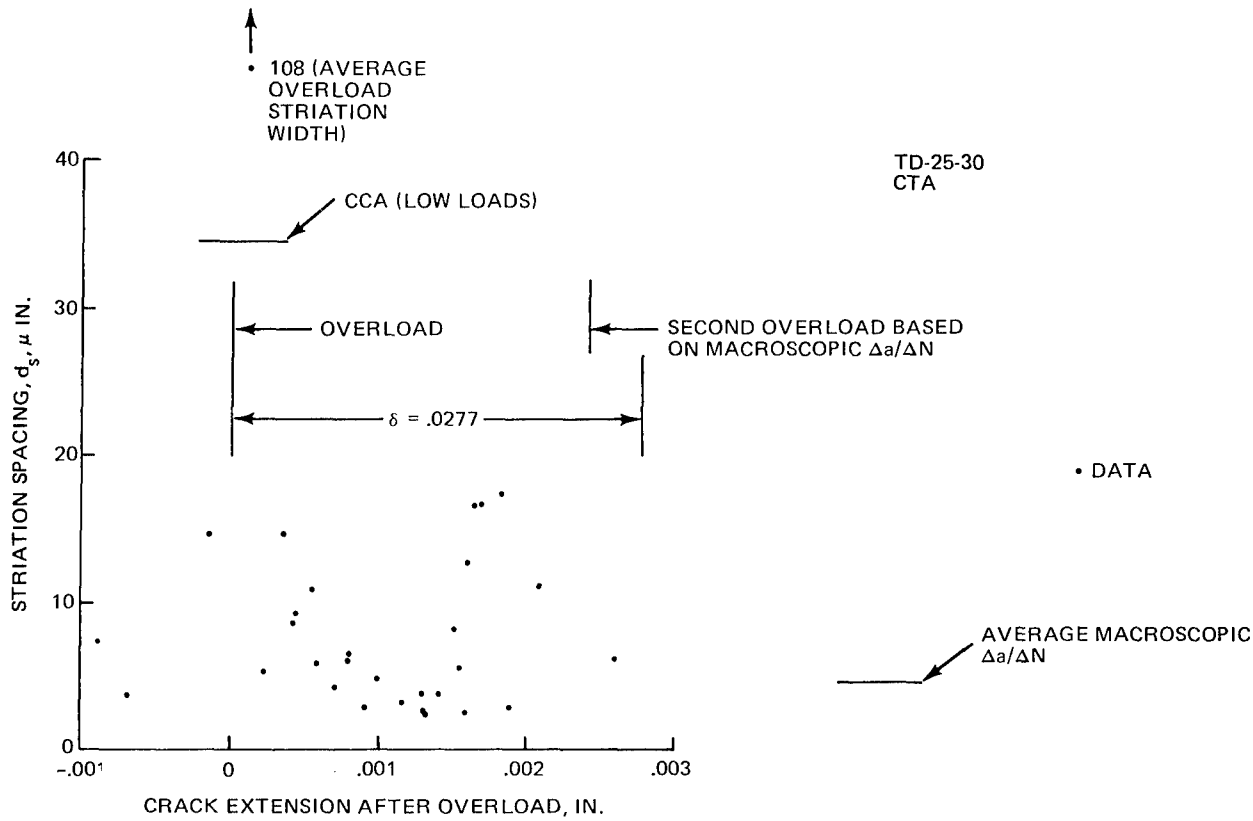


**Figure 90** Single Periodic Overloads, $a_{ref}$ = 1.5 In., O/L = 1.8, $N_{OL}/N$ = 1/500, Ti 6Al-4V Titanium

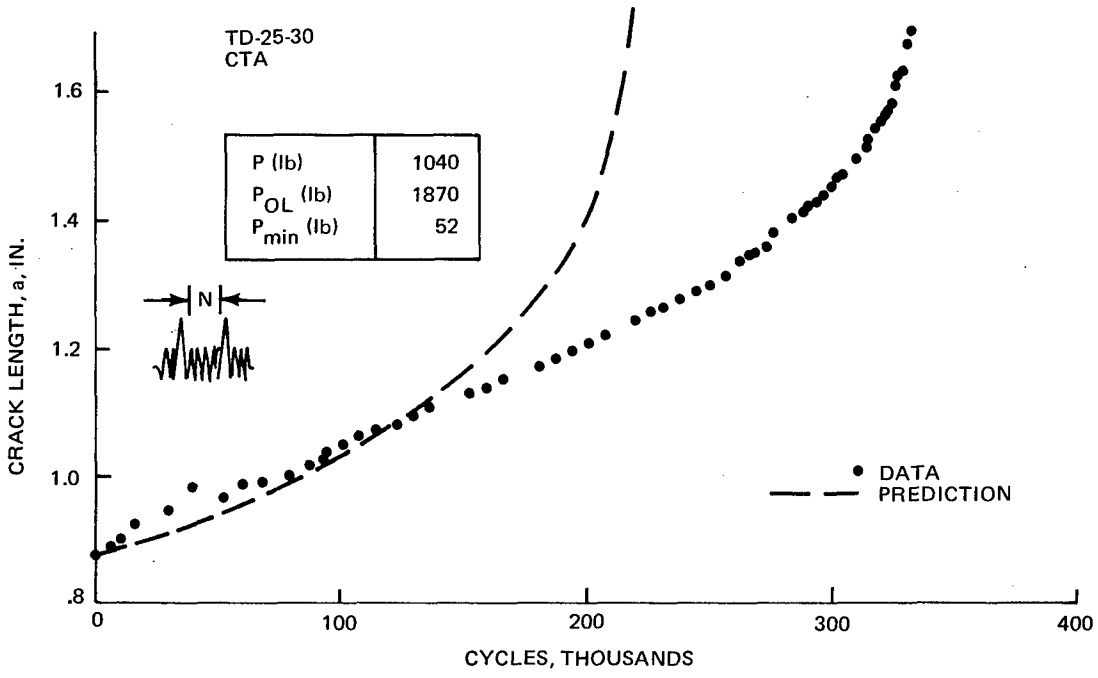


**Figure 91 Predicted a vs N for O/L = 1.8, N = 500, Single Periodic Overloads, Ti 6Al-4V Titanium**

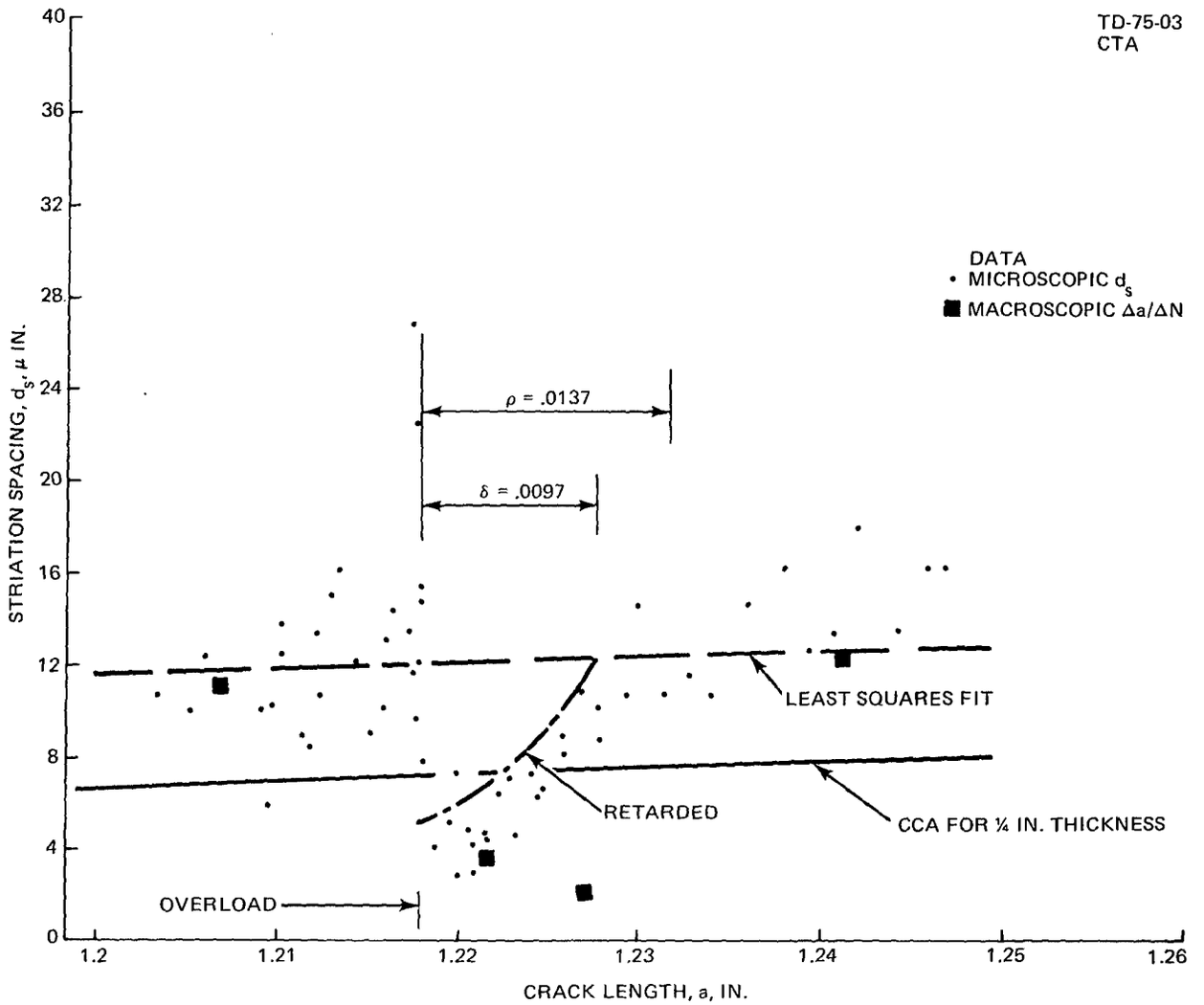


**Figure 92 Thickness Effects, O/L = 1.8, $a_{OL}$ = 1.218 In., Centerline, t = 0.75 In., Ti 6Al-4V Titanium**

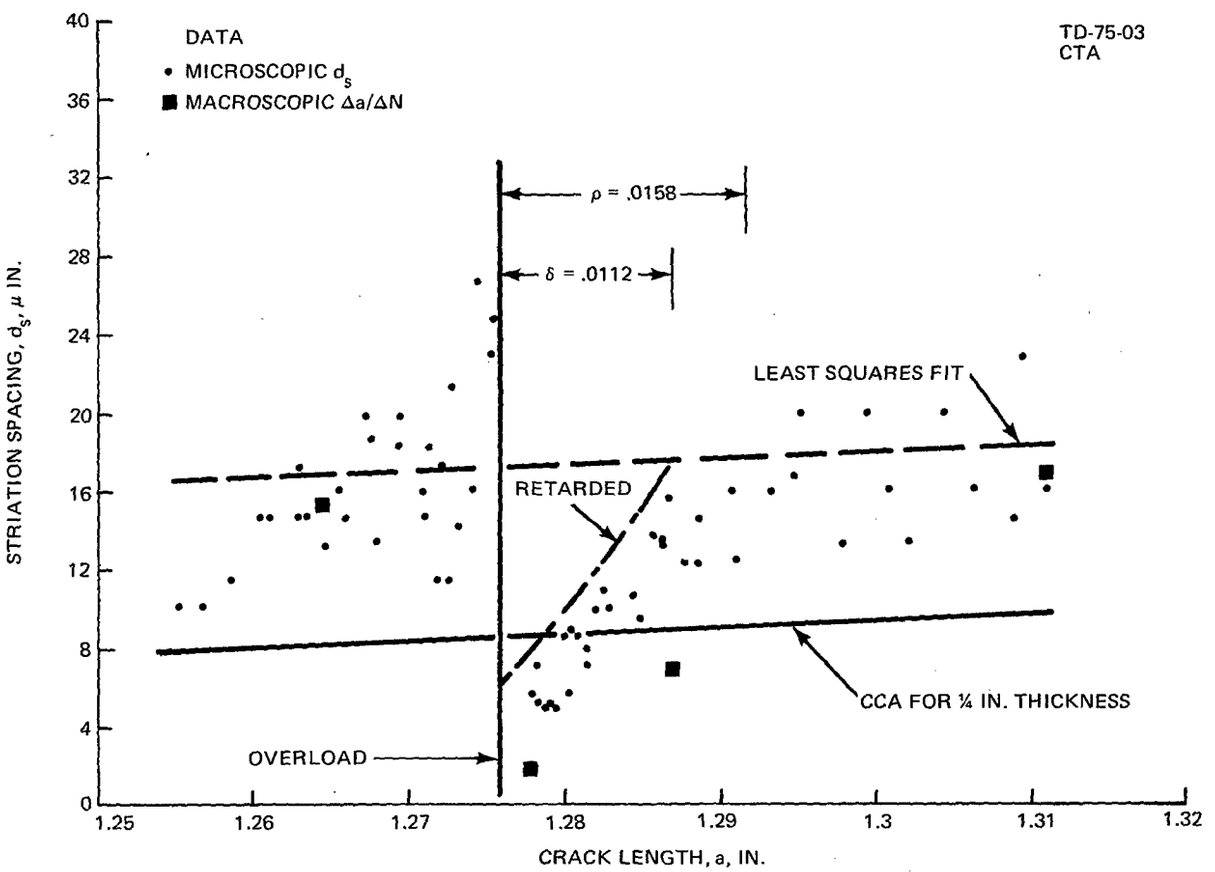


*Figure 93* **Thickness Effects, O/L = 1.8, $a_{OL}$ = 1.276 In., Centerline, t = 0.75 In., Ti 6Al-4V Titanium**

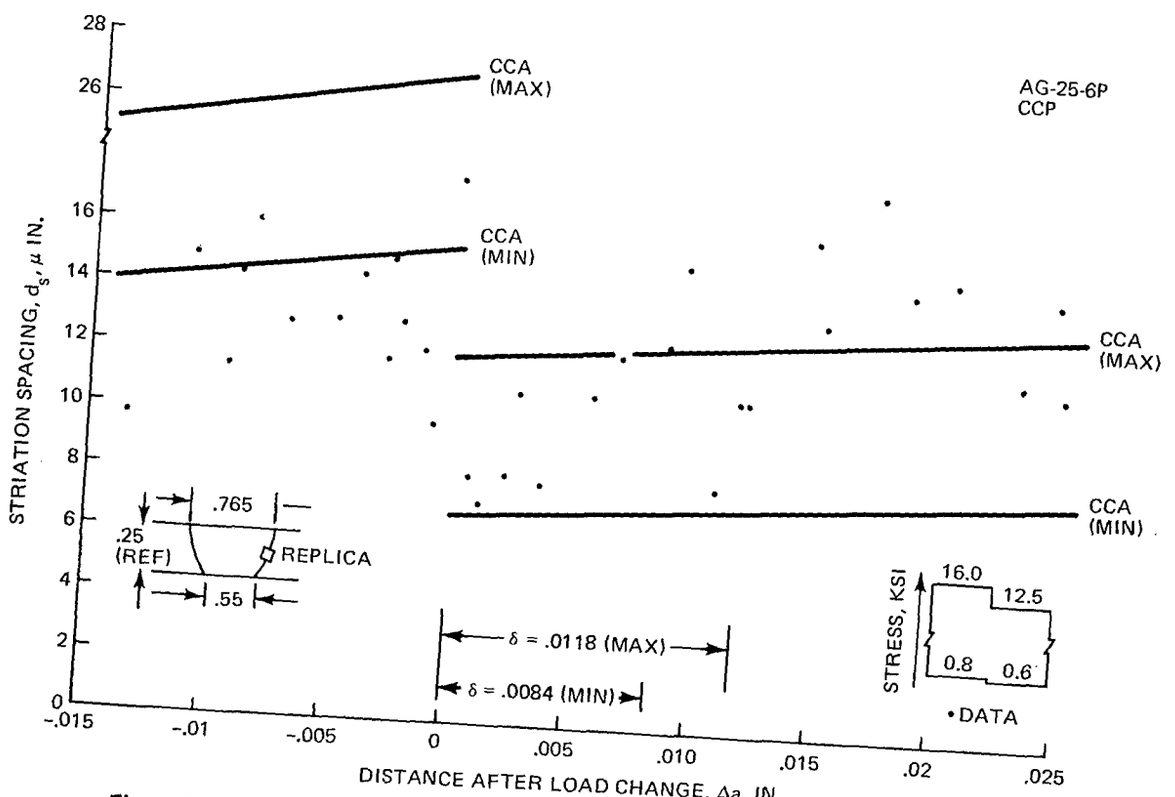


**Figure 94 Transition Crack, High-Low Load, $a_{ref}$ = 0.383 In., 2219-T851 Aluminum**

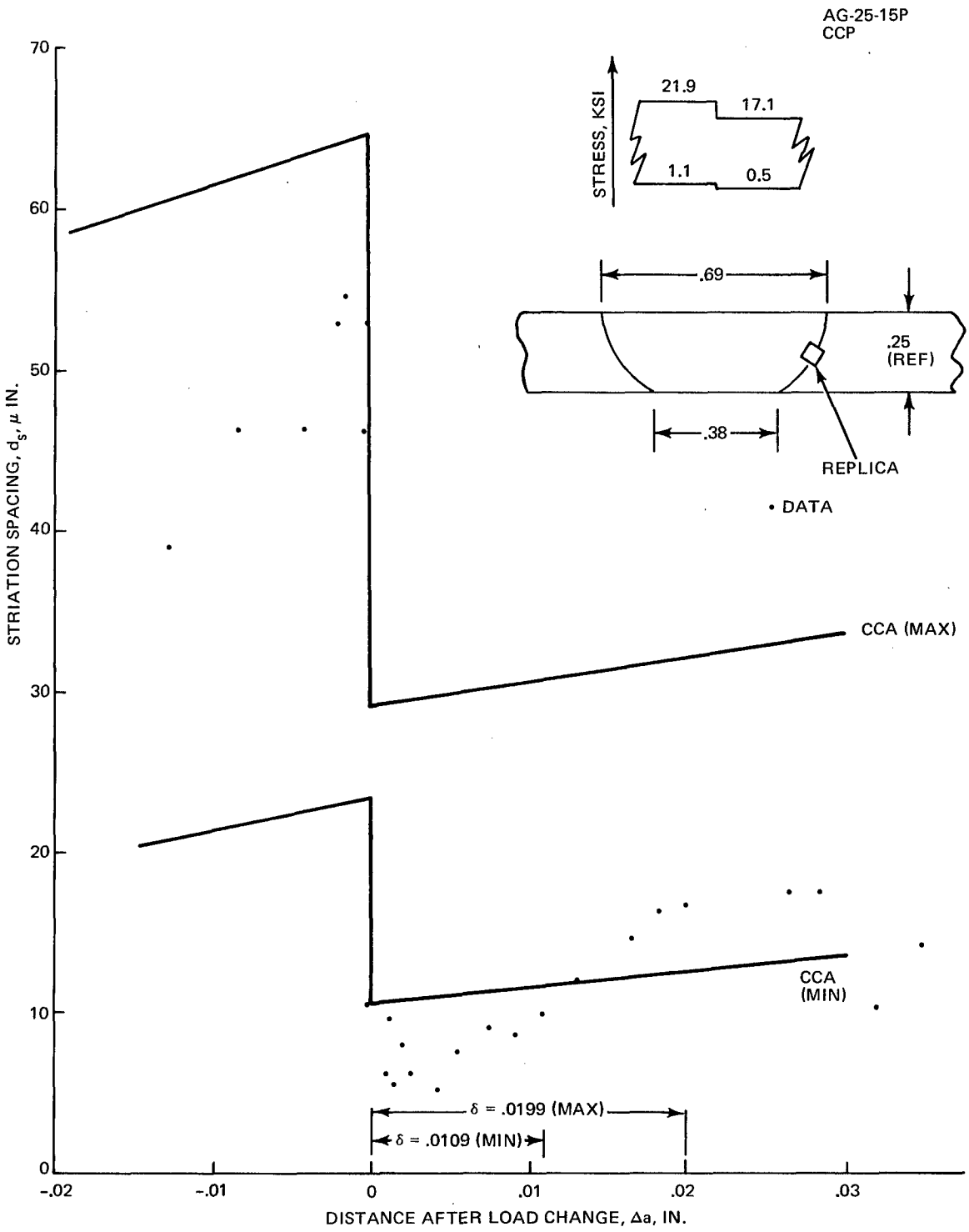


**Figure 95 Transition Crack, High-Low Load, $a_{ref}$ = 0.345 In., 2219-T851 Aluminum**

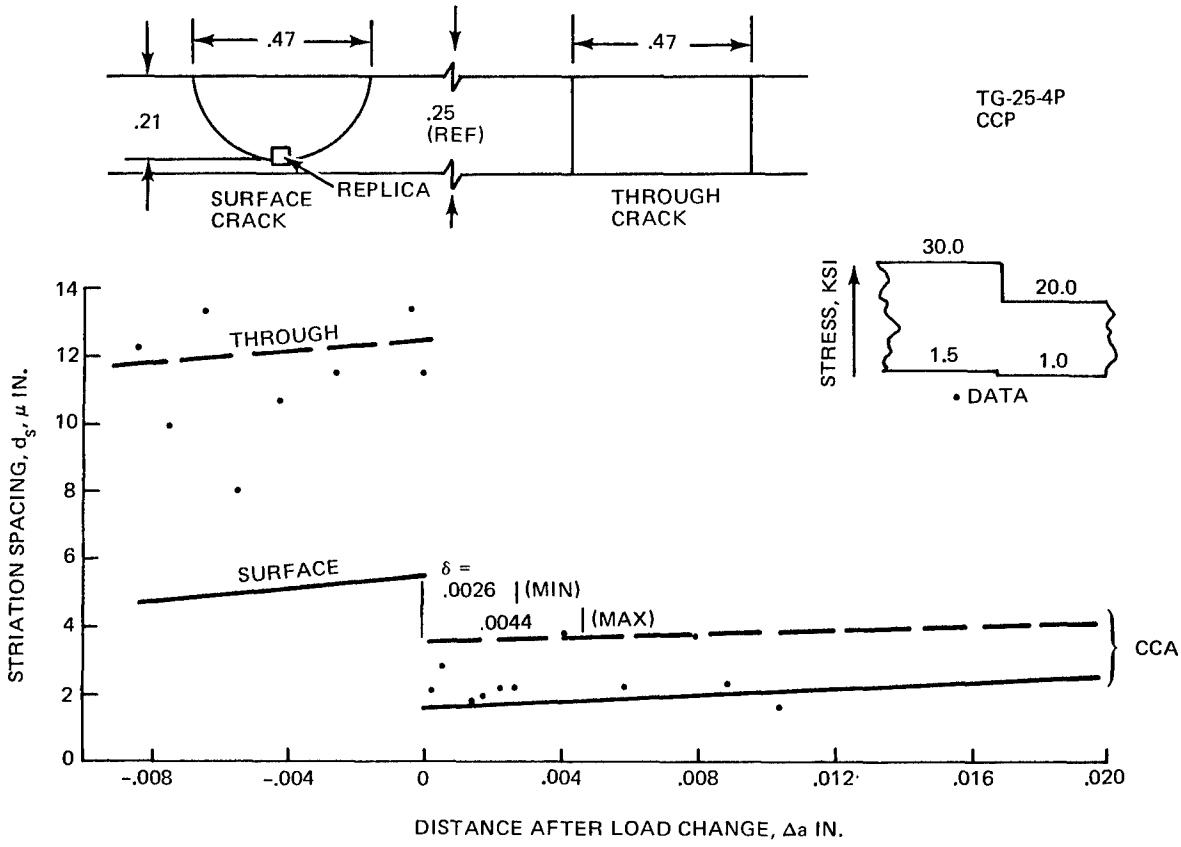


**Figure 96 Surface Crack, High-Low Load, $a_{ref}$ = 0.235 In., Ti 6Al-4V Titanium**

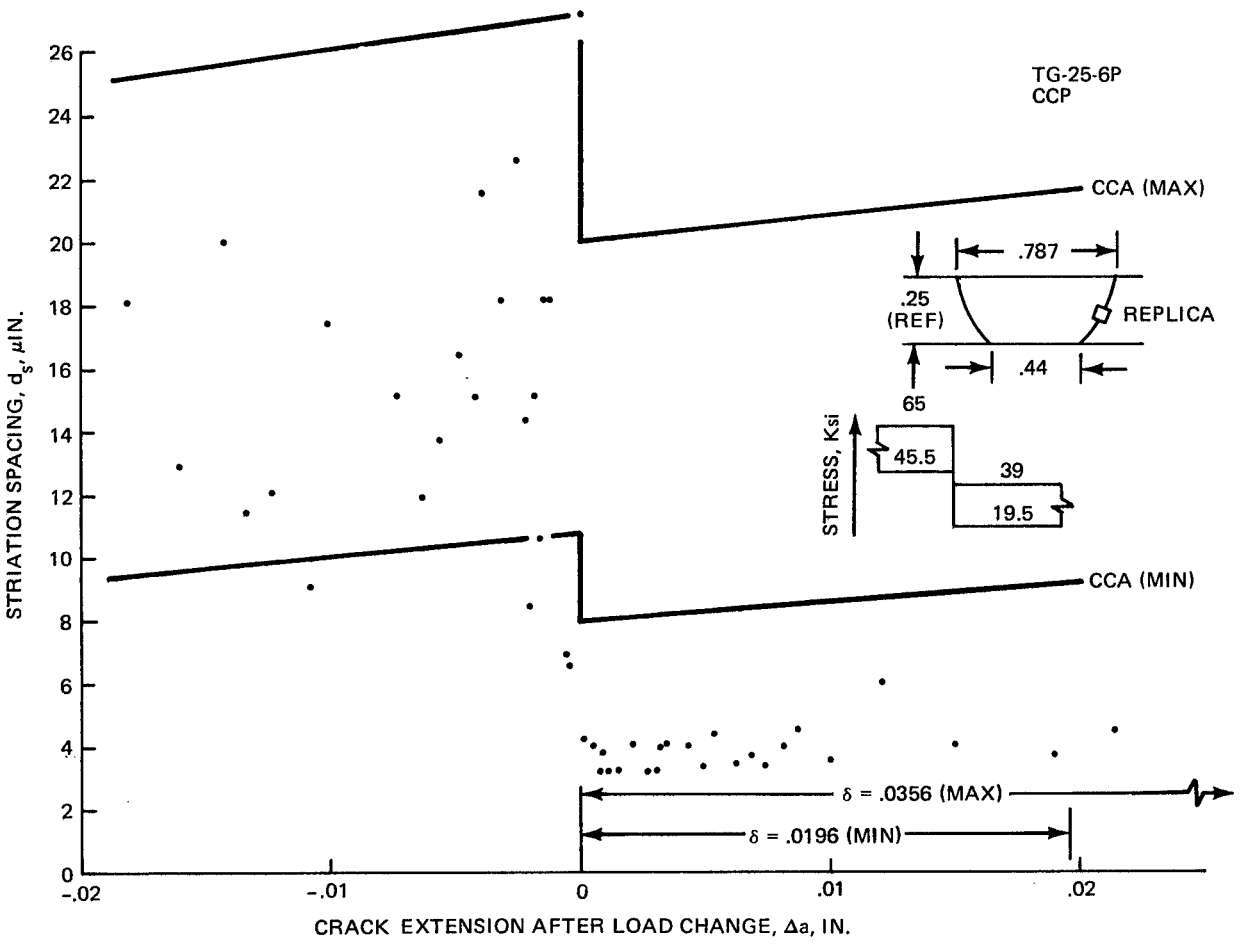


**Figure 97 Transition Crack, High-Low Load, $a_{ref}$ = .394 In., Ti 6Al-4V Titanium**

TABLE 1 MICROSCOPIC AND MACROSCOPIC SPECIMENS

| MATERIAL | SPECIMEN NUMBER | SPECIMEN TYPE | MAXIMUM APPLIED LOAD OR STRESS | STRESS RATIO | CRACK LENGTH a, in. |
|---|---|---|---|---|---|
| 2219-T851 Aluminum | AG-25-1 P | CCP | 10 ksi<br>6 ksi | 0.05 | 0.87 - .93<br>1.1 - 1.5 |
| | AG-25-1P | CCP | 6 ksi | 0.50 | 1.58 - 1.63 |
| Ti6Al-4V Titanium | TG-25-02 | CTB | 1100 lb | 0.05 | 1.05 - 1.45 |
| | TD-25-03 | CTA | 1220 lb | 0.50 | 1.27 - 1.32 |



TABLE 2 SURFACE AND FRACTURE FACE SPECIMENS

| MATERIAL | SPECIMEN NUMBER | SPECIMEN TYPE | MAXIMUM LOAD (OR STRESS) BASELINE | MAXIMUM LOAD (OR STRESS) OVERLOAD | MINIMUM LOAD (OR STRESS) | CRACK LENGTH, a, in. |
|---|---|---|---|---|---|---|
| 2219-T851 Aluminum | AG-25-1P | CCP | 6 ksi | CA* | 0.3 ksi | 1.1 - 1.5 |
| | AD-25-11 | CTA | 525 lb | 656 lb | 26 lb | 1.22 - 1.26 |
| | AD-25-15 | CTA | 550 lb | 825 lb | 27 lb | 1.26 - 1.32 |
| | AG-25-3P | CCP | 10 ksi | 18 Ksi | 0.5 ksi | .49 - .56 |
| Ti 6Al-4V Titanium | TG-25-02 | CTB | 1100 lb | CA | 55 lb | 1.1 - 1.5 |
| | TD-25-13 | CTA | 850 lb | 1062 lb | 43 lb | 1.31 - 1.37 |
| | TG-25-10 | CTB | 1000 lb | 1500 lb | 75 lb | 1.47 - 1.53 |
| | TD-25-106 | CTA | 900 lb | 1620 lb | 45 lb | 1.04 - 1.16 |

*CA - Constant Amplitude

TABLE 3 MATERIAL PROPERTIES

| CHARACTERISTIC | 2219-T851 ALUMINUM | Ti 6Al-4V TITANIUM |
|---|---|---|
| Tensile Yield Stress, ksi | 54.7 | 130.0 |
| Stable Tear Threshold Stress Intensity, ksi$\sqrt{in.}$ | 30.0 | 72.5 |
| Crack Growth Rate, in./cycle | $1.96 \times 10^{-9}$ (1 + 0.6R) $\Delta K^{3.34}$ $0 \leqslant R \leqslant 0.5$ | $5.9 \times 10^{-10}$ (1 + 0.7R) $\Delta K^{3.08}$ $0 \leqslant R \leqslant 0.7$ |
| Closure Factor, $C_f$ | $0.347 + (0.4-0.347)(1+R)^{3.93}$ | $0.338 + (0.4-0.338)(1+R)^{3.33}$ |



TABLE 4 AFFECTED CRACK LENGTH SPECIMENS

| MATERIAL | SPECIMEN NUMBER | SPECIMEN TYPE | LOCATION | OL (1) | $a_{OL}$ (2) | MAXIMUM LOAD (OR STRESS) | | MINIMUM LOAD (OR STRESS) | $K_{max_{OL}}$, ksi$\sqrt{in.}$ |
|---|---|---|---|---|---|---|---|---|---|
| | | | | | | BASELINE | OVERLOAD | | |
| 2219-T851 Aluminum | AD-25-11 | CTA | $\mathcal{L}$ | 1.25 | 1.245 | 525 lb | 656 lb | 26 lb | 16.0 |
| | AD-25-15 | CTA | $\mathcal{L}$, Edge | 1.5 | 1.282 | 550 lb | 825 lb | 27 lb | 21.0 |
| | AD-25-07 | CTA | $\mathcal{L}$ | 1.8 | 1.375 | 350 lb | 630 lb | 17 lb | 18.7 |
| | | | | 1.8 | 1.603 | 350 lb | 630 lb | 17 lb | 25.8 |
| | AG-25-3P | CCP | $\mathcal{L}$ | 1.8 | .495 | 10 Ksi | 18 ksi | 0.5 ksi | 22.8 |
| Ti 6Al-4V Titanium | TD-25-13 | CTA | $\mathcal{L}$, Edge | 1.25 | 1.327 | 850 lb | 1062 lb | 43 lb | 28.7 |
| | TG-25-10 | CTB | $\mathcal{L}$, Edge | 1.5 | 1.483 | 1000 lb | 1500 lb | 75 lb | 49.6 |
| | TG-25-11 | CTB | $\mathcal{L}$ | 1.8 | 1.059 | 1000 lb | 1800 lb | 75 lb | 32.6 |
| | TD-25-106 | CTA | $\mathcal{L}$, Edge | 1.8 | 1.074 | 900 lb | 1620 lb | 45 lb | 40.8 |
| | | | | | 1.127 | 900 lb | 1620 lb | 45 lb | 43.9 |

Notes: 1 Overload Ratio
2 Crack Length at Overload

TABLE 5 DELAYED RETARDATION SPECIMENS

| MATERIAL | SPECIMEN NUMBER | TYPE | LOCATION | O/L | $^{a}$OL, IN. | $\delta$ IN. | $\rho$, IN. |
|---|---|---|---|---|---|---|---|
| | AD-25-12 | CTA | ℄ | 1.25 | 1.352 | .0107 | .0151 |
| | AD-25-11 | CTA | ℄ | 1.25 | 1.245 | .0095 | .0135 |
| | AD-25-15 | CTA | ℄, Edge | 1.5 | 1.282 | .0166 | .0235 |
| 2219-T851 | AG-25-2P | CCP | ℄, Edge | 1.5 | .841 | .0249 | .0347 |
| | AG-25-2P | CCP | ℄ | 1.5 | .908 | .0272 | .0384 |
| Aluminum | AD-25-07 | CTA | ℄ | 1.8 | 1.375 | .0132 | .0136 |
| | AD-25-07 | CTA | ℄ | 1.8 | 1.603 | .0251 | .0355 |
| | AG-25-3P | CCP | ℄, Edge | 1.8 | .495 | .0196 | .0277 |
| | AG-25-3P | CCP | ℄ | 1.8 | 1.343 | .0617 | .0872 |
| | AG-25-3P | CCP | ℄ | 1.8 | 1.548 | .0759 | .1073 |
| | TD-25-13 | CTA | ℄, Edge | 1.25 | 1.327 | .0054 | .0077 |
| | TG-25-10 | CTB | ℄, Edge | 1.5 | 1.483 | .0163 | .0231 |
| Ti 6Al-4V | TD-25-16 | CTA | ℄ | 1.5 | 1.430 | .0093 | .0131 |
| Titanium | TG-25-11 | CTB | ℄ | 1.8 | 1.059 | .0071 | .0100 |
| | TD-25-106 | CTA | ℄, Edge | 1.8 | 1.074 | .0110 | .0156 |
| | TD-25-106 | CTA | ℄ | 1.8 | 1.127 | .0129 | .0182 |

TABLE 6 DELAYED RETARDATION SURVEY RESULTS

| FIGURE NO. | SPECIMEN NO. | O/L | APPARENT DELAYED RETARDATION ? |
|---|---|---|---|
| 34 | AD-25-12* | 1.25 | (1) |
| 35 | AD-25-11 | 1.25 | (1) |
| 36 | AD-25-15* | 1.5 | No |
| 37 | AD-25-15* | 1.5 | Possible |
| 38 | AG-25-2P* | 1.5 | Yes |
| 39 | AG-25-2P* | 1.5 | Yes |
| 40 | AG-25-2P* | 1.5 | Possible |
| 41 | AD-25-07* | 1.8 | (1) |
| 42 | AD-25-07* | 1.8 | No |
| 43 | AG-25-3P* | 1.8 | Yes |
| 44 | AG-25-3P* | 1.8 | Possible |
| 45 | AG-25-3P* | 1.8 | (2) |
| 46 | AG-25-3P* | 1.8 | (2) |
| 47 | TD-25-13 | 1.25 | (1) |
| 48 | TD-25-13 | 1.25 | (1) |
| 49 | TG-25-10* | 1.5 | No |
| 50 | TG-25-10* | 1.5 | Yes |
| 51 | TD-25-16 | 1.5 | No |
| 52 | TD-25-11 | 1.8 | No |
| 53 | TD-25-106 | 1.8 | Possible |
| 54 | TD-25-106 | 1.8 | Possible |
| 54 | TD-25-106 | 1.8 | No |

Notes:
1 Not Apparent from the data
2 Large scale yielding, see text.
* See photo section.

TABLE 7 DELAYED RETARDATION – NUMERICAL VALUES

| | FIGURE NO. | SPECIMEN NO. | O/L | $a_{OL}$, IN. | $a_{MIN}$,(1) IN. | MINIMUM $f_n$ | $\Delta a_{DR}$,(2) IN. | $\frac{\Delta a_{DR}}{\delta}$ |
|---|---|---|---|---|---|---|---|---|
| Definite Delayed Retardation | 38 | AG-25-2P | 1.5 | .841 | .843 | 0.4 | .002 | .092 |
| | 39 | AG-25-2P | 1.5 | .841 | .849 | 0.4 | .008 | .369 |
| | 43 | AG-25-3P | 1.8 | .495 | .500 | 0.5 | .005 | .255 |
| | 50 | TG-25-10 | 1.5 | 1.483 | 1.4895 | 0.3 | .0065 | .399 |
| Possible Delayed Retardation | 37 | AD-25-15 | 1.5 | 1.282 | 1.284 | 0.6 | .002 | .120 |
| | 40 | AG-25-2P | 1.5 | .908 | .9105 | 0.3 | .0025 | .092 |
| | 44 | AG-25-3P | 1.8 | .495 | .498 | 0.5 | .003 | .153 |
| | 53 | TD-25-106 | 1.8 | 1.074 | ~1.077 | 0.6 | .003 | .273 |
| | 54 | TD-25-106 | 1.8 | 1.074 | ~1.079 | 0.7 | .005 | .455 |

Notes:
1 Crack length at minimum striation spacing
2 $a_{min} - a_{OL}$

TABLE 8 LEAST SQUARES RESULTS FOR DELAYED RETARDATION SPECIMENS

| MATERIAL | FIGURE NO. | SPECIMEN NO. | O/L | $\gamma_1$ | B |
|---|---|---|---|---|---|
| 2219-T851 Aluminum | 36 | AD-25-15 | 1.5 | .86 | .31 |
| | 37 | AD-25-15 | 1.5 | .77 (84)(1) | 1.20 (.58)(1) |
| | 38 | AG-25-2P | 1.5 | .84 | 1.54 |
| | 39 | AG-25-2P | 1.5 | .86 | 7.0 |
| | 40 | AG-25-2P | 1.5 | .84 | 1.05 |
| | 42 | AD-25-07 | 1.8 | .79 | 1.00 |
| | 43 | AG-25-3P | 1.8 | .67(2) | 20.7(2) |
| | 44 | AG-25-3P | 1.8 | .78 | .64 |
| Ti 6Al-4V Titanium | 49 | TG-25-10 | 1.5 | .91 | 1.75 |
| | 50 | TG-25-10 | 1.5 | 1.00 | 1.92 |
| | 51 | TD-25-16 | 1.5 | .88 | .26 |
| | 52 | TD-25-11 | 1.8 | .87 | .35 |
| | 53 | TD-25-106 | 1.8 | .79(3) | .50(3) |
| | 54 | TD-25-106 | 1.8 | .78 | 1.12 |
| | 55 | TD-25-106 | 1.8 | .81 | .91 |

Notes:
1 Data in 0.001 in increment after overload excluded
2 Data in 0.002 increment after overload excluded
3 Data in 0.001 increment after overload and $f_n$ value at a = 1.082 in. excluded

TABLE 9 ACCELERATION SPECIMENS

| MATERIAL | SPECIMEN NO. | TYPE | O/L | $a_{OL}$ in. | MAXIMUM LOAD, LB | | MINIMUM LOAD LB | NO. OF OVERLOAD CYCLES |
|---|---|---|---|---|---|---|---|---|
| | | | | | BASELINE | OVERLOAD | | |
| 2219-T851 Aluminum | AD-25-12 | CTA | 1.5 | 1.069 | 450 | 675 | 23 | 730 |
| | AD-25-19 | CTA | 1.25 | 1.396 | 400 | 500 | 20 | 610 |
| Ti 6Al-4V Titanium | TD-25-05 | CTA | 1.25 | 1.418 | 650 | 813 | 33 | 880 |
| | TD-25-110 | CTA | 1.8 | .692 | 900 | 1620 | 45 | 500 |

TABLE 10 ACCELERATION MEASUREMENT RESULTS

| SPECIMEN NO. | O/L | da/dn(1) $\mu$ IN./CYCLE | 1ST OVERLOAD CYCLE STRIATION WIDTH, $d_S$, $\mu$ IN. | | STABILIZED $d_s$, $\mu$ IN. | | $\frac{3}{2}$ | $\frac{4}{2}$ | $\frac{5}{1}$ |
|---|---|---|---|---|---|---|---|---|---|
| | | | (2) | MEASURED | STAGE 1 | STAGE 2 | | | |
| | | 1 | 2 | 3 | 4 | 5 | 6 | 7 | 8 |
| AD-25-12 | 1.5 | 10.8 | 21 | 51-89 (70)(3) | 20 | 12 | 3.3 | .95 | 1.11 |
| AD-25-19 | 1.25 | 15.2 | 23 | 47.5-52.5 (50) | 26 | – | 2.2 | 1.13 | – |
| TD-25-05 | 1.25 | 11.2 | 17 | $\geqslant$40 | 19 | – | $\geqslant$2.4 | 1.12 | – |
| TD-25-110 | 1.8 | 12.2 | 27 | 100 | 22 | $\approx$12 | 3.7 | .81 | .98 |

Notes :
1 CCA value during overloads
2 Crack closure model prediction
3 Average

TABLE 11 SINGLE PERIODIC OVERLOAD SPECIMENS

| MATERIAL | SPECIMEN NO. | SPECIMEN TYPE | O/L | $a_{ref}$,* IN | MAXIMUM LOAD, LB | | MINIMUM LOAD, LB | FREQUENCY OF OVERLOADS CYCLES |
|---|---|---|---|---|---|---|---|---|
| | | | | | BASELINE | OVERLOAD | | |
| 2219-T851 Aluminum | AD-25-29 | CTA | 1.25 | 1.44 | 500 | 625 | 25 | 50 |
| | AD-25-38 | CTA | 1.8 | 1.36 | 500 | 900 | 25 | 500 |
| Ti 6Al-4V Titanium | TD-25-32 | CTA | 1.25 | 1.40 | 800 | 1000 | 40 | 50 |
| | TD-25-30 | CTA | 1.8 | 1.50 | 1040 | 1870 | 52 | 500 |

*Approximate crack length examined

# Appendix

## FRACTOGRAPHS

The fractographs of this appendix supplement the essential illustrations referenced in the body of this report. They are reproduced here for the convenience of those readers interested in evaluating the data base they represent

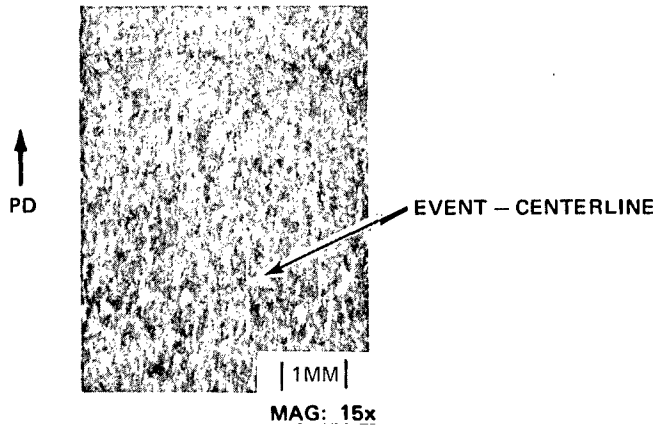


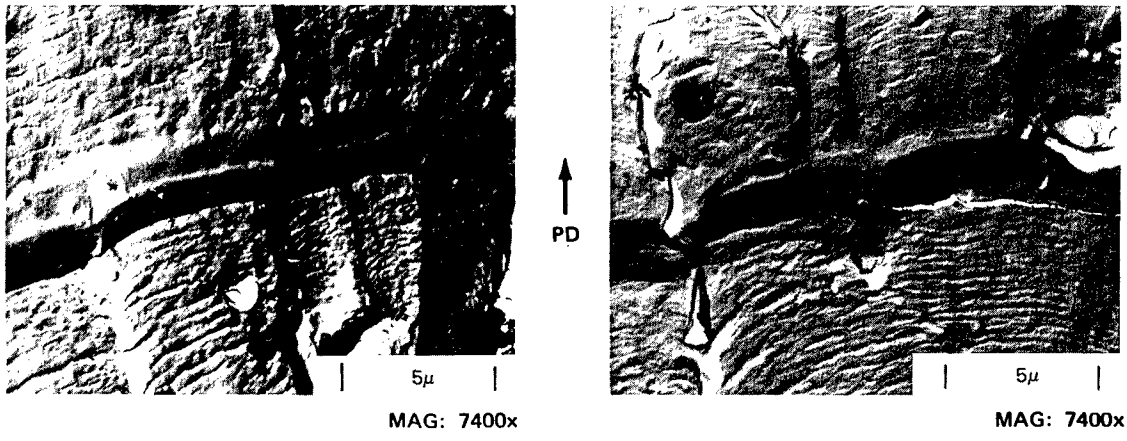


Peak load plastic zone showing well-defined fatigue striations before and poorly defined striations after.

**Figure A-1 Single Overload, $a_{OL}$ = 1.282 In., O/L = 1.5, 2219-T851 Aluminum (Sheet 1 of 2)**

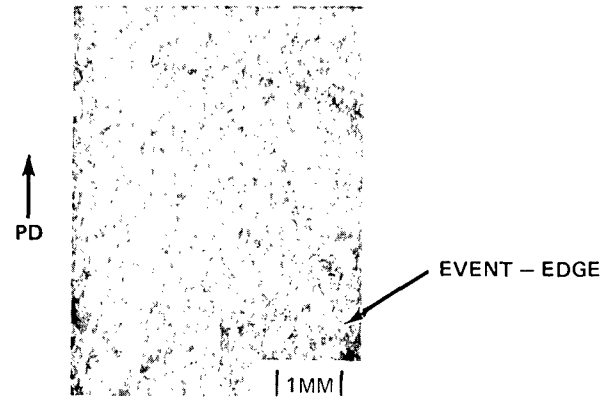


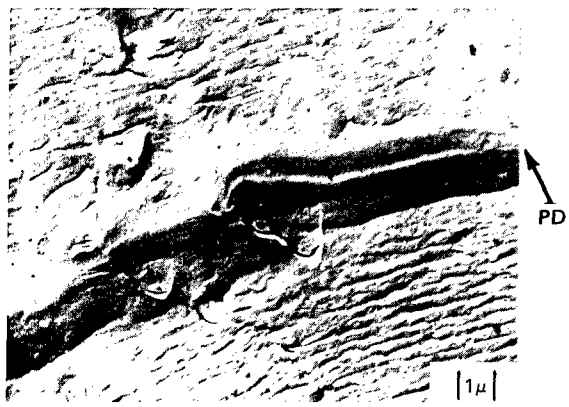


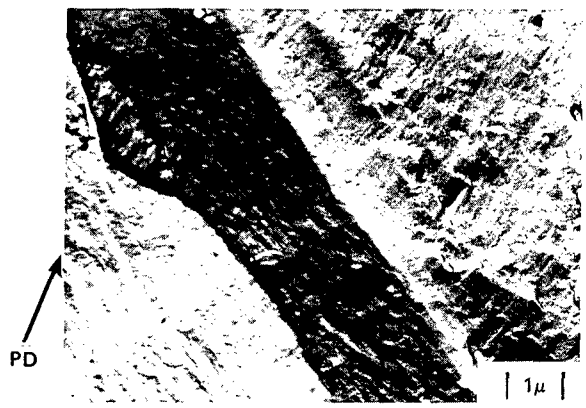


Peak load plastic zone showing well-defined fatigue striations before and poorly defined striations after.

**Figure A-1 Single Overload, $a_{OL}$ = 1.282 In., Edge, O/L = 1.5, 2219-T851 Aluminum (Sheet 2 of 2)**

AD-25-07
CTA

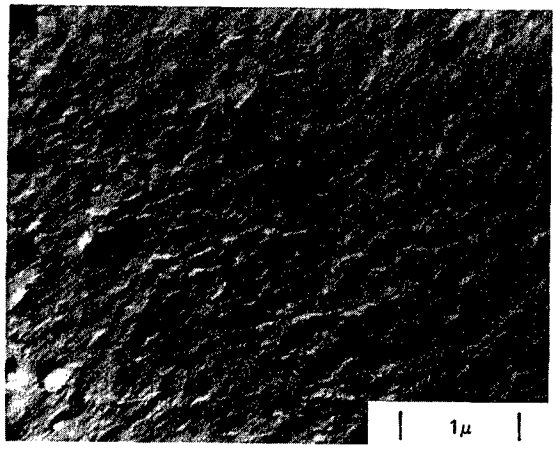


MAG: 26,320X

Typical poorly defined fine striations observed immediately after the peak overload showing crack growth retardation.

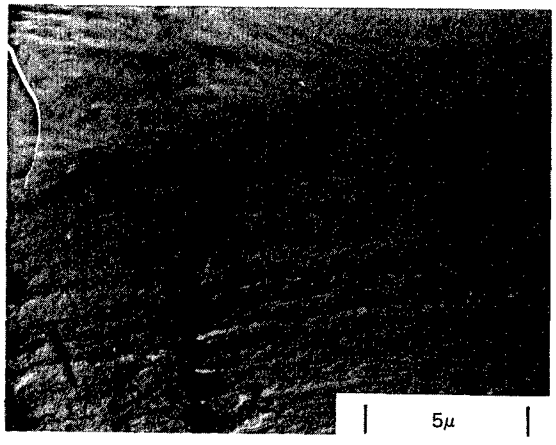


MAG: 7400X

Detail of transition from fatigue to peak load plastic load.

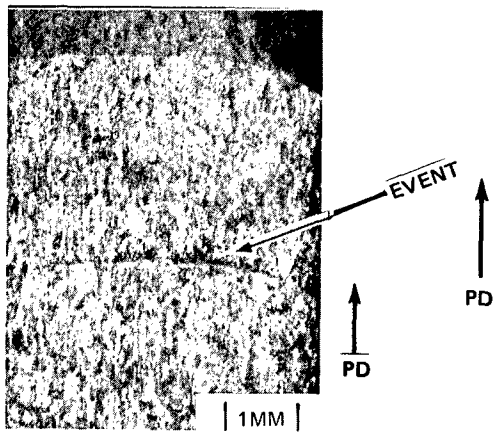


MAG: 15X

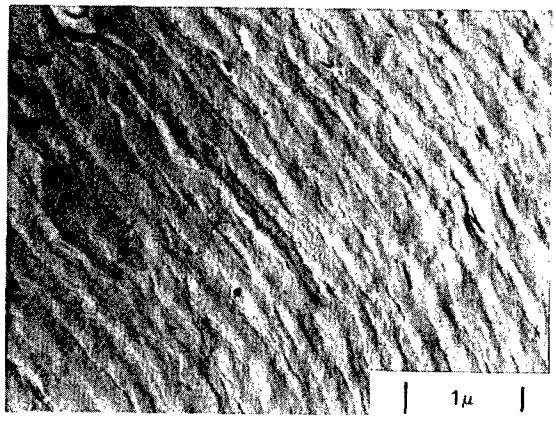


MAG: 26,300X

Coarse striations observed before the peak overload.

**Figure A-2 Single Overload, $a_{OL}$ = 1.375 In., Centerline, O/L = 1.8, 2219-T851 Aluminum**

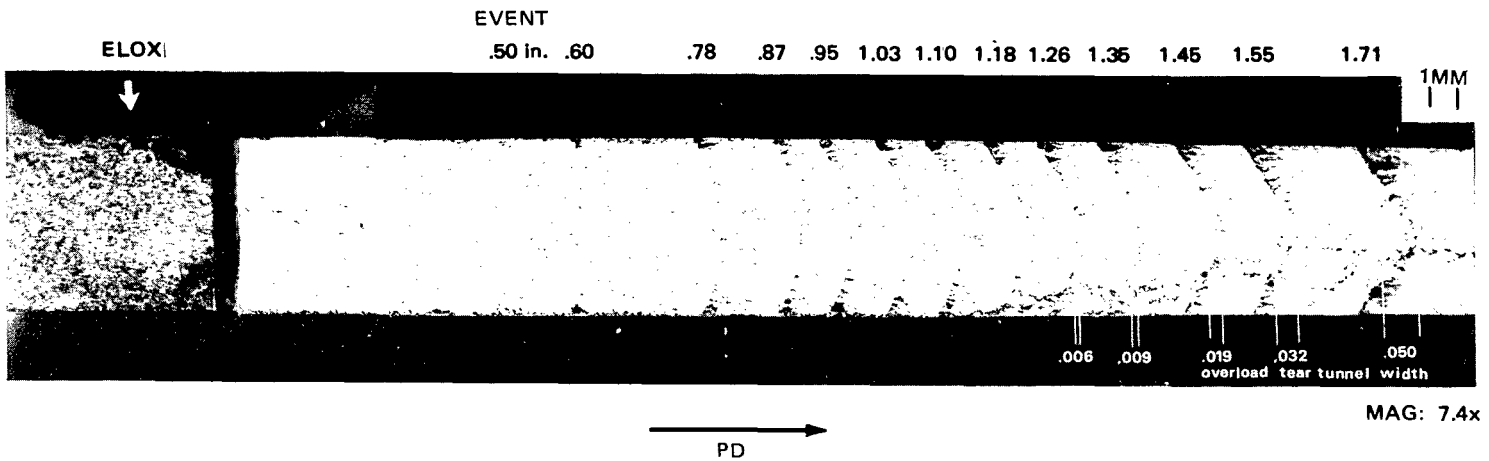


Overall view of fracture face showing fatigue arrest marks. Note that an overload tear tunnel appears with increasing crack length.

**Figure A-3 Multiple Arrest Marks Caused By Single Overloads, O/L = 1.8, 2219-T851 Aluminum (Sheet 1 of 2)**

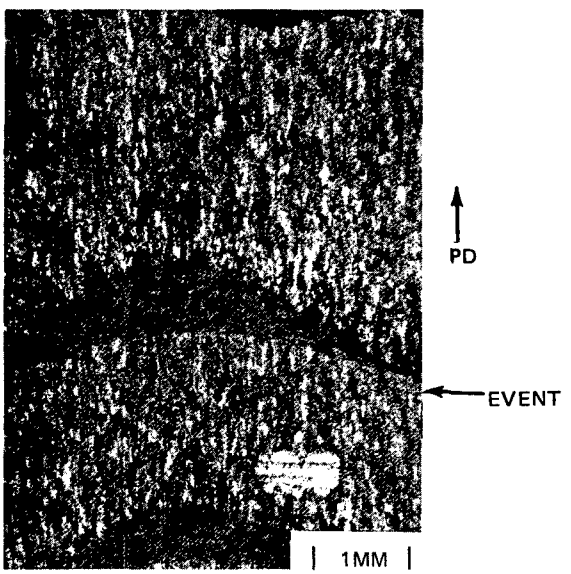


MAG: 15X

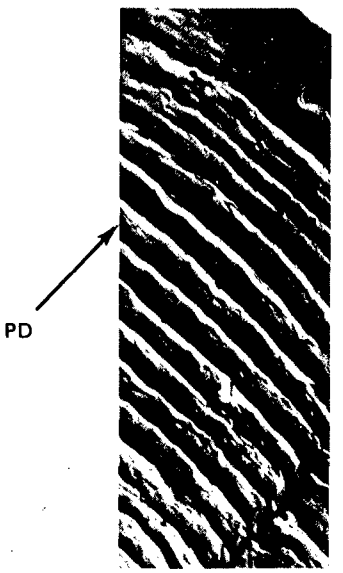


Increasing striation sp
to stretching of the e

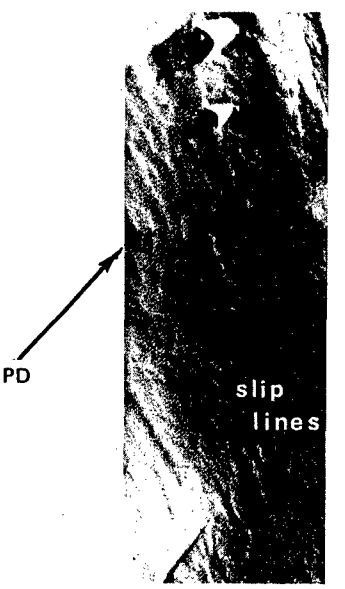


The event in sc
characterized b

**Figure A-3 High Stress Inten
(Sheet 2 of 2)**

AG-25-3P
CCP


MAG: 7400X

Increasing striation spacing just before event. This effect is believed to be due to stretching of the existing fatigue fracture surface by the overload peak.

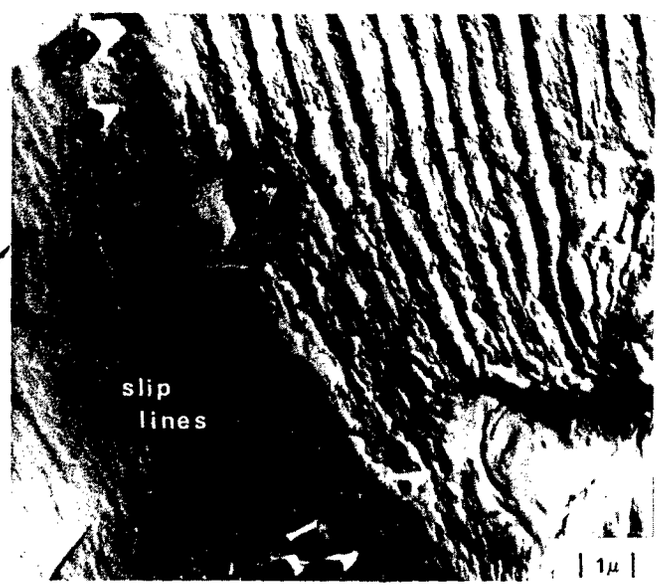


MAG: 7400X

The event in some areas of the peak load plastic zone was characterized by slip lines.

**Figure A-3 High Stress Intensity, Single Overload, $a_{OL}$ = 1.55 In., Centerline, O/L = 1.8, 2219-T851 Aluminum (Sheet 2 of 2)**



2

TG-25-10
CTB

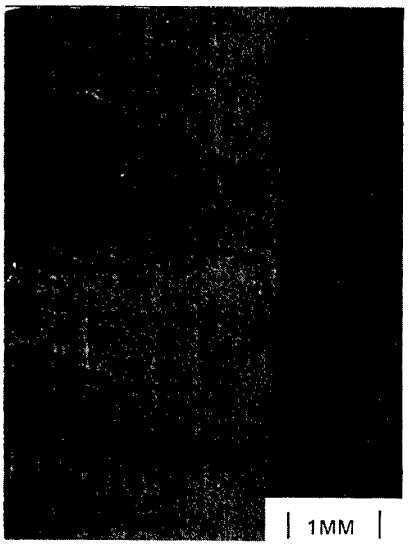


MAG: 15X


MAG: 9200X

Distinct band due to peak load.

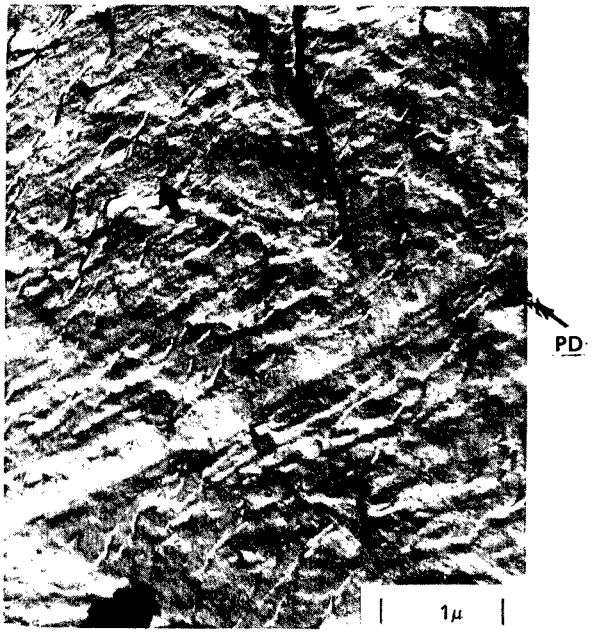


MAG: 21,000X

High magnification view of peak load event showing coarse striations before and fine striations after (arrow).

**Figure A-4 Single Overload, $a_{OL}$ = 1.483 In., Edge, O/L = 1.5, Ti 6Al-4V Titanium**

TG-25-10
CTB

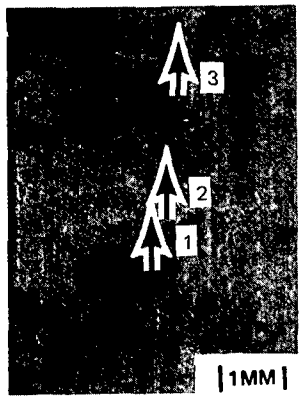


MAG: 15x

PD

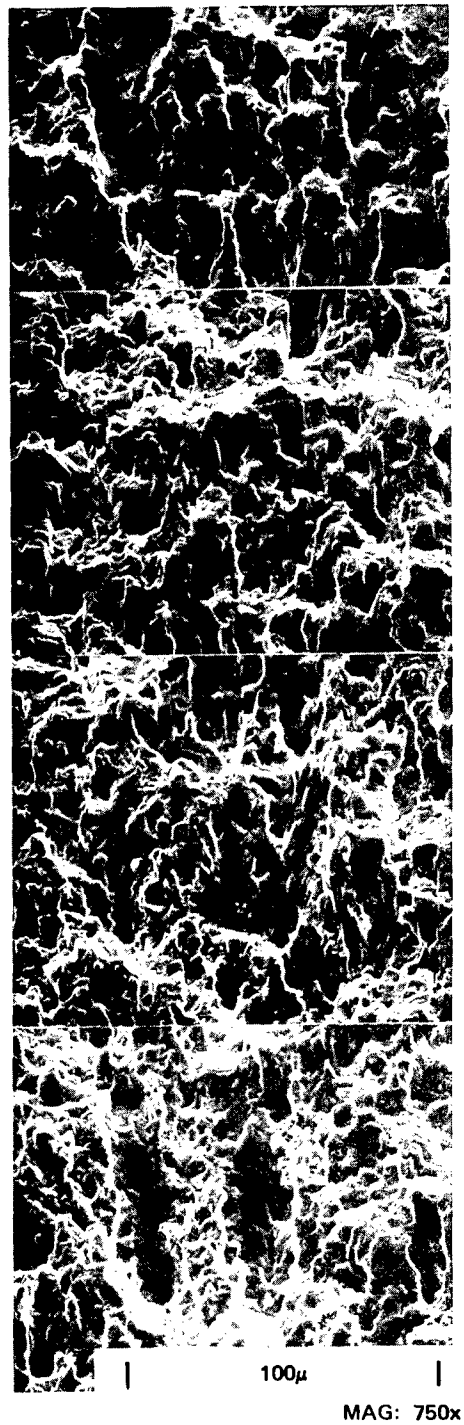


MAG: 750x

Scanning electron microscope view of three peak overload arrest bands.
Location 1, $a_{OL}$ = 1.483 in.
2, $a_{OL}$ = 1.50 in.
3, $a_{OL}$ = 1.58 in.

**Figure A-5 Single Overload, $a_{OL}$ = 1.483 In., Centerline, O/L = 1.5, Ti 6Al-4V Titanium (Sheet 1 of 2)**

TG-25-10
CTB

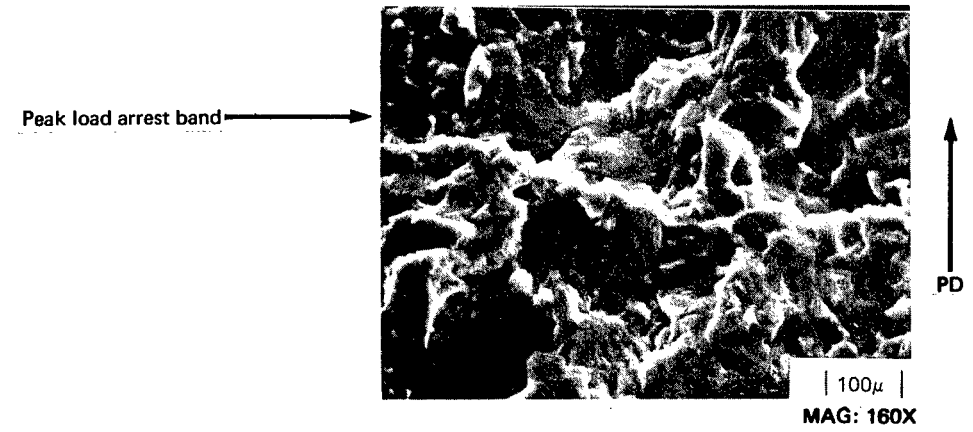


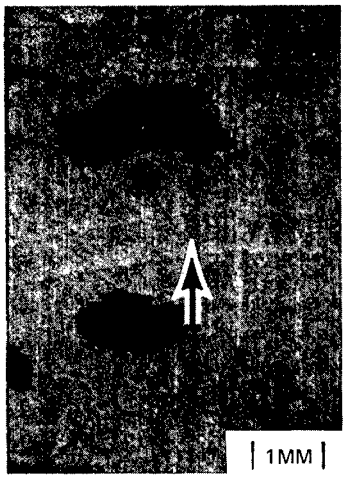


PD

Peak load arrest band

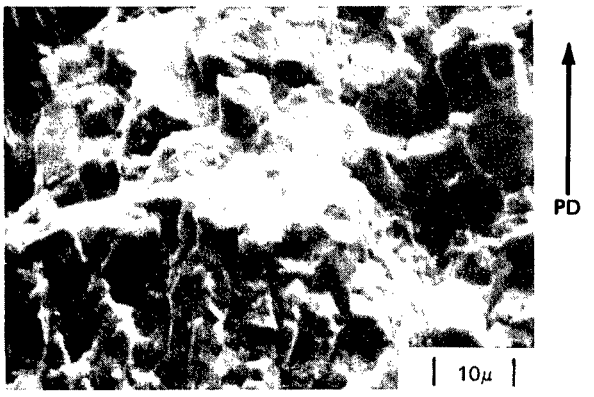


Peak load arrest band

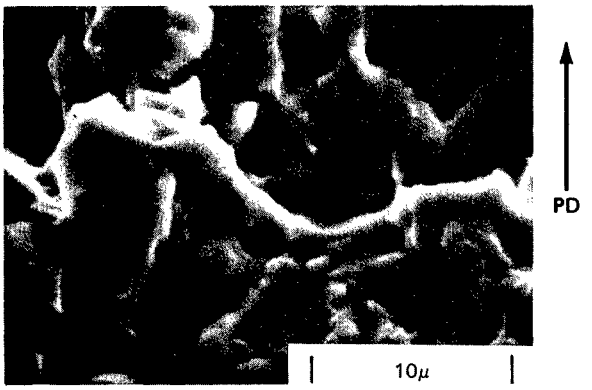


Increasing high magnification scanning election microscope (SEM) views of a 1.5 overload ratio peak load. The plastic zone associated with this load, shown clearly by transmission election microscopy (TEM), is not evident by SEM. The scanning view of the peak load suggests an abrupt change in elevation of the flat fatigue fracture.

**Figure A-5 Single Overload, $a_{OL}$ = 1.483 In., Centerline, O/L = 1.5, Ti 6Al-4V Titanium, SEM Photographs (Sheet 2 of 2)**

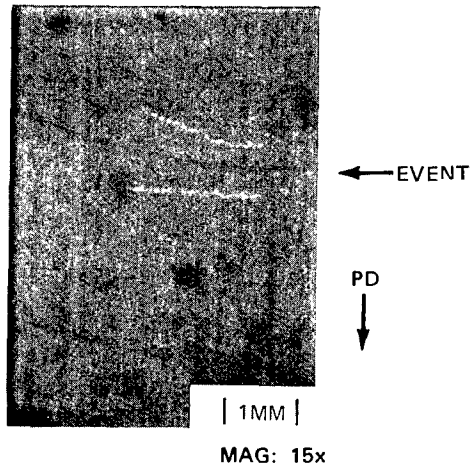


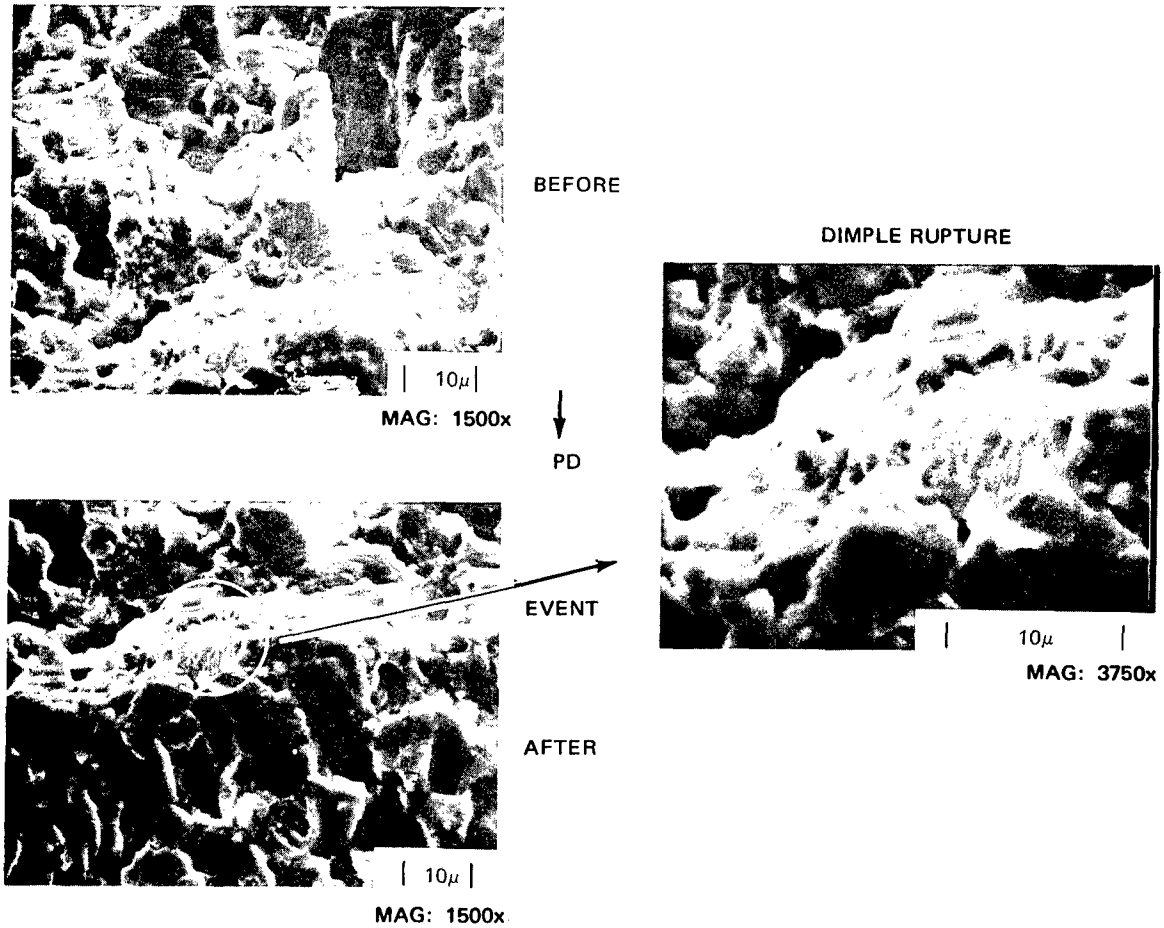


Event consists of dimple rupture at an elevation change as shown by SEM.

**Figure A-6 Single Overload $a_{OL}$ = 1.059 In., Centerline, O/L = 1.8, Ti 6Al-4V Titanium (Sheet 1 of 2)**

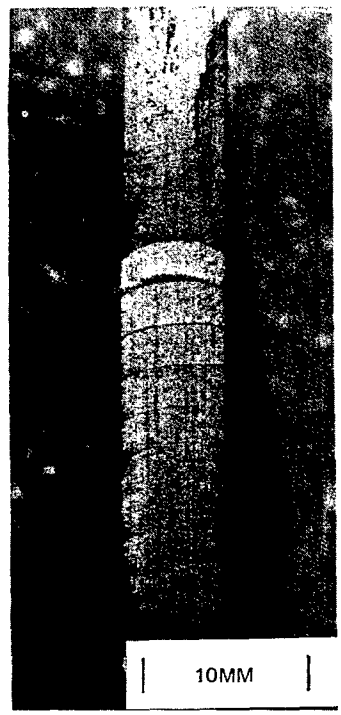


P D

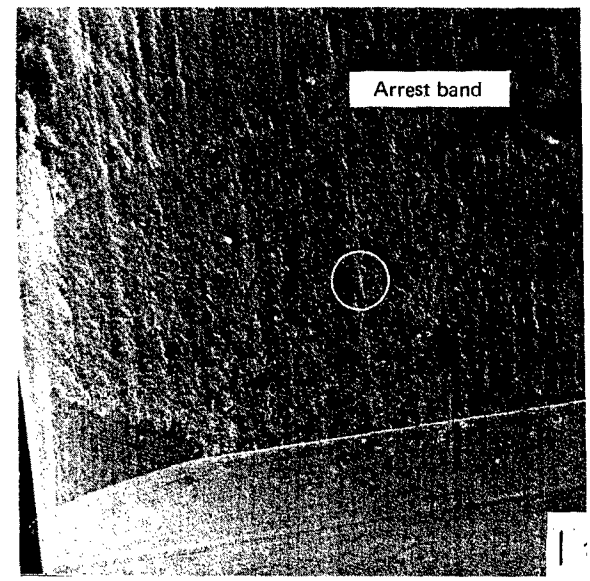


MAG: 5.5X

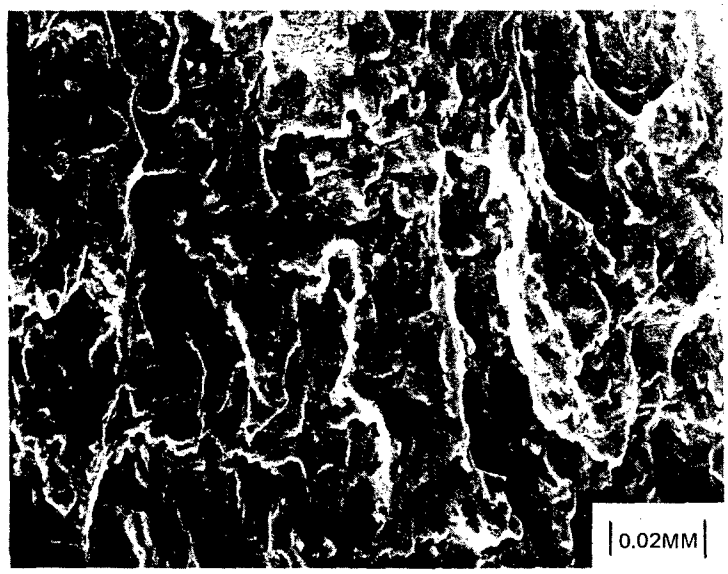


P D

MAG: 1500X

Increasing magnification SEM views of fracture face at a = .438 in., (area within white circle) on specimen TG-25-11. Note poor resolution under normal working conditions of the microscope. This lack of good resolution prevented this program from being done on the SEM.


P D

MAG: 33X

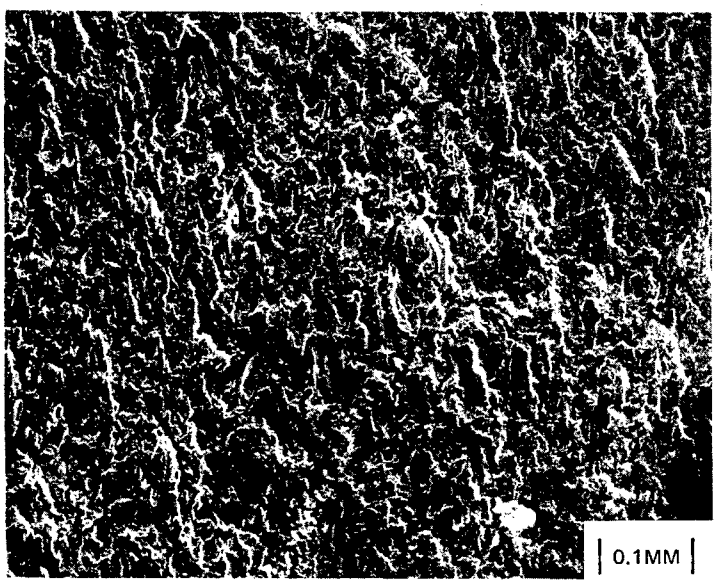


P D

MAG: 300X


P D

MAG: 3000X


P D

MAG: 7500X

poor resolution of the fatigue striations on the SEM.

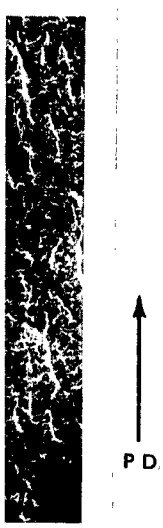

P D

1MM

3: 300X

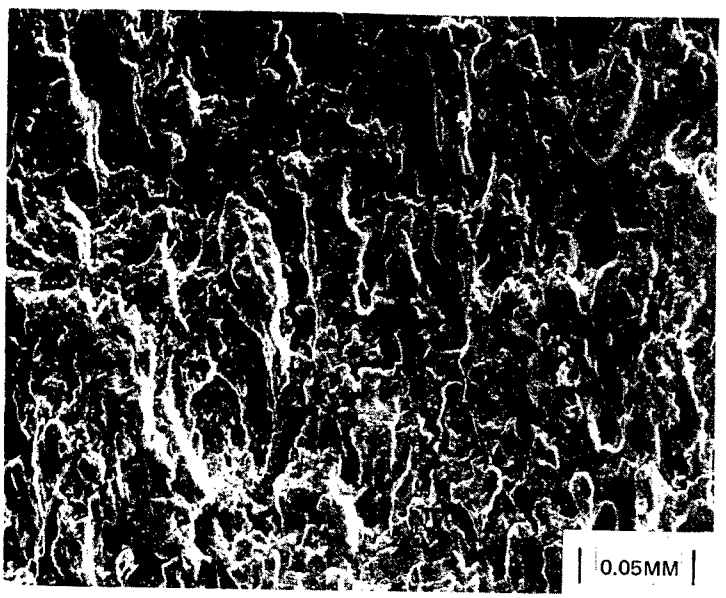

P.D

0.05MM

MAG: 750X

P D

5μ

MAG: 7500X

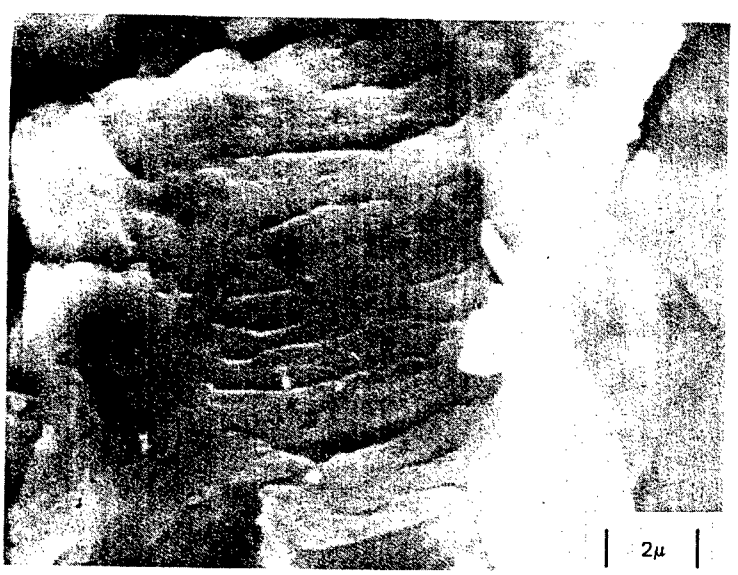

P D

2μ

MAG: 15000X

**Figure A-6 Scanning Electron Microscope (SEM) Resolution Study (Sheet 2 of 2)**

PD

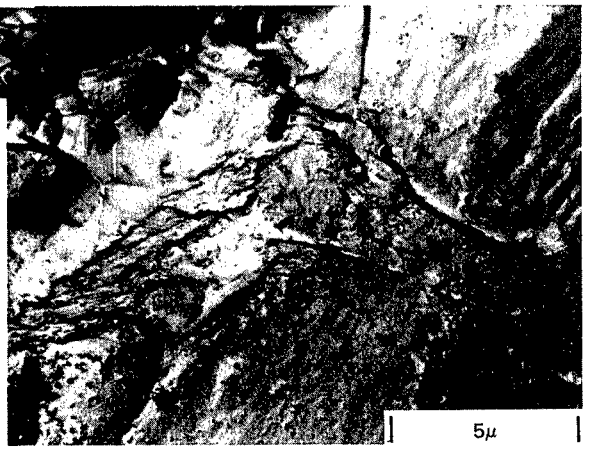


MAG: 6100x

Overload dimples and peak load plastic zone at event.

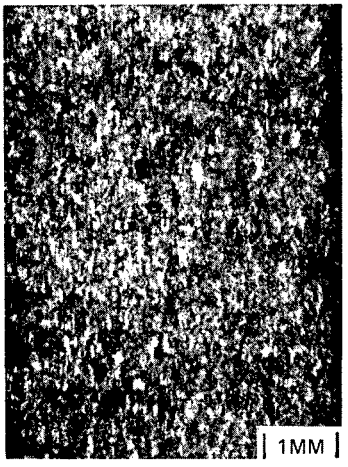


MAG: 15x

PD

EVENT

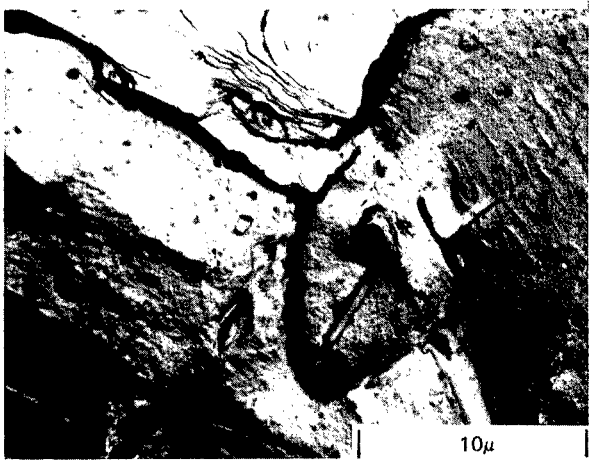


PD

MAG: 4700x

Peak load plastic zone showing striation spacing change before and after event.

**Figure A-7 Single Overload, $a_{OL}$ = 0.84 In., Edge, O/L = 1.5, 2219-T851 Aluminum (Sheet 1 of 2)**

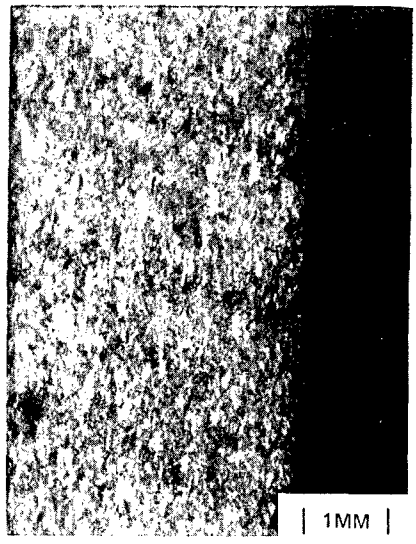


Mag: 15X


MAG: 4700X

Typical striation field near inclusions.

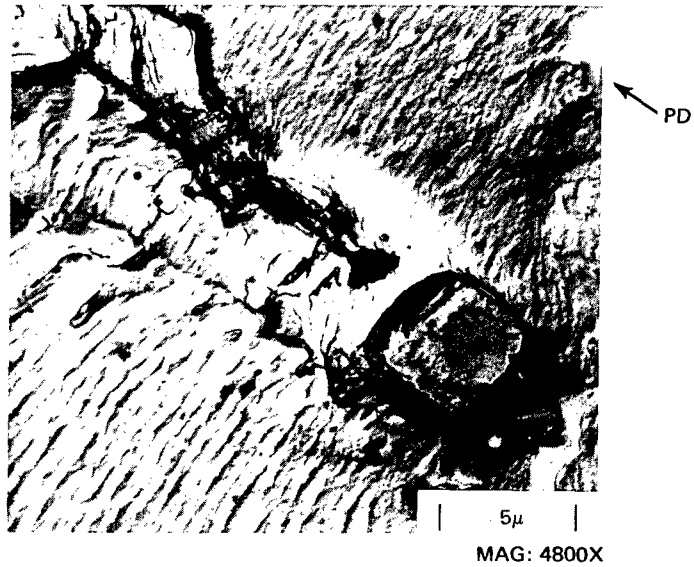


MAG: 4800X

Variation in striation spacing (compare upper and lower) resulting in data scatter.

**Figure A-7 Single Overload, $a_{OL}$ = 0.84 In., Edge, O/L = 1.5, 2219-T851 Aluminum (Sheet 2 of 2)**

AD-25-12
CTA

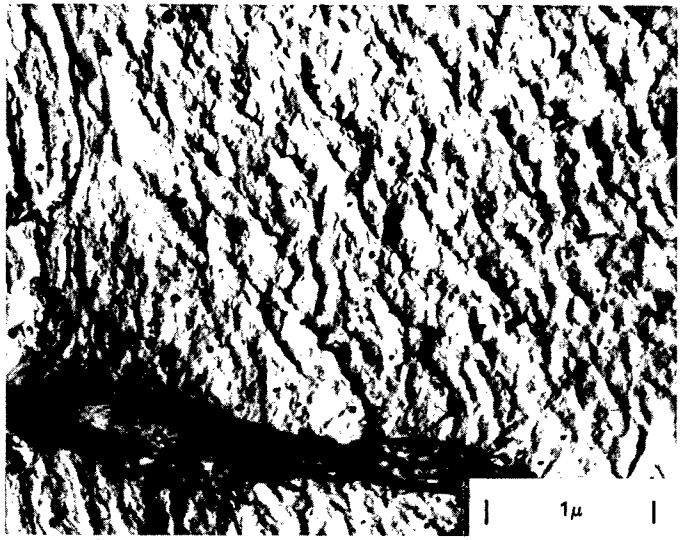



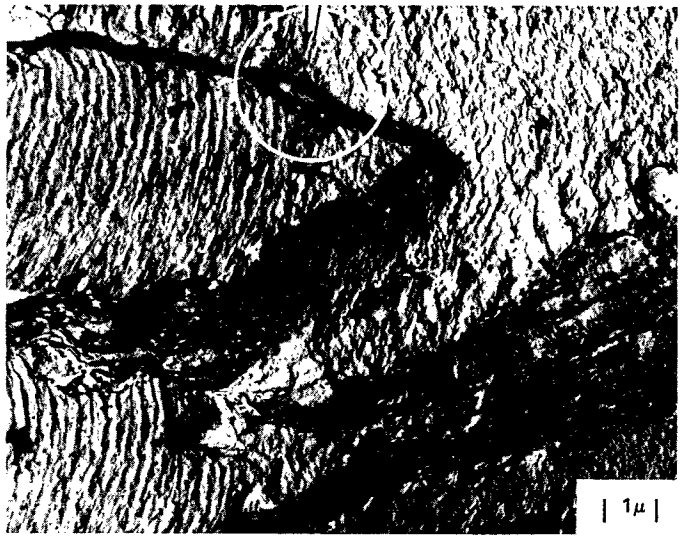


High load to low load fracture progression. Coarse striations are on left and brittle fine striations are on right. Note lack of slip band seen on Sheet 2 when load progression is from low load to high load.

**Figure A-8 Acceleration, $a_{OL}$ = 1.069 In., Centerline, O/L = 1.5, 2219-T851 Aluminum (Sheet 1 of 2)**

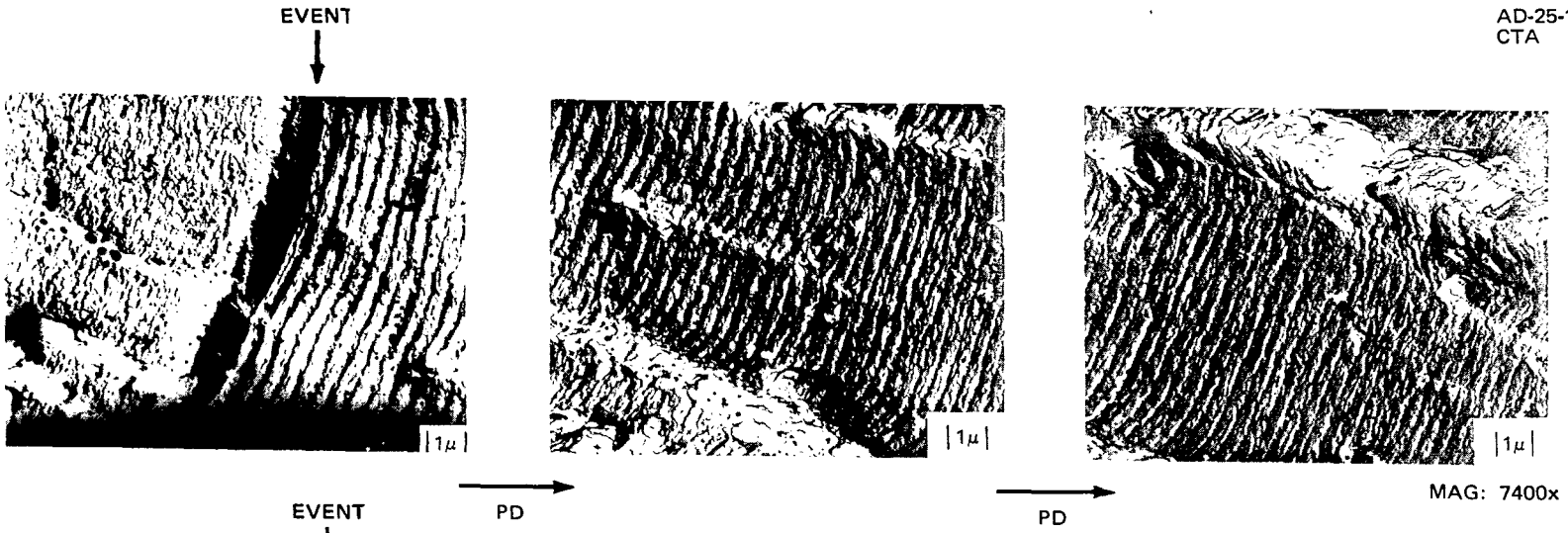


Low load to high load fracture progression. Overload ratio 1.5.

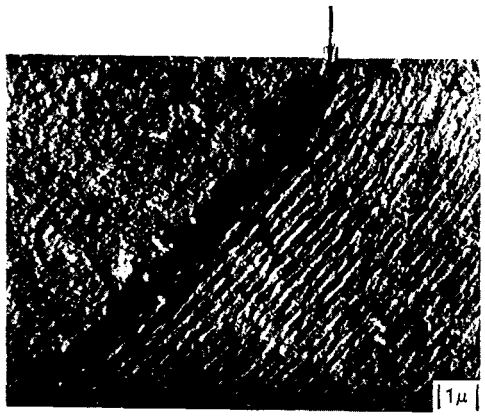


MAG: 7400x

Brittle fine striations on left (low load) and coarse striation on right (high load). Overload ratio 1.5

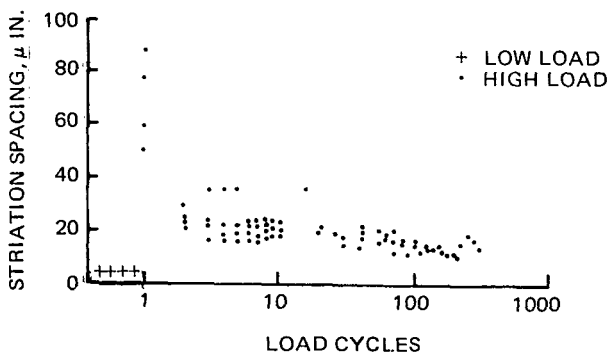


**Figure A-8 Acceleration, $a_{OL}$ = 1.069, In., Centerline, O/L = 1.5, 2219-T851 Aluminum (Sheet 2 of 2)**

AD-25-19
CTA

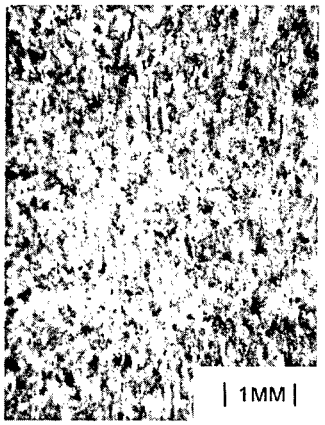


EVENT


MAG: 6075x
Low magnification view of event (Low load to high load) showing change from fine to coarse striations.

EVENT

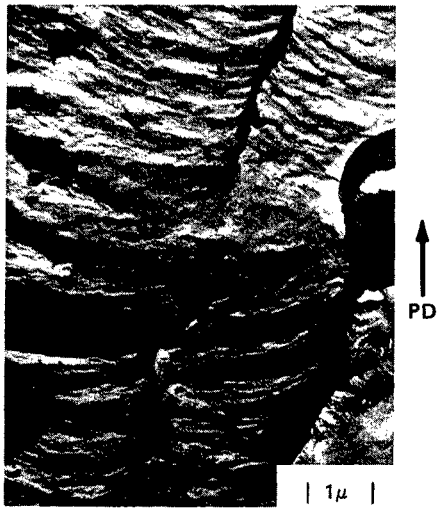


MAG: 14,000x
High magnification view of event (Low load to high load).

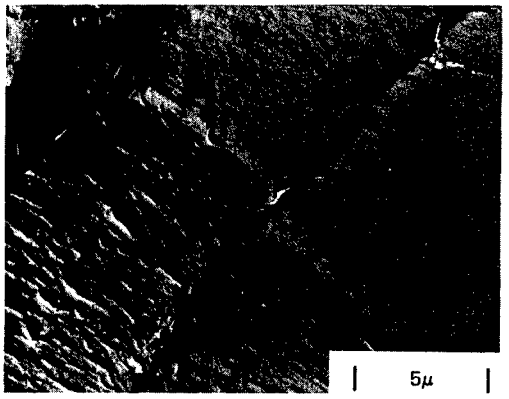


MAG: 6075x
Low magnification view of next event (high load to low load) showing change from coarse to fine striations.

**Figure A-9 Acceleration, $a_{OL}$ = 1.396 In., Centerline, O/L = 1.25, 2219-T851 Aluminum**

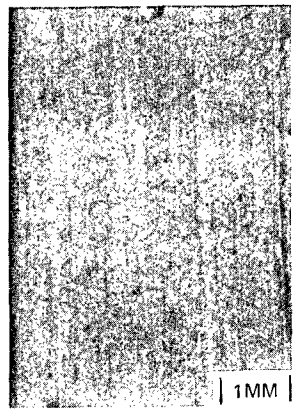


MAG: 15x

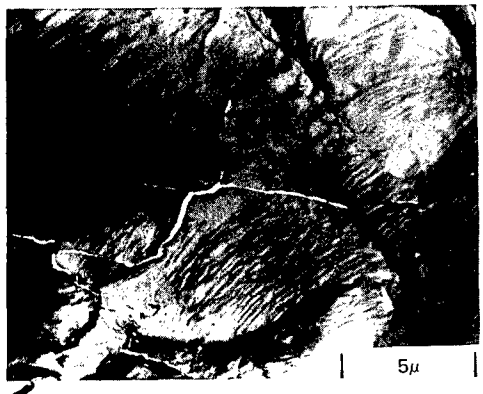


MAG: 5900x

View showing transition in event area from low load to high load (Acceleration).

EVENT

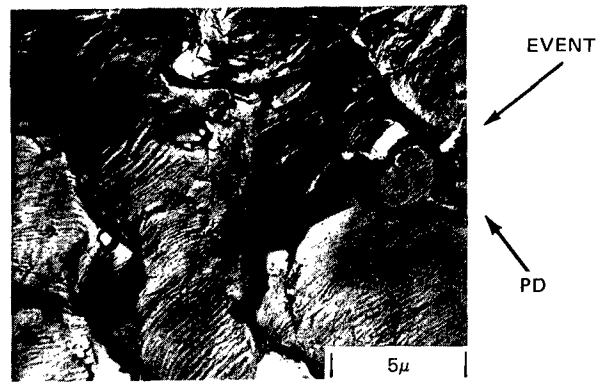


MAG: 6050x

View showing gradual change in striation spacing going from low load to high load.

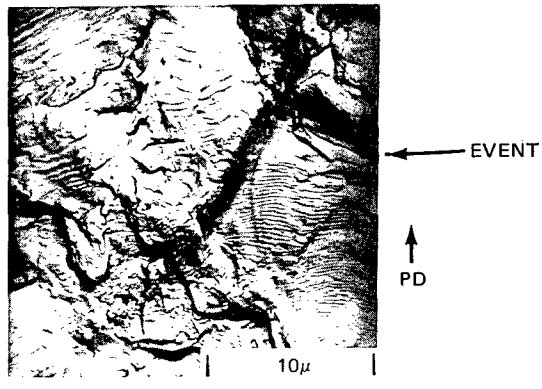


MAG: 3820x

At lower magnification the transition from low to high load is clearly evident.

**Figure A-10 Acceleration, $a_{OL}$ = 1.418 In., Centerline, O/L = 1.25, Ti 6Al-4V Titanium**

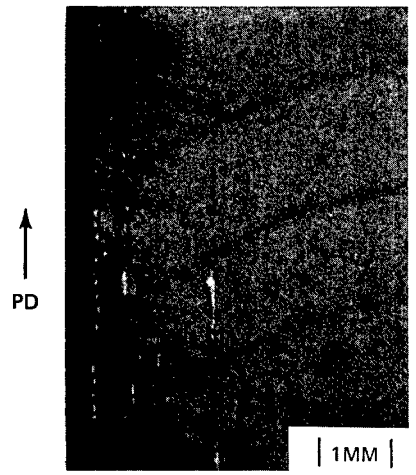


MAG: 15X


MAG: 6030X

Overall view of event. Detail in right photograph.

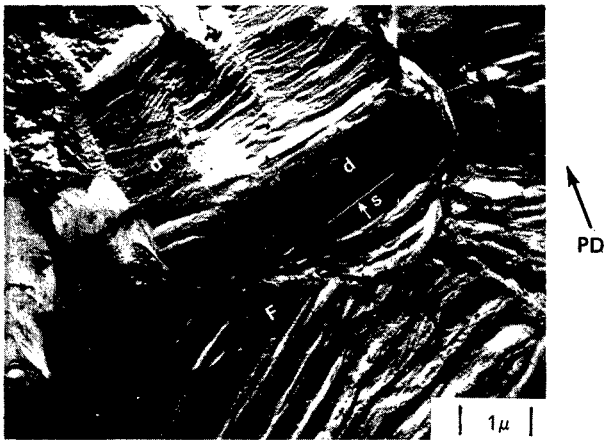


MAG: 14,400X

High magnification view of left photograph. "F" is coarse striations before peak load. "S" is the peak load application line. "d is deformation bands. "f" is fine striations after peak load.

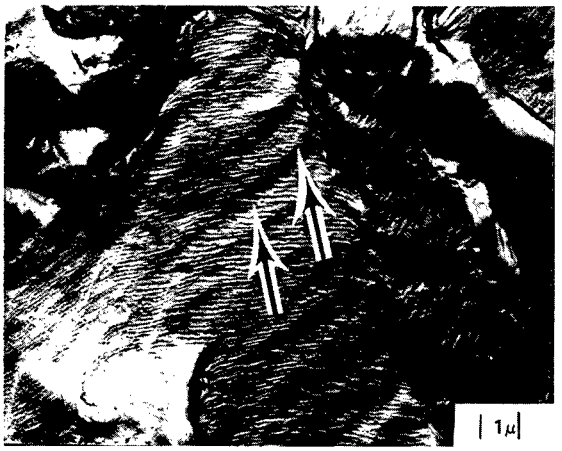


MAG: 3,850X

Example of microstructural texturing creating false impression of course striations (arrows). True fine striations are observable overall.

**Figure A-11 Acceleration, $a_{OL}$ = 0.692 In., Centerline, O/L = 1.25, Ti 6Al-4V Titanium (Sheet 1 of 2)**

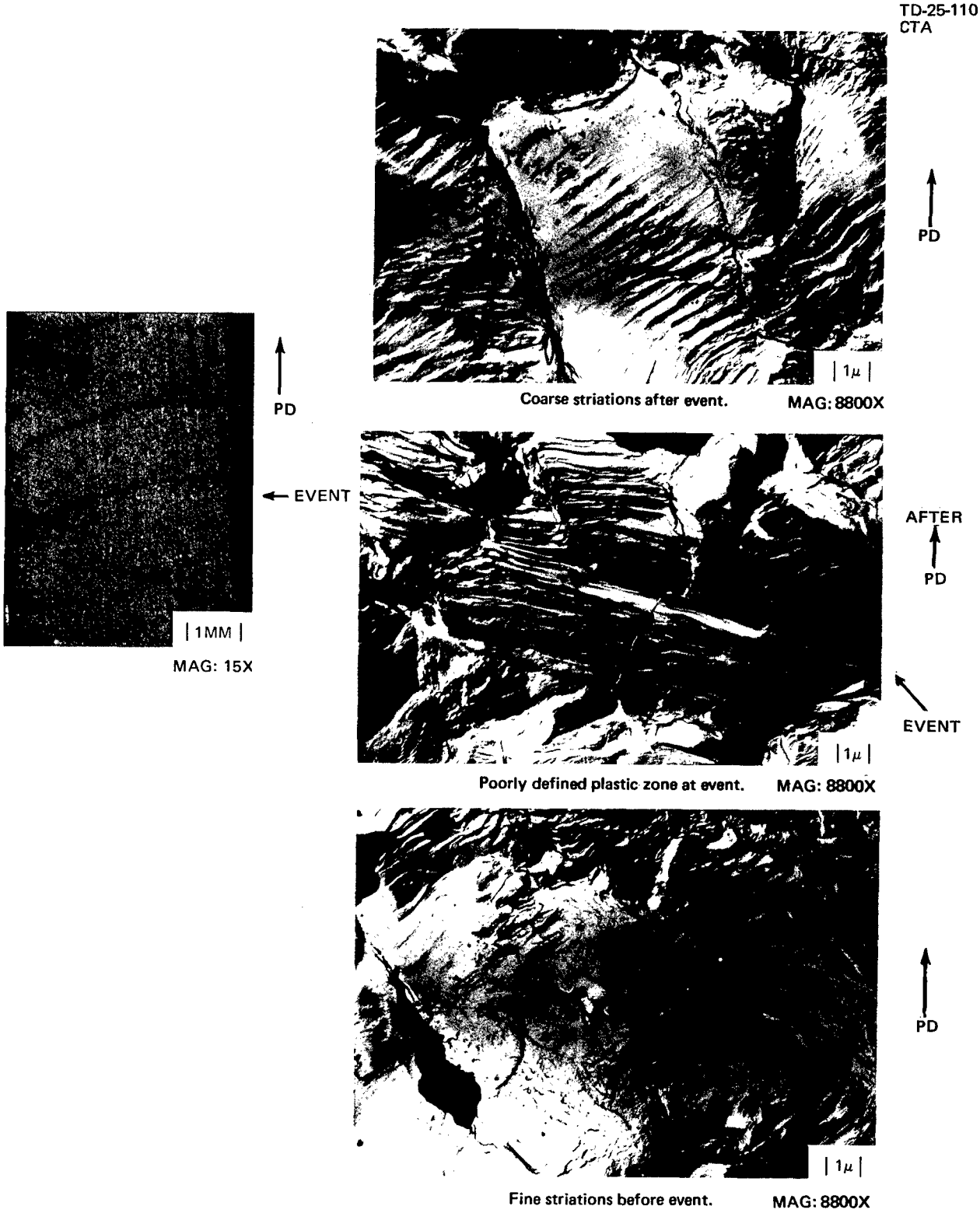


**Figure A-11 Acceleration, $a_{OL}$ = .692 In., Centerline, O/L = 1.8, Ti 6Al-4V Titanium (Sheet 2 of 2)**

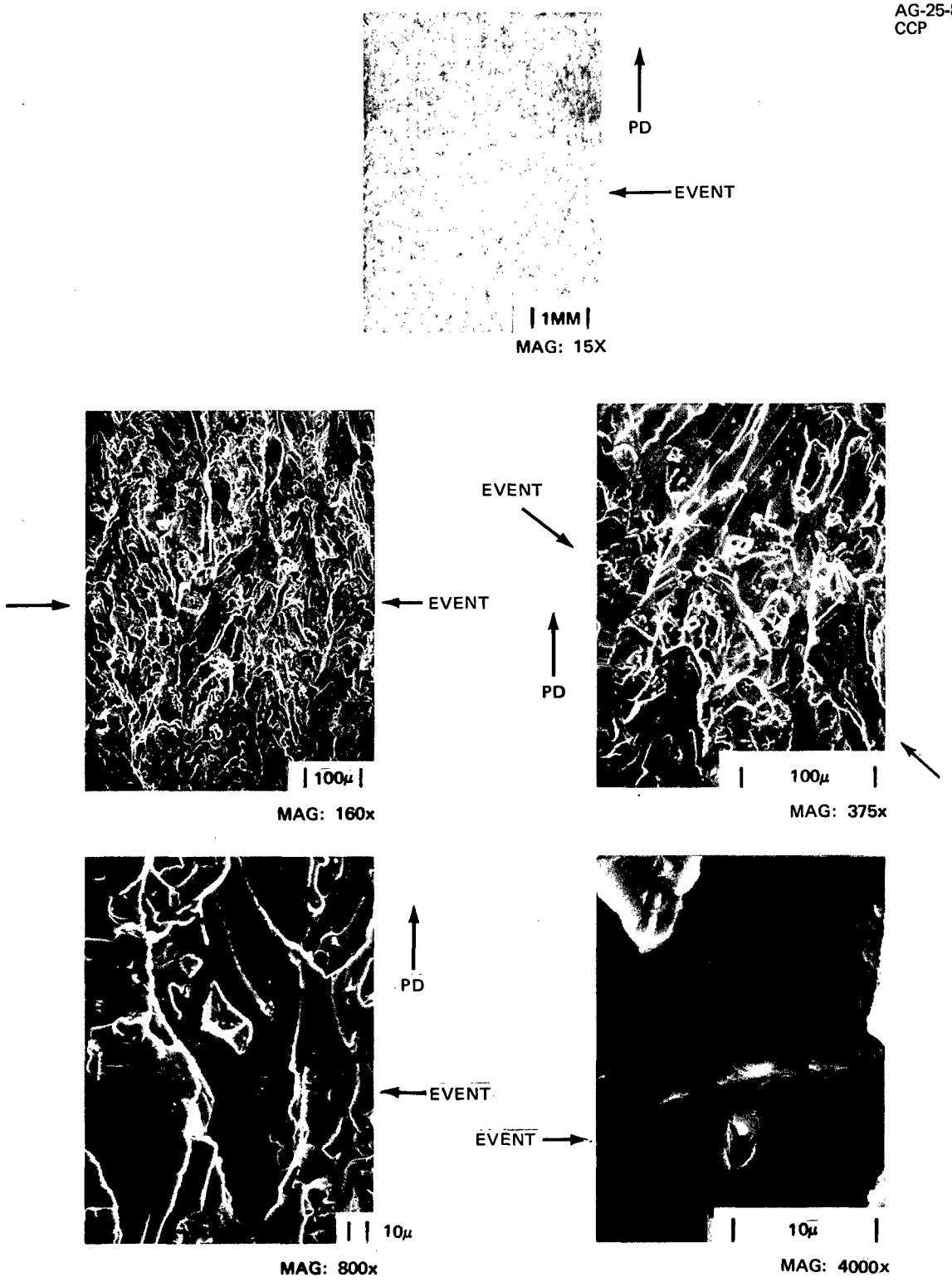


Scanning electron microscope view of discontinuous indications of compression spike event.

**Figure A-12 Compression Spike, $a_{ref}$ = 1.329 In., Centerline, 2219-T851 Aluminum (Sheet 1 of 2)**

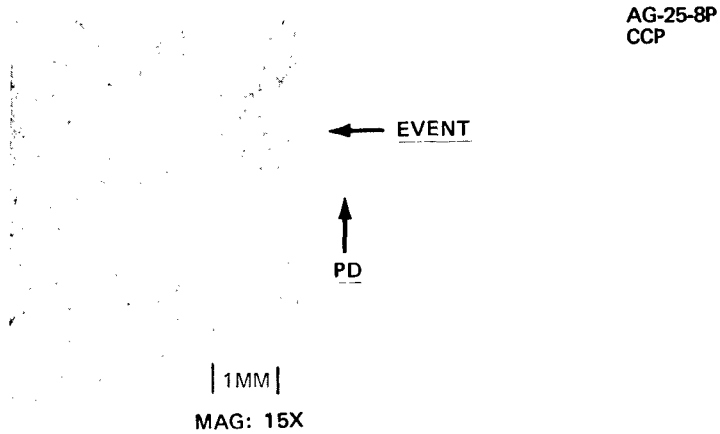


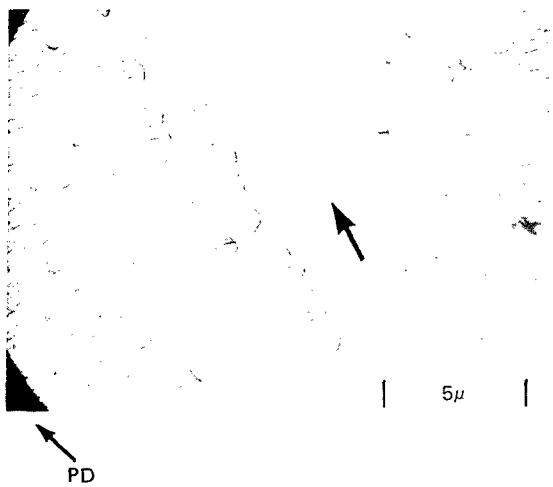


Typical striation spacing observed approaching event with unexplained flattening of one striation (arrow).

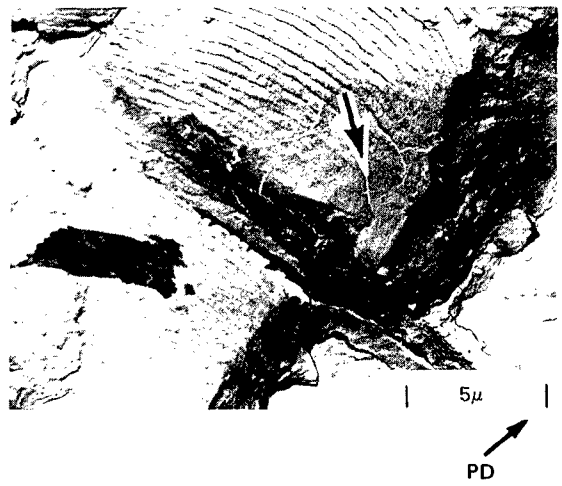


Flattening and rubbing out of existing fatigue fracture (arrow) by subsequent compressive load.

The compression event is not shown in either photo.

**Figure A-12 Compression Spike, $a_{ref}$ = 1.329 In., Centerline, 2219-T851 Aluminum (Sheet 2 of 2)**

AG-25-10P
CCP

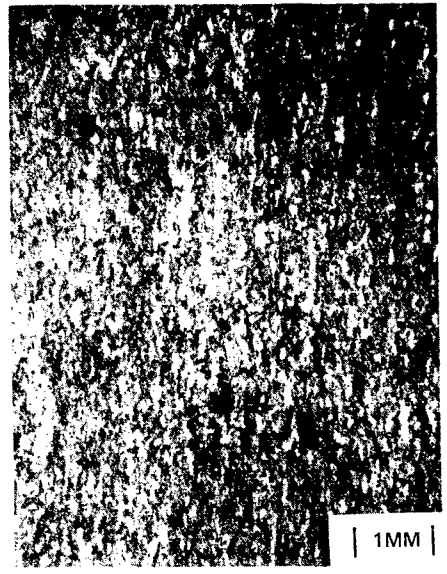


MAG: 15X


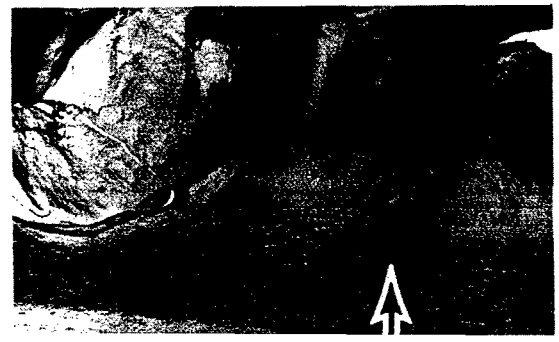

MAG: 15X


MAG: 4100X

Uniform striation spacing before and after event.

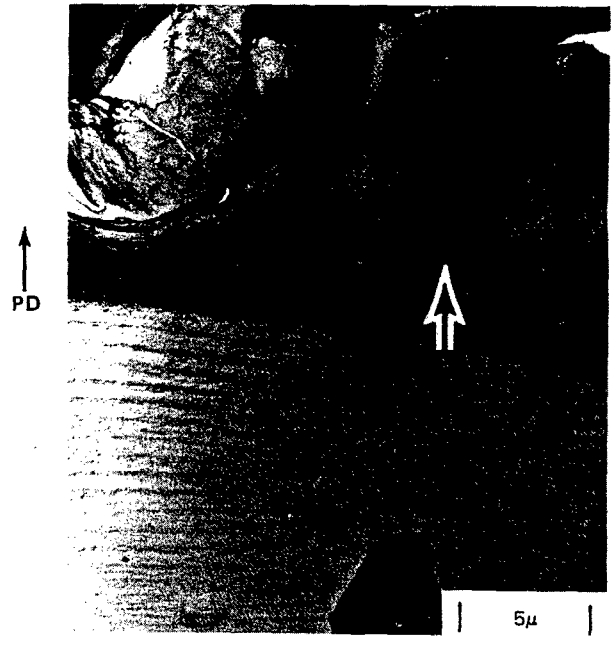


MAG: 4300X

Fatigue striations followed by deformation *marks in plastic zone (arrow).*

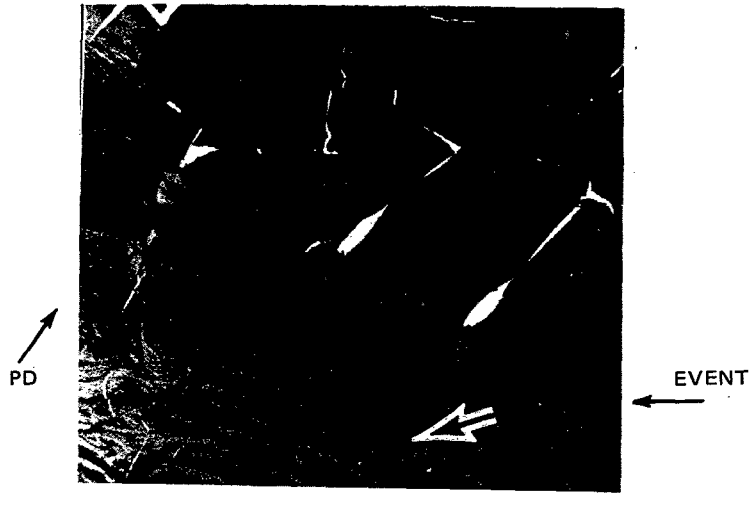


MAG: 4100X

Uniform striation spacing before and after event.


MAG: 4300X

Fatigue striations followed by deformation marks in plastic zone (arrow).

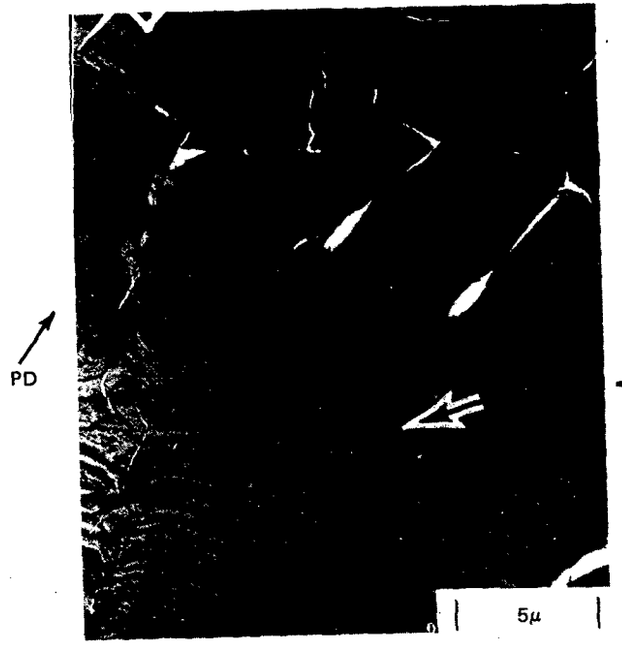


MAG: 4600X

Stretching of existing striations (arrow) just before event.

**Figure A-13 Tension/Compression Spikes, $a_{OL}$ = 1.546 In., 2219-T851 Aluminum (Sheet 1 of 2)**

AG-19-25-10P
CCP

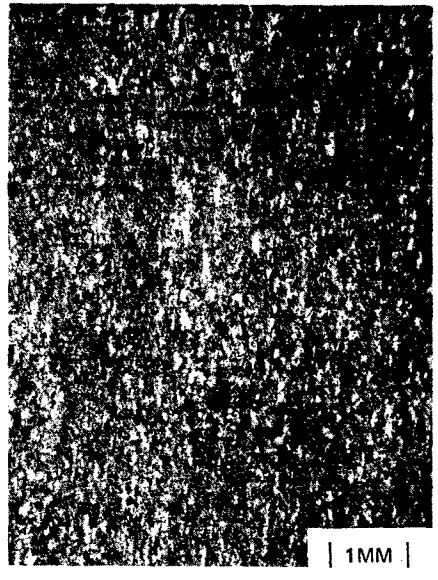


MAG: 15X


MAG: 15X


MAG: 3900X

Overload pocket at event. Note course striations before (lower left) and fine striatons after (upper right).


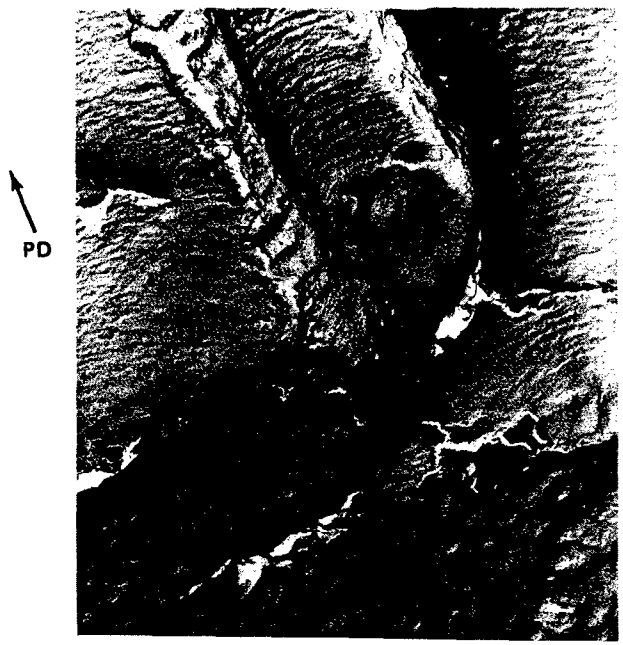


2

181/18


MAG: 3900X

Overload pocket at event. Note course striations before (lower left) and fine striatons after (upper right).


MAG: 7000X

High magnification view of course striations before event.

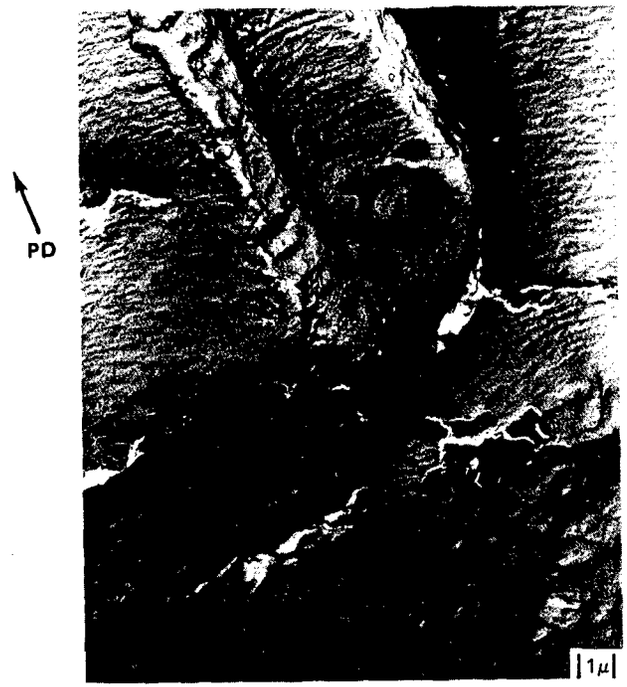


MAG: 6100X

High magnification view of fine striations after event.

**Figure A-13 Tension/Compression Spikes, $a_{OL}$ = 1.363 In., Centerline, 2219-T851 Aluminum (Sheet 2 of 2)**



3

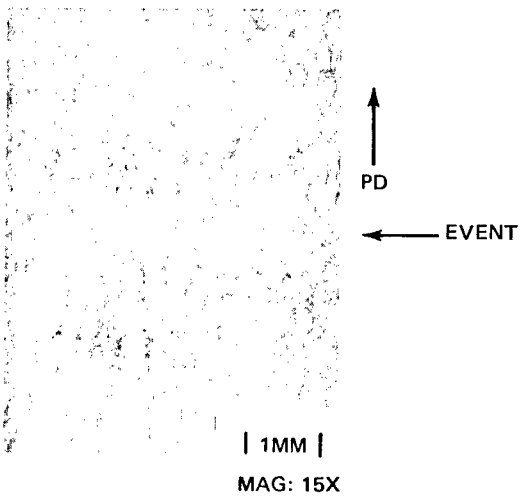


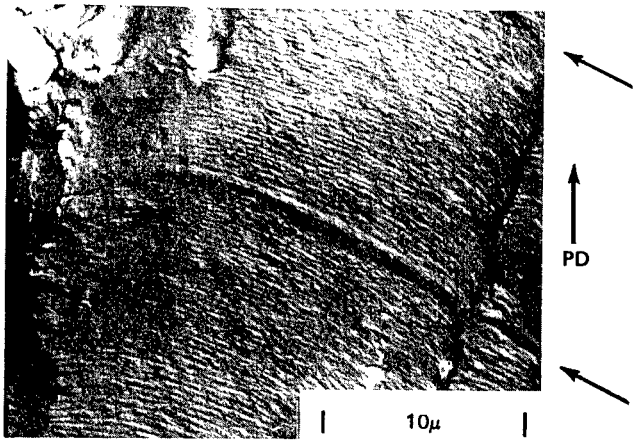


Periodic overload bands

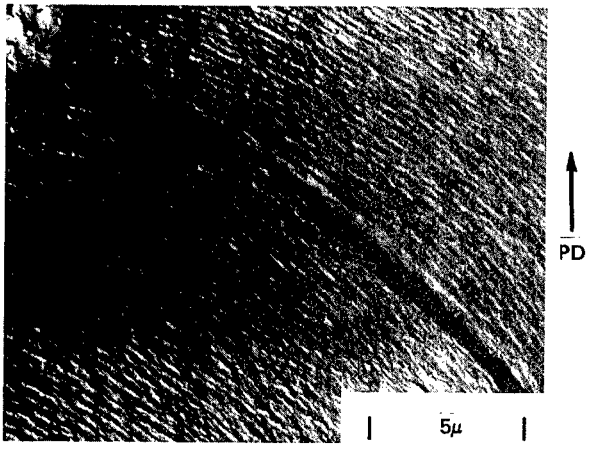


Higher magnification view of overload band

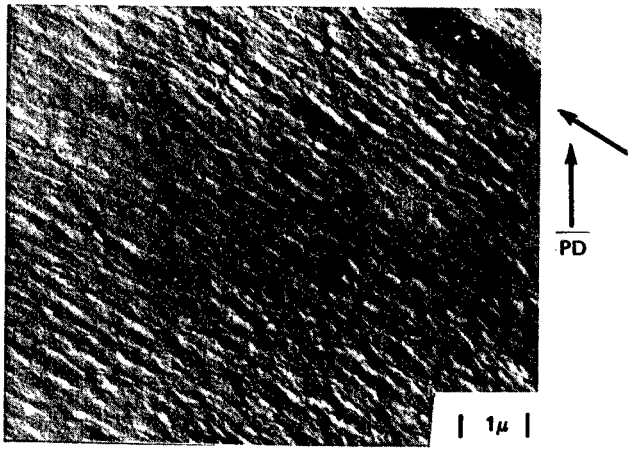


Uniform striation spacing before band (arrow)

**Figure A-14 Single Periodic Overloads, $a_{ref}$ = 1.44 In., Centerline, O/L = 1.25, $N_{OL}/N$ = 1/50, 2219-T851 Aluminum**

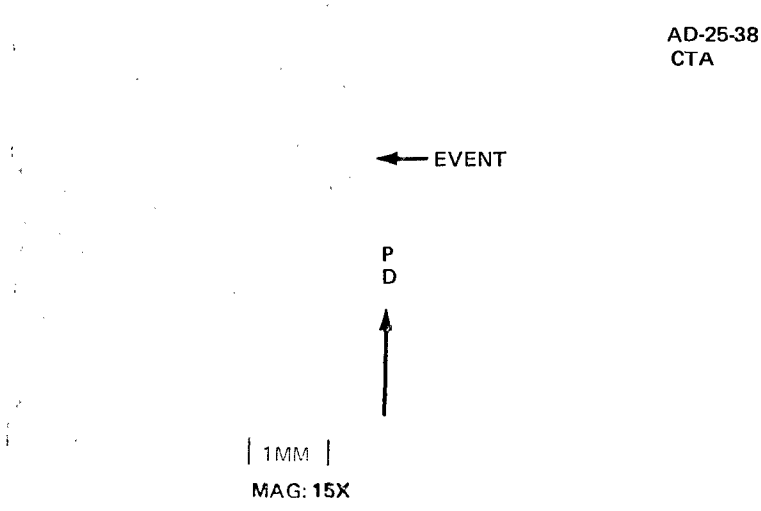


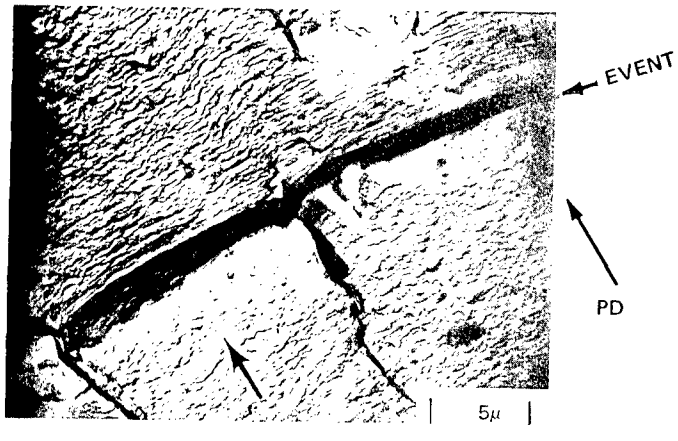


MAG: 3700X

Poorly defined striations before event (arrow)

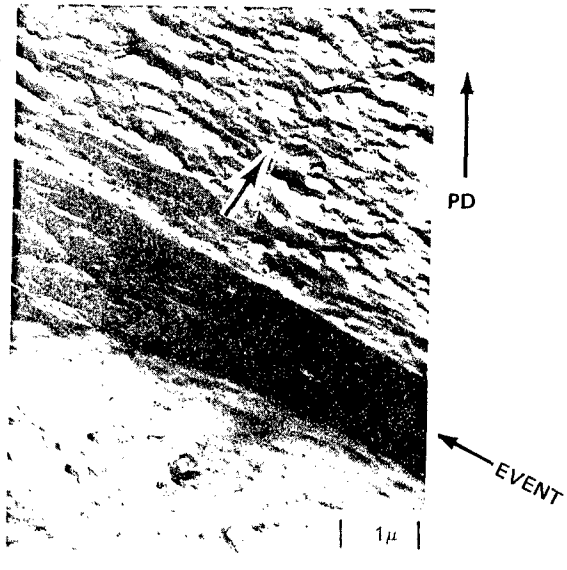


MAG: 15,100X

Striations are difficult to count and measure after event. (arrow)

**Figure A-15 Single Periodic Overloads, $a_{ref}$ = 1.36 In., Centerline, O/L = 1.8, $N_{OL}/N$ = 1/500, 2219-T851 Aluminum**

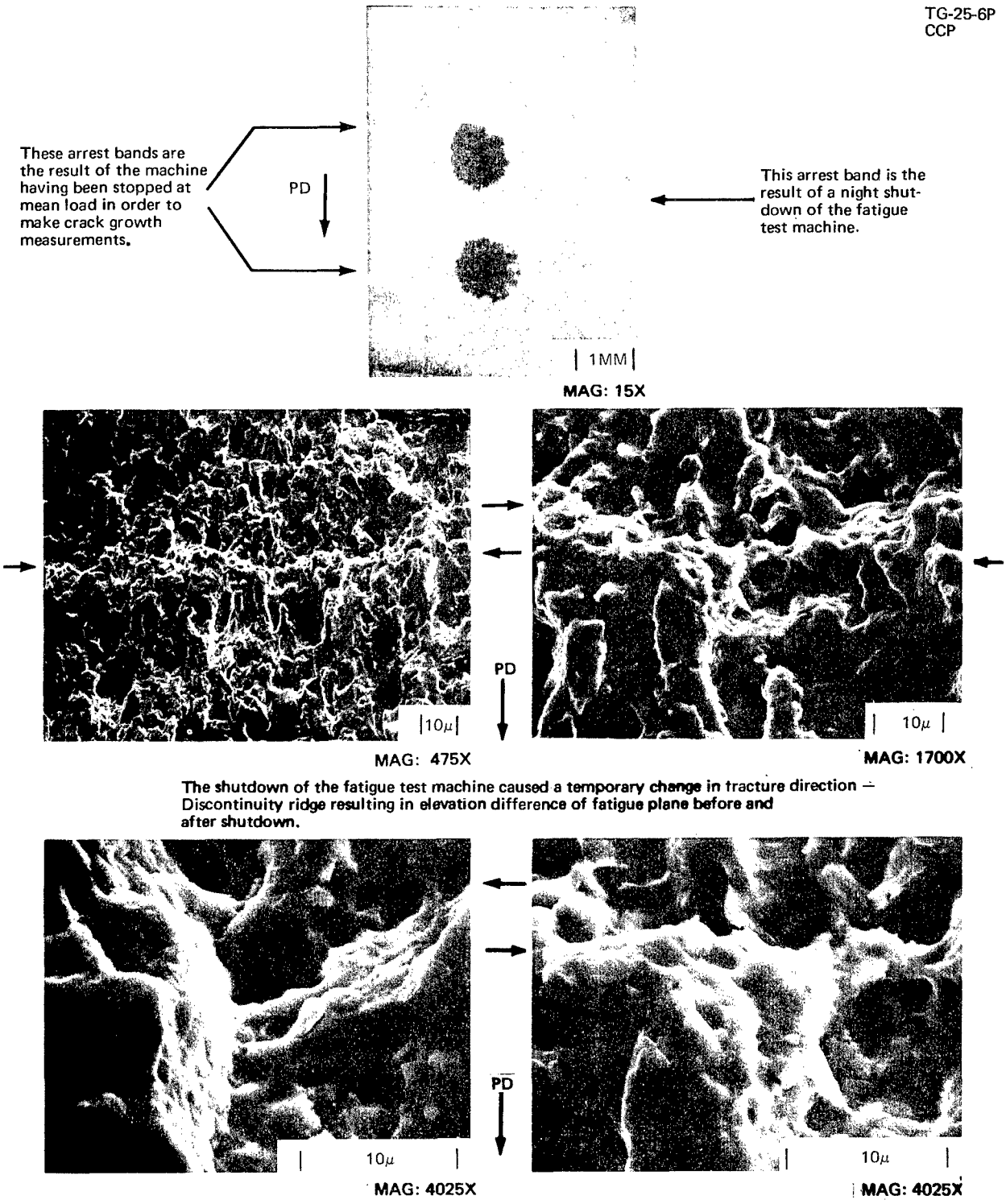


The shutdown of the fatigue test machine caused a temporary change in fracture direction – Discontinuity ridge resulting in elevation difference of fatigue plane before and after shutdown.




The machine shut down event contained a ridge separating the two fatigue planes. This ridge contained a combination of dimple rupture and fatigue striations.

**Figure A-16 Machine Shut Down Event $a_{ref}$ = 1.506 In.**



☆ U. S. GOVERNMENT PRINTING OFFICE: 1976 — 657-630/673

AG-25-6P
CCP

CENTER

NEAR EDGE

EDGE

CRACK LENGTH – .704 .705

Scanning electron microscope fracture edge, midway from edge to center and center traverse. Ductile and brittle striations were c
midway position while the edge traverse shows a heavily rubbed area.

PD

PD

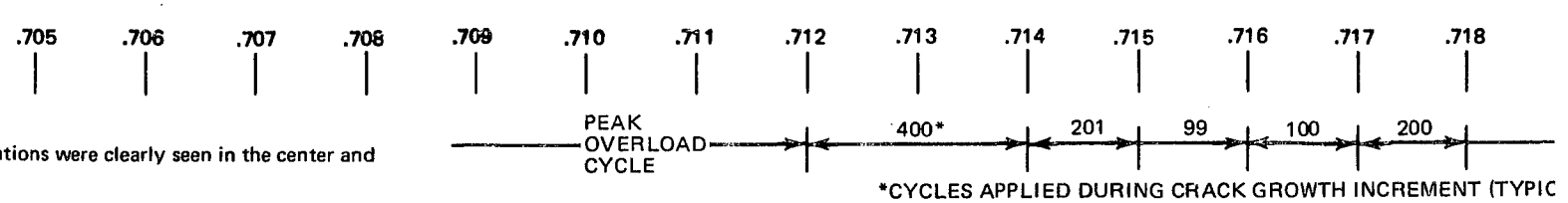


triations were clearly seen in the center and

*CYCLES APPLIED DURING CRACK GROWTH INCREMENT (TYPIC



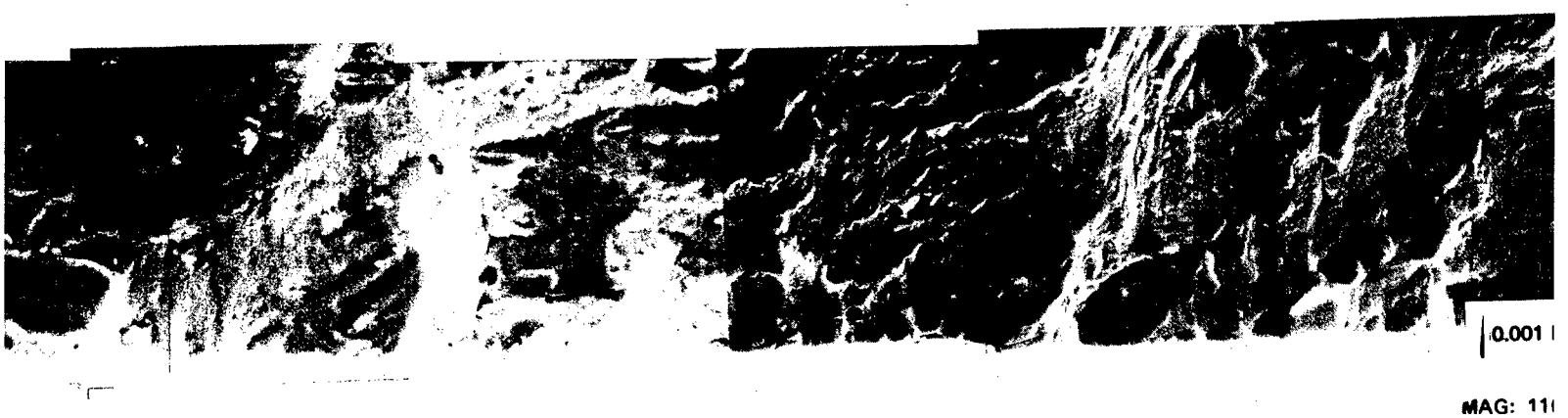


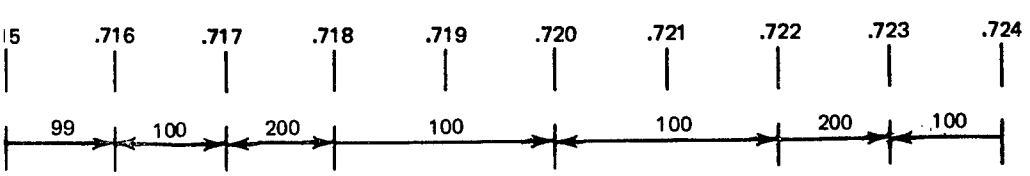


**Figure A-17 SEM Comparison of Edge, Nea Centerline Topography, Single $a_{ref} \cong 0.7$ in., O/L = 2.1, 2219 Aluminum**



3

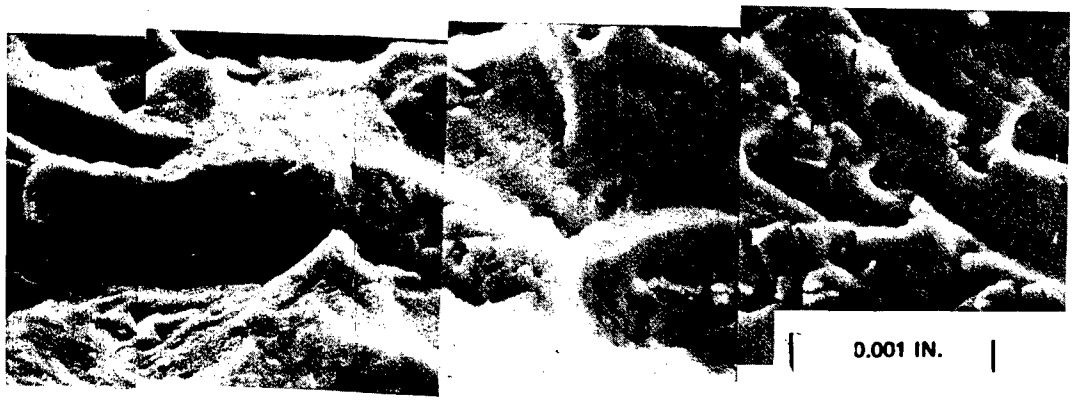


MAG: 2100X

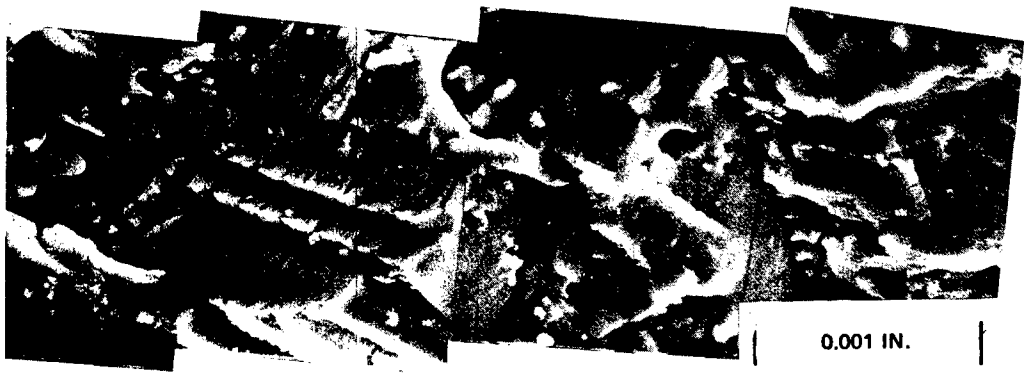


MAG: 2300X


MAG: 1160X

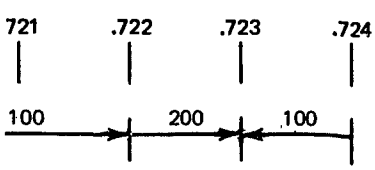


Figure A-17 SEM Comparison of Edge, Near Edge and Centerline Topography, Single Overload, $a_{ref} \cong 0.7$ in., O/L = 2.1, 2219-T851 Aluminum